The immunological role of cell wall components from diverse *Mycobacterium tuberculosis* clinical isolates in regulating HIV-1 replication in human macrophages

By

Mthawelanga Ndengane (NDNMTH001)

A thesis submitted for the degree of

DOCTOR OF PHILOSOPHY

in the department of Medical Microbiology

Faculty of Health Sciences,

UNIVERSITY OF CAPE TOWN

December 2022

Supervisor: Dr Anna K. Coussens

Co-supervisors: Dr Anastasia Koch, Dr Nashied Peton, Dr Joanna Evans, and Honorary Prof. Robert J. Wilkinson

Abstract

Human immunodeficiency virus type 1 (HIV-1) and *Mycobacterium tuberculosis* (*Mtb*) co-infection remains a major global health threat. Both pathogens synergistically drive pathogenesis of the other. The risk of developing active tuberculosis (TB) is increased in people living with HIV-1, even in those receiving antiretroviral therapy (ART), whilst TB was responsible for 15 % of HIV-related deaths in 2020. *Mtb* co-infection increases the likelihood of transcriptionally activating HIV-1 replication potentially due to bioactive *Mtb* lipids engaging macrophage surface receptors, thus triggering signalling pathways which activate human transcriptional factors (hTF) and production of inflammatory cytokines capable of activating HIV-1 transcription. This work investigated the hypothesis that clinical *Mtb* strains with single nucleotide polymorphisms (SNP) in lipid-metabolizing genes, required for cell wall lipid biosynthesis, differentially affect HIV-1 replication and human macrophage inflammatory response during *Mtb*-HIV-1 co-infection *in vitro*. Monocyte derived macrophages (MDM) were the predominant model used to investigate this phenomenon. Infections, in the presence or absence of HIV-1 co-infection, were performed using either lineage 2 or lineage 4 clinical strains with non-synonymous SNP in polyketide synthase 2 (*pks2)* required for sulfolipid 1 (SL-1) biosynthesis and compared to control infections using phylogenetically close clinical strains without the SNP of interest and canonical lineage 2 and 4 laboratory strains (H37Rv$^{P1939/T605}$, CDC1551^{WT} and HN878^{WT}). Secreted cytokines and chemokines were measured in supernatant (SN) by Luminex. The effect of *Mtb* on HIV-1 viral production was assessed by measuring HIV-1 Gag p24 in the SN of co-infected MDM or SN of HIV-1 infected MDM incubated with conditioned media from *Mtb*-infected MDM. The influence of *Mtb* on HIV-1 transcriptional activity was measured using a transgenic cell line (TZM-bl) with Luciferase reporter under HIV-1 long terminal repeat (LTR) expression. The impact of incubating TZM-bl cells in *Mtb*-induced conditioned media before or after HIV-1 infection was assessed. One pair of phylogenetically close clinical strains with and without a *pks2* SNP of interest (EX30$^{Q1939/A605}$ and MRC16$^{P1939/A605}$) with interesting lipid and inflammatory phenotypes, and H37Rv$^{P1939/T605}$ as a lineage 4 control, were subject to single nucleotide mutagenesis using recombineering to either revert SNP of interest to match the alleles of H37Rv or introduce the SNP of interest into the control strains. The wild-type and mutant strains were used in a trans-well assay to infect MDM in the presence of HIV-1 co-infection in the top chamber, while simultaneously mimicking the bystander effect of cytokine-mediated HIV-1 regulation in the bottom chamber which was only infected with HIV-1.

Results demonstrate there was increased cytokine production by MDM infected with MRC16$^{P1939/A605}$ in both the presence and absence of HIV-1 co-infection compared to its phylogenetically close paired strain EX30$^{Q1939/A605}$. The data shows that there was no difference in LTR activity in TZM-bl cells co-incubated with inflammatory environment between the strains of interests, however co-incubation of TZM-bl cells with *Mtb*-induced inflammatory environment generally increased LTR activity during HIV-1; a proxy for HIV-1 replication. In the trans-well co-infection assay, a significant positive association between production of HIVp24 and secretion of CCL2 was observed, whilst IL-1β secretion showed a significant negative relationship with the production of HIVp24, with donor variability in baseline cytokine production also associated with the extent of HIVp24, CCL2, IL-1β and IL-8 production. Introduction of the *pks2* T605A SNP into H37Rv$^{P1939/T605}$ and reversion in EX30$^{Q1939/A605T}$ significantly modified their inflammatory phenotype. Together these results support the hypothesis that *Mtb* clinical stains with genetic variation in cell wall lipid biosynthesis impacts the inflammatory milieu and, subsequently, HIV-1 replication during co-infection. The outcome of *Mtb*-HIV co-infection is therefore not homogenous but contingent on the phenotype of infecting *Mtb* strain and individual.

Table of Contents

Abstract ..... ***i***

Table of Contents ..... ***iii***

Declaration ..... ***vii***

Dedications ..... ***viii***

List of figures ..... ***ix***

List of tables ..... ***xi***

List of abbreviations ..... ***xiii***

Chapter 1. Mycobacterium tuberculosis and human immunodeficiency virus 1 synergistically worsen each other's disease outcome ***16***

1.1. The TB HIV-1 syndemic **16**

1.2. The life cycle of HIV-1 infection **17**

1.2.1. Invasion and viral tropism 17

1.3. Cellular entry and genome integration **19**

1.3.1. HIV-1 systemic infection and reservoir formation 19

1.3.2. HIV-1 replication 20

1.4. Genomic diversity with *Mtb* populations influences TB pathogenesis **22**

1.4.1. *Mtb* has highly diverse and bioactive lipids that influence the phenotype of immune response to infection 24

1.5. *Mtb* co-infection worsens HIV-1/AIDS disease outcome by increasing susceptibility to HIV-1 infection, viral set-point, and spread **26**

1.5.1. *Mtb*-specific T cells have increased susceptibility to HIV-1 infection 26

1.5.2. Mechanisms of *Mtb*-induced viral spread 27

1.5.3. The bystander cell effect: a role for *Mtb*-induced cytokines in regulating HIV-1 replication 28

1.6. Hypothesis **29**

1.7. The aims of this project to address this hypothesis were: **29**

1.8. References **30**

Chapter 2. Materials and Methods ***37***

2.1. Materials **37**

2.2. Methods **40**

2.2.1. Study ethical approval 40

2.2.2. Generating *Mtb* single-cell stocks **41**

2.2.3. Harvesting *Mtb* stocks for single cells 42

2.2.4. Analysis of *Mtb* lipids with thin layer chromatography 42

2.2.5. *Mtb* genetic engineering using recombineering 43

2.2.6. Preparing stocks of HIV bronchoalveolar lavage 51

2.2.7. Generating monocyte derived macrophages (MDM) 56

2.2.8. Infecting MDM with HIV-1 and *Mtb* 57
2.2.9. MDM cytokine measurement by Luminex 59
2.2.10. Analysis of HIV p24 from supernatant using a custom made Luminex assay 62
2.2.11. Analysis of HIV-1 replication in TZM-bl cells using *Mtb* conditioned media 64
2.2.12. Analysis of HIV-1 replication in M2 MDM co-incubated with *Mtb* conditioned media 64
2.2.13. Trans-well assay infection of MDM with *Mtb* WT and mutant strains to assess the impact of SNP on cytokine production and HIV-1 replication 65
2.2.14. Statistical analysis of cytokine and HIV-1 p24 production data 66

2.3. References 66

Chapter 3. Characterization of clinical and laboratory strains of Mtb to assess the effect of SNP in lipid metabolising genes on growth, lipid production and human macrophage infection phenotypes 68

3.1. Introduction 68
3.1.1. *Mtb* cell wall structural components and diversity 68
3.1.2. *Mtb* clinical isolates with mutations in lipid metabolism associated with HIV-1 positive directional selection 68
3.1.3. Impact of *Mtb* cell wall lipids on immune response to infection 69
3.1.4. *Mtb* clinical isolates selected to study in this thesis 71

3.2. Results 73
3.2.1. Characterising cording phenotypes of clinical strains cultured in the absence of Tween 80 73
3.2.2. Lipid characteristics of *Mtb* laboratory and clinical strains analysed by thin layer chromatography 76
3.2.3. Analysis of cytokine secretion by MDM infected with the different strains of *Mtb* 82
3.2.4. Host response to infection with *Mtb* laboratory strains is diverse 85
3.2.5. $MRC16^{P1939/A605}$ increases the secretion of cytokines compared to $EX30^{Q1939/A605}$ 87
3.2.6. $EU111^{N1759}$ and $EU40^{T1759}$ comparably induce the secretion of most cytokines measured in MDM 91

3.3. Discussion 95

3.4. Conclusion 98

3.5. References 98

3.6. Supplementary material 102

Chapter 4. Direct Mtb co-infection and cytokine bystander effects on HIV-1 replication dynamics to a panel of Mtb clinical isolates 110

4.1. Introduction 110

4.2. Results 111
4.2.1. Assessing regulation of HIV-1 replication by measuring LTR activity in TZM-bl cells 111
4.2.2. Impact of *Mtb*-induced cytokines on productive HIV-1 infection 124
4.2.3. Analysis of cytokines from M1 and M2 polarised MDM co-infected with HIV-1 and a panel of *Mtb* strains 128
4.2.4. Analysis of individual cytokine secretion by MDM co-infected with HIV-1 and the different strains of *Mtb* 130
4.2.5. Analysis of HIV-1 productive infection 139
4.2.6. Analysis of productive HIV-1 between M1 and M2 MDM ..... **Error! Bookmark not defined.**
4.2.7. Analysis of HIV-1 production in MDM co-infected with different strains of *Mtb* 139

4.3. Discussion 141

4.4. Conclusion 146

4.5. References 147

4.6. Supplementary material 152

Chapter 5. Genetic engineering of SNP in pks2 of Mycobacterium tuberculosis clinical and laboratory strains: reverting clinical strain SNP to wildtype and introducing clinical variant SNP into wildtype laboratory strain 161

5.1. Introduction 161

5.2. Results 163

5.2.1. Protein modelling to predict functional consequence of the two pks2 mutations in clinical strains. 163

5.2.2. Recombineering of *pks2* in EX30$^{Q1939/A605}$, MRC16$^{P1939/A605}$ and H37Rv$^{P1939/T605}$ 165

5.2.3. Mutation confirmation: SNP-1817 is more amenable to change than SNP-5817 173

5.2.4. Analysis of wild-type and mutant *Mtb* strain lipid profiles by TLC 176

5.3. Discussion 178

5.4. Conclusion 181

Supplementary Figure 5.1. thin layer chromatography analysis of lipids from different strains of *Mtb* 181

5.5. References 182

Chapter 6. Linking Mtb pks2 genotype to cytokine and HIV-1 phenotype in co-infected human macrophages 184

6.1. Introduction 184

6.2. Results **185**

6.2.1. Trans-well assay set-up to monitor direct co-infection and bystander effects of *Mtb* infection on HIV-1 production. 185

6.2.2. Trans-well baseline parameters: HIV-1 migration is similar between the top and the bottom chamber 186

6.2.3. Cytokine secretion is influenced differently between top and bottom chamber 190

6.2.4. Analysis of p24 secretion in MDM co-infected with different strains of *Mtb* in the presence of HIV-1 co-infection 191

6.2.5. Analysis of cytokine secretion in MDM directly infected with *Mtb* in the presence of HIV-1 co-infection 196

6.2.6. HIV-1 production correlated with cytokine secretion 201

6.3. Discussion **204**

6.4. Conclusion **210**

6.5. References **210**

6.6. Supplementary material 214

Chapter 7. Discussion 221

7.1. Background and rationale for the study 221

7.2. Different *Mtb* strains with SNP in lipid metabolising genes have altered cell wall lipid profiles, and cording phenotypes 222

7.3. Diverse *Mtb* strains with cell wall lipid differences differentially induce cytokines in mono-infected and HIV-1 co-infected MDM 225

7.3.1. Phylogenetically close *Mtb* strains with different SNP in lipid metabolising genes differentially induce the secretion of cytokines implicated in HIV-1 infection 226

7.4. *Mtb*-induced soluble factors induce the transcription of HIV-1 LTR but do not increase active HIV-1 productive infection 228

7.4.1. *Mtb*-induced soluble factors increase HIV-1 infection and replication into TZM-bl cells 229

7.4.2. HIV-1 productive infection in MDM was either decreased or unaffected in the presence of *Mtb*-induced soluble factors 231

7.5. HIV-1 production was not affected in MDM co-infected with different strains of *Mtb* despite elevated HIV-1 inducing cytokines 232

7.6. Engineering the *pks2* SNP in *Mtb* strains changed cytokine secretion in *Mtb* infected MDM 235

7.6.1. Genetically engineered *Mtb* strains modify HIV-1 productive infection compared to wildtype 237

7.6.2. Secretion of p24 correlates with donor inflammatory phenotype 238

7.7. Limitations of the study 241

7.7.1. *Mtb* culture 241

7.7.2. *In vitro* models of infection 242

7.7.3. Mutation and interpretation of results 242

7.8. Relevance of study in the field 243

7.9. Future research 246

7.10. Conclusions 247

7.11. References 248

Declaration

I, Mthawelanga Ndengane, hereby declare that the work on which this dissertation/thesis is based is my original work (except where acknowledgements indicate otherwise) and that neither the whole work nor any part of it has been, is being, or is to be submitted for another degree in this or any other university.

I empower the university to reproduce for research either the whole or any portion of the contents in any manner whatsoever.

Signature: M. Ndengane

Date: 11 – February – 2023

Dedications

This thesis is dedicated to the memory of my father the late, great Malwande "Greatman" Ndengane, my grandparents, Malungelo Ndengane, Nontsikelelo Shangase, Thamsanqa Joninga, Nozimasile Joninga and my uncle Solomzi Joninga. I will carry your courage, love, and support with me through life. You will always be in my heart.

To my family that is still with me in this life, this journey would never have been possible without every sacrifice you all have made along the way to ensure that as difficult as this journey has been, it is a little comfortable.

A special thank you to the following for their uncompromising support:
Prof. Nolutho Diko, Mrs Zukiswa Ndengane, Mr Nkosinathi Mgciza Mrs Nozibele Mgciza, Miss Sikelewa Joninga, Miss Thubakazi Ndengane, Mr Xhanti Mgciza, Mr Mzuvukile Joninga, Miss Yolani Ndengane, Liyabona Joninga, Anoyolo Joninga, Iminathi Ndengane and Onesisa Joninga

To my wife, Linamandla Ndengane, my rock, my point of sanity during insanity, no words could ever come close to explaining the gratitude I feel for the love and support you have afforded me through this period. The best I can say is thank you.

This work would not have been successful without the support of Prof. Robert J Wilkinson, you took a chance and had faith in me, you supported me through the years despite times when it seems we were not making progress, I give a special thanks to you. Dr Anastasia Koch, always insightful, calm, and understanding, I have given you lots of headaches, but always you were calm, supportive, and understanding, thank you. Dr Anna Coussens, I am lost for words when I think about how your vast insight, expertise and sternness have moulded me into the researcher I have become, thank you. A special thanks to Dr Nashied Peton, Dr Joanna Evans and Dr Apoorva Bhatt who have contributed to ensuring this work is completed. I reserve a thank you to colleagues in CIDRI-AFRICA, Robyn Waters, Rudranil Hazra, Raymond Moeketsi, Avuyonke Balfour and Muki Shey for their support. I would also like to acknowledge NRF and EU Pathco for funding.

List of figures

Figure 1.1. The life cycle of HIV-1. ..... **18**
Figure 1.2. The long terminal repeat (LTR) region of HIV-1. ..... **21**
Figure 1.3. A detailed structure of the Mtb cell wall. **25**
Figure 2.1. Generation of HIV-1 from PBMC of multiple donors. **52**
Figure 3.1. Phylogenetic analysis of strains used in this project. **72**
Figure 3.2. A schematic showing show the visualisation of Mtb strains under the widefield microscope. **74**
Figure 3.3. Gross phenotype of *Mtb* laboratory strains grown in absence of Tween 80. ..... **75**
Figure 3.4. Cording phenotype of *Mtb* clinical strains used in this project. **76**
Figure 3.5. Schematic of preparing *Mtb* clinical and laboratory strains for lipid analysis. **77**
Figure 3.6. TLC analysis of SL-1, TDM, GMM and DAT from the cell wall of clinical and laboratory strains. **78**
Figure 3.7. Analysis of PDIM in the cell wall of clinical and laboratory strains of Mtb. **79**
Figure 3.8. TLC analysis of free fatty acids and mycolic acids from clinical and laboratory strains. **80**
Figure 3.9. TLC analysis of AC2PMI6, AC2PMI2 and phospholipid a of clinical and laboratory strains. **82**
Figure 3.10. Experimental flow of MDM infection with Mtb and analysis of cytokines from the SN. **83**
Figure 3.11. Principal component analysis showing multiple variables contributing to variation in cytokine production by MDM infected with a panel of Mtb strains. **85**
Figure 4.1. A schematic that shows the flow of how TZM-bl cells were used as a model for HIV-1 replication in the presence of *Mtb* induced SN. **112**
Figure 4.2. Analysis of LTR activity in TZM-bl cells infected with HIV-1 pre and post incubation with SN harvested from uninfected MDM or media only. **114**
Figure 4.3. Analysis of TZM-bl cells infection with HIV-1 pre incubation with harvested 24-hours post-infection from MDM infected with from MDM infected with laboratory strains. **117**
Figure 4.4. Analysis of TZM-bl cells infection with HIV-1 pre-incubation with SN harvested 96-hours post-infection from MDM infected with clinical and laboratory strains. **119**
Figure 4.5. Analysis of HIV-1 LTR activity in TZM-bl cells incubated with SN harvested 24-hours post-infection of MDM infected with clinical and laboratory strains. **122**
Figure 4.6. Analysis of HIV-1 LTR activity in TZM-bl cells incubated with SN harvested 96-hours post-infection of MDM infected with clinical and laboratory strains. **124**
Figure 4.7. A schematic that shows the flow of incubating HIV-1 infected M2 MDM with SN harvested from *Mtb* infected MDM and analysis of secreted p24 antigen. **125**
Figure 4.8. Secretion of HIV-1 p24 by MDM incubated with laboratory strain induced SN. **128**

Figure 4.9. A simple schematic that shows the flow of the co-infection experiments performed and analysis of SN with Luminex assay. 128
Figure 4.10. Principal component analysis of cytokine secretion 96 hours after HIV *Mtb* co-infection. Dates stratified by (A) MDM phenotype, (B) donor and (C) HIV-1 co-infected *Mtb* strain. ... 130
Figure 4.11. HIV-1 production by M1 and M2 polarised MDM harvested 96-hours post-co-infection. ..... Error! Bookmark not defined.
Figure 4.12. HIV-1 production from MDM co-infected with different clinical and laboratory strains. 140
Figure 5.1. Simplified schematic of recombineering. 162
Figure 5.2. A computer-generated model of pks2 protein from Mycobacterium tuberculosis showing proline in position 1939. 164
Figure 5.3. A computer-generated model of pks2 protein from Mycobacterium tuberculosis showing threonine in position 605. 165
Figure 5.4. Agarose gel of APH(3') gene amplified from a colony of EX30$^{Q1939/A605}$:pNIT. 167
Figure 5.5. Schematic of protein analysis in Mtb strains following induction with IVN. 168
Figure 5.6. SDS-PAGE of gp61 protein induced in EX30$^{Q1939/A605}$::pNIT using IVN. 169
Figure 5.7. Average CFU following electroporation in the presence of ssDNA and/or pOLYG to change two SNP in pks2. 173
Figure 5.8. Sanger sequencing data representation of base modification at amino acid position 605. 174
Figure 5.9. Thin layer chromatography analysis of apolar cell wall lipids from Mtb WT and mutant strains. 177
Figure 5.10. Thin layer chromatography analysis of apolar cell wall lipids from Mtb WT and mutant strains. 182
Figure 6.1. Schematic trans-well plate infectin conditions used to assess the impact of *Mtb* strains on HIV-1 replication in co-infected and bystander cells. 186
Figure 6.2. Secretion of p24 by MDM infected with HIV-1. 189
Figure 6.3. Secretion of p24 by MDM infected with HIV-1 and a panel of *Mtb* strains and p24 from bystander cells exposed to HIV-1/*Mtb* co-infection environment. 193
Figure 6.4. Secretion of p24 by MDM infected with HIV-1 or bystander cells exposed to HIV-1/*Mtb* co-infection environment. 195
Figure 6.5. PCA analysis showing differences in cytokines production by MDM seeded in the top chamber and the bottom chamber of a trans-well plate. 197
Figure 6.6. A correlation plot for the association of cytokine secretion and the production of HIV-1 in MDM. 203
Figure 6.7. A correlation plot for the association of cytokine secretion and the production of HIV-1 in MDM. 203

List of tables

Table 2.1 List of the reagents and chemicals that were used in the project 37
Table 2.2 List of the equipment that were used in the project..... 39
Table 2.3. Laboratory-adapted and clinical Mtb strains used in the project..... 41
Table 2.4. SNP details of the Mtb strains that were used for recombineering 44
Table 2.5. Single-stranded DNA substrates designed and used to insert SNP in clinical and laboratory *Mtb* strains. 44
Table 2.6. Plasmids used for electroporation of the Mtb strains 45
Table 2.7. Experimental and control conditions of electroporation in the presence of pNIT and pOLYG 46
Table 2.8. Details of the PCR master mix using the Roche FastStart Taq kit..... 47
Table 2.9. Details of PCR conditions used in the project 48
Table 2.10. Recipe for making SDS-PAGE gels for protein analysis 48
Table 2.11. Electroporation conditions of the strains with pNIT to transform them with ssDNA substrates..... 49
Table 2.12. Plating conditions used strains following electroporation to insert ssDNA and pOLYG 50
Table 2.13. Primers used for colony PCR and sequencing..... 51
Table 2.14. Plates used for incubating CD14+ cells stimulated with M-CSF and GM-CSF 57
Table 2.15. The analytes measured and respective bead regions for 25-plex Luminex (Thermofiischer) 61
Table 2.16. The analytes measured and respective bead regions for 13-plex Luminex..... 62
Table 3.1. The resulting amino acid change by the SNP identified to be under HIV-1 selective pressure in the clinical isolate and its phylogenetically close paired strain. 73
Table 3.2. Comparison of cytokines secreted 24 hours and 96 hours post-infection of MDM with the laboratory strains..... 86
Table 3.3. Comparison of cytokines secreted by EX30$^{Q1939/A605}$ and MRC16$^{P1939/A605}$ infected MDM 89
Table 3.4. Comparison of cytokines secreted by *EU111*^{N1759} and EU40^{T1759} infected MDM..... 93
Table 4.1. Comparison of cytokine secretion induced by the laboratory strains in HIV-1 co-infected MDM 24-hours and 96-hours 131
Table 4.2. Comparison of cytokines secretion induced by Mtb EX30$^{Q1939/A605}$ and MRC16$^{P1939/A605}$ in HIV-1 co-infected MDM 133
Table 4.3. Comparison of cytokine secretion induced by *EU111*^{N1759} and EU40^{T1759} in HIV-1 co-infected MDM 137
Table 5.1. Colony counts of Mtb strains electroporated following electroporation to insert pNIT plasmid..... 166
Table 5.2. Colony counts of Mtb strains electroporated following electroporation to insert pNIT plasmid..... 170
Table 5.3. The rate of positive mutants in the number of screened colonies for the Mtb strains..... 175

Table 5.4. The combination of wildtype and their mutant strains that were successfully created with genetic engineering. 176
Table 6.1. Analysis of HIV-1 p24 production by MDM in the trans-well plate..... 188
Table 6.2. The comparison of cytokine secretion between the top and the bottom chamber of trans-well infected with HIV-1..... 191
Table 6.3. Comparison of cytokines secreted in HIV-1 infected bystander MDM exposed to cytokines from HIV-1/H37RvP1939/T605 or HIV-1/H37Rv$^{P1939/T605A}$ 199
Table 6.4. Cytokines secreted by MDM co-infected with HIV-1/MRC16$^{P1939/A605}$ or HIV-1/MRC16$^{P1939/A605T}$ 201
Table 6.5. Analysis of the source of variation in HIV-1 production using a Two-way Anova 202

List of abbreviations

Abbreviation	
1-Ethyl-3-(3-dimethylaminopropyl) carbodiimide	EDC
Acquired immunodeficiency syndrome	AIDS
Activator protein 1	AP-1
Active TB	aTB
Albumin dextrose catalase	ADC
Alveolar macrophages	AM
Aminoglycoside-3'-phosphotransferase	aph3’
Antiretroviral therapy	ART
Biosafety cabinet	BSC
Bone marrow derived macrophages	BMDM
Carbon dioxide	CO2
CCAAT/ Enhancer Binding Protein	C/EBP
Colony-forming units	CFU
Complementary DNA	cDNA
Degrees Celsius	°C
Dendritic cells	DC
Dimethyl sulfoxide	DMSO
Dulbecco's Modified Eagle Medium	DMEM
Fetal bovine serum	FBS
Gut-associated lymphoid tissue	GALT
Highly active antiretroviral therapy	HAART
Hour	h
human AB serum	hAB
Human immunodeficiency virus 1	HIV-1
Human transcriptional factors	hTF
Hygromycin	Hyg
Interleukin	IL
Isovaleronitrile	IVN
Kanamycin	Kan
Kilovolts	kV

Liquid nitrogen	LN2
Long terminal repeat	LTR
Luria-Bertani	LB
Lymph nodes	LN
Microlitres	mL
Milligrams	mg
Milliliter	mL
Millimolar	mM
Monocyte derived macrophages	MDM
Mycobacterium tuberculosis	*Mtb*
***Mycobacterium tuberculosis* complex**	MTBC
N-hydroxysulfosuccinimide	NHS
Nanograms	ng
Nuclear factor kappa B	NF-kB
Nuclear factor of activated T cells 5	NFAT5
Oleic albumin dextrose catalase	OADC
Optical Density	OD
Pathogen associated molecular patterns	PAMP
Pattern recognition receptor	PRR
Percent	%
Peripheral blood mononuclear cells	PBMC
Phosphate buffered saline	PBS
Phthioceranic/hydroxyphthioceranic acid synthase 2	Pks2
Polymerase chain reaction	PCR
Principal component analysis	PCA
Regions of difference	RD
Revolutions per minute	Rpm
Ribose nucleic acid	RNA
Roswell Park Memorial Institute 1640 Medium	RPMI
Single nucleotide polymorphism	SNP
Single-stranded DNA	ssDNA
Sodium dodecyl sulphate	SDS
Specificity protein 1	SP-1

Supernatant	SN
Tb-specific deletion 1	TbD1
Thin layer chromatography	TLC
Toll-like receptor	TLR
Tuberculosis	TB
Whole-genome sequencing	WGS
Wild type	WT
World health organization	WHO
Room temperature	RT
Endosomal Sorting Complexes Required for Transport	ESCRT

Chapter 1. *Mycobacterium tuberculosis* and human immunodeficiency virus 1 synergistically worsen each other's disease outcome

1.1. The TB HIV-1 syndemic

There were 5.8 million newly infected people with *Mycobacterium tuberculosis* (*Mtb*), the causative agent of tuberculosis (TB), in 2020 according to the World Health Organization (WHO) estimates [1]. The human immunodifociency virus type-1 (HIV-1), the etiological agent of acquired immunodeficiency syndrome (AIDS), is estimated to have newly infected 1.5 million people [2]. The WHO notes that both HIV-1 and TB worsen the outcomes of each disease, with HIV-1 increasing the chances of an individual infected with *Mtb* developing active TB disease by between 16 to 27 times (WHO, 2020), whilst TB was associated with 214,000 deaths in HIV-1 infected people were due to TB in 2020 [1]. This thesis will investigate how *Mtb* co-infection may contribute to exacerbating HIV-1 infection by assessing the impact of *Mtb* clinical strain diversity and more specifically their cell wall lipid composition on the immune environment in monocyte derived macrophages (MDM) and how these changes may affect HIV-1 replication and productive infection. This literature review will give a brief background on the epidemiology of HIV-1-TB disease, the lifecycle of HIV-1 infection, the diversity of *Mtb*, and the mechanisms of *Mtb*-influenced HIV-1 infection and replication.

The HIV-1/AIDS pandemic remains a major concern, despite antiretroviral therapy (ART) having drastically reduced global AIDS-related deaths [3]. Studies have found that HIV-1 infection is a major risk factor for *Mtb* infection and reinfection despite ART treatment and that HIV-1 infected people in high TB burden settings are five times more likely to get TB compared to HIV-1 uninfected community members [4, 5]. This is despite HIV-1 infected study participants being on ART for over five years and having $CD4^+$ T cell counts of over 700 cells/ mL [4]. A modelled study from Cape Town showed that TB notification rates were significantly higher in the HIV-1 infected population with notifications increasing from when people reached about 20 years and remaining high throughout their lifetime [6]. Much has been done to investigate the epidemiology of HIV-1/*Mtb* co-infection, revealing important information about how the disease spreads within communities and what the major risk factors for infection are known [7-9]. Moreover, many studies have attempted to investigate how HIV-

1 influences TB disease on an immunological level, so as to understand why HIV-1 co-infection increases TB disease progression risk. However, *Mtb* co-infection is likely to precede *Mtb* infection in high burden settings, studies have shown high levels of non-HIV-1 associated TB cases compared to HIV-1 associated TB cases [10], and about half of HIV-1 uninfected youths had latent TB in a high TB burden setting [5], suggesting that HIV-1 infection likely comes second. It is important to understand the impact of *Mtb* infection on HIV-1 replication, particularly given that *Mtb* infection increases the susceptibility of host cells to HIV-1 co-infection [11], and that HIV-1 replication is increased locally at the sites with *Mtb* co-infection [12] and systemically in HIV-1/*Mtb* co-infected patients [13]. In the mid-90s, Nakata *et al.,* (1997) [14], showed HIV-1 RNA load was significantly increased in BAL of patients co-infected with *Mtb* compared to RNA load in BAL of patients who were only infected with HIV-1 [14]. Importantly, the authors also compared samples in radiologically involved versus radiologically uninvolved lung segments from the same patients, and they reported a 10-fold increase in HIV-1 replication from the involved lung segment compared to the uninvolved lung segment [14]. These data point to the stimulus for HIV-1 replication being local.

1.2. The life cycle of HIV-1 infection

1.2.1. Invasion and viral tropism

Transmission of HIV-1 occurs through the transfer of viral particles by infected bodily fluids, such as seminal and vaginal fluids; blood, contact between broken skin and wounds; intravenous drug use and mother to child transmission [15]. HIV-1 crosses the physical barrier of the epithelial lining and preferentially infects mucosal membranes, including genital and rectal tissues [14]. For successful invasion, HIV-1 particles cross the epithelial barrier by a process called transcytosis [16], trojan-horsing resident mucosa Langerhan's cells [17], and dendritic cells (DC) [18] or direct disruption of mucosal membrane integrity by HIV-1 envelope glycoprotein 120 (Gp120) [19]. To facilitate cellular entry, the HIV-1 gp120 envelope protein binds with high affinity to host CD4 and the interaction facilitates the recruitment of co-receptors CCR5 and CXCR4 to enable viral entry (Fig. 1.1) [24]. CD4, CCR5 and CXCR4 engagement is a critical step to HIV-1 entry because viral entry can be inhibited or modified by co-receptor mutation or the use of co-receptor inhibitors [25, 26].

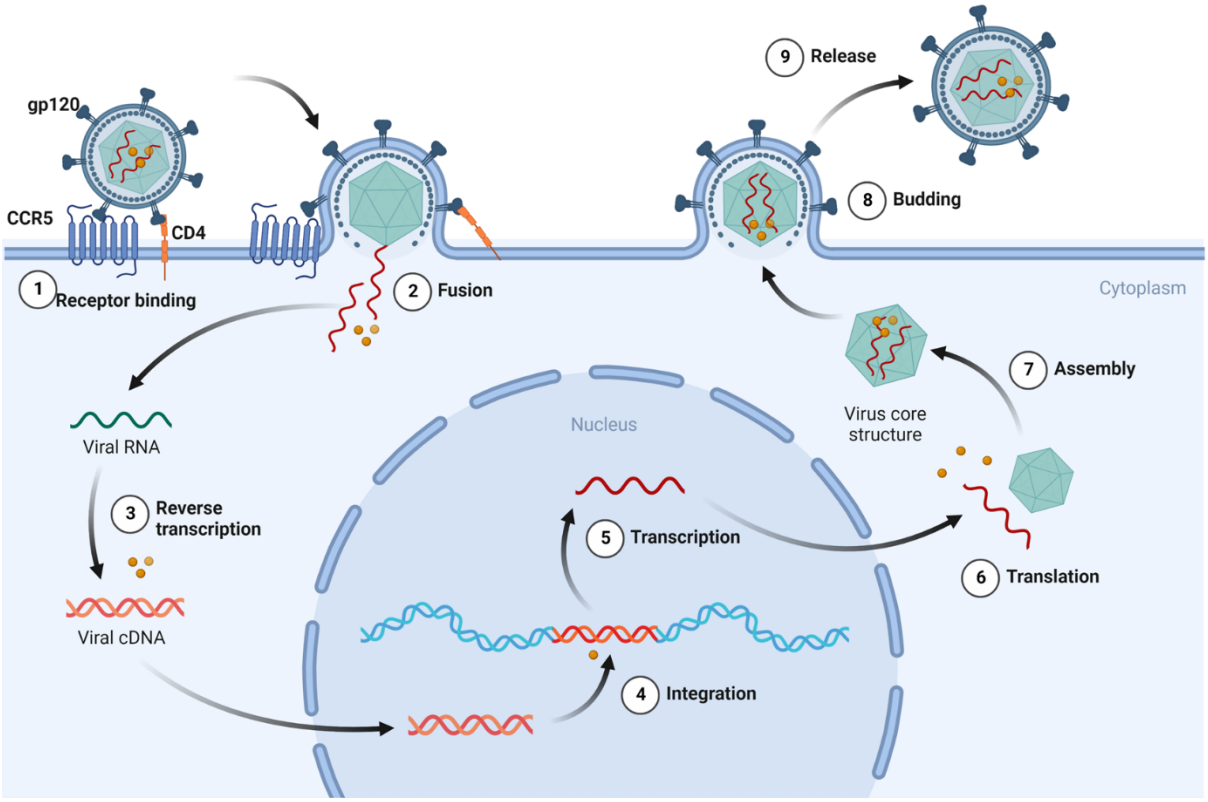

Figure 1.1. The life cycle of HIV-1.
Step 1: To facilitate entry into host cells, the HIV-1 gp120 protein binds with high affinity to CD4 receptor, which leads to the recruitment of CCR5 co-receptor. 2: Viral protein-human receptor interaction facilitates membrane fusion and viral entry which is followed by the infection of the viral genome and accessory proteins into the host cells cytoplasm. 3: Viral single stranded RNA is reverse transcribed into a double stranded complimentary cDNA. 4: The viral cDNA translocates to the nucleus, where it is integrated into the host genome.5, 6 and 7: Transcription, translation and assembly of viral RNA and proteins uses host cellular machinery and energy. 8 – 9: The viral progeny buds off the cells and new mature virions are released from the cells. Image creatred with Biorender.com.

HIV-1 particles that make it through the primary barrier infect frontline mucosal resident $CD4^+$, $CCR5^+$ and $CXCR4^+$ T lymphocytes, tissue macrophages and DC [20]. The majority of HIV-1 particles are produced by activated $CD4^+$ T cells *in vivo*, and *in vitro* studies have shown increased permissiveness of $CD4^+$ T cells to HIV-1 infection due to surface expression of CD4 and CCR5 [21]. However, other $CD4^+$, $CCR5^+$ and $CXCR4^+$ cells can also be infected by HIV-1, including tissue macrophages and DC [21].

HIV-1 strains are classified according to the co-receptor used during infection: strains that use CCR5 as a co-receptor are R5-tropic, and strains that use CXCR4 are called X4-tropic. Dual-tropic R5/X4 strains which use either CCR5 or CXCR4 co-receptor are also found [22]. For unknown reasons, in most cases, infection founders are R5 strains, despite evidence that all HIV-1 strains are present in semen, blood, cervicovaginal and rectal secretions [23]. X4 strains

only seem to be selected for in the later stages of the disease and are associated with a rapid loss of CD4+ T cells and accelerated progression to AIDS [23].

1.3. Cellular entry and genome integration

Following initial HIV-1 gp120 host cell receptor engagement, the HIV-1 viral capsid fuses with the host cell membrane through the HIV-1 gp41 protein, allowing the HIV-1 genetic material to be injected into the cytoplasm of the host cell (Fig. 1.1) [27, 28]. The HIV-1 genome is composed of a single-stranded RNA which is converted to a double-stranded complementary DNA (cDNA) by HIV-1 reverse transcriptase enzyme, shortly following viral entry [29]. The double-stranded cDNA translocates to the nucleus, where a HIV-1 integrase enzyme facilitates the nicking of the host DNA and integration of the cDNA into the host genome (Fig. 1.1) [29]. Since the viral DNA is integrated into the host genome, viral DNA replicates along with cellular DNA during cycles of cell division, as with any cellular gene [29]. The provirus serves as a template for the production of viral proteins and progeny virions (Fig. 1.1) [29]. This is how HIV-1 establishes a permanent viral reservoir within host cells and is thus carried throughout the body.

1.3.1. HIV-1 systemic infection and reservoir formation

HIV-1 viral reservoir cells are highly stable and long-lived [30] and it is thought the most abundant source is a subset of resting $CD4^+$ T cells [31]. Abrahams and colleagues (2019) [32] showed that most reservoirs cells were from resting, long-lived ($CD25^{low}$, $CD69^-$, and $HLA\text{-}DR^-$) $CD4^+$ T cells, and that this subset of cells could still produce replication competent viruses despite being from patients who were on ART for average of five years.

Viral reservoirs are also established in organs [33]. The lungs are very active immunological effector sites that are constantly exposed to viral and bacterial airborne pathogens and represent potential HIV-1 lymphoid reservoir [34]. The lungs have features that render them ideal as havens for HIV-1 persistence, HIV-1 has been isolated from lung cell-free BAL fluid, $CD4^+$ T cells and alveolar macrophages of untreated patients [14, 35] and HIV-1 DNA and RNA have been isolated from alveolar macrophages (AM) of patients receiving ART [36]. Also, the presence of millions of alveoli that are close together spatially increases the chance of cell-to-cell viral spread [35]. AM which are abundant in the lung spaces provide an ideal niche for persistent HIV-1 due to their resistance to HIV-1-induced apoptosis [37]. Given that the lungs

are also the primary site of *Mtb* infection, the lungs present an important site for HIV-1 and *Mtb* interaction.

The gut-associated lymphoid tissue (GALT) contains significant numbers of $CD4^+$ $CCR5^+$ T cells and counts as one of the major sites for early HIV-1 infection [38]. The GALT becomes a factory for virus production and ultimately systemic infection of secondary lymphoid tissue sites [38], like the lymph nodes (LN), which are a major source of replication-competent HIV-1 even in virally suppressed patients [33]. The LN immune complexes shield HIV-1, permitting replication, production, and storage of viral particles [39]. HIV-1 is carried to the LN by DC which accumulates in the LN and viruses can be transported by central memory T cells which are selectively retained in the lymph nodes due to their homing receptor expression [33]. Given that both DC and T cell types are infected by HIV-1, this provides a mechanism by which viral reservoirs can be established in the LN. Other lymphoid organs such as the spleen, thymus and bone marrow have also been implicated as potential HIV-1 reservoirs [40]. Bone marrow, as a secondary lymphoid organ and site of haematopoiesis, contains progenitor cells that are not only long-lived but divide and thus can act as replicating points, producing progeny with integrated HIV-1-DNA [41]. In ART-naïve individuals, HIV-1 has been identified in bone marrow in $CD133^+$ haematopoetic stem cells, mesenchymal stem cells, macrophages, and memory $CD4^+$ T cells [41]. Some of these sites are identified as sites for extrapulmonary TB and provide important niches for the interaction of *Mtb* and HIV-1.

1.3.2. HIV-1 replication

The central transcriptional regulatory element in HIV-1 is a 5' gene promoter called the long terminal repeat (LTR) [42]. The promoter, enhancer, and modulatory elements of LTR are activated by a plethora of human transcriptional factors (hTFs) (Fig. 1.2), which activate, repress, or act as adapter proteins for LTR leading to the upregulation of HIV-1 transcription [43-44] Important and well-documented hTFs involved in HIV-1 transcription include nuclear factor kappa-light-chain-enhancer of activated B cells (NF-kB), activator protein 1 (AP-1) [45], specificity protein 1 (SP1) [46], nuclear factor of activated T cells 5 (NFAT5) [47]. A lack of HIV-1 activating hTFs has been reported as one of the bottlenecks to HIV-1 replication [44]. Although replication of HIV-1 genes is predominantly regulated by hTFs, HIV-1 accessory proteins such as Vpr and other putative elements have been reported to influence transcription [48].

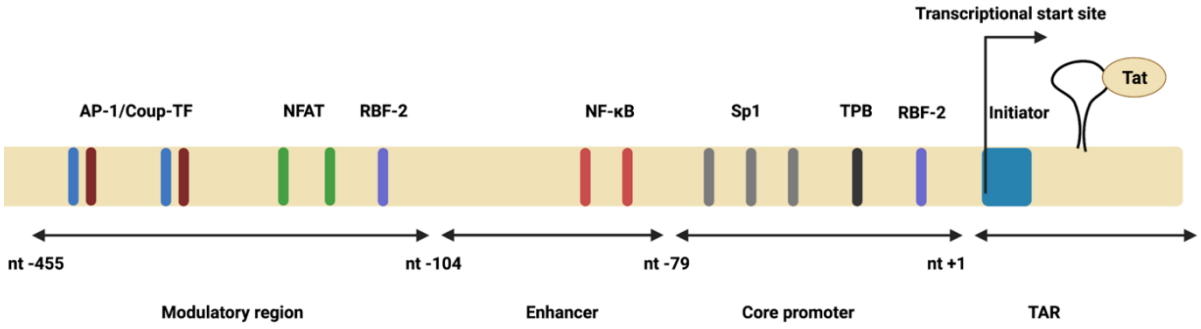

Figure 1.2. The long terminal repeat (LTR) region of HIV-1.
The HIV-1 LTR is a promoter of HIV-1 transcription. The LTR contains four regions: the modulatory region, the enhancer, the core promoter, and the transactivation responsive (TAR) element region. Human transcriptional factors bind to the first three regions and regulate HIV-1 transcription. Activator protein 1 (AP-1), COUP Transcription Factor 1 (COUP-TF), nuclear factor of activated T cells 5 (NFAT5) and Retinoblastoma-family protein 2 (RBF2) bind the modulatory region. include nuclear factor kappa-light-chain-enhancer of activated B cells (NF-kB) binds to the enhancer region. The core region binds, specificity protein 1 (Sp-1), TATA-binding protein (TPB) and RBF-2. The TAR region contains a hair pin structure that binds the HIV-1 encoded Tat protein, capable of initiating transcription independent of human transcriptional factors. Image created with Biorender.com (Adapted from Roebuck and Saifuddin, 1999) [45].

NF-kB plays an important role in early HIV-1 transcription in activated CD4+ T cells and the initial interaction of NF-kB with the HIV-1 LTR stimulates the generation of several full-length transcripts of HIV-1, permitting the transcription of HIV-1 Tat [44]. Tat recognizes the transactivation responsive element region (TAR) in the primary transcript, triggering a cascade of events including the phosphorylation of RNA polymerase II and subsequently increasing HIV-1 transcriptional efficiency [43]. The successful packaging of viral components into a mature virion and budding out of infected cells is a crucial part of the infectious cycle [49]. The packing of the HIV-1 components occurs in the cytoplasm, where two copies of the RNA genomic material, tRNA, cDNA synthesis priming molecules, viral envelope proteins, Gag polyprotein and the viral enzymes reverse transcriptase, integrase and protease are packaged to make a mature HIV-1 virion [49].

HIV-1 escapes the intracellular environment through usurping the endosomal sorting complexes required for transport (ESCRT) machinery [50]. The ESCRT machinery is responsible for the trafficking of ubiquitylated multivesicular bodies from the endosome to the lysosome [51] as well as mediating a diverse array of membrane remodelling activities [52]. Membrane fission during cytokinesis is facilitated by a coordinated recruitment of ESCRT-II proteins by ESCRT-1. ESCRT-II in turn recruits ESCRT-III proteins complex member CHMP6, CHMP2/4 resulting in membrane fission [53]. HIV-1 achieves budding by active recruitment of host ESCRT-I and ESCORT-III complexes respectively via Gag p6 protein [54,

55]. Recently, it was elucidated that budding of HIV-1 is enhanced by monocyte chemoattractant protein 1 (MCP1 also referred to as CCL2) [56]. The authors showed a CCL2 dependent recruitment of ALIX (an ESCRT-III accessory protein) and HIV-1 production [56]. The study also showed that the absence of CCL2 improves ALIX solubility and enhanced binding to Gag p6 and thus increased HIV-1 release. However, conversely, there was decreased HIV-1 released from cells when treated with an anti-CCL2 antibody [56], demonstrating a complex role of CCL2 in regulating the amount of virus released.

1.4. Genomic diversity with *Mtb* populations influences TB pathogenesis

While early genetic comparison of *Mtb* strains suggested that given the MTBC was genetically monomorphic, 20th century studies showed differences in virulence capacities between strains. For example, a study conducted on guinea pigs in the 1960s found that clinical strains from India exhibited lower virulence compared to strains from the UK [57]. As genomic typing and WGS of *Mtb* became more sophisticated, greater genetic diversity was observed between strains [58]. With that, studies also began to show differences in virulence phenotypes between strains. For example, Tsenova *et al*., (2005) [59], showed that HN878, a laboratory adapted lineage 2 (L2) strain, has a consistent hypervirulent phenotype in mice and rabbits compared to lineage 4 (L4) CDC1551 [59].

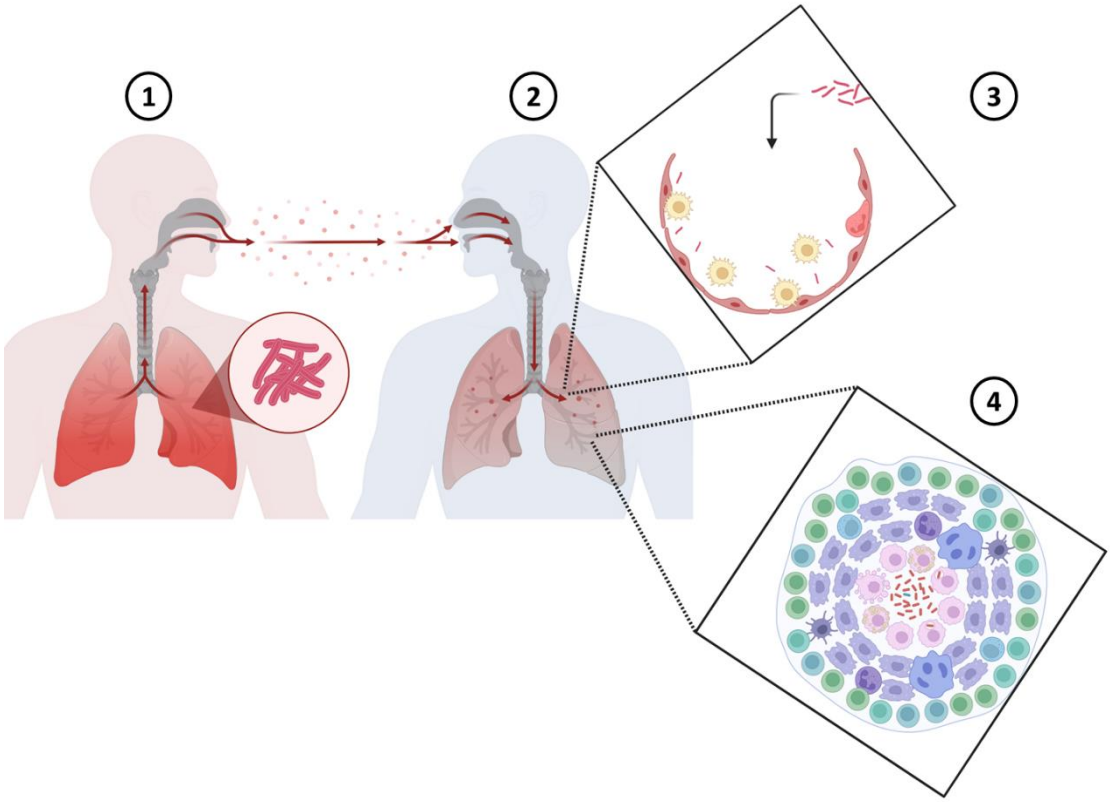

Figure 1.3. The infectious lifecycle of *Mtb*.
(1) *Mtb* infected person releases *Mtb* through droplets by either tidal breathing or coughing [93], (2) the droplets are inhaled from the air by uninfected person, (3) *Mtb* makes to the alveolar space and infects alveolar macrophages, (4) *Mtb* infection results in a granuloma, an organised structure containing an abundance of cells including macrophages, multinucleated giant cells, epithelioid cells and surrounded by a rim of lymphocytes [91]. Figure created using biorender.

One of the important determinants of disease outcome is the interaction of pathogen-associated molecular patterns (PAMPs) with host pattern recognition receptors (PRRs) during infection [60]. The association of PRRs and PAMPs controls cytokine production, expression of co-stimulatory molecules, as well as antigen presentation [61]. It is recognized in the literature that the immune response phenotype can be altered by the concentration of PAMPs and the manner of PRR activation [61]. These studies' data suggest that the diversity of PAMPs in *Mtb* strains might inevitably lead to strain-specific immune modulation. Carmona et al., (2013) [60], showed that two strains of HN878 preferentially engaged Toll-like receptor 4 (TLR4) and Toll-like receptor 2 (TLR2), respectively, in mice bone marrow derived macrophages, which resulted in significant differences in cytokine induction by these strains [60]. Interestingly, variation in the induction of pro-inflammatory molecules have also been observed between strains that engage the same receptor [60]. These differences in receptor usage as well as differential recognition by the same receptor could influence disease outcomes, including the

production of pro- and anti-inflammatory cytokines and chemokines as well as anti-microbial molecules [60].

1.4.1. *Mtb* has highly diverse and bioactive lipids that influence the phenotype of immune response to infection

Mtb contains an abundance of diverse, bioactive, and surface-exposed lipids that form the first point of contact with host receptors [62-64]. The diversity of lipids in *Mtb* is one of the most studied aspects of *Mtb* pathobiology and may be an important component of infection phenotype. *Mtb* lipids are found in a complex multi-layered cell wall composed of a capsule, located in the outermost layer, a cell wall core, and a conventional plasma membrane (Fig. 1.3) [65]. The cell wall core of *Mtb* is composed of, amongst other entities, a layer of free, non-covalently attached lipids and glycolipids [65]. Glycolipids including trehalose monomycolates (TMM), trehalose dimycolates (TDM), glycerol monomycolates, glucose monomycolates, phthiocerol dimycocerosates (PDIM), poly-acylated threaloses (PAT), sulfolipids (SL), phosphatidylinositol mannosides (PIM), phenolic glycolipids (PGL) and mannose-capped lipoarabinomannans (Man-LAM) are some of the best-described *Mtb* virulence factors [65].

Lipids play a critical role in cellular entry and phagocytosis mechanisms, modulation of phagosome maturation, granuloma biogenesis [65] and modulation of the immune response [67, 68]. Variation in infection is affected by *Mtb* lipids. For example, an *in vitro* study found that a collection of L2 clinical strains were defective in uptake by monocyte derived macrophages (MDM) compared to Erdman [68]. The authors report that the L2 strains had highly branched and truncated surface Man-LAM which hindered receptor engagement and thus could not be phagocytosed [68].

The phagocytosis of *Mtb* by immune cells, including macrophages and DC [69], is meant to enable elimination of *Mtb*, however, the bacteria have evolved strategies that permit evasion of eradication by these cells [69]. Furthermore, Cambier *et al.* (2014) [70], noted that *Mtb* favours the recruitment of macrophages that are permissive to its survival while evading microbicidal macrophages [70]. These authors showed that mice infected with an isogenic H37Rv strain, lacking the machinery to recruit PDIM to the surface, resulted in a greater proportion of iNOS-producing monocytes recruited to the lungs compared to lungs of mice

infected with wildtype H37Rv [70]. Furthermore, Blanc *et al.* (2017) [71], found that a tetraacylated sulfoglycolipid (Ac4SGL) on the surface of *Mtb* inhibited TLR2 activation by acting as a competitive inhibitor of natural *Mtb* TLR2 antagonists. They showed in THP-1 cells, a human monocytic cell line, that Ac4SGL could inhibit activation of Nf-kB in a dose-dependent manner [71]. These studies suggest that cell surface-exposed lipids of pathogenic mycobacteria interact with host cell receptors and can manipulate the subsequent immune response.

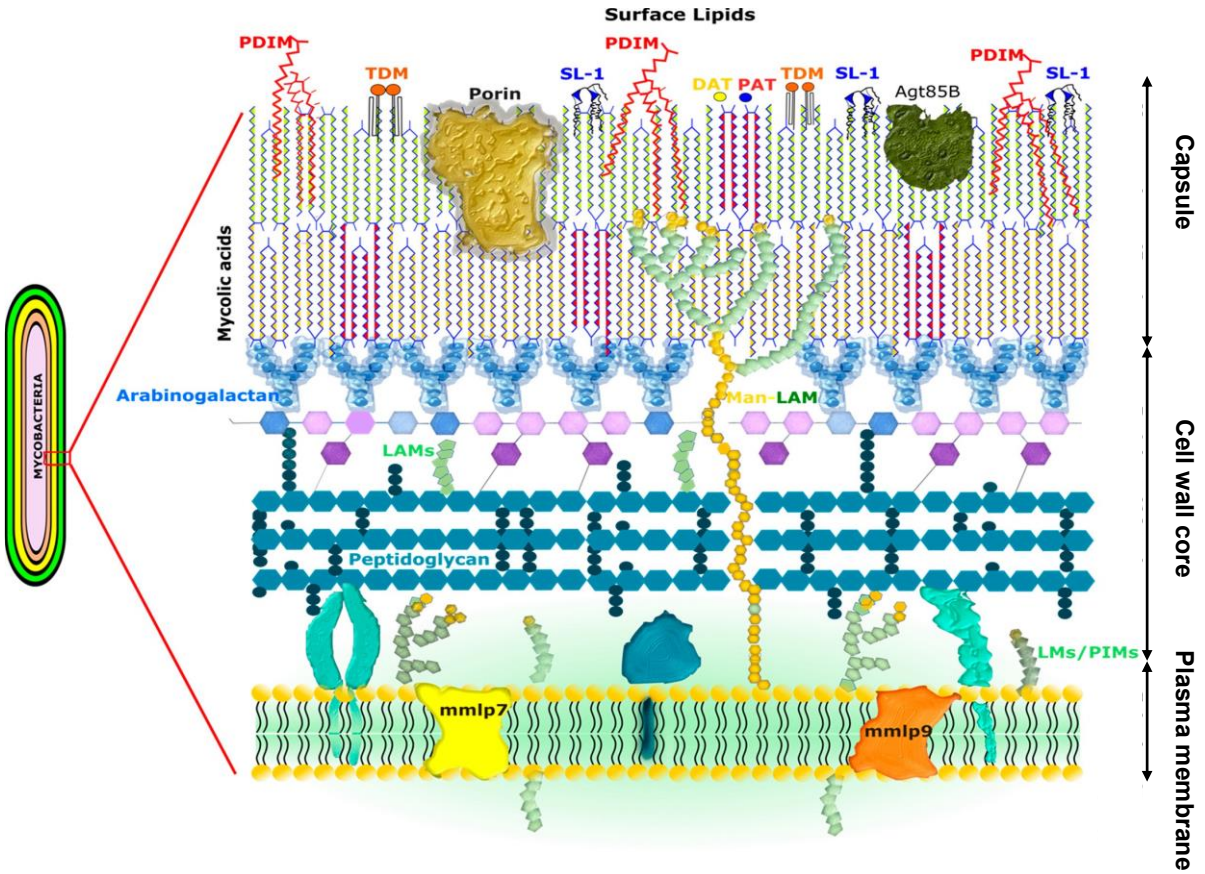

Figure 1.4. A detailed structure of the *Mtb* cell wall.
The *Mtb* cell wall is composed of the inner plasma membrane, the cell wall core, and the capsule. The outer capsule of *Mtb* contains surface exposed lipids, Phthiocerol dimycocerosates (PDIM), Trehalose 6,6'-dimycolate (TDM), Sulfolipid-1 (SL-), Diacyltrehaloses (DAT), poly-acylated threalоses (PAT) which form the first point contact with host cell receptors during infection and are the most studied virulence factors of *Mtb.* The cell wall core contains, Lipoarabinomannan (LAM) and Mannose-capped Lipoarabinomannan (Man-LAM). The plamsa membrane harbours, Mycobacterial membrane protein Large 7 (MmpL7), Mycobacterial membrane protein Large 9 (MmpL9), phosphatidylinositol mono-mannosides (PIMs) and Lipomannan (LM). Figure taken from Modak *et al.,* (2022) [66].

Cytokines and chemokines play a key role in regulating inflammation during infection [72]. These molecules offer a channel of communication for immune cells to migrate to the site of infection and provide specific instructions to the immune cells about actions to be taken during

immunity [73]. A variety of *Mtb* lipids have been shown to either directly or indirectly be involved in inducing cytokines and chemokines. A study in 2020 showed that peripheral blood mononuclear cells (PBMC) stimulated with apolar lipids from wild-type (WT) *Mtb* Erdman strain significantly induced cytokine production relative to untreated PBMC, but a strain disrupted in a 13-gene operon *Mce*1 did not significantly induce cytokines compared to untreated PBMC [73]. The *Mce1* operon is involved in lipid transport across the membrane [74]. The authors note that the two strains are different by about 400 lipid species [75].

Other studies have shown that mice which were exposed to liposomes containing TDM via intratracheal instillation showed highly induced tumour necrosis factor (TNF) compared to mice treated with liposomes only [76]. Additionally, TDM was found to interact with membrane receptor C-type lectin (Mincle) resulting in increased production of TNF and macrophage inflammatory protein (MIP-2) [77]. Mice exposed to liposomes incorporating mycolic acids (MA) via intratracheal instillation produced a robust interleukin (IL)-6 and IL-12 response [76].

Mtb lipids have also been found to impede the production of cytokines. For example, Reed *et al.* (2004) [78], showed the presence of a PGL in HN878 significantly hampered cytokine production compared to H37Rv in murine bone marrow derived macrophages (BMDM) [78]. Furthermore, a HN878 deletion mutant of PGL significantly increased cytokine production in BMDM compared to H37Rv complemented with PGL [78] – demonstrating the key role that PGL plays in cytokine induction. Taken together, this information highlights the significance of *Mtb* lipids on the immunological response to *Mtb* and consequent inflammatory microenvironment.

1.5. *Mtb* co-infection worsens HIV-1/AIDS disease outcome by increasing susceptibility to HIV-1 infection, viral set-point, and spread

1.5.1. *Mtb*-specific T cells have increased susceptibility to HIV-1 infection

HIV-1 has a propensity to readily and selectively infect *Mtb* specific T cells more than other antigen-specific T cells [79]. An early study showed that LN or PBMC from patients who are latently infected with *Mtb* are preferentially infected by HIV-1 compared with healthy individuals [80], a phenotype that is enhanced by pathogenic mycobacteria compared to non-pathogenic mycobacteria [11]. An experiment in which PBMC were stimulated with: *Mtb*,

Mycobacterium bovis Bacille Calmette-Guerin (BCG), *Mycobacterium smegmatis* or left unstimulated for 72 h and then exposed to either X4 or R5 strains of HIV-1, showed that T cells stimulated with pathogenic *Mtb* were highly susceptible to HIV-1 infection with both X4 and R5 strains compared to the non-pathogenic mycobacteria BCG and *M. smegmatis* [11]. A clinical study in TB patients in Tanzania showed a decline of 89.4 % in *Mtb* specific CD4+ T cells in the first-year post-HIV-1+ seroconversion, compared to 40.6 % of cytomegalovirus (CMV) specific CD4+ T cells [79]. This evidence indicates that *Mtb* infection creates a permissive environment for HIV-1 infection of T cells.

Susceptibility of *Mtb* specific T cells to HIV-1 infection also means that *Mtb*-co-infection has the potential to increase HIV-1 viral set-point, by creating an increased pool of HIV-1 susceptible cells [81]. HIV-1 replicates rapidly following initial infection, reaching peak viremia approximately two weeks post-infection [82]. The viral load then decreases after a few weeks post-infection and remains in a steady state called the viral set-point: the set-point is influenced by the height of the initial peak, with a greater initial replication resulting in a higher viral set-point [83-84]. Individuals with a high viral set-point tend to progress faster to AIDS compared to individuals with a low viral set-point [85]. A higher viral set-point was one of the predictors of death amongst a study in African woman with HIV-1 infection [86].

1.5.2. Mechanisms of *Mtb*-induced viral spread

HIV-1 spreads beyond the initial site of infection through cell-free virions migrating via the bloodstream and lymphatic vessels and through the circulation of HIV-1 infected cells [87-89]. Transmission by direct cell-to-cell spread is known to be the most efficient form of viral spread [90], signifying that an environment with an overabundance of cells and/or tightly packed cells creates a niche ideal for HIV-1 spread. Initial *Mtb* infection results in a granuloma, an organised structure containing an abundance of cells including macrophages, multinucleated giant cells, epithelioid cells and surrounded by a rim of lymphocytes [91]. The granuloma with activated cells nearby provides a niche for HIV-1 cell-to-cell spread. Additionally, peripheral cells are continually recruited to the granuloma [91], supplying HIV-1 with uninfected peripheral cells. Secondly, HIV-1 infected circulating peripheral cells may be recruited to the site of *Mtb* infection and thereby inescapably transport HIV-1 to the granuloma. The interplay of cells between the periphery and site of infection provides a mechanism for HIV-1 spread.

1.5.3. The bystander cell effect: a role for *Mtb*-induced cytokines in regulating HIV-1 replication.

The signal transduction pathways involved in the regulation of genes related to innate immunity are exploited by HIV-1 for activation of HIV-1-LTR and consequently replication of HIV-1 [92]. Promoters of genes involved in innate immunity are activated through the NF-κB, MAPK, and C/EBP pathways [92]. However, it is recognised that direct co-infection of the same cell is not necessary for *Mtb* to impact the regulation of HIV-1 replication [12]. Some *in vitro* studies have drawn a link between the regulation of HIV-1 replication and the cytokine milieu of the cellular microenvironment [93, 94]. Jacobs and colleagues showed that *in vitro* stimulation of PBMC with a cocktail of SDF-1, CCL21, XCL1, CCL14, and CCL27 cytokines significantly downregulated HIV-1 replication [93]. The authors used this combination of cytokines because they were shown to be significantly increased in a cohort of elite HIV-1 controllers [93]. The authors infected PBMC depleted of CD8+ T cells with two strains of HIV-1 and co-cultured either individual or a cocktail of cytokines and described a significant suppression of HIV-1 replication by both individual cytokines and a cocktail of cytokines [93].

An interesting paper published in 2009 showed that two genetically different laboratory strains of *Mtb* lineage 2 HN878 and lineage 4 CDC1551 differentially activated HIV-1 p24 production in PBMC after 10 days of infection. The authors suggested that this difference was brought about by differential cytokine induction associated with the immune regulatory capabilities of the cell wall lipid PGL on the surface of HN878, which is not present in CDC1551 [94]. To validate this, the authors created a mutant of HN878 lacking PGL. Ranjbar *et al.* (2009) [94], first showed that CDC1551 significantly increased secretion of IL-6, TNF and CCL2 from PBMC compared to HN878, but not compared to the PGL deficient mutant of HN878. Additionally, they showed HIV-1 p24 production was not significantly different between CDC1551 and the PGL deficient HN878 mutant [94]. To further validate the involvement of cytokines, the authors showed a dose-dependent reduction of HIV-1 in PBMC co-infected with CDC1551 and subsequently treated with varying doses of anti-TNF, anti-CCL2, and anti-IL-6 antibodies [94]. Collectively, these data show differential regulation of HIV-1 viral production during co-infection with *Mtb* associated with the absence/presence of cell wall lipid components and differential cytokine production. However, the experiments by Ranjbar and colleagues [94], used two different lineage strains of *Mtb* with varying genetic backgrounds and the entire lipid of focus was missing in one strain. More work is required to determined

how small genetic differences which exist in clinical isolates of the same lineage may impact the amount of lipid or structure of the lipid in the cell membrane and whether this results in subtle differences in cytokine production with the ability to impact HIV-1 replication during co-infection.

1.6. Hypothesis

Natural genetic variation in cell wall lipid metabolising genes in clinical *Mtb* isolates confers differential cell wall lipid phenotypes that modify human macrophage cytokine production and, consequently, HIV-1 replication during co-infection.

1.7. The aims of this project to address this hypothesis were:

Aim 1

- **A.** To identify lipid phenotypes which differ between phylogenetically close *Mtb* clinical isolates with single nucleotide polymorphism (SNP) in lipid metabolising genes that are predicted to confer a lipid phenotype change.
- **B.** To determine whether phylogenetically close *Mtb* strains with SNP in lipid metabolising genes differentially regulate macrophage cytokine production *in vitro*, and whether these are further modified during HIV-1 co-infection.
- **C.** To assess whether differential cytokine induction by *Mtb* strains with different lipid phenotypes correlate with changes in HIV-1 replication and productive infection in co-infected MDM.

Aim 2

- **A.** To genetically revert or introduce SNP of interest into the *Mtb* clinical isolates with identified phenotypic differences and their lineage-matched laboratory strain.
- **B.** To determine whether genetic modulation of SNP in lipid metabolising genes changes *Mtb* lipid phenotypes.

Aim 3

- **A.** To compare MDM cytokine induction following *in vitro* infection with wild-type and genetically modified *Mtb* strains.
- **B.** To assess whether genetically engineered strains differentially alter HIV-1 replication and productive infection in MDM, via either direct co-infection or in by stander cells.

1.8. References

1. WHO, *Global Tuberculosis report 2021.* 2021.
2. WHO, *Global progress report on HIV, viral hepatitis amd sexually transmitted infection.* 2021.
3. Fettig, J., et al., *Global epidemiology of HIV.* Infect Dis Clin North Am, 2014. 28(3): p. 323-37.
4. Gupta, A., et al., *Tuberculosis incidence rates during 8 years of follow-up of an antiretroviral treatment cohort in South Africa: comparison with rates in the community.* PLoS One, 2012. 7(3): p. e34156.
5. Middelkoop, K., et al., *Transmission of tuberculosis in a South African community with a high prevalence of HIV infection.* J Infect Dis, 2015. 211(1): p. 53-61.
6. Blaser, N., et al., *Tuberculosis in Cape Town: An age-structured transmission model.* Epidemics, 2016. 14: p. 54-61.
7. Martinson, N.A., C.J. Hoffmann, and R.E. Chaisson, *Epidemiology of tuberculosis and HIV: recent advances in understanding and responses.* Proc Am Thorac Soc, 2011. 8(3): p. 288-93.
8. Getahun, H., et al., *Development of a standardized screening rule for tuberculosis in people living with HIV in resource-constrained settings: individual participant data meta-analysis of observational studies.* PLoS Med, 2011. 8(1): p. e1000391.
9. Belay, M., G. Bjune, and F. Abebe, *Prevalence of tuberculosis, HIV, and TB-HIV co-infection among pulmonary tuberculosis suspects in a predominantly pastoralist area, northeast Ethiopia.* Glob Health Action, 2015. 8: p. 27949.
10. Corbett, E.L., et al., *The growing burden of tuberculosis: global trends and interactions with the HIV epidemic.* Arch Intern Med, 2003. 163(9): p. 1009-21.
11. Thayil, S.M., et al., *Mycobacterium tuberculosis complex enhances susceptibility of CD4 T cells to HIV through a TLR2-mediated pathway.* PLoS One, 2012. 7(7): p. e41093.
12. Toossi, Z., et al., *Impact of tuberculosis (TB) on HIV-1 activity in dually infected patients.* Clin Exp Immunol, 2001. 123(2): p. 233-8.
13. Goletti, D., et al., *Inhibition of HIV-1 replication in monocyte-derived macrophages by Mycobacterium tuberculosis.* J Infect Dis, 2004. 189(4): p. 624-33.
14. Nakata, K., et al., *Mycobacterium tuberculosis enhances human immunodeficiency virus-1 replication in the lung.* Am J Respir Crit Care Med, 1997. 155(3): p. 996-1003.

15. Kariuki, S.M., et al., *The HIV-1 transmission bottleneck.* Retrovirology, 2017. 14(1): p. 22.
16. Kinlock, B.L., et al., *Transcytosis of HIV-1 through vaginal epithelial cells is dependent on trafficking to the endocytic recycling pathway.* PLoS One, 2014. 9(5): p. e96760.
17. Sarrami-Forooshani, R., et al., *Human immature Langerhans cells restrict CXCR4-using HIV-1 transmission.* Retrovirology, 2014. 11: p. 52.
18. Cavarelli, M., et al., *R5 HIV-1 envelope attracts dendritic cells to cross the human intestinal epithelium and sample luminal virions via engagement of the CCR5.* EMBO Mol Med, 2013. 5(5): p. 776-94.
19. Imran, M., et al., *HIV-1 and hijacking of the host immune system: the current scenario.* APMIS, 2016. 124(10): p. 817-31.
20. Hladik, F. and M.J. McElrath, *Setting the stage: host invasion by HIV.* Nat Rev Immunol, 2008. 8(6): p. 447-57.
21. Lee, B., et al., *Quantification of CD4, CCR5, and CXCR4 levels on lymphocyte subsets, dendritic cells, and differentially conditioned monocyte-derived macrophages.* Proc Natl Acad Sci U S A, 1999. 96(9): p. 5215-20.
22. Doranz, B.J., et al., *A dual-tropic primary HIV-1 isolate that uses fusin and the beta-chemokine receptors CKR-5, CKR-3, and CKR-2b as fusion cofactors.* Cell, 1996. 85(7): p. 1149-58.
23. Yamamoto, T., et al., *Selective transmission of R5 HIV-1 over X4 HIV-1 at the dendritic cell-T cell infectious synapse is determined by the T cell activation state.* PLoS Pathog, 2009. 5(1): p. e1000279.
24. Checkley, M.A., B.G. Luttge, and E.O. Freed, *HIV-1 envelope glycoprotein biosynthesis, trafficking, and incorporation.* J Mol Biol, 2011. 410(4): p. 582-608.
25. Brandt, S.M., et al., *Association of chemokine-mediated block to HIV entry with coreceptor internalization.* J Biol Chem, 2002. 277(19): p. 17291-9.
26. Alkhatib, G., *The biology of CCR5 and CXCR4.* Curr Opin HIV AIDS, 2009. 4(2): p. 96-103.
27. Liu, Z., et al., *Genome editing of the HIV co-receptors CCR5 and CXCR4 by CRISPR-Cas9 protects CD4(+) T cells from HIV-1 infection.* Cell Biosci, 2017. 7: p. 47.
28. Moore, P.L., et al., *Nature of nonfunctional envelope proteins on the surface of human immunodeficiency virus type 1.* J Virol, 2006. 80(5): p. 2515-28.
29. Craigie, R. and F.D. Bushman, *HIV DNA integration.* Cold Spring Harb Perspect Med, 2012. 2(7): p. a006890.

30. Finzi, D., et al., *Latent infection of CD4+ T cells provides a mechanism for lifelong persistence of HIV-1, even in patients on effective combination therapy.* Nat Med, 1999. 5(5): p. 512-7.
31. Zaikos, T.D. and K.L. Collins, *Long-lived reservoirs of HIV-1.* Trends Microbiol, 2014. 22(4): p. 173-5.
32. Abrahams, M.R., et al., *The replication-competent HIV-1 latent reservoir is primarily established near the time of therapy initiation.* Sci Transl Med, 2019. 11(513).
33. Karris, M.A. and D.M. Smith, *Tissue-specific HIV-1 infection: why it matters.* Future Virol, 2011. 6(7): p. 869-882.
34. Costiniuk, C.T. and M.A. Jenabian, *HIV reservoir dynamics in the face of highly active antiretroviral therapy.* AIDS Patient Care STDS, 2015. 29(2): p. 55-68.
35. Costiniuk, C.T. and M.A. Jenabian, *The lungs as anatomical reservoirs of HIV infection.* Rev Med Virol, 2014. 24(1): p. 35-54.
36. Jambo, K.C., et al., *Small alveolar macrophages are infected preferentially by HIV and exhibit impaired phagocytic function.* Mucosal Immunol, 2014. 7(5): p. 1116-26.
37. Collini, P.J., et al., *HIV gp120 in the Lungs of Antiretroviral Therapy-treated Individuals Impairs Alveolar Macrophage Responses to Pneumococci.* Am J Respir Crit Care Med, 2018. 197(12): p. 1604-1615.
38. Arthos, J., et al., *The Role of Integrin alpha4beta7 in HIV Pathogenesis and Treatment.* Curr HIV/AIDS Rep, 2018. 15(2): p. 127-135.
39. Lorenzo-Redondo, R., et al., *Persistent HIV-1 replication maintains the tissue reservoir during therapy.* Nature, 2016. 530(7588): p. 51-56.
40. Wong, J.K. and S.A. Yukl, *Tissue reservoirs of HIV.* Curr Opin HIV AIDS, 2016. 11(4): p. 362-70.
41. El Hed, A., et al., *Susceptibility of human Th17 cells to human immunodeficiency virus and their perturbation during infection.* J Infect Dis, 2010. 201(6): p. 843-54.
42. Gaynore, R., *Cellular Transcription Factors Involved in the Regulation of HIV-1 Gene Expression.* AIDS, 1992. 6(4): p. 347 - 364.
43. Nielsen, M.H., F.S. Pedersen, and J. Kjems, *Molecular strategies to inhibit HIV-1 replication.* Retrovirology, 2005. 2: p. 10.
44. Schiralli Lester, G.M. and A.J. Henderson, *Mechanisms of HIV Transcriptional Regulation and Their Contribution to Latency.* Mol Biol Int, 2012. 2012: p. 614120.
45. Roebuck, K.A. and M. Saifuddin, *Regulation of HIV-1 transcription.* Gene Expr, 1999. 8(2): p. 67-84.

46. Chun, T.W., et al., *Quantification of latent tissue reservoirs and total body viral load in HIV-1 infection.* Nature, 1997. 387(6629): p. 183-8.
47. Pereira, L.A., et al., *A compilation of cellular transcription factor interactions with the HIV-1 LTR promoter.* Nucleic Acids Res, 2000. 28(3): p. 663-8.
48. Marsden, M.D., B.P. Burke, and J.A. Zack, *HIV latency is influenced by regions of the viral genome outside of the long terminal repeats and regulatory genes.* Virology, 2011. 417(2): p. 394-9.
49. Sundquist, W.I. and H.G. Krausslich, *HIV-1 assembly, budding, and maturation.* Cold Spring Harb Perspect Med, 2012. 2(7): p. a006924.
50. Votteler, J. and W.I. Sundquist, *Virus budding and the ESCRT pathway.* Cell Host Microbe, 2013. 14(3): p. 232-41.
51. Williams, R.L. and S. Urbe, *The emerging shape of the ESCRT machinery.* Nat Rev Mol Cell Biol, 2007. 8(5): p. 355-68.
52. Im, Y.J., et al., *Crystallographic and functional analysis of the ESCRT-I /HIV-1 Gag PTAP interaction.* Structure, 2010. 18(11): p. 1536-47.
53. Bhutta, M.S., C.J. McInerny, and G.W. Gould, *ESCRT function in cytokinesis: location, dynamics and regulation by mitotic kinases.* Int J Mol Sci, 2014. 15(12): p. 21723-39.
54. VerPlank, L., et al., *Tsg101, a homologue of ubiquitin-conjugating (E2) enzymes, binds the L domain in HIV type 1 Pr55(Gag).* Proc Natl Acad Sci U S A, 2001. 98(14): p. 7724-9.
55. Usami, Y., S. Popov, and H.G. Gottlinger, *Potent rescue of human immunodeficiency virus type 1 late domain mutants by ALIX/AIP1 depends on its CHMP4 binding site.* J Virol, 2007. 81(12): p. 6614-22.
56. Ajasin, D.O., et al., *CCL2 mobilizes ALIX to facilitate Gag-p6 mediated HIV-1 virion release.* Elife, 2019. 8.
57. Mitchison, D.A., et al., *A comparison of the virulence in guinea-pigs of South Indian and British tubercle bacilli.* Tubercle, 1960. 41: p. 1-22.
58. Niemann, S., et al., *Impact of Genetic Diversity on the Biology of Mycobacterium tuberculosis Complex Strains.* Microbiol Spectr, 2016. 4(6).
59. Tsenova, L., et al., *Virulence of selected Mycobacterium tuberculosis clinical isolates in the rabbit model of meningitis is dependent on phenolic glycolipid produced by the bacilli.* J Infect Dis, 2005. 192(1): p. 98-106.
60. Carmona, J., et al., *Mycobacterium tuberculosis Strains Are Differentially Recognized by TLRs with an Impact on the Immune Response.* PLoS One, 2013. 8(6): p. e67277.

61. Demento, S.L., et al., *Pathogen-associated molecular patterns on biomaterials: a paradigm for engineering new vaccines.* Trends Biotechnol, 2011. 29(6): p. 294-306.
62. Brennan, P.J., *Structure, function, and biogenesis of the cell wall of Mycobacterium tuberculosis.* Tuberculosis, 2003. 83(1-3): p. 91-97.
63. Yang, L., et al., *Changes in the major cell envelope components of Mycobacterium tuberculosis during in vitro growth.* Glycobiology, 2013. 23(8): p. 926-34.
64. Jackson, M., *The mycobacterial cell envelope-lipids.* Cold Spring Harb Perspect Med, 2014. 4(10).
65. Gago, G., L. Diacovich, and H. Gramajo, *Lipid metabolism and its implication in mycobacteria-host interaction.* Curr Opin Microbiol, 2018. 41: p. 36-42.
66. Reed, M.B., et al., *A glycolipid of hypervirulent tuberculosis strains that inhibits the innate immune response.* Nature, 2004. 431(7004): p. 84-7.
67. Queiroz, A. and L.W. Riley, *Bacterial immunostat: Mycobacterium tuberculosis lipids and their role in the host immune response.* Rev Soc Bras Med Trop, 2017. 50(1): p. 9-18.
68. Torrelles, J.B., et al., *Inactivation of Mycobacterium tuberculosis mannosyltransferase pimB reduces the cell wall lipoarabinomannan and lipomannan content and increases the rate of bacterial-induced human macrophage cell death.* Glycobiology, 2009. 19(7): p. 743-55.
69. Sakamoto, K., *The pathology of Mycobacterium tuberculosis infection.* Vet Pathol, 2012. 49(3): p. 423-39.
70. Cambier, C.J., S. Falkow, and L. Ramakrishnan, *Host evasion and exploitation schemes of Mycobacterium tuberculosis.* Cell, 2014. 159(7): p. 1497-509.
71. Blanc, L., et al., *Mycobacterium tuberculosis inhibits human innate immune responses via the production of TLR2 antagonist glycolipids.* Proc Natl Acad Sci U S A, 2017. 114(42): p. 11205-11210.
72. Chaudhry, H., et al., *Role of cytokines as a double-edged sword in sepsis.* In Vivo, 2013. 27(6): p. 669-84.
73. Domingo-Gonzalez, R., et al., *Cytokines and Chemokines in Mycobacterium tuberculosis Infection.* Microbiol Spectr, 2016. 4(5).
74. Lima, P., et al., *Enhanced mortality despite control of lung infection in mice aerogenically infected with a Mycobacterium tuberculosis mce1 operon mutant.* Microbes Infect, 2007. 9(11): p. 1285-90.

75. Petrilli, J.D., et al., *Differential Host Pro-Inflammatory Response to Mycobacterial Cell Wall Lipids Regulated by the Mce1 Operon.* Frontiers in Immunology, 2020. 11.
76. Korf, J., et al., *The Mycobacterium tuberculosis cell wall component mycolic acid elicits pathogen-associated host innate immune responses.* Eur J Immunol, 2005. 35(3): p. 890-900.
77. Ishikawa, E., et al., *Direct recognition of the mycobacterial glycolipid, trehalose dimycolate, by C-type lectin Mincle.* J Exp Med, 2009. 206(13): p. 2879-88.
78. Geldmacher, C., et al., *Preferential infection and depletion of Mycobacterium tuberculosis-specific CD4 T cells after HIV-1 infection.* J Exp Med, 2010. 207(13): p. 2869-81.
79. Garrait, V., et al., *Tuberculosis generates a microenvironment enhancing the productive infection of local lymphocytes by HIV.* J Immunol, 1997. 159(6): p. 2824-30.
80. Ramkissoon, S., H.G. Mwambi, and A.P. Matthews, *Modelling HIV and MTB co-infection including combined treatment strategies.* PLoS One, 2012. 7(11): p. e49492.
81. Little, S.J., et al., *Viral dynamics of acute HIV-1 infection.* J Exp Med, 1999. 190(6): p. 841-50.
82. Geskus, R.B., et al., *The HIV RNA setpoint theory revisited.* Retrovirology, 2007. 4: p. 65.
83. Hodcroft, E., et al., *The contribution of viral genotype to plasma viral set-point in HIV infection.* PLoS Pathog, 2014. 10(5): p. e1004112.
84. Chang, H.H., et al., *Transcriptional network predicts viral set point during acute HIV-1 infection.* J Am Med Inform Assoc, 2012. 19(6): p. 1103-9.
85. Lavreys, L., et al., *Higher set point plasma viral load and more-severe acute HIV type 1 (HIV-1) illness predict mortality among high-risk HIV-1-infected African women.* Clin Infect Dis, 2006. 42(9): p. 1333-9.
86. Costigliola, P., et al., *Detection of circulating p24 antigen-positive CD4 T cells during HIV infection by flow cytometry.* AIDS, 1992. 6: p. 1121 - 1125.
87. Zhong, P., et al., *Cell-to-cell transmission can overcome multiple donor and target cell barriers imposed on cell-free HIV.* PLoS One, 2013. 8(1): p. e53138.
88. Bobardt, M.D., et al., *Cell-free human immunodeficiency virus type 1 transcytosis through primary genital epithelial cells.* J Virol, 2007. 81(1): p. 395-405.
89. Sattentau, Q.J. and M. Stevenson, *Macrophages and HIV-1: An Unhealthy Constellation.* Cell Host Microbe, 2016. 19(3): p. 304-10.

90. Silva Miranda, M., et al., *The Tuberculous Granuloma: An Unsuccessful Host Defence Mechanism Providing a Safety Shelter for the Bacteria?* Clinical and Developmental Immunology, 2012. 2012: p. 1-14.
91. Falvo, J.V., et al., *Arc of a vicious circle: pathways activated by Mycobacterium tuberculosis that target the HIV-1 long terminal repeat.* Am J Respir Cell Mol Biol, 2011. 45(6): p. 1116-24.
92. Sandberg, J.K., et al., *HIV-1 Replication Is Differentially Regulated by Distinct Clinical Strains of Mycobacterium tuberculosis.* PLoS ONE, 2009. 4(7).
93. Jacobs, E.S., et al., *Cytokines Elevated in HIV Elite Controllers Reduce HIV Replication In Vitro and Modulate HIV Restriction Factor Expression.* J Virol, 2017. 91(6).
94. Dinkele, R, et al., Aerosolization of Mycobacterium tuberculosis by Tidal Breathing. Am J Respir Crit Care Med. 2022. 206(2): p. 206–216

Chapter 2. Materials and Methods

2.1. Materials

General reagents, chemicals, equipment, and software referred to in Methods Section 2.2 are described in Table 2.1 and 2.2.

Table 2.1 List of the reagents and chemicals that were used in the project

Reagent/chemical	Supplier	Catalogue number
1-Ethyl-3-(3-dimethylaminopropyl) Carbodiimide	Thermo Fisher	E6383-1G
25-Plex human cytokine panel	Thermo Fischer scientific	LHC0009M
Accutase	Sigma-Aldrich	A1110501
Acrylamide	Bio-rad	1610154
Agarose powder	Sigma-Aldrich	11816586001
ADC	BD Life Sciences	212240
Anti-CD14 Magnetic beads	Biocom Africa	130-097-052
Ammonium Persulfate (APS)	Thermo Fisher	17874
Borosilicate solid-glass beads	Sigma-Aldrich	Z143944-1EA
Bovine Serum Albumin (BSA)	Thermo Fisher	A23018
Bright-Glo reagent	Promega	E2610
Buffy coats	Western Cape Blood Service	
Dimethyl sulfoxide (DMSO)	Sigma-Aldrich	D8418
DNA loading dye	Sigma-Aldrich	G2526
Dul'ecco's Modified 'agle's Medium (DMEM)	Sigma-Aldrich	D0819
Ethidium Bromide solution	Sigma-Aldrich	E1510
Ethylenediaminetetraacetic acid (EDTA)	Sigma-Aldrich	27285
Fetal Calf serum (FBS)	Thermo Fischer scientific	A4766801
Glycerol	Sigma-Aldrich	447498-1G
Glycine	Sigma-Aldrich	G8898

Granulocyte-macrophage colony-stimulating factor (GM-CSF)	Biocom Africa	G5035-5UG
Goat serum	Thermo Fisher	G5018
Human AB serum (HAB)	Sigma-Aldrich	H4522
Hygromycin B (Hyg B)	Thermo Fisher	10687010
Interleukin-2	Sigma-Aldrich	I2644
Isovaleronitrile (IVN)	Sigma-Aldrich	08528
Kanamycin Sulfate (Kan)	Sigma-Aldrich	PHR1487
KC57-RD1 antibody	Beckman Coulter	6604667
Lymphoprep	Thermo Fischer	15257179
Lysozyme	Thermo Fisher	89833
M-CSF	Biocom Africa	130-096-491
Middlebrook 7H10	Sigma-Aldrich	M0303
Middlebrook 7H9	Sigma-Aldrich	M0178
Mouse serum	Thermo Fisher	10410
N-hydroxysulfosuccinimide (NHS)	Thermo Fisher	24510
Oleic Albumin Dextrose Catalase (OADC)	BD Life Sciences	212240
Penicillin-Streptomycin	Sigma-Aldrich	P4333
Phosphate Buffered Saline (PBS)	Sigma-Aldrich	D1283
QIAquick PCR purification kit	Qiagen	28104
Recombinant HIV-1 p24 full-length protein	Abcam	ab127888
Roswell Park Memorial Institute (RPMI)	Sigma-Aldrich	R6504
Sodium chloride	Sigma-Aldrich	S9888
Sodium dodecyl sulfate (SDS)	Sigma-Aldrich	L3771
Sucrose	Sigma-Aldrich	S0389
Tetramethylethylenediamine (TEMED)	Thermo Fisher	15524010
Tris	Sigma-Aldrich	10708976001
Triton X-100	Sigma-Aldrich	X100
Trypan blue	Sigma-Aldrich	302643

Tryptone	Sigma-Aldrich	T9410
Tween 80	Sigma-Aldrich	P1754
xMAP® antibody coupling kit	Luminex corp	MC100XX-ID
Yeast extract	Sigma-Aldrich	Y1625
ZR Plasmid Miniprep™-Classic	Zymo research	D4015

Table 2.2 List of the equipment that were used in the project

Types of equipment	Supplier	Catalog number
Falcon tubes	Sigma-Aldrich	15 mL CLS430055 50 mL CLS430055
Allegra X-12 Benchtop Centrifuge	Beckman Coulter	392932
Petri-dishes (90X15mm)	White scientific	PLAS-HP0005
Thermo Heraeus centrifuge	Thermo Scientific	8000195472
TC automated cell counter	Bio-Rad	1450102
T75 flask	Sigma-Aldrich	Z707503
Beckman Ultracentrifuge Optima L-100XP ultracentrifuge	Beckman Coulter	PN LXP-IM-7AB
0.45 mM sterile filter	Sigma-Aldrich	SLHV033N
96 well plates round bottom clear wells	Sigma-Aldrich	CLS3922
96-Well Black Polystyrene Plate	Sigma-Aldrich	CLS3601
GeneXbright software	Promega	Software v1.9.3
MS/LS ferromagnetic sphere columns	Miltenyi Biotec	MS 130-090-543 LS 130-042-401
MACS® magnetic separator	Miltenyi Biotec	130-108-934
6-well tissue culture plate	Thermo Scientific	140675
Large Petri tissue culture dish	Thermo Scientific	171099

96-well TPP tissue culture plates	Greiner Bio-one	T1096
Corning 96 well 0.2 pvdf filter plate	Sigma-Aldrich	CLS3508
Bio-Plex Pro II Wash Station Microplate Washer	Bio-Rad	5703
Bio-Plex® 200 Luminex Reader	Bio-Rad	6006
Stuart SB1 Blood Tube Rotator	Akribis Scientific Limited	P105
Gene Pulser Xcell™ Electroporation Systems	Bio-Rad	1652662
Electroporation cuvettes	Sigma-Aldrich	Z706094
Eppendorf 5417C desktop centrifuge	Eppendorf	Z366021
Water bath	Memmert	WNB 7
ProFlex™ 2 x 384-well PCR System	Thermo Scientific	Z374911
Sub-Cell GT cell horizontal DNA electrophoresis cell	Bio-Rad	1704401
Optical adhesive covers starter kit	Thermo Scientific	4313663
Whatman® flexible TLC Plate	Sigma-Aldrich	Z742864

2.2. Methods

2.2.1. Study ethical approval

Ethical clearance for the study was approved by the University of Cape Town Faculty of Health Sciences Human Research Ethics Committee with HREC reference number 575/2022, under the main study with the HREC reference number 317/2016.

2.2.2. Generating *Mtb* single-cell stocks

Mtb strains that were used in the project are listed in Table 2.3. The *Mtb* clinical strains used in this project were originally isolated from HIV-1 infected and uninfected individuals living in Khayelitsha, South Africa, as described in Koch *et al.* [1]. All strains were routinely cultured in a biosafety level 3 (BSL3) facility, in Middlebrook 7H9 broth (Sigma-Aldrich) containing 0.2 % glycerol, 0.05 % Tween 80 (Sigma-Aldrich) and supplemented with albumin dextrose catalase (ADC) (BD Life Sciences). Individual freezer stocks (0.5 mL) were inoculated into 4.5 mL 7H9/ADC in a 50 mL Falcon tube (NEST Biotechnology) and cultures were incubated at 37 °C in the presence of 5 % carbon dioxide (CO2) without shaking for a total of 10 days. Cultures were aerated for 10 minutes and swirled to disperse clumps every three days. When the optical density at 600 nm (OD600) reached between 0.6 and 0.8, 1 mL of the starter culture was sub-cultured into 50 mL 7H9/ADC without Tween 80 and incubated for a further ten days at 37 °C with 5 % CO2, with 10 minutes swirling and aeration every three days. Cultures to make infection stocks were grown without adding Tween 80 to ensure the lipid membrane was intact.

Table 2.3. Laboratory-adapted and clinical *Mtb* strains used in the project

Strain name	Reason for selection	Sub-lineage
Experimental strains		
EX30$^{Q1939/A605}$ a	Predicted HIV-1 positive directional selection SNP in *pks2* position 5817: amino acid: Q1939, with an additional SNP in position 1815: amino acid A605	4
***EU111^{N1759}* a**	Predicted HIV-1 positive directional selection SNP in *pks2*: position 5277: amino acid	2
EX86S12 a	Predicted HIV-1 positive directional selection SNP in *pks2*: position 36	4
Control strains		
MRC16$^{P1939/A605}$ a	Phylogenomically close to EX30$^{Q1939/A605}$ with a SNP in position 1815 of *pks2* and no SNP in position in 5817	4
EU40^{T1759} a	Phylogenomically close to *EU111^{N1759}* without the SNP in *pks2* position 5277	2

EU268^{R12} [a]	Clinical strain phylogenomically close to EX86S12 without the SNP in *pk2* position 36	4
CDC1551^{WT} [b]	Well characterised laboratory strain. Matched H37Rv$^{P1939/T605}$ in position on interest	4
H37Rv$^{P1939/T605}$ [c]	Well characterised laboratory strain	4
HN878^{WT} [d]	Well characterised laboratory strain. Matched H37Rv$^{P1939/T605}$ in position of interest.	2

[a] Koch *et al.,* 2017; [b] Valway *et al.,* 1998; [c] Ioerger *et al.,* 2010; [d] Manca *et al.,* 2001

2.2.3. Harvesting *Mtb* stocks for single cells

To harvest bacteria for single cell stocks, cultures were centrifuged at room temperature (RT) for 5 minutes at 1450 x g using an Allegra X-12 Benchtop Centrifuge (Beckman Coulter). The supernatants (SN) were discarded and borosilicate solid-glass beads (Sigma-Aldrich), 2-3 mm in diameter, were added directly to the pellet, to disperse clumps. Following vigorous shaking for one minute, the tubes were left to stand for 5 minutes to allow aerosols to settle before the lid was opened. A volume of 6 mL sterile phosphate buffered saline (PBS), pH 7.4 (Sigma-Aldrich), was added and the tube was inverted 6 times and then left to stand for 10 minutes to allow bigger clumps to settle. After 10 minutes, the upper 5 mL of the SN was transferred into a new 15 mL Falcon tube and centrifuged for 10 minutes at 1400 x g, following which the upper 4.5 mL SN was added to a Falcon tube containing 0.5 mL of 50 % sterile glycerol. Final stocks were made into aliquots of 200 µL, 400 µL and 600 µL for each strain. The stocks were frozen at -80 °C until further use. One hundred microlitres of the stocks were used to determine the colony-forming units (CFU). To determine CFU, a 10-fold serial dilution was carried out by diluting 100µl in 900 µL of media from 10-1 to 10-6 for each strain. One hundred microlitres of the dilutions were plated on Petri-dishes (Whitesci) with Middlebrook 7H10 agar containing 0.5 % glycerol and supplemented with oleic albumin dextrose catalase (OADC) (BD Life Sciences). Two days post-freezing, 100 µL was taken again for each strain, to determine the effect freezing has on viability. Plates were checked for the presence of colonies starting on day 14 following incubation at 37 °C and were counted every three days for up to 4 weeks.

2.2.4. Analysis of *Mtb* lipids with thin layer chromatography

Lipids from *Mtb* strains were analysed with TLC to establish cell wall lipid production between the strains. *Mtb* strains were cultured as described in section 2.2.2. To harvest bacteria for TLC,

cultures were centrifuged at RT for 5 minutes at 1450 x g using an Allegra X-12 Benchtop Centrifuge (Beckman Coulter), they were resuspended in 5 mL PBS and the transferred to 2 mL tubes and heat-killed in 80 °C water bath for 1 h. Heat killed bacteria were centrifuged at 3000 x g, and the SN was discarded. The remaining pellets were shipped to Dr Apoorva Bhatt, at the University of Birmingham for TLC analysis. Briefly, this involved weighing the culture pellets to ensure the equal weight of each pellet was used for lipid extraction. The total lipid extraction was performed as follows: cells were transferred into 20 ml of methanol: 0.3 % aqueous sodium chloride. Then 10 ml of petroleum ether was added, and the solution was vigorously shaken for 15 minutes using a magnetic stirrer bar to facilitate complete emulsification of the polar and apolar layers. The mixture was allowed to separate, and the top layer was transferred into a 5 ml falcon tube. Ten millilitres of petroleum ether were further added to the lower aqueous phase and stirred further for 15 minutes. The mixture was allowed to separate again and more of the top layer solution was added to the first top layer harvested, this is the apolar lipids layer. To the lower layer, 17.3 mL of chloroform: methanol 0.3 % aqueous sodium chloride was added, and the solution was vigorously stirred for 1 h. The cell debris was pelleted at 750 x g for 15 minutes and the SN was transferred into a 50 ml falcon tube. The pellet was resuspended in 5.6 mL of chloroform: methanol: 0.3 % aqueous sodium chloride and stirred for 30 minutes. The solution was centrifuged for 30 minutes at 750 x g and the SN was combined with the previous SN of polar lipids. The apolar and polar lipids (?) were dried by using rotary vacuum evaporation. Following lipid extraction Dr Apoorva ran the TLC plates as follows: the dried lipid pellets were dissolved in chloroform, 2 µL of each sample were loaded to a TLC plate (Sigma-Aldrich), the mobile phase made up of chloroform/methanol/water (60:12:1, v/v). To visualise the spots, TLC plates were dipped in 0.5 % α-naphthol dissolved in 50 % methanol and charred in 50 % concentrated sulphuric acid.

2.2.5. *Mtb* genetic engineering using recombineering

Genetic engineering of the strains was applied to investigate whether any observed phenotypic difference in the strains could be directly linked to genetic variation. SNP were introduced into strains using recombineering, a homologous recombination-based technique used in molecular biology for genetic engineering [2, 3]. In *Mtb*, recombineering is achieved using *E. coli* RecE and RecT homologs gp60 and gp61, from mycobacteriophage (Che9c), together with single-stranded DNA (ssDNA) substrates homologous to the region of interest [2]. The ssDNA

substrates are homologous to the region of interest except for the single base change that will be introduced. The details of the SNP and strains are highlighted in Table 2.4.

Table 2.4. SNP details of the *Mtb* strains that were used for recombineering

SNP	EX30$^{Q1939/A605}$	MRC16$^{P1939/A605}$	H37Rv$^{P1939/T605}$
Pks2: 5817[a]	**C** **Glutamine(Q)1939**	**G** **Proline(P)1939**	**G** **Proline(P)1939**
Pks2: 1815	**T** **Alanine(A)605**	**T** **Alanine (A)605**	**C** **Threonine (T)605**

[a] SNP predicted to be under HIV-1 positive directional selection.
Red base = SNP compared to H37Rv; Black base = base as seen in H37Rv

2.2.5.1. *Designing the ssDNA substrates*

There is evidence that recombineering has a lagging strand bias [2] and therefore the efficiency of recombineering is increased when the ssDNA substrate is designed to match the lagging strand. The ssDNA substrates (Table 2.5) used in the project were based on the sequences for both the leading and lagging strand of *Mtb pks2* (*Rv3825c*), which were obtained from MycoBrowser (https://mycobrowser.epfl.ch/) [4].

Table 2.5. Single-stranded DNA substrates designed and used to insert SNP in clinical and laboratory *Mtb* strains.

SNP/position	ssDNA substrate designed
SNP: g to t lagging strand **Position: *pks2* 5817** **Amino acid: 1939**	5'-ccgaccaggctccccacgcgatcgcggtagcctgcaggccctgagcttgccgccaatgcgcgaaggcgtc-3'
SNP: t to g lagging strand **Position: *pks2* 5817** **Amino acid: 1939**	5'-gatatccgaccaggctccccacgcgatcgcggtagccggcaggccctgagcttgccgccaatgcgcgaaggc-3'
SNP: c to a leading strand **Position: *pks2* 1939**	5'-gacgccttcgcgcattggcggcaagctcagggcctgcaggctaccgcgatcgcgtggggagcctggtcgg-3'

SNP: a to c leading strand **Position: pks2 1939**	5'-gacgccttcgcgcattggcggcaagctcagggcctg**ccg**gctaccgcgatcgcgtggggagcctggtcggat-3'
SNP: t to c lagging strand **Position: *pks2* 605**	5'-tgccgcccgccggggcacctgacgaccgtt**ggc**gggccacggtgtggtcacctcggggcacgaa-3'
SNP: c to t lagging strand **Position: *pks2* 605**	5'-tgccgcccgccggggcacctgacgaccgtt**ggt**gggccacggtgtggtcacctcggggcacgaa-3'

2.2.5.2. *Preparing pNIT and pOLYG plasmids*

Stocks of *E. coli* cells containing pNIT [5, 6] (Table 2.6) and pOLYG [7] (Table 2.6), were a gift from Dr Anastasia Koch. A pipette tip was used to pick at the frozen stock, which was resuspended in 5 mL of Luria-Bertani (LB) media and incubated at 37 °C overnight. The media was prepared by weighing out 10 g of Tryptone, 10 g sodium chloride, and 5 g of yeast extract and made up to 1 L using distilled water. Bacteria were harvested and plasmid isolated using the ZR Plasmid Miniprep™-Classic from Zymo research according to manufacturer's protocol.

Table 2.6. Plasmids used for electroporation of the *Mtb* strains.

Plasmid	Function of plasmid
apNIT: ET	The plasmid was used for expression of the phage Che9c RecET system for Recombineering in mycobacteria with
bpOLYG	The plasmid was used as a marker of electroporation efficiency in clinical strains

2.2.5.3. *Electroporating strains in the presence of pNIT*

Stocks of EX30$^{Q1939/A605}$, MRC16$^{P1939/A605}$ and H37Rv were inoculated in 5 mL of 7H9 media with 0.05 % Tween 80 and no antibiotic, as described previously (Section 2.2.2). Bacteria were allowed to grow for 5 days at 37 °C with no shaking until the OD600 was between 0.6-0.8. One millilitre of the starter culture was sub-cultured into 50 mL of 7H9 media with 0.05 % Tween 80. Glycine was added to a final concentration of 1.5 % at least 24 hours before

electroporation. Bacteria were harvested by centrifugation at 1450 x g for 10 minutes and the SN was discarded. The pellet was resuspended in 40 mL of a 10 % glycerol solution and centrifuged again; this was step was repeated 3 times. The final pellet was resuspended in a volume appropriate to add 400 mL cells in each of the experimental conditions (see table 2.7). Electroporation cuvettes (Sigma-Aldrich) were placed in the BSC and 500 ng of pNIT plasmid DNA (van Kessel *et al.,* 2008), water, or 100 ng, 250 ng and 500 ng of pOLYG were added to the electroporation cuvette respectively and then 400 µL of cells were added to the cuvette and mixed with DNA. Electroporation was carried out in the BSC using a Gene Pulser X cell™ Electroporation System (BioRad) with the following settings: 2.5 kV, 25 µF, 1000Ω. Time constant results were recorded after each electroporation. Following electroporation 800 µL of 7H9 media was added to the cuvette and the cells were transferred into a 1.5 mL Eppendorf tube and incubated at 37 °C overnight without shaking to allow for cell recovery. Electroporated cells were centrifuged using Eppendorf 5417C desktop centrifuge at 25 000 x g for 5 minutes and the pellet was resuspended in 300 mL 7H9/ADC media. A 10-fold serial dilution was carried out in 900 mL of 7H9/ADC media until 10-6. The cells were plated onto 7H10/OADC plates with either no antibiotic or 25 mg/mL of kanamycin (kan) or 50 mg/mL hygromycin B (hyg) (Table 2.7) and the plates were incubated at 37 °C for 3 – 6 weeks, until colonies appeared.

Table 2.7. Experimental and control conditions of electroporation in the presence of pNIT and pOLYG

Controls used	Antibiotic used
500 ng pNIT	25 mg/mL kan
100 ng pOLYG **250 ng pOLYG** **500 ng pOLYG**	25 mg/mL hyg
Water	No antibiotic
Water	25 mg/mL hyg
Water	25 mg/mL kan

2.2.5.4. PCR screening for the successful uptake of pNIT

Colonies on plates on which individual colonies could be observed were counted and, thereafter, single colonies were picked and resuspended in 50 mL of Tris-EDTA (TE) buffer.

Five microliters were transferred to 7H10/OADC media supplemented with kan to create a "spot plate" to maintain the strain, and the remaining colony suspension was boiled at 80 °C for 1 hour using a water bath (Memmert). Forty-five microliters of chloroform were added to tubes and shaken vigorously to mix. The tube was centrifuged at 25 000 x g for 10 minutes. The upper layer of the suspension was used as the template for polymerase chain reaction (PCR). The components of the PCR are listed in Table 2.8 and the conditions of the PCR are listed in table 2.9.

A 1 % agarose gel was prepared to analyse PCR products. The gel was prepared by weighing 1 g of agarose powder (Sigma-Aldrich), the powder was resuspended in 100 mL of a buffer containing Tris base, acetic acid and EDTA (TEA). The agarose was dissolved by heating, and then 1 mL of Ethidium Bromide solution (Sigma-Aldrich) was added. The solution was added to a gel electrophoresis casting tray and allowed to solidify. Once solidified, 2 uL of a 6 X DNA loading dye (Thermo Fisher Scientific) was mixed with 10 uL of PCR product and then loaded to the agarose gel. The DNA was analysed using the Sub-Cell GT cell horizontal DNA electrophoresis cell (BioRad) at 80 volts for 80 minutes and the gel image was captured. Once a colony was identified to be successfully transformed with pNIT by gel electrophoresis, the corresponding colony was picked from the spot plate and resuspended in 10 mL of 7H9/ADC supplemented with 0.05 % Tween and 25 mg/mL kan. The culture was allowed to grow to OD600 of 0.6 – 0.8, cells were harvested and stored in 500 mL aliquots at -80 °C until further use.

Table 2.8. Details of the PCR master mix using the Roche FastStart Taq kit

PCR contents	V0 of reagent in mL/20 mL reaction
10 X PCR buffer	2
5 X GC rich buffer	4
dNTPs	0.4
F primer	2
R primer	2
DNA polymerase	0.25
Template DNA	4 mL

Table 2.9. Details of PCR conditions used in the project

Temperature	Duration	Reaction	Cycles
95 °C	5 minutes	Initial denaturation	1 cycle
95 °C	30 seconds	Denaturation	25 cycles
53 °C	30 seconds	Annealing	
72 °C	1 minute	Elongation	
72 °C	7 minutes	Final elongation	1 cycle

2.2.5.5. SDS-PAGE to determine the induction of gp60/61 proteins in pNIT

The pNIT plasmid contains genes for two proteins gp60 & gp61, whose production can be induced by the addition of isovaleronitrile (IVN). To confirm induction by IVN, 500 uL of the $EX30^{Q1939/A605}$ strain was resuspended in 5 mL of 7H10 media supplemented with 25 mg/ mL of kan. Bacteria were allowed to grow until the OD600 readings were between 0.6 – and 0.8. At the desired OD600, 1 mL of the culture was harvested to serve as a "before induction sample", and then 1 mM of IVN was added to the remaining culture. The culture was incubated for 8 hours, following which a second 2 mL sample was harvested and used as the "8 hours after induction sample" and the culture was incubated for a further 18 hours and then the remaining culture was harvested. Harvested bacteria were heat-killed at 80 °C for 1 hour and then centrifuged at 1760 x g for 10 minutes. The cell pellets were resuspended in 50 µL lysozyme and 100 µL 100 mM Tris-HCl pH 7.6. For protein solubilization, 10 % of sodium dodecyl sulphate (SDS) was added. The samples were then incubated at 60 °C for 30 minutes, centrifuged at 13 000 x g at 4 °C for 5 minutes and the supernatant was used to analyse the protein. Proteins were analysed using 15 % SDS-PAGE, the recipe for making SDS-PAGE can be seen in Table 2.10.

Table 2.10. Recipe for making SDS-PAGE gels for protein analysis

10 % Separating gel	6 % stacking gel
5 mL acrylamide (30 %)	0.8 mL acrylamide (30 %)
2.5 mL Tris 1.5 M (pH 8.8)	0.5 mL Tris 1 M (pH 6.8)
50 mL SDS (20 %)	20 mL SDS (20 %)

100 mL APS (10 %)	40 mL APS (10 %)
10 mL TEMED	10 mL TEMED
2.4 mL water	2.7 mL water

2.2.5.6. Electroporating pNIT positive strains in the presence of ssDNA substrates and pOLYG

Following successful identification of protein induction and production, the *Mtb* strains carrying the pNIT plasmid were cultured in 5 mL 7H9 media supplemented with kan (25 ug/ml). Bacteria were allowed to grow an OD600 of between 0.6 and 0.8, and 1 mL was subsequently used to sub-culture 50 mL media supplemented with 0.05 % Tween 80, 0.05 % glycerol and ADC media. The expression of the recombinase enzyme, carried in the pNIT plasmid, was induced with 1 mM IVN (Sigma-Aldrich) for 8 hours. Cultures were supplemented with 1.5 % glycine 24 hours before electroporation, and the strains were electroporated in the presence of ssDNA or ssDNA + pOLYG (Table 2.11). Furthermore, pOLYG was used alone as a positive control as it is easily taken up by bacteria during electroporation and therefore serves as a control to facilitate the calculation of electroporation efficiencies. Electroporation and plating were carried out as described in section 2.2.3. The electroporated strains were plated under the conditions stated in Table 2.12.

Table 2.11. Electroporation conditions of the strains with pNIT to transform them with ssDNA substrates

Strain details	DNA used
EX30$^{Q1939/A605}$, MRC16$^{P1939/A605}$ and H37Rv with pNIT	100 ng ssDNA substrate 250 ng ssDNA substrate 500 ng ssDNA substrate
EX30$^{Q1939/A605}$, MRC16$^{P1939/A605}$ and H37Rv with pNIT	100 ng ssDNA substrate + 500 ng pOLYG 250 ng ssDNA substrate + 500 ng pOLYG 500 ng ssDNA substrate + 500 ng pOLYG
EX30$^{Q1939/A605}$, MRC16$^{P1939/A605}$ and H37Rv with pNIT	100 ng pOLYG 250 ng pOLYG 500 ng pOLYG

EX30$^{Q1939/A605}$, MRC16$^{P1939/A605}$ and H37Rv with pNIT	Water

Table 2.12. Plating conditions used strains following electroporation to insert ssDNA and pOLYG

Experiment	Media conditions used
EX30$^{Q1939/A605}$:pNIT + ssDNA **MRC16$^{P1939/A605}$:pNIT + ssDNA** **H37Rv:pNIT + ssDNA**	Plate in 7H10/OADC supplemented without antibiotic
EX30$^{Q1939/A605}$:pNIT + ssDNA and pOLYG **MRC16$^{P1939/A605}$:pNIT + ssDNA and pOLYG** **H37Rv:pNIT + ssDNA and pOLYG**	Plate in 7H10/OADC supplemented 25 mg/mL hyg
EX30$^{Q1939/A605}$:pNIT + pOLYG **MRC16$^{P1939/A605}$:pNIT + pOLYG** **H37Rv:pNIT + pOLYG**	Plate in 7H10/OADC supplemented with 25 mg/mL hyg
EX30$^{Q1939/A605}$:pNIT water **EX30$^{Q1939/A605}$:pNIT water** **EX30$^{Q1939/A605}$:pNIT water**	Plate in 7H10/OADC supplemented with 25 mg/mL hyg Plate in 7H10/OADC supplemented with 25 mg/mL kanamycin Plate in 7H10/OADC without antibiotic

2.2.5.7. Confirming substitution of SNP

Colonies were counted, spot-plated and heat-killed as described previously (section 2.2.3). A 421 bp region containing T605A and a 491 bp region containing P1939Q of *Pks2* were amplified using the same PCR conditions as Table 2.9. Five microlitres of the PCR products were analysed using 1 % agarose gel. Samples identified to have the correct product were purified using the QIAquick PCR purification kit (Qiagen) according to the manufacturer's protocol. The presence or absence of the mutation of interest was determined via Sanger sequencing of purified PCR products. Sanger sequencing was conducted at the Central Analytic Facility at Stellenbosch University: http://www.sun.ac.za/english/faculty/science/CAF. The sequences were analysed with SnapGene software.

Table 2.13. Primers used for colony PCR and sequencing

Primers	Sequences
***APH(3')* colony PCR primers**	Forward: 5'-tcaacgggaaacgtcttgctc-3' Reverse: 5'-aaactcaccgaggcagttcc-3'
***Pks2* 605 colony PCR primers**	Forward: 5'-gtggacgccgcgacggtcggcatggtcgaa-3' Reverse: 5'-gatgaccgccgtgcgcaccgaccggtgcgt-3'
***Pks2* 605 sequencing primers**	Forward: 5'-atgagattgctggcatcaccaccaacctct-3' Reverse: 5'-cgttcgttcccgagaacccataagacgaca-3'
***Pks2* 1939 colony PCR primers**	Forward: 5'-gagcggttggtggcgaccgctgtggccacc-3' Reverse: 5'-tggcagctcgttcagctcgacgcggaatttgc-3'
***Pks2* 1939 sequencing primers**	Forward: 5'-actcagcggccaacagctggctggacgcct-3' Reverse: 5'-tgccgaccaccaccccaactggccgatatc-3'

2.2.6. Preparing stocks of HIV bronchoalveolar lavage

The HIV-1 strain used for the experiments was HIV-1 BaL, a CCR5 tropic strain of HIV-1 known to infect macrophages (Tsang *et al*., 2010), which was a kind gift from Dr Anna Coussens. HIV-1 was propagated to make infection stocks by chronologically infecting PBMC isolated from four healthy donors and harvesting the SN (Fig. 2.1). from which the virus was purified by sucrose gradient. All the HIV-1 work was completed in a BSL2+ tissue culture laboratory.

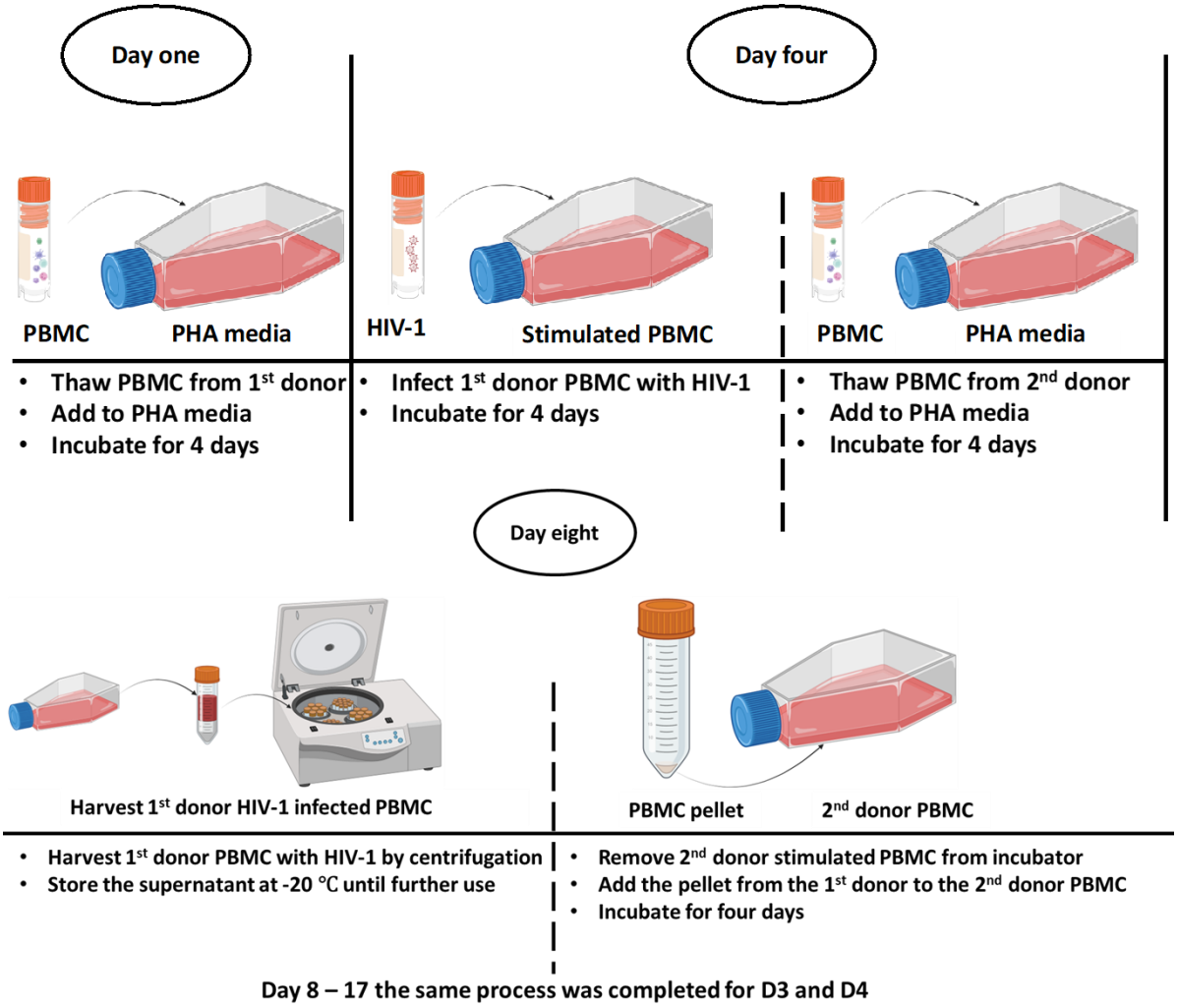

Figure 2.1. Generation of HIV-1 from PBMC of multiple donors.
PBMC from the 1st donor were added to PHA media and incubated for four days. The PBMC were infected with HIV-1 and incubated for a further four days, simultaneously PBMC from a 2nd donor were added to PHA media and incubated for four days. Harvest the SN by centrifugation from the 1st donor and store. The pellet of 1st donor was added to the PBMC of the 2nd donor and incubated for four days. The same process was completed for donor 3 and donor 4 of PBMC.

2.2.6.1. PBMC Isolation

Buffy coats from four healthy donors were purchased from Western Cape Blood Transfusion Service. Each buffy coat was split into 15 mL volumes in 50 mL Falcon tubes and mixed with 15 mL PBS. To isolate PBMC via gradient centrifugation, 15 ml of Lymphoprep solution (Sigma-Aldrich) was added to 50 mL tubes and the blood/PBS mixture was overlaid gently on top of the Lymphoprep, ensuring blood/PBS mixture was maintained as a layer above, and did not mix with Lymphoprep. The tubes were centrifuged at 700 x g, for 20 minutes using a Thermo Heraeus centrifuge (Thermo Scientific). The break option was removed from the centrifugation settings for deceleration to minimise disturbance of the peripheral blood

mononuclear cell (PBMC) layer. The PBMC layer was carefully transferred to a 15 mL Falcon tube containing 5 mL PBS and centrifuged for 10 minutes at 600 x g. The pellet was resuspended in 10 mL PBS and centrifuged for a further 10 minutes at 400 x g. The pellet was resuspended in 4 mL of media, and PBMC were counted using a TC automated cell counter (Bio-Rad), by adding 20 µL of PBMC sample to 20 µL of Trypan blue solution (Sigma Aldrich). The PBMC were pelleted by centrifugation at 400 x g for 10 minutes before resuspension in ice-cold Roswell Park Memorial Institute 1640 Medium (RPMI) (Sigma-Aldrich). PBCM were frozen to a final freezer stock concentration of 20 million cells/mL by transferring 500 µL of PBMC to a 1 mL cryovial kept on ice and then adding 500 µL of a freezing medium containing 90 % fetal bovine serum (FBS) (Separation scientific) and 10 % dimethyl sulfoxide (DMSO) (Sigma-Aldrich) to the PBMC suspension drop-by-drop. The PBMC were stored at -80 °C overnight and then transferred to liquid nitrogen (LN2) until further use.

2.2.6.2. PBMC Infections

To prepare HIV-1 stocks, four different donors of PBMC were used. PBMC from the 1st donor were removed from LN2 allowed to thaw and then resuspended in PHA media (RPMI + 20 % FCS + PHA 0.5 mg/mL) in a T75 flask (Sigma-Aldrich) (Fig. 2.1). The PBMC were incubated for 3 days at 37 °C, 5% CO2. PBMC were transferred to a Falcon tube and centrifuged at 500 x g for 5 minutes. While the PBMC were spinning, a HIV-1 stock was removed from LN2 and allowed to thaw at room temperature. After centrifugation, PBMC SN was discarded, and the 300 µL of the thawed virus was used to resuspend the pellet (Fig. 2.1). The PBMC and virus were incubated for 2 hours at 37 °C, 5% CO2, with occasional agitation every 30 minutes for sufficient infection to occur. Infected PBMC were topped up with ~20 mL IL-2 media (RPMI-1460 + 20 % FCS + P/S + 20 U/ml IL-2) to give a final concentration of $1x10^6$ cells/mL, and then incubated at 37 °C 5% CO2 in a T75 flask for 4 days. On the same day, a 2nd donor's PBMC were allowed to thaw, then transferred to a Falcon tube with 5 mL of RPMI, and then centrifuged for 5 minutes at 500 x g (Fig. 2.1). The pellet was resuspended in PHA media to make $1x10^6$ cells/mL. PBMC were transferred into a T75 flask and incubated lying flat at 37 °C and 5 % CO_2 for 4 days, the same as the donor.

The 2nd donor's PBMC were removed from the incubator, transferred into a 50 mL Falcon tube, and centrifuged at 500 x g for 5 minutes. The pellet was resuspended in IL-2 media to

make $1x10^6$ cell/mL. Then, the HIV-1 infected 1st donor's PBMC were transferred into a 50 mL Falcon tube and centrifuged at 500 g for 5 minutes. The SN was collected into a 50 mL Falcon marked "HIV harvest one" and stored at -80 °C until further use. The 2nd donor PBMC were used to resuspend the 1st donor pellets and then, incubated at 37 °C and 5 % CO2 for four days. A 3rd donor's PBMC were removed from the LN2, prepared the same as above in PHA media and then incubated at 37 °C for four days.

The 3rd donor's PBMC was centrifuged and resuspended in IL-2 media the same as the 2nd donor. The SN was harvested from the 2nd donor and stored at -80 °C until further use same as above. The 3rd donor's PBMC was used to resuspend, and cells were incubated at 37 °C for four days. The 4th donor's PBMC were in PHA media and then incubated at 37 °C and 5 % CO2 the same as above.

On the 15th day, the 4th donor PBMC were centrifuged and resuspended in IL-2 media. The HIV-1 infected PBMC were transferred into a 50 mL Falcon tube and centrifuged at 500 x g for 5 minutes. The SN was harvested from the 3rd donor and stored at -80 °C until further use. The 4th donor's PBMC was used to resuspend, and cells were incubated at 37 °C and 5 % CO2 for four days.

On the 19th day, SN was harvested from the 4th donor was harvested and stored at -80 °C until further use. The pellet was discarded in water with Actichlor™ overnight.

2.2.6.3. Purification of HIV through 25 % sucrose

All four HIV-1 SN harvests were removed from the -80 °C freezer and allowed to thaw. A Beckman Ultracentrifuge Optima L-100XP ultracentrifuge (Beckman Coulter) was switched on, the rotor properly placed inside, the temperature was set to 4 °C and the vacuum setting was started. Ultracentrifuge buckets were sterilized with 70 % EtOH in a BSC. Thawed HIV-1 SN were pooled and filtered using a 0.45 mM sterile filter (Lasec). Twenty-four millilitres of the virus were transferred to ultracentrifuge tubes (Beckman Coulter), and then 6 mL of a 25 % sucrose solution was gently underlaid in the bottom of the virus solution according to Bess *et al.,* (1993). The centrifuge tubes were weighed to ensure they are balanced. The virus was centrifuged at 4 °C for 2 hours at 140 000 x g. The SN was discarded in Actichlor™ and centrifuge tubes were inverted into a 6-well plate to ensure that all SN drains. Each pellet was

resuspended in 1 mL of RPMI supplemented with 5 % human AB (hAB) serum (Sigma-Aldrich) and all pellets were pooled and 100 µL aliquots were made. Aliquots were stored at -80 °C overnight and then transferred to LN2 until further use.

2.2.6.4. Quantification of HIV-1 stocks using TZM-bl cells

Viral quantification was completed using a TZM-bl cell assay. TZM-bl cells are a HeLa derived cell line that expresses high levels of CD4 as well as CCR5 and CXCR4, which also contains a luciferase gene under the control of the HIV LTR (Platt *et al.,*1998), production of luciferase allows quantification of HIV-1 LTR activity using a luciferase assay. TZM-bl cells were donated by Dr Anna Coussens. Cells were removed from LN2, allowed to thaw, and transferred to 5 mL of Dulbecco's Modified Eagle Medium (DMEM) media (Sigma-Aldrich), and counted using a TC counter. The TZM-bl cells were centrifuged at 500 x g for 5 minutes and the pellet was resuspended in DMEM media supplemented with 10 % FCS to make $1x10^6$cells/mL. The cells were transferred to a T75 tissue culture flasks and were incubated at 37 °C with 5 % CO2, with daily monitoring, until ~80 % confluent (~80 % of the flask surface was covered with cells). The media was discarded, and the cells were washed with 10 mL of PBS. TZM-bl cells attached strongly surface of the tissue culture flask, so 2 mL of Accutase, Sigma-Aldrich) was added to the cells followed by incubating at 37 °C and 5 % CO2 for 15 minutes. Accutase is used for detaching the cells from the surface of tissue culture plasticware. Detached TZM-bl were transferred into 5 mL of DMEM media, centrifuged at 500 x g for 5 minutes, and then resuspended in DMEM media supplemented with 10 % FBS. The cells were plated at $1x10^5$ cells/well in a 96 well plate in triplicates and incubated at 37 °C with 5 % CO2 overnight. An HIV-1 stock aliquot was removed from the LN2 and allowed to thaw. Two hundred microlitre serial dilutions were carried out in triplicate in a 96-well plate from 10-1 until 10-9 in DMEM/10 % FBS solution. The overnight plate with TZM-bl cells was moved to the BSC and the media was discarded. The media was replaced with triplicate HIV-1 stock dilutions, to have an infection from 10-3 until 10-9, a blank well was left in the last row. The plate was sealed with Millipore tape and incubated at 37 °C with 5 % CO2 for 48h.

The plate was removed from the incubator into the BSC and 100 µL of media was discarded into a waste container. One hundred microlitres of Bright-Glo reagent (Promega) was added, and the plate was sealed, covered with foil, and placed on a shaker for 2 minutes. The plate was placed back in the BSC and then 150 mL was removed and transferred into Corning

Costar® 96-Well Black Polystyrene Plate (Sigma-Aldrich). Luciferase activity was measured on the GloMax® 96 microplate Luminometer (Promega), using the GeneXbright software (Promega).

2.2.7. Generating monocyte derived macrophages (MDM)

MDM were polarized from fresh or frozen PBMC obtained from buffy coats of healthy donors. PBMC were isolated from buffy coats (as described in 2.3.1). Monocytes are a $CD14^+$ cell type in PBMC and can differentiate into macrophages when stimulated [8]. Here the monocytes were stimulated with GM-CSF to polarise into M1 MDM and M-CSF to make M2 MDM. The polarisation of monocytes to M1 or M2 using either GM-CSF and M-CSF has been validated in literature by both cytokine expression (14) and gene expression (15). Another study also showed that stimulation of monocytes with GM-CSF was sufficient to generate M1 macrophages characterised by increased production of IL-6, IL-12p40/p70 and TNFα poststimulation, in contrast M-CSF polarised MDM produced higher levels of anti-inflammatory IL-10 [16].

Isolated PBMC were counted and then centrifuged at 300 x g for 10 minutes. The pellet was resuspended in MACS buffer (PBS with 0.5 % FBS and 2 mM ethylenediaminetetraacetic acid (EDTA) in a volume equivalent to 80 µL of MACS buffer per 10^7 PBMC. Magnetic beads coated with anti-CD14 antibody (Miltenyi Biotec) were added in a volume that is equivalent to 18 µL of beads per 107 PBMC. The cells mixed with the beads were incubated at 4 °C for 15 minutes. After incubation, 1.5 mL of MACS buffer was added per 107 PBMC and centrifuged at 300 x g for 10 minutes. The supernatant was discarded, and the pellet was resuspended in 1 mL of MACS buffer.

A column with ferromagnetic spheres (Miltenyi Biotec) was mounted on a MACS® magnetic separator (Miltenyi Biotec) with a strong magnetic field inside the BSC. The columns used were either the MS column for cells up to $2x10^8$, or the LS column for cells up to $2x10^9$. The MS or LS columns were equilibrated with 500 µL or 3 µL of MACS buffer, respectively. The PBMC/beads mixture was added to the column and the volume was allowed to flow through by gravitational force. The MS or LS columns were washed three times with 500 µL or 3 µL of MACS buffer, respectively. The volume was allowed to drain each time completely before adding the next wash. The following step was done quickly: the column was removed from the

magnetic separator and placed in a 15 mL Falcon tube, 1 mL of MACS buffer was added to the column and the column plunger was used to plunge the volume into the 15 mL Falcon tube. The isolated monocytes were counted and centrifuged at 300 x g for 10 minutes. The cells were resuspended in RPMI/10 % hAB media to make $2x10^6$ cell/3 mL of media. The cells were split into two equal volumes in 50 mL tubes, to make either type 1 polarised MDM (M1) using GM-CSF, or type 2 polarised MDM (M2) using M-CSF. Human AB serum to a final concentration of 10 % and 5 ng/mL of GM-CSF (Biocom Africa) was added to the first tube, then hAB to a final concentration of 10 % and 20 ng/mL of M-CSF (Biocom Africa) were added to the 2nd tube. The cells were plated in either a small tissue culture dish, 6-well plate, or large tissue culture petri dish according to the concentration of cells (Table 2.4). The cells were incubated at 37 °C with 5 % CO2 for seven days, the dishes were left untouched for 4 days before the cells were checked for attachment to the plates.

Table 2.14. Plates used for incubating CD14+ cells stimulated with M-CSF and GM-CSF

Dish	Size	Volume/compartment	Max cells/compartment
6-well plate	10 cm2	3 ml	$2 x10^6$
Small dish	21.5 cm2	6 ml	$4 x10^6$
Large dish	56.7 cm2	18 ml	$12 x 10^6$

2.2.7.1. Harvesting MDM

After 7 days of differentiation, the used media was discarded from the plates and the cells were washed with 10 mL of PBS. MDM were harvested by adding 2 mL of Accutase to Petri-dishes or 1 mL to a small dish or 500 mL to a 6-well plate. The plates were incubated 37 °C and 5 % CO2 for 15 minutes and then cells were detached from the plates by pipetting up and down. The cycle of Accutase treatment and incubation was repeated if a significant number of MDM remain adhered after the first round. The cells were transferred into a Falcon tube with 5 mL of RPMI and counted using a TC cell counter and centrifuged at 1500 x g for 5 minutes. The pellet was resuspended in RPMI/5 % hAB media. The MDM were transferred to 96-well TPP tissue culture plates (TC plates) (Greiner Bio-one) at $1x10^5$ cell/well in 100 µL.

2.2.8. Infecting MDM with HIV-1 and *Mtb*

A HIV-1 infection stock aliquot was removed from LN2 to thaw. Thawed HIV-1 stocks were prepared for infection by making an inoculum of $3x10^5$ viral particles per 100 µL volume in

RPMI/5 % hAB media. To establish a confluent HIV-1 infection, duplicate M1 and M2 cells were infected by adding 100 mL of HIV at a multiplicity of infection (MOI) of 3 and cultured for a total of 7 days. Duplicate MDM for each condition were left uninfected with HIV and all plates were incubated for 24 hours. The media from all cells was removed and discarded into an Antichlor™ waste container and replaced with RPMI/5 % hAB to a final volume of 200 µL. The media was refreshed every 3 days until day 7.

Once MDM were infected with HIV-1, the plates were moved to the BSL3 for *Mtb* infection. *Mtb* stocks were allowed to thaw and an inoculum volume of $1x10^5$ bacteria per 200 µL was made for each strain in RPMI/5 % hAB. The media was removed from MDM plates and replaced with 200 µL of bacterial inoculum. The plates were incubated at 37 °C with 5 % CO2 for 4 hours. Extracellular bacteria were removed after 4 hours by discarding the media and refreshing with RPMI/5 % hAB media incubating for a further 20-92 hours. The best measures were done to ensure the number of bacteria used to infect each condition were consistent by completing a cfu count prior to infection as well as cfu count with bacteria on the day of infection to compare irregularities of the bacterial counts.

After 24 h infection, 100 µL of SN was harvested from each plate and transferred to a clean 96-well plate, that was clearly labelled to eliminate the confusion of samples. The plate was properly sealed, surface decontaminated, placed in a zip lock bag, and stored at -80 °C until further use. One hundred microlitres of fresh media were used to replace the SN after harvesting and plates were incubated further for 72 hours. The remaining 200 µL of SN was harvested from each plate and transferred to a clean 96-well plate after 96 hours total infection.

2.2.8.1. Sterilising SN of Mtb and HIV-1 for analysis of cytokines and HIV-1

To sterilise the SN to enable cytokine and HIV-1 p24 measurement, SN from the different time points were double filtered to remove *Mtb* using corning 96 well 0.2 mM polyvinylidene difluoride (PVDF) filter plate (Sigma-Aldrich) and centrifuged at 1400 x g for 10 minutes. The SN was transferred to a clean low-binding polypropylene 96-well plate and moved to the BSL2+ laboratory. SN from each duplicate well was pooled and frozen at -80 °C until further use. When ready to first analyse the SN, frozen SN from -80 °C were allowed to thaw. To lyse HIV-1, once thawed, 55 µL of the SN was transferred into a corning costar® 96-well black

polystyrene plate and 1 % Triton X-100 was added to a final concentration of 0.08 % Triton-X, and the plate was incubated for 2 hours at 37 °C with 5 % CO2.

2.2.9. MDM cytokine measurement by Luminex

A Luminex assay allows the simultaneous measurement of analytes in a single sample [9]. Luminex uses microspheres with a unique fluorescent signature, therefore a different analyte may be conjugated to distinct microsphere within a single reaction [9, 10]. In the Luminex machine a 635 nm diode laser is used excite the red and infrared classifier fluorophores which are part of the unique fluorescent signatures of the microspheres, while a second 523 nm laser excites phycoerythrin, the orange reporter fluorophore used in the Luminex-based assays [10].

Experimental set-up followed the manufacturer's instructions for the Thermo Fisher Scientific 25-Plex magnetic human cytokine panel (LHC0009M) with the following modifications: Briefly statute changes made, the serial dilution for the standard curve was modified from 3:1 serial dilution to 2:1 which used 11 points, rather than 7, to increase accuracy of the extrapolation. To enable quantification of more samples per plate, added bead volumes were reduced from 25µL to 12.5µL and the beads were resuspended in a final volume of 90µL when running on the machine. This enable 3 plates of samples to be analysed per kit. Additional buffers and Streptavidin antibody were purchased as additional kits, for each additional plate. The list of analytes and their range of detection is listed in Table 2.15.

2.2.9.1. Preparation of Luminex standards

Each Luminex kit for the 25-plex assay contains two lyophilized standard vials, a 16-plex standard vial and a 14-plex standard vial. Each standard was reconstituted in 500 µL of a solution containing 50 % assay diluent (Thermo Fisher) and 50 % RPMI /10 % hAB media (diluent mixture). The standards were allowed to hydrate in the diluent mixture for 10 minutes at RT and then combined to make 1 mL. The standards were serially diluted in a 1:2 ratio, by adding 150 µL of the diluent mixture to eleven Eppendorf tubes and serially diluting 150 µL of the reconstituted standards.

2.2.9.2. Setting up the Luminex assay

A 1X wash solution was prepared by adding 50 mL of a 20 X wash solution concentrate (Thermo Fisher) to 950 µL of deionized water. Antibody beads (1 X) (Thermo Fisher) were

vortexed for 30 seconds and then sonicated for 30 seconds, then 12.5 µL of beads were transferred to a black 96-well F-bottom, µclear®, cell culture microplate (Luminex plate) (Greiner Bio-One). The beads were protected from light once added to the plate. The Luminex plate was placed on a Bio-Plex Pro II Wash Station Microplate Washer (BioRad) and washed as follows: the plate was placed on the magnetic surface of the wash station for 60 seconds and the machine was programmed to wash twice with 200 µL of 1X wash solution. After the wash, 50 µL of incubation buffer (Thermo Fisher) was added to each well, and then 100 µL of standards and blank (50/50 diluent mixture) were added to their respective wells.

Fifty microlitres of the sample were mixed with 50 µL of assay diluent and then transferred to the Luminex plate. The plate was covered with foil and incubated for 2 hours at room temperature under agitation on an orbital plate shaker.

Biotinylated antibody (Thermo Fisher) and streptavidin-RPE (Thermo Fisher) were prepared to 1X concentration by adding 10 mL of a 10 X biotinylated antibody to 100 µL of biotin diluent (Thermo Fisher) or 10 µL of 10 X streptavidin-RPE to a 100 µL solution of RPE-diluent (Thermo Fisher), respectively. The appropriate volume was adjusted according to the number of wells to be assayed.

The plate was removed from the shaker and placed on the wash station and the beads were washed as previously described. One hundred microlitres of the 1 X biotinylated antibody were added to each well and the plate was covered with foil and incubated for 1 hour at room temperature under agitation on an orbital plate shaker. The plate was removed from the shaker and the beads were washed as previously described. One hundred microlitres of the 1 X biotinylated antibody were added to each well and the plate was covered with foil and incubated for 30 minutes at room temperature under agitation on an orbital plate shaker. The plate was removed from the shaker and placed on the wash station and the beads were washed as previously described.

The 1 X wash solution was added to make 90 µL/well and then the plate was placed in the orbital plate shaker for 2 minutes. The plate was analysed using a Bio-Plex® 200 Reader (BioRad). The machine was set to run at a flow rate of 60 µL/minute with 50 events/bead. The

sample size was set at 50 μL with default double discriminator gates and reporter gain settings. The region for each bead is listed Table 2.15.

Table 2.15. The analytes measured and respective bead regions for 25-plex Luminex (Thermofischer)

Analyte	Bead region	Limits of detection (pg/ml)	
		Upper limit	Lower limit
Eotaxin (CCL11)	2	3905	5.36
GM-CSF	27	7235	9.92
IFN alpha	43	9725	13
IFN gamma	38	2160	2.96
IL-1 beta	13	10465	14
IL-10	15	13280	18
IL-12/IL-23p40	20	6880	9.44
IL-13	18	10710	15
IL-15	30	18625	26
IL-17A (CTLA-8)	25	22955	31
IL-1RA	51	98730	135
IL-2	54	15445	21
IL-2R	61	17210	24
IL-4	77	39100	54
IL-5	34	3953	16
IL-6	19	12755	17
IL-7	55	17320	24
IL-8 (CXCL8)	78	5790	7.94
IP-10 (CXCL10)	56	2085	2.86
MCP-1 (CCL2)	29	18550	25
MIG (CXCL9)	63	3650	5.01
MIP-1 alpha (CCL3)	26	14115	19
MIP-1 beta (CCL4)	28	13410	18
RANTES (CCL5)	21	3723	15
TNF alpha	52	4615	6.33

Table 2.16. The analytes measured and respective bead regions for 13-plex Luminex

Analyte	Bead region	Limits of detection (pg/ml)	
		Upper limit	Lower limit
Eotaxin (CCL11)	77	60.7	14.750
GM-CSF	46	12.2	2.970
IFN gamma	38	58.5	14.209
IL-1 beta	28	19.5	4.744
IL-10	22	4.8	1.162
IL-6	13	4.8	1.154
IL-8 (CXCL8)	18	5.2	1.255
IP-10 (CXCL10)	21	1.03	250
MCP-1 (CCL2)	25	33	8.017
MIP-1 alpha (CCL3)	35	101.2	24.580
MIP-1 beta (CCL4)	37	150.2	36.493
RANTES (CCL5)	36	22.6	5.488
TNF alpha	12	9.7	2.359

2.2.10. Analysis of HIV p24 from supernatant using a custom made Luminex assay

2.2.10.1. Preparing p24 beads

To quantify HIV-1 Gag p24 levels in SN as a measure of released viral particles, a custom Luminex assay was developed according to Biancotto *et al.* (2009) [11] with modifications described by Coussens *et al.* (2015) [12]. All reagents in the xMAP® antibody coupling kit (Luminex corp) were removed from the fridge and allowed to warm to RT. Stock solutions (20 mg/mL) solutions of N-hydroxysulfosuccinimide (sulfo-NHS) (Thermo Fisher) and 20 mg/mL working stock solution of 1-Ethyl-3-(3-dimethylaminopropyl) carbodiimide (EDC) (Thermo Fisher) were made by weighing out 10 mg of the compound and resuspending in 500 µL of activation buffer, respectively. Both solutions were filtered using a 0.22 µm filter, sonicated for 30 seconds and vortexed for 30 seconds. The solutions were mixed to make a final

concentration of 10 mg/mL of each solution in the EDC-NHS solution. Once the reagents warmed up, MagPlex® microspheres (beads) with region 42 (Luminex corp) were sonicated for 30 seconds and vortexed for 30 seconds and then transferred to a 1.5 mL Eppendorf tube. The beads were washed by adding 500 µL of activation buffer (Luminex Corp) followed by 30 seconds of sonication and vortex. The tube was placed on the magnetic separator for 2 minutes and the liquid was removed using a pasture pipette. The wash step was repeated. Thereafter 250 µL of the activation buffer was added to the tube and the beads were sonicated and vortexed for 30 seconds. After vortexing, 250 µL of EDC-NHS mixture was added to the tube, which was then placed on a blood rotator (Stuart SB1 Blood Tube Rotator, Akribis Scientific Limited) for 30 minutes at 30 rpm. The beads were washed 3 times with 500 uL of activation buffer and then resuspended in 990 mL of activation buffer.

A recombinant HIV-1 p24 full-length antibody was reconstituted in 100 µL of PBS to make a 1 mg/mL stock of capture antibody (per manufacturer's instruction) (Luminex corp). Ten microlitres of the antibody were added to the beads and then vortexed. The tube was covered in foil and placed on the blood rotator for 2 hours at 30 rpm. The tube was placed on the magnetic separator for 2 minutes and the liquid was removed. A wash step was carried out by adding 500 µL of wash buffer followed by sonication for 30 seconds and vortex for 30 seconds, which was repeated three times. The beads were resuspended in 1 mL of wash buffer. The beads were counted using the TC cells counter using 1/10 dilution: 10 mL of beads + 90 µL of PBS. The beads were stored at 4 °C and covered in foil until further use.

2.2.10.2. Preparing HIV-1 p24 for Luminex assay standards and samples

To measure HIV-1 Gag p24, SN had HIV-1 lysed with triton-X as described in section 2.6.1. Buffers and standards were prepared as follows: Assay buffer (PBS (no Mg or Ca), 0.1 % BSA, 0.1 % Mouse serum, 0.1 % Goat serum, 0.02 % Tween 20). Standard buffer (Assay Buffer + 1 % triton-X). Wash Buffer **(**PBS (no Mg or Ca) + 0.02 % Tween 20). A recombinant 1 mg/mL HIV-1 p24 full-length protein (Abcam) was used to make the standard curve and the protein was diluted to a 10 mg/mL working stock, the protein was further diluted to 750 ng/mL in standard one, followed by a 10-point 1:3 serial dilution.

The SN were diluted at 1:3 in assay buffer. The HIV p24 antibody-conjugated beads were removed from the fridge, sonicated for 30 seconds and vortexed for 30 seconds. Fifty

microlitres of beads were added to the Luminex black plate at 2000 beads/well. Fifty microlitres of the standards and samples were added to the respective wells black 96-well F-bottom, μclear®, cell culture microplate (Luminex plate). The plate was covered with adhesive foil land incubated at room temperature for 1 hour in a rotation shaker at 800 rpm. The plate was placed on the wash station and the beads were washed as stated in section 2.6.4. A fluorescently conjugated KC57-RD1 antibody (Beckman Coulter) that detect HIV p24 was diluted 1:1000 in the assay buffer. The volume of antibody added made was scaled to add 100 μL of antibody to each well. The plate was covered with adhesive foil, incubated at room temperature for 1 hour in a rotation shaker. The was washed as stated previously on the wash station. Ninety microlitres of assay buffer were added to the wells. The plate was analysed using a Bio-Plex® 200 Reader. The machine was set to run at a flow rate of 60 μL/minute with 50 events/bead. The sample size was set at 50 μL with default double discriminator gates and reporter gain settings.

2.2.11. Analysis of HIV-1 replication in TZM-bl cells using *Mtb* conditioned media

SN from GM-CSF and M-CSF polarized MDM infected with *Mtb* only strains, were thawed in the BSC. The SN harvested 24- and 96-hours post-infection were diluted to 50 % 25, %, 12.5 % and 6.25 % SN using RPMI/ 5 % hAB media. Following analysis of the data, the 50 % SN was used for the experiments. TZM-bl cells were plated at $1x10^5$ cells/well in 200 μL of DMEM/ 10 % FBS media in two plates labelled as "pre-infection" for the plate incubated with SN before HIV infection and "post-infection" for the plate incubated with SN after HIV-1 infection, for 4 hours. Media was discarded from both plates, the post-infection plate was replaced with 90 μL DMEM/ 10 % FBS media, while the pre-infection plate was replaced with 90 μL of the 50 % SN and both plates were incubated at 37 °C for 18 hours. Both plates were infected with 20 μL of HIV for a 1:5 MOI and then placed back in the incubator for 6 h. Then, 90 μL of media was added to the pre-infection plate and 90 μL of the 50 % SN was added to the post-infection plate, both plates were placed back in the incubator for 48 hours. The plates were treated with Bright-Glo reagent as described in section 2.4.4, and luminescence was read using the GloMax® 96 microplate Luminometer, using GeneXbright software.

2.2.12. Analysis of HIV-1 replication in M2 MDM co-incubated with *Mtb* conditioned media

To assess the impact of *Mtb*-induced conditioned media on HIV-1 replication in MDM, M1 and M2 media conditioned with the clinical and laboratory *Mtb* strains, harvested at 96 hours,

across different donors was pooled to make a donor heterologous conditioned media for each strain type. MN from PBMC of five healthy buffy coats were polarized with M-CSF as described in section 2.2.7 to make M2 MDM. On day 7, the MDM were harvested and plated at $1x10^5$ cells per well in 85 µL of media. HIV-1 was prepared to make a 1:2 MOI. MDM were infected by adding 15 µL of HIV-1 to each well and incubating for 18 hours. All the media volume was removed and replaced with 100 µL of donor heterologous conditioned media, then the wells were topped up to 200 µL using 100 µL of media and further incubated for 72 hours. Following incubation, the SN was harvested, and HIV-1 Gag p24 measured using Luminex assay as section 2.2.10.

2.2.13. Trans-well assay infection of MDM with *Mtb* WT and mutant strains to assess the impact of SNP on cytokine production and HIV-1 replication

The mutant strains that were generated in section 2.2.5 above and their original WT strains were used to infect M2 MDM in a trans-well plate in the presence of HIV-1 co-infection. The trans-well plate was used to simultaneously accomplish co-infection (the top chamber) and the effect of cytokines in bystander MDM (bottom chamber). The trans-well plate was used to mimic a co-infected environment by infecting MDM seeded in the top chamber with HIV-1 and then co-infecting with various strains of *Mtb*. The bottom chamber was used to mimic the effect of cytokine produced by HIV-1/*Mtb* co-infection on bystander cells infected with HIV-1 only and exposed to cytokines for nearby *Mtb*-infected cells.

2.2.13.1. Measuring cytokine production and HIV-1 replication in MDM using a trans-well plate

The trans-well infection was carried out in a 96-well, 0.4 mM, polycarbonate membrane trans-well plate corning plate (Sigma-Aldrich). The top chamber and bottom chamber were not allowed to mix until co-infection with *Mtb*.

PBMC isolation from six donors followed the same protocol as in (section 2.2.6), the polarisation to MDM using M-CSF was done the same as in (section 2.2.7) The MDM were harvested and seeded at $1x10^5$ cell/well in the using 150 µL in the top chamber and 200 µL in the bottom chamber of a 96-well trans-well plate. HIV-1 infection of MDM was completed the same as (section 2.2.8) and the trans-well plates were moved to the BSL3 for co-infection with *Mtb.* While kept separated, the top chamber of the trans-well was co-infected with *Mtb* the

same as (section 2.2.8) and incubated for 4 h. Media in the bottom chamber was discarded and replaced with 200 µL of fresh RPMI/5% hAB media. Media in the top chamber was discarded to remove bacteria not infecting cells and the two chambers were combined to allow flow-through of cytokines between the chambers. The SN was harvested and processed the same as (section 2.2.8.1) and the analysis of cytokines was completed using a 13-Plex Luminex human discovery assay with catalogue number LXSAHM-13 and the same protocol was followed in (section 2.2.9) The HIVp24 protein was measured from both the top and the bottom chamber using the HIVp24 Luminex protocol in (section 2.2.10.1).

2.2.14. Statistical analysis of cytokine and HIV-1 p24 production data.

Analysis of data was performed using Qlucore Omics Explorer (Qlucore, version 3.8.11) and GraphPad prism (GraphPad Software Inc, version 9.4.1). All the data was first log transformed for normal distribution and then normalised using the z-score normalisation on Qlucore omics, such that the mean is equal to zero and the standard deviation is equal to 1. The PCA plots were generated using Qlucore, in principal PCA plots are used to reduce dimensionality of a large data while preserving as much of the variation as possible [13]. The PCA clusters variables based on their correlation with all other variables and distinct clusters represent the least correlated variables [13], allowing the observation of patterns within the data set. GraphPad was used to analyse statistical significance between all the groups compared and the significance cut of value was $P<0.05$ for all analyses. An un-parametric paired Mann-Whitney t-test was performed when comparing two groups with equal samples and an un-parametric Wilcoxon t-test was performed for groups with unequal samples. One-Way ANOVA was used for three or more groups, for paired data using Friedman's test or the Kruskal-Wallis's test for unpaired data, with Dunn's multiple comparison test for both. The two-stage linear step-up procedure of Benjamini, Krieger and Yekutieli was used for False Discovery Rate (FDR) of 0.1 for multiple comparison of tests.

2.3. References

1. Koch, A.S., et al., *The Influence of HIV on the Evolution of Mycobacterium tuberculosis.* Mol Biol Evol, 2017. **34**(7): p. 1654-1668.
2. van Kessel, J.C. and G.F. Hatfull, *Efficient point mutagenesis in mycobacteria using single-stranded DNA recombineering: characterization of antimycobacterial drug targets.* Mol Microbiol, 2008. **67**(5): p. 1094-107.

3. Sharan, S.K., et al., *Recombineering: a homologous recombination-based method of genetic engineering.* Nat Protoc, 2009. **4**(2): p. 206-23.
4. Kapopoulou, A., J.M. Lew, and S.T. Cole, *The MycoBrowser portal: a comprehensive and manually annotated resource for mycobacterial genomes.* Tuberculosis (Edinb), 2011. **91**(1): p. 8-13.
5. Pandey, A.K., et al., *Nitrile-inducible gene expression in mycobacteria.* Tuberculosis (Edinb), 2009. **89**(1): p. 12-6.
6. Murphy, K.C., K. Papavinasasundaram, and C.M. Sassetti, *Mycobacterial recombineering.* Methods Mol Biol, 2015. **1285**: p. 177-99.
7. Garbe, T.R., et al., *Transformation of mycobacterial species using hygromycin resistance as selectable marker.* Microbiology (Reading), 1994. **140 (Pt 1)**: p. 133-8.
8. Girgis, N.M., et al., *Ly6C(high) monocytes become alternatively activated macrophages in schistosome granulomas with help from CD4+ cells.* PLoS Pathog, 2014. **10**(6): p. e1004080.
9. Carson, R.T. and D.A. Vignali, *Simultaneous quantitation of 15 cytokines using a multiplexed flow cytometric assay.* J Immunol Methods, 1999. **227**(1-2): p. 41-52.
10. Pang, S., et al., *A comparability study of the emerging protein array platforms with established ELISA procedures.* J Immunol Methods, 2005. **302**(1-2): p. 1-12.
11. Biancotto, A., et al., *A highly sensitive and dynamic immunofluorescent cytometric bead assay for the detection of HIV-1 p24.* J Virol Methods, 2009. **157**(1): p. 98-101.
12. Coussens, A.K., et al., *High-dose vitamin D3 reduces deficiency caused by low UVB exposure and limits HIV-1 replication in urban Southern Africans.* Proc Natl Acad Sci U S A, 2015. **112**(26): p. 8052-7.
13. Jolliffe, I.T. and J. Cadima, *Principal component analysis: a review and recent developments.* Philos Trans A Math Phys Eng Sci, 2016. **374**(2065): p. 20150202.
14. Verreck , F.A.W., *et al*. Human IL-23-producing type 1 macrophages promote but IL-10-producing type 2 macrophages subvert immunity to (myco)bacteria. PNAS, 2004. **13**(101): p. 4560–4565.
15. Lacy, D.C., Defining GM-CSF– and Macrophage-CSF–Dependent Macrophage Responses by In Vitro Models. The Journal of Immunology, 2012. **188** (11): p. 5752–5765.
16. Portevin, D., et al., Human Macrophage Responses to Clinical Isolates from the Mycobacterium tuberculosis Complex Discriminate between Ancient and Modern Lineages. PLoS Pathog, 2011. 7(3) .

Chapter 3. Characterization of clinical and laboratory strains of *Mtb* to assess the effect of SNP in lipid metabolising genes on growth, lipid production and human macrophage infection phenotypes

3.1. Introduction

3.1.1. *Mtb* cell wall structural components and diversity

Studies with new molecular techniques for analysis of genomes revealed a greater *Mtb* strain diversity than originally thought [1]. It is now well recognised that human adapted *Mtb* strains fall into seven lineages [2, 3] which have major genomic differences [3]. Genetic diversity between *Mtb* strains has implications for virulence, *in vitro* and *in vivo* growth patterns, as well as cell wall composition. The *Mtb* cell wall is a complex multi-layered structure with an abundance of diverse, bioactive, and surface exposed lipids that form the first point of contact with host receptors [4-6]. The abundance of exposed lipids on the surface of the *Mtb* cell wall means that lipids set the course of infection, including cellular entry, modulation of phagosome maturation, immune response, and the biogenesis of the granuloma [5, 7, 8]. *Mtb* cell wall lipids that have been implicated in modifying the macrophage response to infection include phthiocerol dimycocerosates (PDIM), free fatty acids (FA) and mycolic acids (MA), sulfolipid-1 (SL-1), trehalose dimycolate (TDM), diacyltrehaloses (DAT), tetraacylated phosphatidylinositol hexamannoside (Ac2PMI6), di-acyl phosphatidylinositol mannoside di-mannose (Ac2PMI2), phenolicglycolipid (PGL) and phospholipids (P). The unique nature of the *Mtb* cell wall generates different interactions with host PRR and may influence the outcomes of infection [9]. Cell wall components such as lipomannan (LM), lipoarabinomannan (LAM) and mannose-capped lipoarabinomannan (ManLAM), lipoproteins, PDIM, and MA are unique to mycobacterial species and will therefore result in mycobacteria specific immune responses [9]. The nature of PAMP and PRR interaction are important determinants of host-pathogen interactions. Differences in PAMP on pathogens, including different concentration, alteration in structure and presence or absence of a PAMP will determine the host immune cell response to infection [10].

3.1.2. *Mtb* clinical isolates with mutations in lipid metabolism associated with HIV-1 positive directional selection

The clinical strains used in this thesis were identified as strains of interest following work conducted by Koch *et al.* (2017) [28], in which WGS of *Mtb* strains isolated from TB patients

with and without HIV co-infection, living in Khayelitsha, a peri-urban township located in Cape Town, South Africa, was carried out (Figure 3.1). Analysis by Koch *et al*. identified SNP that exhibited potential signs of HIV-1 positive directional selection, using the evolutionary predictive model MEDS [28]. The SNP selected for this study were in *pks2,* a gene that is involved in the metabolism of SL-1 [29], and *Rv2954c* which encodes a methyltransferase involved in the metabolism of PGL [30]. The selective advantage conferred by each SNP positively selected by HIV-1 is not obvious and requires further investigation [28]. However, it is worth noting that host derived immune cytokines are important to HIV-1 replication *in vivo* and selection of SNP which increase the pro-inflammatory phenotype of strains may serve to enhance HIV-1 replication.

3.1.3. Impact of *Mtb* cell wall lipids on immune response to infection

Mtb cell wall lipids are implicated in variety of virulence processes during the infection cycle of *Mtb*. SL-1, which requires *pks2* for biosynthesis, was recently shown to induce cough in a guinea pig model of *Mtb* infection and thus was proposed to be involved in the transmission of *Mtb* [17]. These authors infected guinea pigs with WT strains of *Mtb* Erdman or *Mtb* Erdman with a knockout for a gene coding a sulfotransferase (*stf*) involved in the biosynthesis of SL-1. They showed that six weeks post infection coughing in the guinea pigs infected with WT strains was more severe compared to coughing in guinea pigs infected with mutant strain [17]. Furthermore, the authors showed that complementing the gene encoding Stf in the mutant strain reverts coughing in guinea pigs to levels observed with WT [17]. SL-1 was shown to also increase the biogenesis of lysosomes in human THP-1 macrophages [18]. Interestingly, THP-1 cells that were infected with a mutant of CDC1551 lacking *pks2*, which therefore does not produce SL-1, were shown to be less effective in making lysosomes [18].

The cell wall of *Mtb* also contains PDIM and the structurally associated, glycosylated PGL [19]. PDIM has been shown to be spontaneously lost during *in vitro* culture [20], which could have implications for virulence. For example, a study showed that WT *M. marinum* resulted in the recruitment of a significantly smaller number of iNOS-producing macrophages compared to PDIM-deficient strains in a Zebra fish model [21]. Furthermore, another study showed that PDIM is important in protecting *Mtb* against IFN-γ immunity [22]. Reed *et al.* (2004) [7], showed the *Mtb* lipid PGL significantly hampered the production of cytokine by (Bone marrow-derive macrophages) BMM [7], while other studies have shown other lipids increase in the production of cytokines, such as TDM increasing the production of TNF in mice

following intratracheal instillation [23], or a robust IL-6 and IL-2 response by mycolic acids incorporated into liposomes [23].

Other cell wall lipids involved in the pathogenesis of *Mtb* include those involved in the formation of serpentine-like structures, known as cording [11, 12]. Laboratory culture of *Mtb* in the presence of detergents to avoid cording results in shedding of the capsule into the media [12], and the understanding that *Mtb* cell wall lipids are important virulence factors creates controversy about culturing *Mtb* in the presence of Tween 80 [12]. The *Mtb* glycolipid TDM, also known as cord factor, is involved in cord formation [13]. TDM is important to *Mtb* pathobiology, and studies by Indrigo *et al.* (2003) [14] showed that *Mtb* strains devoid of TDM were killed quickly upon infection in murine macrophages as compared to native *Mtb* strains. The survival of TDM-deficient strains could be restored by addition of pure TDM to macrophage culture [14]. Other experiments showed that mice infected with a *Mtb* strain lacking the machinery to make a cyclopropane ring in the TDM structure were deficient in cording and, subsequently, these mutants were not able to kill infected mice and were quickly cleared from the system of the mice [15]. Cording may also offer survival advantages, including resistance to drugs, as noted by Trivedi *et al.* (2016) [16] who demonstrated that *Mtb* biofilms were still metabolically active even at 100x minimum inhibitory concentration (MIC) of first line antitubercular drugs like isoniazid [16].

Fatty acids (FA) are found in high content in the human granuloma [24], and *Mtb* is thought to scavenge FA to fuel metabolism for biosynthetic pathways [25]. *Mtb* synthesizes C16-22 fatty acids through the fatty acid synthase-I (FAS-I) enzyme, although β-oxidation of scavenged FA is a more energy efficient option [25]. FA are integrated directly into membrane phospholipids and are therefore indirectly required for the maintenance of cytoplasmic membrane integrity (Daniel *et al.,* 2011). The *Mtb* cell wall contains mycolic acids (MA) covalently linked to trehalose and arabinogalactan, however an association between free MA and *Mtb* biofilm formation under certain growth conditions and media has been described [26]. In this study, the authors showed that, despite bacteria in the biofilms being drug sensitive, they harbour an elevated number of bacteria that survive high concentrations of antibiotics [26]. Furthermore, the Ac_2PMI_6, and Ac_2PMI_2 in the inner membrane of the *Mtb* cell wall increases stability, decreases fluidity and reduces drug permeability due the tight packing of acyl chains from Ac_2PMI_6, and Ac_2PMI_2 [27]. Taken together, these data show the importance of *Mtb* cell wall

lipids on the biology of *Mtb* and illustrate how changes to the lipid structures or absence of lipids may result in alteration of *Mtb* infection patterns.

3.1.4. *Mtb* clinical isolates selected to study in this thesis

Three clinical strains with SNP predicted to be under HIV-1 positive directional selection were selected for study in this thesis. Two clinical strains named EX30$^{Q1939/A605}$ and EU111^{N1759} contained SNP in *pks2* whilst a third, EX86S^{12}, contained a SNP in *Rv2954c*. To reduce any impact of background genetic difference which may exist between these three clinical strains and control laboratory strains used for comparisons, three phylogenetically close strains to each of the three clinical strains with SNP of interest were also selected for analysis.

The phylogenetic tree of all strains analysed by Koch *et al*. (2017) [28] shows the close relationship between the strains predicted to have a SNP under HIV-1 positive directional selection and their selected phylogenetically close clinical control strains (Figure 3.1). The tree shows that the clinical pairs EX86S12/EU268R12 as well as *EU111^{N1759}*/EU40^{T1759} were the most closely related of the pairs. EX30$^{Q1939/A605}$ and MRC16$^{P1939/A605}$ are also closely related with MRC16$^{P1939/A605}$ in a close out group of the EX30$^{Q1939/A605}$ node. All strains except MRC16$^{P1939/A605}$ were isolated from HIV co-infected TB patients. EX86S12S12, EU268R12, EX30$^{Q1939/A605}$ and MRC16$^{P1939/A605}$ are lineage 4, whilst *EU111^{N1759}* and EU40^{T1759} are lineage 2.

EX30$^{Q1939/A605}$ contains a SNP in position 5817 in *pks2*, which changes a proline in position 1939 to a glutamine (P1939Q) (Fig. 3.1; Table 3.2), and EX86S12 contains a SNP in position 36 of *Rv2956* which changes an arginine in position 12 to serine (R12S) (Fig. 3.1, Table 3.2). The identified SNP under HIV-1 selective pressure in *EU111^{N1759}* was in *pks2* at position 5277 that results in a threonine to asparagine substitution in position 1759 (T1759N) (Fig. 3.1; Table 3.2). These strains were paired with strains that are phylogenetically close but did not have the SNP of interest.

Strain EX86S12 was paired with a phylogenetically close strain EU268R12 (Fig. 3.1, Table 3.1) without the SNP of interest in position R12S and *EU111^{N1759}* was paired with strain EU40^{T1759}, lacking the SNP at position T1759N. EX30$^{Q1939/A605}$ was paired with a phylogenetically close strain MRC16$^{P1939/A605}$, which does not have the SNP predicted to be under HIV-1 positive directional selection at position 1939. However, further analysis of

EX30$^{Q1939/A605}$ and MRC16$^{P1939/A605}$ sequences identified an additional non-synonymous SNP in *pks2* in position 1815 of which is shared by both strains, in comparison to H37Rv, and changes a threonine in position 605 to an alanine (T605A). This SNP was included in the project to determine whether it augments the phenotype of EX30$^{Q1939/A605}$ which has both P1939Q and T605A, whilst MRC16$^{P1939/A605}$ only has T605A, in comparison to their same lineage (4) reference strain H37Rv.

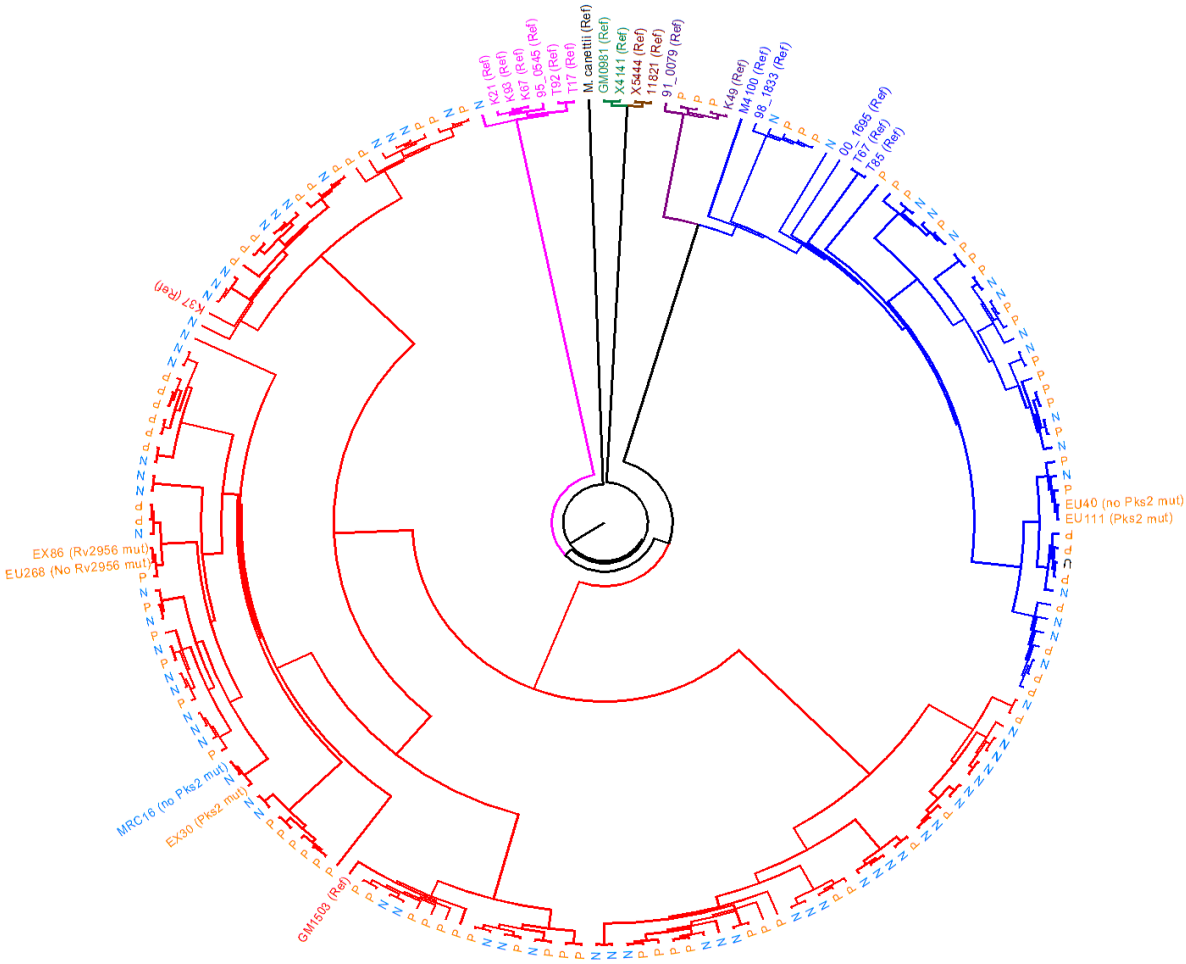

Figure 3.1. Phylogenetic analysis of strains used in this project.
Strains isolated from Khayelitsha, South Africa, underwent whole genome sequencing. An evolutionary predictive model MEDS was used to detect SNP under HIV-1 positive selection [28]. This figure is adapted from (Koch et al., 2017). Strains EX30$^{Q1939/A605}$ and EU111^{N1759} have non-synonymous SNP in pks2, whilst and EX86S12 has a SNP in gene Rv2956c. The closely related strains MRC16$^{P1939/A605}$ (paired with EX30$^{Q1939/A605}$) and EU40^{T1759} (paired with EU111^{N1759}) and EU268R12 (paired with EX86S12) do not have the SNP predicted to under HIV-1 positive directional selection. Branch nodes indicate TB patient HIV status: uninfected (N, blue) or infected (P, orange). Strains branches are coloured by lineage; red: lineage 4, blue lineage 2, pink: lineage 1, maroon: lineage 3.

In this chapter the phenotype of these six clinical strains was compared to three well characterised laboratory strains: two L4 strains, H37Rv$^{P1939/T605}$ and CDC1551^{WT}, and one L2 strain HN878^{WT} (Table 3.1). The following results describe the cording phenotype, lipid production and *in vitro* cytokine profiles produced by MDM infected with these selected clinical and laboratory strains of *Mtb.*

Table 3.1. The resulting amino acid change by the SNP identified to be under HIV-1 selective pressure in the clinical isolate and its phylogenetically close paired strain.

Strain	SNP under HIV-1 selection	Amino acid change	Paired Strain
EX30$^{Q1939/A605}$	*Pks2*: 5817	Proline → Glutamine	MRC16$^{P1939/A605}$
EU111^{N1759}	*Pks2:* 5277	Threonine → Asparagine	EU40^{T1759}
EX86S12	*Rv2956:* 36	Arginine → Serine	EU268R12
Laboratory control strains			
H37Rv$^{P1939/T605}$	Lineage 4 matched control strain		
CDC1551^{WT}	Lineage 4 matched control strain		
HN878^{WT}	Lineage 2 matched control strain		

3.2. Results

3.2.1. Characterising cording phenotypes of clinical strains cultured in the absence of Tween-80

Firstly, I wanted to analyse whether the strains differed in cording phenotype when grown in liquid media without a detergent, as the impact of SNP on lipid-induced phenotypes, such as cording [13], are important to understand. To achieve this, I cultured the laboratory and clinical strains in liquid 7H9 media without adding Tween 80 detergent and analysed samples using a widefield microscope (ZOE Fluorescent Cell Imager, BioRad), as illustrated in Fig. 3.2.

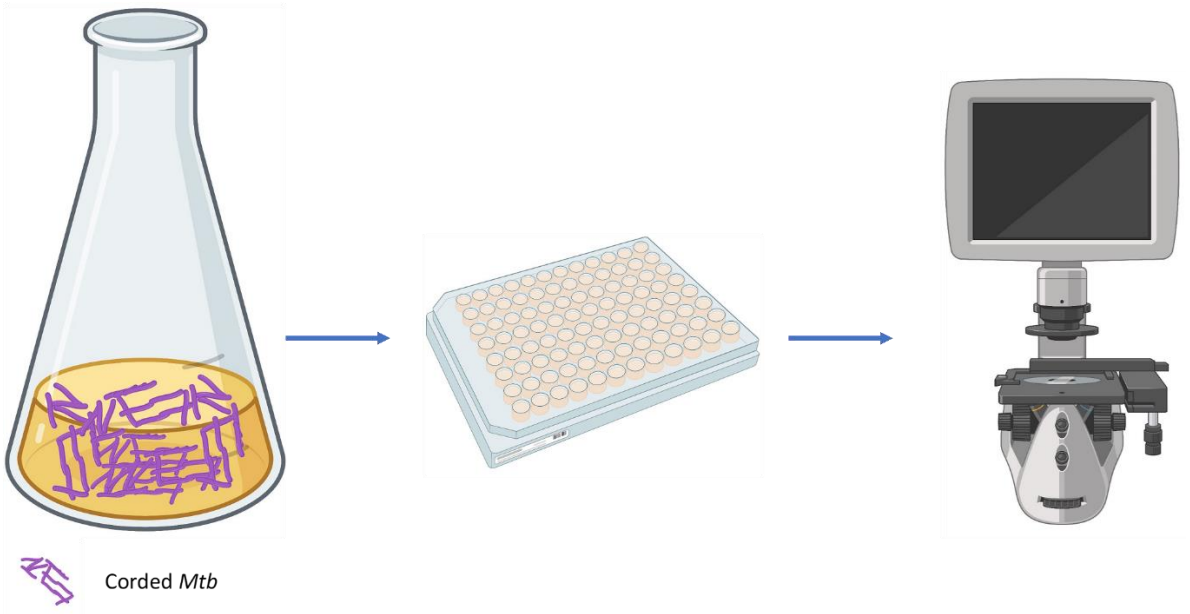

Figure 3.2. A schematic showing show the visualisation of Mtb strains under the widefield microscope.

Mtb cultures were grown in 7H9 broth for 10 days in the absence of Tween 80, 100 µL were transferred to a flat bottomed 96-well plate and then viewed using the ZOE cell imager.

To start, I examined cording of laboratory strains H37Rv$^{P1939/T605}$, HN878^{WT} and CDC1551^{WT} cultured for 10 days without shaking in detergent free media. I observed that all formed clumps to different degrees, but a distinct cording phenotype was absent (Fig. 3.3).

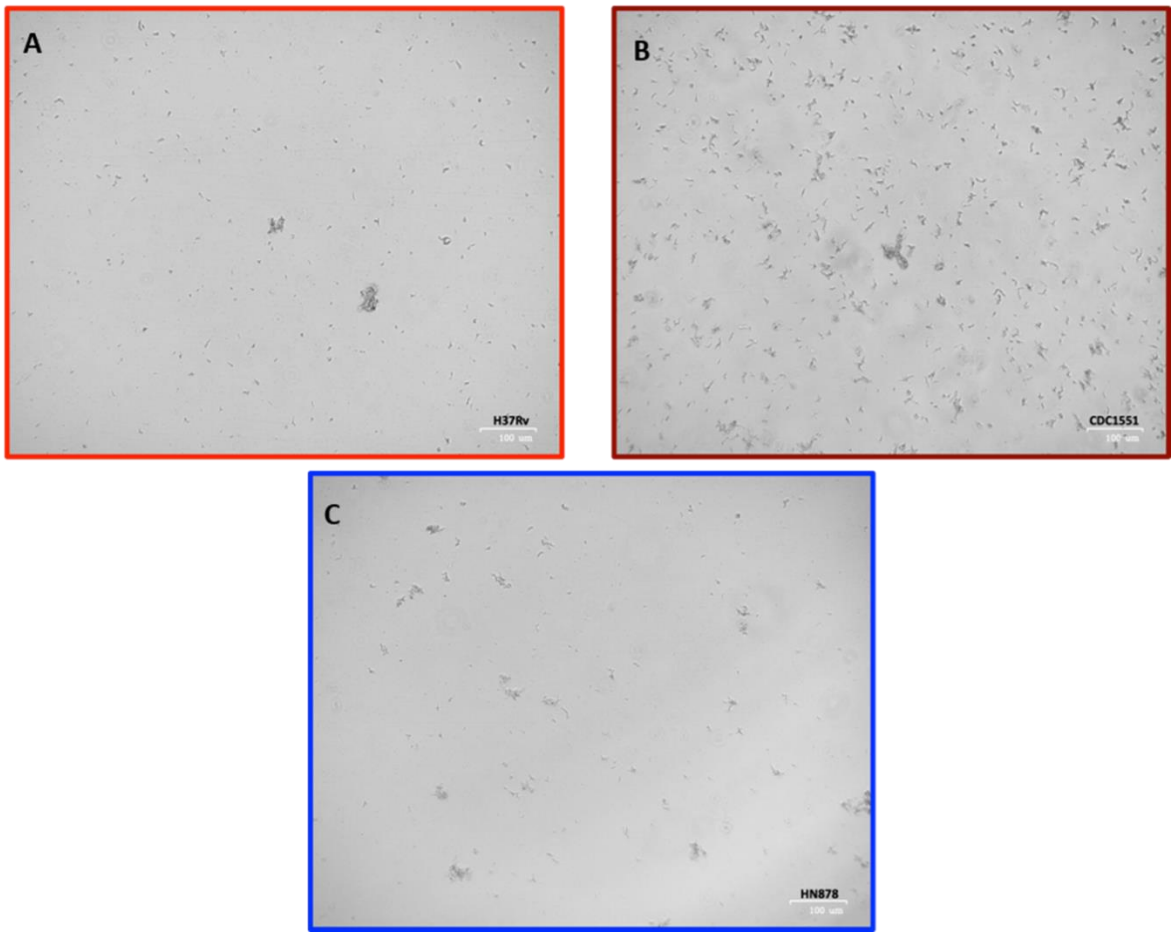

Figure 3.3. Gross phenotype of *Mtb* laboratory strains grown in absence of Tween 80.

Mtb laboratory strains H37Rv$^{P1939/T605}$ (A), CDC1551^{WT} (B) and HN878^{WT} (C) were cultured in 5 mL 7H9 media with Tween 80 for 10 days. The 10th day culture was used to sub-culture 1 mL into 50 mL of 7H9 media without Tween 80. One hundred microliters of culture were viewed using a Zoe fluorescent Cell Imager. The images show clumping. Scale bar indicates 100 μm.

Next, I wanted to assess whether the cording phenotype was present in any of the selected clinical strains (Fig. 3.4). I observed that the degree of clumping observed in EX86^{S12} (Fig. 3.4A), EU268^{R12} (Fig. 3.4B) and EU40^{T1759} (Fig. 3.4F) cultures was minimal and these strains did not exhibit cording. By comparison, the other three clinical strains, EX30$^{Q1939/A605}$ (Fig. 3.4B), EU111^{N1759} (Fig. 3.4C) and MRC16$^{P1939/A605}$ (Fig. 3.4E) displayed severe cording and clumping during growth in the absence of Tween 80. The degree of the cording and clumping phenotype varied between the strains. EU111^{N1759}, one of the clinical strains of interest, was the least corded amongst the three strains that showed cording. EX30$^{Q1939/A605}$, another clinical strain of interest, formed long cords and spiral shaped serpentine structures. Its control strain, MRC16$^{P1939/A605}$, had the most severe cording phenotype observed of all the *Mtb* cultures. The cords observed in strains was accompanied by a dark clumpy material. MRC16$^{P1939/A605}$ had

the strongest phenotype, with cords that were long and thick in width compared to cording from all other strains.

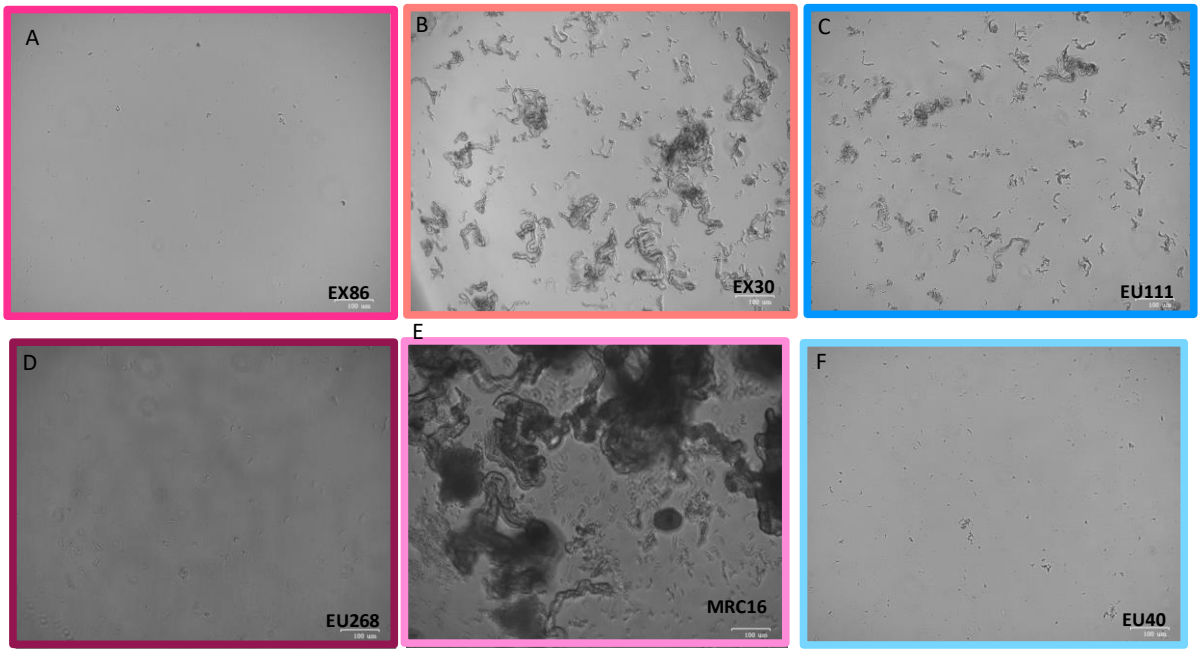

Figure 3.4. Cording phenotype of *Mtb* clinical strains used in this project.

Mtb clinical strains were cultured in 7H9 broth for 10 days in the absence of Tween 80. One hundred microliters of culture were viewed using a Zoe fluorescent Cell Imager. The images shown here represent cording phenotype in (**A**) EX86^{S12}, (**B**) EX30$^{Q1939/A605}$, (**C**) EU111^{N1759}, (**D**) EU268^{R12}, (**E**) MRC16$^{P1939/A605}$ and (**F**) EU40^{T1759}. Lineage 4 strains are outlined in shades of red and lineage 2 strains in shades of blue. Scale bar indicates 100 μm.

3.2.2. Lipid characteristics of *Mtb* laboratory and clinical strains analysed by thin layer chromatography

To describe the lipid phenotypes in strains analysed, thin layer chromatography (TLC) was used to analyse the lipids. To this end, I cultured the different *Mtb* clinical and laboratory strains in media without Tween 80 supplementation. Heat-killed culture pellets were shipped to Dr Apoorva Bhatt at Birmingham University. Dr Bhatt extracted polar and apolar lipids from the different strains and performed TLC analysis on equivalent quantities of extracted lipids from each strain (Fig. 3.5).

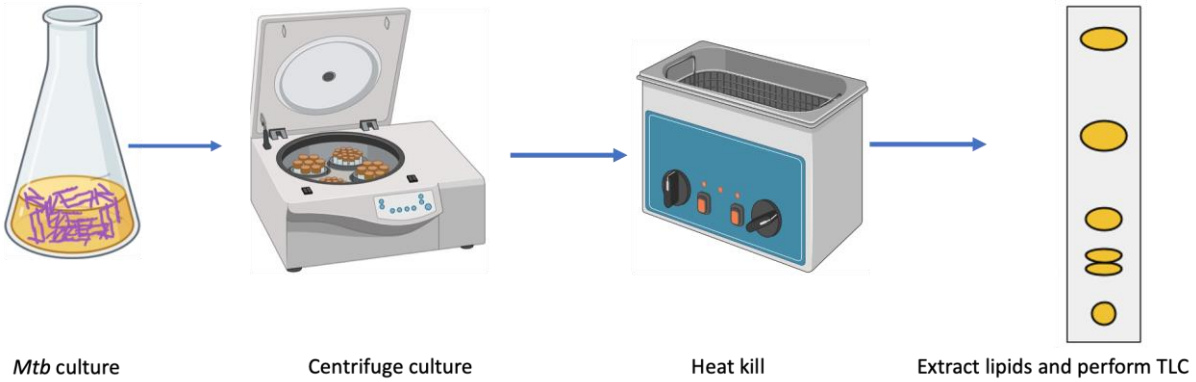

Figure 3.5. Schematic of preparing *Mtb* clinical and laboratory strains for lipid analysis.
Mtb clinical strains were cultured in 5 mL of 7H9 media without detergent supplementation for 10 days. One millilitre of the 5 mL culture was sub-cultured in 50 mL of 7H9 media without detergent supplementation for 10 days. The cultures were centrifuged, supernatant removed, and bacterial pellets heat-killed at 80 °C for 1 hour in a water bath. Heat-killed *Mtb* pellets were sent to Dr Apoorva Bhatt for lipid extraction and thin layer chromatography (TLC) analysis.

Extracted lipids were first analysed for the presence of SL-1, TDM, and DAT in the cell wall of the panel of *Mtb* strains. As expected, SL-1 is present in the cell wall extract of all the laboratory strains (Fig. 3.6A-C). This lipid was also detected in the extract of clinical strain MRC16$^{P1939/A605}$ (Fig. 3.6 H), and there is a spot in *EU111*^{N1759} (Fig. 3.6F) and EU40^{T1759} (Fig. 3.6I) which could be SL-1, but in these gels this lipid spot is observed to have migrated lower in the TLC than where SL-1 is expected, in comparison to the gels from the other strains. Other clinical strains including EX30$^{Q1939/A605}$ (Fig. 3.6E), EX86^{S12} (Fig. 3.6D), and EU268^{R12} (Fig. 3.6G) are all missing SL-1 in their lipid extracts. Interestingly EX30$^{Q1939/A605}$ and MRC16$^{P1939/A605}$ are paired clinical isolates with EX30$^{Q1939/A605}$ containing a SNP in *pks2* and MRC16$^{P1939/A605}$ without (Table 3.2). The TLC data for these strains provides tentative but tantalising evidence that the SNP of interest in these strains may be responsible for the TLC phenotype, with EX30$^{Q1939/A605}$ missing SL-1 whilst it is present in MRC16$^{P1939/A605}$. Other lipids analysed here were DAT and TDM, with both lipids present in the lipid extract for all the strains analysed here (Fig. 3.6).

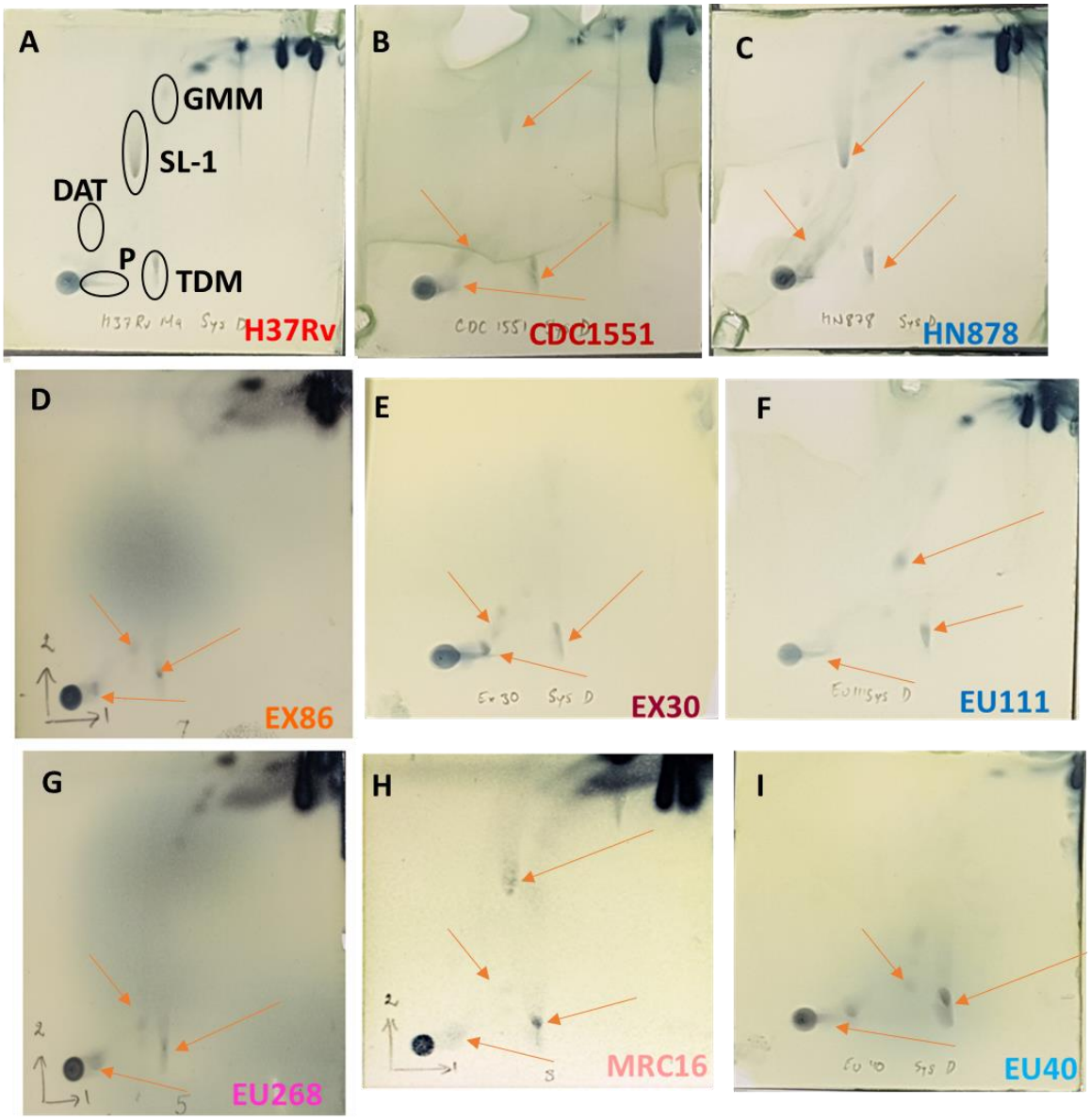

Figure 3.6. TLC analysis of SL-1, TDM, GMM and DAT from the cell wall of clinical and laboratory strains.

All the strains were cultured media without Tween 80. The strains were allowed to grow for 10 days. The cultures were centrifuged, and the media discarded, and the pellet was heat-killed at 80 °C for 1 h. The pellet was used to extract polar and apolar lipids, which were analysed by TLC for laboratory strains (**A**) H37Rv$^{P1939/T605}$, (**B**) CDC1551^{WT}, (**C**) HN878^{WT}, and clinical strains (**D**) EX86^{S12}, (**E**) EX30$^{Q1939/A605}$, (**F**) EU111^{N1759}, (**G**) EU268^{R12}, (**H**) MRC16$^{P1939/A605}$, (**I**) EU40^{T1759}. Middle row is clinical strain of interest and below is paired control clinical strain.

Next, the presence of PDIM was analysed in the cell wall of the different strains of *Mtb*. PDIM was present in the cell wall extract of all the strains except the cell wall of MRC16$^{P1939/A605}$ (Fig. 3.7). PDIM spots on the TLC plate for the laboratory strains (Fig. 3.7A-C) and *EU111*^{N1759} (Fig. 3.7F), EU40^{T1759} (Fig. 3.7G) and EU268^{R12} (Fig. 3.7I) were more pronounced than other

strains. Although TLC is not a quantitative method, the quantity of samples loaded on the TLC was standardised for all strains, so a brighter spot could be interpreted as an indication that the lipid quantities may be elevated in the loaded sample. By comparison, the TLC spots for EX86^{S12} (Fig. 3.7D) and EX30$^{Q1939/A605}$ (Fig. 3.7E) were less intense, suggesting that these samples had lower quantities of the lipid. Together with Fig. 3.6, these results show that EX30$^{Q1939/A605}$ has PDIM but is missing SL-1, whilst its close paired strain MRC16$^{P1939/A605}$ is missing PDIM but has SL-1. All the other paired strains appeared to produce similar cell wall lipids, in the panel of lipids that were measured for these experiments.

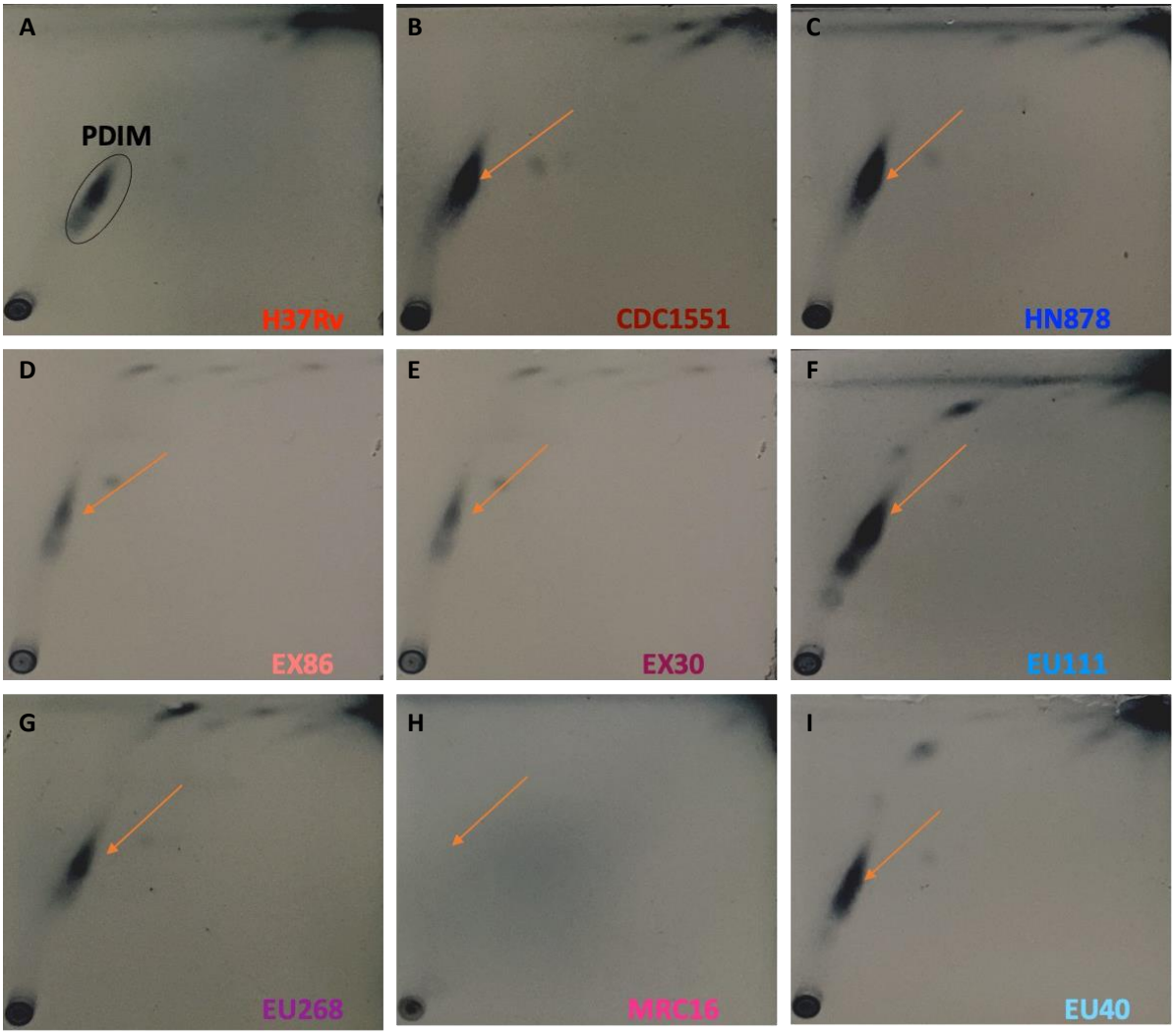

Figure 3.7. Analysis of PDIM in the cell wall of clinical and laboratory strains of Mtb.
All the strains were cultured media without Tween 80. The strains were allowed to grow for 10 days. The cultures were centrifuged, and the media discarded, and the pellet was heat-killed at 80 °C for 1 h. The pellet was used to extract polar and apolar lipids, which were analysed by TLC for laboratory strains (**A**) H37Rv$^{P1939/T605}$, (**B**) CDC1551^{WT}, (**C**) HN878^{WT}, and clinical strains (**D**) EX86^{S12}, (**E**) EX30$^{Q1939/A605}$, (**F**) EU111^{N1759}, (**G**) EU268^{R12}, (**H**) MRC16$^{P1939/A605}$, (**I**) EU40^{T1759}. Middle row is clinical strain of interest and below is paired control clinical strain.

Free FA and free MA from the lipid extracts of the clinical and laboratory strains were also analysed. All the strains here produced free FA and free MA in their cell wall (Fig. 3.8). The TLC spots were brighter in the laboratory strains (Fig. 3.8A-C), suggesting that the lipids are present in higher levels in these strains as compared to clinical strains. The intensity of the spots varied between the clinical strains with EX86^{S12} (Fig. 3.8D), *EU111*^{N1759} (Fig. 3.8F), EU268^{R12} (Fig. 3.8G) and EU40^{T1759} (Fig. 3.8I) showing similar spot intensities. The intensity of the free FA and free MA was lower in the TLC of EX30$^{Q1939/A605}$ (Fig. 3.8E) and MRC16$^{P1939/A605}$ (Fig. 3.8H), and the MRC16$^{P1939/A605}$ lipid extract appears to lack free MA altogether, with a faint spot of free FA.

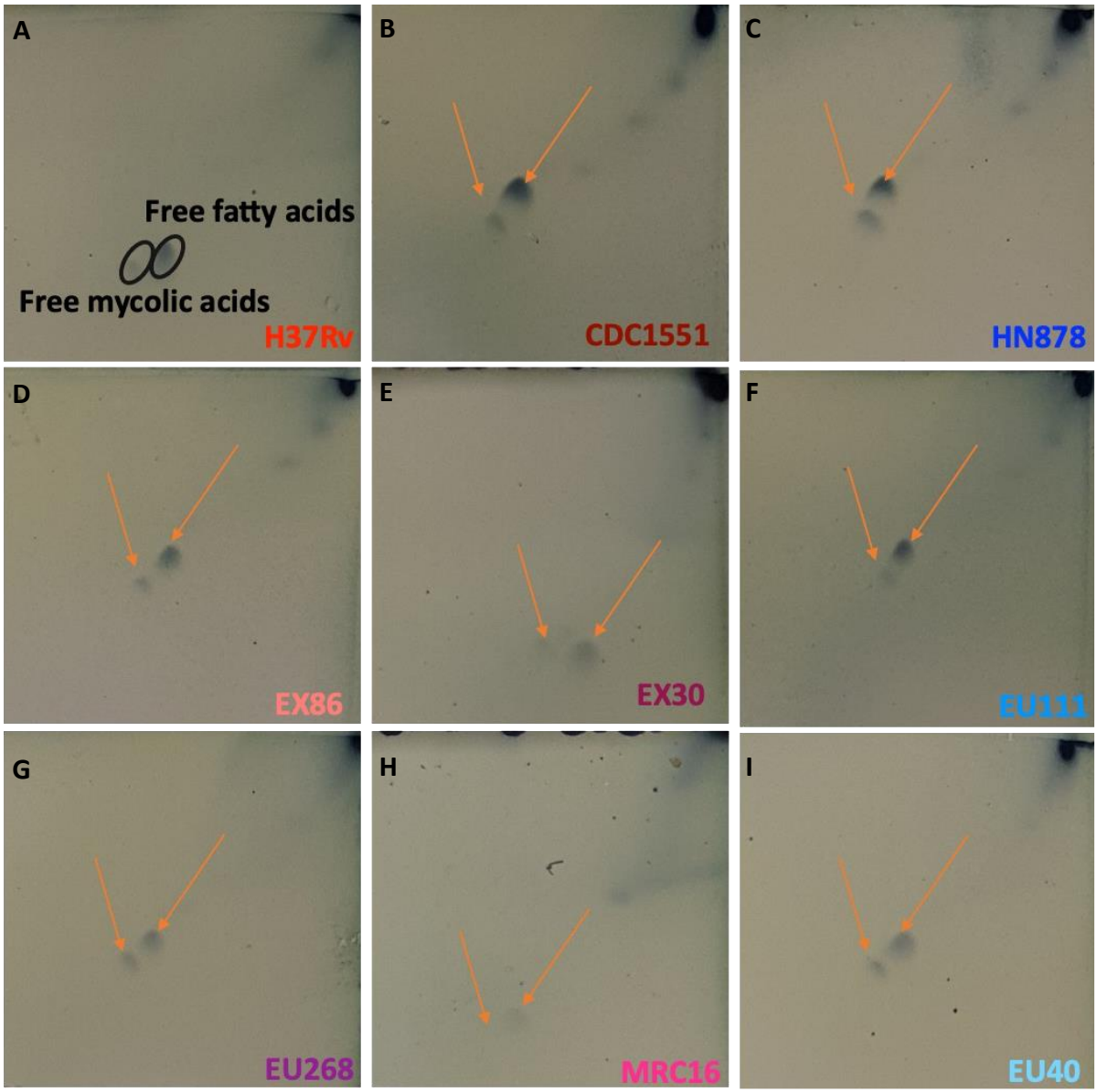

Figure 3.8. TLC analysis of free fatty acids and mycolic acids from clinical and laboratory strains.

The strains were cultured media without Tween 80 for 10 days. The cultures were centrifuged, and the media discarded, and the pellet was heat-killed at 80 °C for 1 h. The pellet was used to extract polar and apolar lipids, which were analysed by TLC for laboratory strains (**A**) H37Rv$^{P1939/T605}$, (**B**) CDC1551^{WT}, (**C**) HN878^{WT}, and clinical strains (**D**) EX86^{S12}, (**E**) EX30$^{Q1939/A605}$, (**F**) EU111^{N1759}, (**G**) EU268^{R12}, (**H**) MRC16$^{P1939/A605}$, (**I**) EU40^{T1759}. Middle row is clinical strain of interest and below is paired control clinical strain.

Finally, the production AC_2PMI_6, AC_2PMI_2 and phospholipid was assessed. These lipids were all clearly present in the lipid extracts from all the laboratory strains (Fig. 3.9A-C) and all the clinical strains EX86^{S12} (Fig. 3.8D), EX30$^{Q1939/A605}$ (Fig. 3.8E), EU111^{N1759} (Fig. 3.8F), EU268^{R12} (Fig. 3.8G) and EU40^{T1759} (Fig. 3.8I), excluding the extract of MRC16$^{P1939/A605}$ (Fig. 3.8H). MRC16$^{P1939/A605}$ lipids ran distinctly different on the gel from other strain extracts, resulting in the lipids not migrating as far and thus complicating the identification of each lipid for this strain. There appears to be strong P lipid profile staining at the top of the gel, whilst AC_2PMI_6, and AC_2PMI_2 spots are harder to distinguish, and fainter compared to extracts from the other strains. Together Fig. 3.6-3.9 show that almost all lipids were low in MRC16$^{P1939/A605}$, yet this strain displayed one of the most pronounced cording phenotypes (Fig. 3.4). One potential explanation is that lipids were less efficiently extracted from this strain due to the strong cording structure.

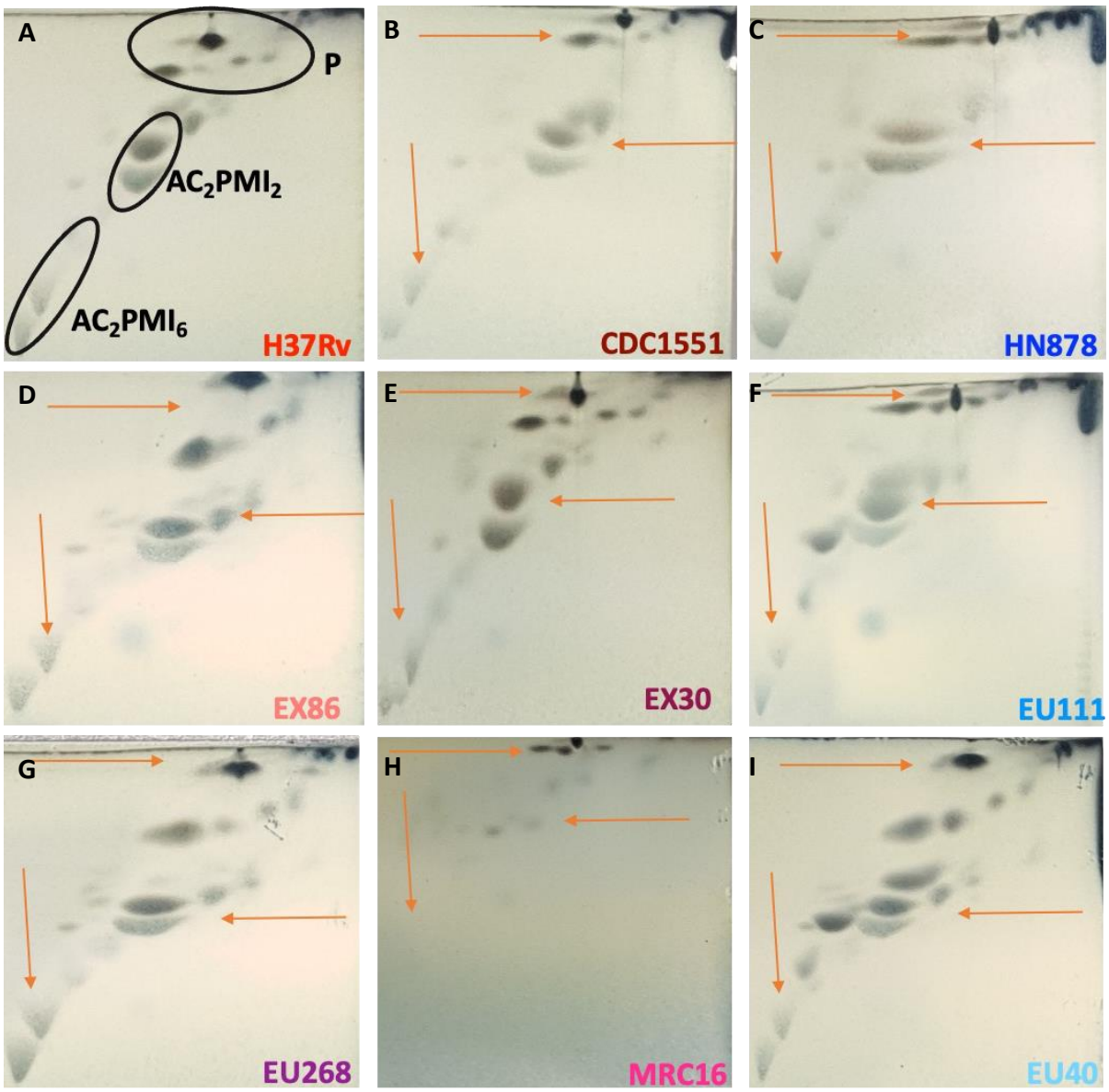

Figure 3.9. TLC analysis of AC2PMI6, AC2PMI2 and phospholipid a of clinical and laboratory strains.

All the strains were cultured media without Tween 80. The strains were allowed to grow for 10 days. The cultures were centrifuged, and the media discarded, and the pellet was heat-killed at 80 °C for 1 h. The pellet was used to extract polar and apolar lipids, which were analysed by TLC for laboratory strains (**A**) H37Rv$^{P1939/T605}$, (**B**) CDC1551^{WT}, (**C**) HN878^{WT}, and clinical strains (**D**) EX86^{S12}, (**E**) EX30$^{Q1939/A605}$, (**F**) EU111^{N1759}, (**G**) EU268^{R12}, (**H**) MRC16$^{P1939/A605}$, (**I**) EU40^{T1759}. Middle row is clinical strain of interest and below is paired control clinical strain.

3.2.3. Analysis of cytokine secretion by MDM infected with the different strains of *Mtb*

A total of nine strains of *Mtb* were selected for this project, including three clinical pairs and three laboratory strains (chapter 2; Table 3.2). The cording and cell wall lipid phenotype were

analysed between all the strains. These data showed that EX86^{S12} and EU268^{R12} showed similarities in both growth in liquid media (Fig. 3.4) and cell wall lipids (Fig. 3.6 – Fig. 3.9). Given that these strains are phylogenetically close pairs (Fig. 3.1), I reasoned that their similar cording phenotype and cell wall lipids are unlikely to result in differential cytokine induction upon MDM infection and therefore unlikely to differentially affect HIV-1 replication and production. To this end, these two strains were not taken forward for infection of MDM in further experiments.

To further characterise the phenotype of the remaining *Mtb* strains being studied, I analysed cytokine production from MDM when infected with three *Mtb* laboratory stains and the two *Mtb* clinical strain pairs of interest following TLC results. To do this, I infected M1 and M2 MDM from six different donors with the panel of *Mtb* strains and harvested the SN for cytokine analysis by Luminex, after 24 and 96 hours of infection. MDM were polarised to both M1 and M2 because, M1 MDM are associated with a pro-inflammatory phenotype, and M2 MDM that are linked to resolution of inflammation and participating in tissue remodelling [31]. Therefore, using both M1 and M2 MDM might provide a broader spectrum of *Mtb* induced cytokine secretion data. Following data cleaning, sample clustering according to raw cytokine concentrations were visualised using principal component analysis (PCA) in Qlucore omics software. A PCA is a multivariate analysis tool that reduces a large multivariate data set to a limited number of principal components which explain the majority of the variance in the dataset [32].

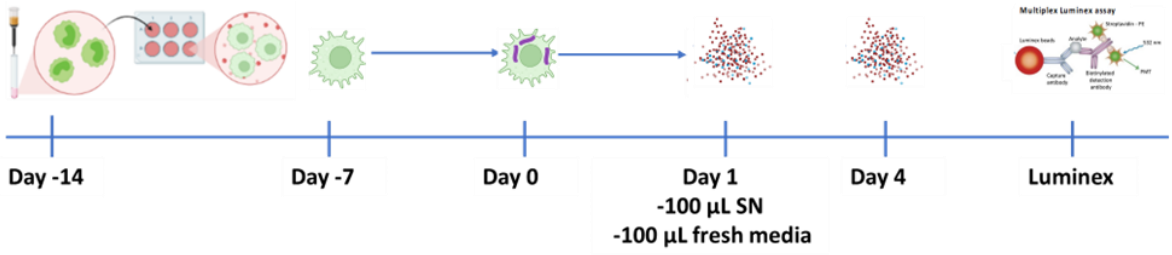

Figure 3.10. Experimental flow of MDM infection with *Mtb* and analysis of cytokines from the SN. Monocytes were polarised over 7 days into either M1 MDM with GM-CSF or M2 MDM with M-CSF. Polarised MDM were incubated for seven days, with the media refreshed every three days, to replicate the period during which HIV-1 infection will be performed in subsequent co-infection experiments. The media was discarded and refreshed with media containing *Mtb* at an MOI of 1. The infection was allowed to continue for four hours (h) and then media was replaced to remove all cell free *Mtb*. The *Mtb* infected MDM

were incubated, and supernatant (SN) was harvested at 24 h and 96 h post *Mtb* infection, with SN cytokines quantified by Luminex assay.

To analyse cytokine secretion induced by infection with the different strains in MDM, first I looked at possible sources of variation other than infection with different strains of *Mtb* by using a PCA plot to analyse sample clustering. Here, I used the PCA to determine the clustering patterns of the MDM phenotypes, to determine how much the MDM phenotype (M1 and M2) contribute to the data variation. As indicated in Fig. 3.9A, M1 and M2 MDM did not have a differential clustering pattern in the PCA. In fact, the clustering pattern of M1 and M2 overlap. Related variables cluster together in PCA plot and distinct clusters represent unrelated variables. As such, these data suggest that differences in MDM phenotype contribute minimally to the cytokine variation observed in the data. I also stratified the analysis according to the donors, to assess whether donor differences also contributed to the variation observed in the data. According to the PCA, data donor variability was not major contributor to the variation in cytokine secretion data (Fig. 3.9B), although there was a small separation evident between donors along principal component 2 (PC2). Next, I applied PCA to determine whether different strains of *Mtb* used during infection contribute to differences in cytokine secretion by MDM. As indicated by Fig. 3.9C, most of the contribution to variation in cytokine secretion along PC1 results from different strains, representing 66% of variation in the data. Uninfected cells are most separated from MRC16$^{P1939/A605}$ infected cells, with MDM infected from the other strains mostly clustering between these two.

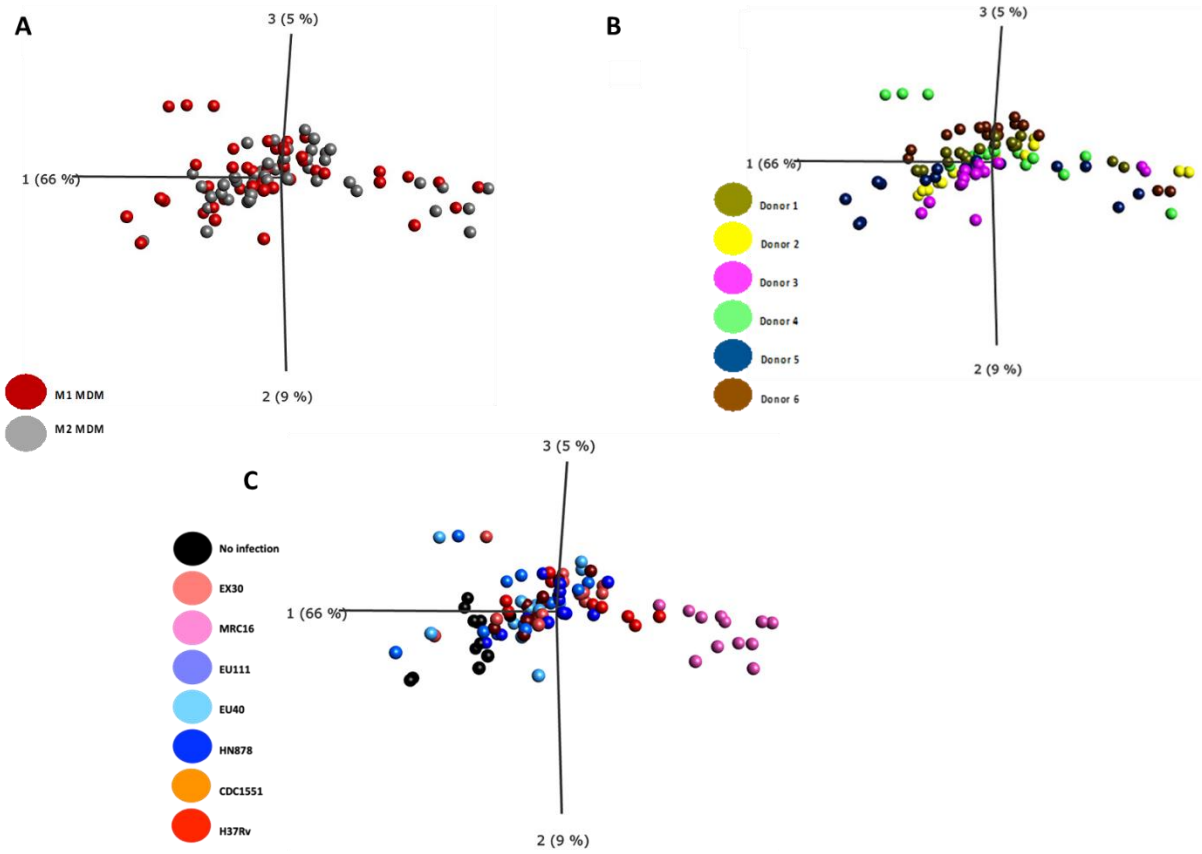

Figure 3.11. Principal component analysis showing multiple variables contributing to variation in cytokine production by MDM infected with a panel of *Mtb* strains.

(A) MDM phenotype had minimal effect on PCS clustering, (B) whilst donor differences were evident. Monocytes from 6 donors were polarised to M1 and M2 MDM. MDM were infected with different *Mtb* strains and incubated for 96 h. The supernatant was harvested and used for quantifying 25 cytokines by Luminex assay. Luminex data was analysed by Qlucore omics, each dot represents coordinates of each donor in the PCA space for n=6 donors.

3.2.4. Host response to infection with *Mtb* laboratory strains is diverse

Comparing individual cytokine differences between strains, first, I compared cytokine secretion induced by the laboratory strains at 96-hours and 24 hour-post-infection. Cytokines that had a significant fold change differences in at least one comparison are listed in the tables below. Where there was no significant fold change difference the value is not indicated, and the p-value is marked with ns. Raw data, including interquartile ranges are in supplementary tables at the end of this section.

At each time point 24-hours and 96-hours, the magnitude of cytokine secretion was comparable for all strains. That is to say that between HN878^{WT}, CDC1551^{WT} and H37Rv$^{P1939/T605}$ all produced comparable cytokines when compared to each other, however, there were certain

cytokines that were increased by each strain relative to uninfected MDM. All the laboratory strains increased secretion of GM-CSF, CXCL8 and CCL4 compared to uninfected MDM 24-hours (Table 3.2; Supplementary Table 3.1), while CXCL8, CCL4, CCL2, IL-12 and IL-6 were increased at the 96-hour time-point (Table 3.2; Supplementary Table 3.3). The L2 HN878^{WT} strain on average increased the secretion of more cytokines compared to L4 CDC1551^{WT} and H37Rv$^{P1939/T605}$ in relation to uninfected controls at 24-hours post-infection. In fact, only infection with HN878^{WT} resulted in increased secretion of CCL3 (5.5-fold change; p = 0.0046) compared to uninfected MDM. There was a further increase in the secretion of cytokines in MDM infected with H37Rv$^{P1939/T605}$ at 96-post infection, with H37Rv$^{P1939/T605}$ having higher average increased in cytokine secretion.

MDM infected with H37Rv$^{P1939/T605}$ secreted twice as much IL-6 96 hours post-infection compared to CDC1551^{WT} infected MDM at the same time point. Furthermore, infection with H37Rv$^{P1939/T605}$ also significantly increased the secretion of CCL3 (5.73-fold; p=0.0051), where these cytokines were not significantly increased by either CDC1551^{WT} or HN878^{WT} 96 hours post-infection. It is surprising that early on during infection H37Rv$^{P1939/T605}$ did not significantly increase the production of cytokines such as IL-6, TNF and CCL3 compared uninfected control. This data points to *Mtb* strains possibly deploying diverse mechanisms during infection which lead to a variation in host responses and the time taken for the host to responds to infection.

Table 3.2. Comparison of cytokines secreted 24 hours and 96 hours post-infection of MDM with the laboratory strains.

	H37Rv$^{P1939/T605}$ v Uninfected		CDC1551^{WT} v Uninfected		HN878^{WT} v Uninfected	
Cytokines harvested 24 hours post infection						
Analyte	Fold change	p-value	Fold change	p-value	Fold change	p-value
CCL4	9.93	0.0245	12.57	0.0100	15.88	0.0021
GM-CSF	1.99	0.0301	2.14	0.0301	2.31	0.0201
CXCL8	1.79	0.0207	23.23	0.0068	23.77	0.0034
IL-6	-	ns	21.25	0.0032	31.35	0.0011
IL-4	-	ns	3.46	0.0050	4.03	0.0021
TNF	-	ns	2.47	0.0153	3.39	0.0097
CCL3	-	ns	-	ns	5.56	0.0046
Cytokines harvested 96 hours post infection						
IL-6	26.05	<0.0001	13.67	0.0001	23.41	<0.0001
CXCL8	15.08	<0.0001	10.14	0.0005	10.79	0.0003
CCL4	10.43	<0.0001	2.48	0.0164	3.19	0.0014
IL-12	8.92	0.0004	7.24	0.0012	9.64	0.0002

CCL3	5.72	0.0051	-	ns	-	ns
IL-1β	4.94	0.0004	-	ns	4.37	0.0065
CCL2	2.38	0.0092	2.33	0.0274	2.68	0.0203
IL-2R	2.77	0.0009				
CXCL9	1.76	0.0076	-	ns	-	ns

Kruskalis-Wallis multiple comparison test with false discovery rate (FDR). p-value shown for comparisons with FDR of <0.1. Fold change of non-significant (ns) values is not shown (-).

3.2.5. MRC16$^{P1939/A605}$ increases the secretion of cytokines compared to EX30$^{Q1939/A605}$

Initial cording analysis (Fig. 3.4) and TLC lipid characterisation (Fig. 3.6 - Fig. 3.9), indicated that there may be interesting phenotypic differences between the two phylogenetically close strains EX30$^{Q1939/A605}$ and MRC16$^{P1939/A605}$, which differ only by a single *pks2* mutation (Table 2.4), and share a second *pks2* mutation as compared to H37Rv$^{P1939/T605}$ (Table 2.4). Therefore, I applied a more in-depth analysis of differences in MDM cytokine production when infected with these two strains and a lineage matched laboratory strain H37Rv$^{P1939/T605}$, comparing each to their uninfected controls and then comparing fold difference in secretion between the strains directly. Infection with MRC16$^{P1939/A605}$ resulted in increased secretion of cytokines compared to the donor-matched uninfected control at both 24-hours and 96-hours post-infection (Table 3.3; Supplementary Table 3.2; Supplementary Table 3.4). Furthermore, MRC16$^{P1939/A605}$ infection increased greater secretion of cytokines 24-hours and 96-hours post-infection compared to both the clinical matched strain EX30$^{Q1939/A605}$ and the laboratory matched strain H37Rv$^{P1939/T605}$ relative to uninfected control (Table 3.3). When comparing the level of induced cytokines between the paired clinical strains, MRC16$^{P1939/A605}$ infection significantly increased 14 of the 25 cytokines measured at 24-hours compared to EX30$^{Q1939/A605}$ (Table 3.3). When compared to H37Rv$^{P1939/T605}$, MRC16$^{P1939/A605}$ significantly increased all the cytokines measured except for CCL2 at 24-hours post-infection (Table 3.3). Specifically, MRC16$^{P1939/A605}$ and H37Rv$^{P1939/T605}$ significantly increased the secretion of HIV-1 infection antagonistic cytokine CCL4 by 120-fold ($p = 0.0005$) and 9.83-fold ($p = 0.0025$), respectively (Table 3.3). MRC16$^{P1939/A605}$ also increased the secretion of CCL3 another HIV-1 infection antagonist by 100-fold ($p = 0.0005$) (Table 3.3). EX30$^{Q1939/A605}$ did not result in any significant increase of cytokines compared to uninfected control at 24-hours post infection (Table 3.3; Supplementary Table 3.2; Supplementary Table 3.4). The secretion of CCL3 and CCL4 varied between 24-hours and 96-hours post-infection. These cytokines were 2x and 3x less compared to 24-hours post-infection in MRC16$^{P1939/A605}$ infection, respectively (Table 3.3). While CCL3 was not different with respect to uninfected control at 24-hours in EX30$^{Q1939/A605}$ and H37Rv$^{P1939/T605}$ infection, EX30$^{Q1939/A605}$ increased CCL3 by 3.76-fold ($p = 0.0143$) and

H37Rv$^{P1939/T605}$ by 5.72 (p = 0.0051) at 96-hours. EX30$^{Q1939/A605}$ and H37Rv$^{P1939/T605}$ also increased CCL4 by 4- and 10-fold respectively (Table 3.3). There was no difference in the induction of cytokines between EX30$^{Q1939/A605}$ and H37Rv$^{P1939/T605}$ at both time points (Table 3.3). Both EX30$^{Q1939/A605}$ and MRC16$^{P1939/A605}$ also significantly increased cytokines such as TNF, IL-6, IL-12, IL-1β, CCL2, and IL-4 which are all associated with regulation of HIV-1 replication compared to uninfected MDM at 96-hours post-infection (Table 3.3; Supplementary Table 3.4). Of these cytokines, only IL-12 was significantly increased by the lineage matched laboratory strain H37Rv$^{P1939/T605}$, compared to uninfected control. There were no cytokines that were comparably secreted by MDM infected with either EX30$^{Q1939/A605}$ or MRC16$^{P1939/A605}$ at the 96-hour time point (Table 3.3). The differences in cytokine and chemokine secretion in MDM infected with the two strains as well as the differences in cytokines between uninfected MDM could potentially influence how co-infection with the strains influences HIV-1 replication.

Table 3.3. Comparison of cytokines secreted by EX30$^{Q1939/A605}$ and MRC16$^{P1939/A605}$ infected MDM 24-hours and 96-hours post-infection

Cytokines harvested 24-hours post infection										
	EX30$^{Q1939/A605}$ v MRC16$^{P1939/A605}$		EX30$^{Q1939/A605}$ v H37Rv$^{P1939/T605}$		MRC16$^{P1939/A605}$ v H37Rv$^{P1939/T605}$		EX30$^{Q1939/A605}$ v Uninfected		MRC16$^{P1939/A605}$ v Uninfected	
Analyte	Fold change	p-value	Fold change	p-value	Fold change	p-value	Fold change	Fold change	Fold change	p-value
CXCL9	-29.02	0.0141	-	ns	44.67	0.0161	-	ns	57.63	0.0061
CXCL10	-23.32	0.0304	-	ns	6.08	0.0251	-	ns	74.40	0.0024
IFN-γ	-13.47	0.0433	-	ns	22.23	0.0023	-	ns	38.08	0.0015
IL-10	-5.31	0.0304	-	ns	8.48	0.0022	-	ns	12.76	0.0024
CCL5	-6.46	0.0061	-	ns	15.47	0.0029	-	ns	5.72	0.0141
IL-15	-4.60	0.0304	-	ns	5.33	0.0080	-	ns	6.84	0.0024
IL-5	-4.26	0.0057	-	ns	3.18	0.0325	-	ns	4.72	0.0017
IL-2	-3.99	0.0433	-	ns	6.25	0.0063	-	ns	9.14	0.0015
CCL11	-3.72	0.0061	-	ns	7.58	0.0029	-	ns	3.46	0.0141
IL-1RA	-3.29	0.0433	-	ns	3.43	0.0100	-	ns	4.12	0.0015
IFNα	-3.02	0.0433	-	ns	3.86	0.0353	-	ns	7.76	0.0015
IL-7	-2.90	0.0433	-	ns	3.82	0.0150	-	ns	5.15	0.0015
IL-17	-2.83	0.0433	-	ns	3.34	0.0162	-	ns	4.05	0.0015
IL-13	-1.63	0.0433	-	ns	2.44	0.0268	-	ns	2.72	0.0015
IL-12	-	ns	-	ns	229.39	0.0013	-	ns	368.51	0.0005
TNF	-	ns	-	ns	65.49	0.0005	-	ns	124.37	0.0005
CCL3	-	ns	-	ns	18.49	0.0034	-	ns	100.51	0.0005
IL-6	-	ns	-	ns	166.67	0.0006	-	ns	1176.30	0.0005
IL-1β	-	ns	-	ns	4.54	0.0181	-	ns	15.49	0.0005
CCL4	-	ns	-	ns	9.55	0.0084	-	ns	120.09	0.0005
IL-2R	-	ns	-	ns	8.85	0.0049	-	ns	15.70	0.0005
GM-CSF	-	ns	-	ns	22.15	0.0020	-	ns	43.32	0.0005
CCL2	-	ns	-	ns	-	ns	3.35	0.0080	6.35	0.0094
IL-4	-	ns	-	ns	7.54	0.0005	-	ns	17.92	0.0005
CXCL8	-	ns	-	ns	2.54	0.0083	-	ns	41.42	0.0009

Cytokines harvested 96-hours post infection										
	EX30$^{Q1939/A605}$ v MRC16$^{P1939/A605}$		EX30$^{Q1939/A605}$ v H37Rv$^{P1939/T605}$		MRC16$^{P1939/A605}$ v H37Rv$^{P1939/T605}$		EX30$^{Q1939/A605}$ v Uninfected		MRC16$^{P1939/A605}$ v Uninfected	
Analyte	Fold change	p-value	Fold change	p-value	Fold change	p-value	Fold change	Fold change	Fold change	p-value
IL-6	-73.47	0.0143	-	ns	58.19	0.0001	20.63	0.0143	1516.18	<0.0001
CXCL9	-27.77	0.0031	-	ns	28.84	<0.0001	1.86	0.1530	50.94	<0.0001
GM-CSF	-37.17	0.0059	-	ns	29.13	0.0024	-	ns	65.95	<0.0001
IL-12	-25.76	0.0143	-	ns	24.84	0.0003	8.89	0.0032	221.59	<0.0001
TNF	-24.65	0.0107	-	ns	50.51	0.0007	3.01	0.0247	74.39	<0.0001
CCL3	-14	0.0143	-	ns	9.19	0.0012	3.76	0.0143	52.65	<0.0001
IL-10	-7.29	0.0005	-	ns	9.1	0.0025	-	ns	8.69	0.0001
IFN-γ	-7.16	0.0059	-	ns	5.54	0.0026	-	ns	10.13	<0.0001
CCL4	-6.57	0.0143	-	ns	4.07	0.0061	6.66	0.0143	43.71	<0.0001
IL-2R	-6.23	0.0043	-	ns	5.32	0.0006	-	ns	14.75	<0.0001
CXCL10	-5.26	0.0107	-	ns	21.22	0.0001	3.18	0.0247	20.78	<0.0001
IL-1β	-4.97	0.0438	-	ns	6.31	0.0299	6.25	0.0408	31.03	<0.0001
IL-15	-4.21	0.0059	-	ns	4.32	0.0059	-	ns	7.28	<0.0001
CCL5	-4.33	0.0043	-	ns	7.6	0.0108	-	ns	4.51	0.0011
IL-5	-4.09	0.0005	-	ns	3.77	0.0393	-	ns	4.18	0.0001
IL-4	-3.48	0.0143	-	ns	5.63	0.0031	3.79	0.0143	13.20	<0.0001
IL-2	-3.32	0.0107	-	ns	4.78	0.0144	2.20	0.0247	7.33	<0.0001
IL-7	-3	0.0059	-	ns	2.8	0.0136	-	ns	5.07	0.0002
IL-17	-2.95	0.0022	-	ns	2.96	0.0296	-	ns	4.04	0.0022
CCL2	-2.77	0.0412	-	ns	3.89	0.0017	3.35	0.0080	9.28	<0.0001
IFNα	-2.56	0.0143	-	ns	3.54	0.0108	2.53	0.0143	6.47	0.0185
CCL11	-2.30	0.0031	-	ns	3.41	0.0006	-	ns	2.49	0.0002
CXCL8	-2.19	0.0143	-	ns	2.08	0.022	14.29	0.0143	31.36	<0.0001
IL-1RA	-2.27	0.0143	-	ns	-	ns	-	ns	4.14	<0.0001
IL-13	-1.76	0.0059	-	ns	-	ns	-	ns	3.40	<0.0001

Friedman's multiple comparison test with false discovery rate (FDR). p-value shown for comparisons with FDR of <0.1. Fold change of non-significant (ns) values is not shown (-).

3.2.6. EU111^{N1759} and EU40^{T1759} comparably induce the secretion of most cytokines measured in MDM

I went further to compare cytokine secretion between the lineage 2 laboratory strain HN878^{WT} and the clinical isolate pair, EU111^{N1759} which has the pks2 5277 mutation and the clinical pair EU40^{T1759}. EU111^{N1759} and HN878^{WT} significantly increased more cytokines at 24-hours post-infection relative to uninfected control compared to EU40^{T1759} (Table 3.4). In fact, IL-6 was the only cytokine that was significantly increased by EU40^{T1759} compared to uninfected control (Table 3.4). At the 96-hour time-point, it was EU111^{N1759} and EU40^{T1759} that resulted in more cytokines secreted than HN878^{WT} (Table 3.4). There were no differences in the induction of cytokines between the clinical matched strains 24-hours post-infection (Table 3.4), however, HN878^{WT}, significantly increased the secretion of IL-12, CCL4 and IL-2 compared to EU40^{T1759} at this time point (Table 3.4). I observed that at 24-hours post-infection only the clinical strain significantly increased the secretion of IL-1β relative to uninfected control (Table 3.3 – Table 3.4). There is an interesting variation in the secretion of CCL3 at both time points following infection with all the strains. In the case of EU111^{N1759} the secretion of CCL3 increased from 6.5-fold ($p = 0.0005$) compared to uninfected control to 13.68-fold ($p = 0.0002$) compared to uninfected control (Table 3.4). While infection with EU40^{T1759} did not significantly increase the secretion of CCL3 at 24-hours post-infection, there was a 7-fold increase in CCL3 at 96-hours post-infection with EU40^{T1759} (Table 3.4). The laboratory matched strain HN878^{WT} resulted in 23-fold ($p = 0.0034$) increase in CCL3 24-hours post-infection, while it did not significantly affect the secretion of CCL3 at the 96-hour time point (Table 3.4). The other HIV-1 antagonist CCL4 was significantly increased by both EU111^{N1759} (17-fold; $p = 0.0005$) and HN878^{WT} (16-fold; $p = 0.0021$) at 24-hours post-infection, while EU40^{T1759} did not affect the secretion of CCL4 at 24-hour time point. All three strains did increase the secretion of CCL4 at the 96-hour time point.

The secretion of IL-6 by EU111^{N1759} was increased by 26.7-fold ($p = 0.0014$) 24-hours post-infection, while it was increased by 17.3-fold ($p = <0.0001$) 96-hours post-infection in MDM (Table 3.4). MDM infected with EU40^{T1759} for 24-hours increased IL-6 secretion by 10.17-fold ($p = 0.008$), while MDM infected for 96-hours increased IL-6 secretion by 4.2-fold ($p = 0.0258$) compared to matched uninfected controls (Table 3.4). While the secretion relative to uninfected control is reduced between 24-hours and 96-hours for the clinical strains, for HN878^{WT} the secretion went from 15-fold ($p = 0.0002$) to 23-fold ($p = <0.0001$), between the 24-hour and

96-hour time point respectively (Table 3.4). The clinical pair EU40^{T1759} increased more cytokines 96-hours post-infection compared to EU111^{N1759} and HN878^{WT} relative to uninfected control (Table 3.4). The strain even significantly increased IL-1RA compared to both *EU111^{N1759}* and HN878^{WT} (Table 3.4), furthermore, IL2R was significantly increased by EU40^{T1759} compared to control, while it was not affected by EU111^{N1759} and HN878^{WT} (Table 3.4). The similarity in cytokine secretion phenotypes between EU111^{N1759} and EU40^{T1759} suggest that co-infection with these strains is unlikely to result in differential regulation of HIV-1 replication.

Table 3.4. Comparison of cytokines secreted in MDM 24-hours and 96hours post-infection with by $EU111^{N1759}$ or $EU40^{T1759}$

Cytokines harvested 24-hours post infection										
	$EU111^{N1759}$ v $EU40^{T1759}$		$EU111^{N1759}$ v $HN878^{WT}$		$EU40^{T1759}$ v $HN878^{WT}$		$EU111^{N1759}$ v Uninfected		$EU40^{T1759}$ V Uninfected	
Analyte	Fold change	p-value	Fold change	p-value	Fold change	p-value	Fold change	Fold change	Fold change	p-value
IL-6	-	ns	-	ns	-	ns	26.66	0.0039	10.17	0.0209
IL-12	-	ns	-	ns	-4.31	0.0433	16.49	0.0094	-	ns
CCL3	-	ns	-	ns	-	ns	6.54	0.0005	-	ns
IFNα	-	ns	-	ns	-	ns	2.49	0.0209	-	ns
CCL4	-	ns	-	ns	-2.31	0.0209	17.21	0.0005	-	ns
IL-1β	-	ns	-	ns	-	ns	4.68	0.0005	-	ns
CCL2	-	ns	-	ns	-	ns	2.62	0.0061	-	ns
IL-2	-	ns	-	ns	-1.74	0.0209	8.11	0.0094	-	ns
IL-4	-	ns	-	ns	-	ns	2.42	0.0024	-	ns
CXCL8	-	ns	-	ns	-	ns	4.21	0.0061	-	ns
Cytokines harvested 96-hours post infection										
	$EU111^{N1759}$ v $EU40^{T1759}$		$EU111^{N1759}$ v $HN878^{WT}$		$EU40^{T1759}$ v $HN878^{WT}$		$EU111^{N1759}$ v Uninfected		$EU40^{T1759}$ V Uninfected	
Analyte	Fold change	p-value	Fold change	p-value	Fold change	p-value	Fold change	p-value	Fold change	p-value
IL-6	-	ns	-1.71	0.0412	-	ns	13.68	0.0002	7.81	0.0002
CCL3	-	ns	-	ns	-	ns	1.55	0.0043	1.82	0.0004
IFNα	-	ns	-	ns	-	ns	10.07	0.0002	9.00	0.0002
CCL4	-	ns	-	ns	-	ns	2.92	0.0011	3.50	<0.0001
CCL2	-	ns	-	ns	-	ns	2.92	0.0011	3.50	<0.0001
IL-2	-	ns	-	ns	-	ns	1.79	0.0321	1.46	0.0043
CXCL8	-	ns	-	ns	-	ns	10.07	0.0002	9.00	0.0002
IL-1β	-	ns	-	ns	-	ns	5.92	0.0004	3.83	0.0002

GM-CSF	-	ns	-1.28	0.0412	-	ns	-	ns	-	ns
IL-1RA	-1.08	ns	-	ns	1.18	0.0080	-	ns	1.51	0.0247
TNF	-	ns	-	ns	-	ns	2.32	0.0412	1.68	0.0107
IL-4	-	ns	-	ns	-	ns	3.24	0.0008	2.30	0.0008
IL2R	-	ns	-	ns	-	ns	-	ns	1.55	0.0107
IL-13	-	ns	-	ns	-	ns	1.60	0.0247	1.38	0.0080
IL-12	-	ns	-	ns	-	ns	6.64	0.0022		4.45
IL-7	-	ns	-	ns	-	ns	-	ns	1.32	0.0247
CXCL10	1.32	0.0412	-	ns	-	ns	-	ns	2.17	0.0005

Friedman's multiple comparison test with false discovery rate (FDR). p-value shown for comparisons with FDR of <0.1. Fold change of non-significant (ns) values is not shown (-).

3.3. Discussion

The data presented herein demonstrate that *Mtb* strains can have different growth patterns and in their cell wall lipid profiles despite having a phylogenetically close relationship. Infection with different strains of *Mtb* results in differential secretion of cytokines by MDM, which can be linked to the presence of specific cell wall lipids. The clinical pairs with most diverse cell wall lipids also showed the most variation in cytokine induction, while clinical pairs with similar cell wall lipids showed overlapping cytokine induction capacity. This suggests that genetic diversity which may result in phenotype diversity in *Mtb* cell wall lipids might lead to strain specific patterns of growth *in vivo* and *in vitro* and strain specific modulation of host cytokine response. Koch *et al.,* (2017) [28], showed that some strains in HIV-1 co-infected patients have SNP predicted to be under HIV-1 positive selection. It is interesting that these SNP occur in genes associated with lipid metabolism, which raises to chance that these strains may induce a differential immune response in a co-infected host, which may benefit the outcome of HIV-1 co-infection. In this chapter, I characterised lipid production by the different strains with SNP in lipid metabolising genes, the cording phenotype of these strains in liquid media and looked and the cytokine induction capacities between the strains.

To reduce a potentially missed variability in *Mtb* phenotypic response, phylogenetically close strains were paired in these experiments (Fig. 3.1.), as identified by Koch *et al*. [28]. Following initial bacterial phenotyping the clinical strains $EX86^{S12}$ and $EU268^{R12}$ were not taken forward for infection of MDM in these experiments as they had a similar cording phenotype when grown in liquid culture and they had similar cell wall lipid phenotypes on TLC. For these reasons, I postulated that these strains are unlikely to result in differential induction of cytokine secretion upon MDM infection. I also reasoned that since they have the same cell wall lipid phenotype, the strains are unlikely to differentially regulate HIV-1 *in vitro*.

The strains that were taken forward for infection of MDM were the three laboratory strains and the clinical strains $EX30^{Q1939/A605}$ and matching clinical pair $MRC16^{P1939/A605}$ as well clinical stain $EU111^{N1759}$ and the matching clinical pair $EU40^{T1759}$. The laboratory strains are well characterised strains which can be used as controls. For example, clinal strains $EU111^{N1759}$ and $EU40^{T1759}$ are L2 strains and so is $HN878^{WT}$ strains, while $EX30^{Q1939/A605}$ and $MRC16^{P1939/A605}$ are L4 strains and so are $H37Rv^{P1939/T605}$ and $CDC1551^{WT}$.

There are limited differences in cytokines induction between the clinical pair of EU111^{N1759} and EU40^{T1759} when infecting MDM *in vitro*. There were more cytokines (IL-12, CCL4 and IL-2) significantly different between MDM infected with HN878^{WT} compared to EU40^{T1759} than MDM infected with EU111^{N1759} compared to EU40^{T1759} at 24-hours post-infection (Table 3.4). No cytokines were different between MDM infected with the both strains at 24-hours post-infection and only two were different at 96-hours post-infection. This data suggests that EU111^{N1759} and EU40^{T1759} likely have a cytokine induction phenotype that is related to each other, then it is to the laboratory matched lineage strain. Analysis of the cording phenotype showed that EU40^{T1759} is closer to HN878^{WT} in cording (Fig. 3.3 – 3.4). However, since the strains were subject to rigorous disruption using silica beads and medium speed centrifugation designed to remove clumps and corded cells, to obtain single cell suspensions before using them for MDM infection. Thus, this cording phenotype may not play a significant role in the observed cytokine induction phenotype. Nonetheless, the lack of difference in cytokine induction between the strains is not surprising, particularly given that these clinical strains are phylogenetically close (Fig. 3.1), and the cell wall lipids analysed here were all similar between EU111^{N1759} and EU40^{T1759} (Fig. 3.6 – 3.9). It is worth noting that TLC here was employed to detect the presence or absence of the lipids analysed. However, lipid mass spectrometry is a more robust technique which would have allowed the detection and quantification (Zarini *et al.,* 2019), of the different lipid species between the different strains.

The biggest difference in cytokine secretion induction was observed between EX30$^{Q1939/A605}$ and MRC16$^{P1939/A605}$ and H37Rv$^{P1939/T605}$ (Table 3.3). These strains had a strong cording phenotype in liquid media, but the degree of the cording was more intense in MRC16$^{P1939/A605}$ compared to EX30$^{Q1939/A605}$, while the cording was minimal for H37Rv$^{P1939/T605}$ (Fig. 3.3 – 3.4 B&E). While these strains were also, subject to the same single cell prep as above, the intensity of the cording phenotype on MRC16$^{P1939/A605}$ may have resulted in residual cording that amplified the cytokine secretion phenotype (Table 3.3). The TLC data also showed that there were several lipids that were different between the strains with EX30$^{Q1939/A605}$ missing SL-1, while MRC16$^{P1939/A605}$ is missing PDIM, and may have a modified AC_2PMI_6, and AC_2PMI_2 phenotype. Previous studies have shown that PDIM deficient strains are attenuated from growth in mice [22] and highly susceptible to early killing [33], while PDIM^{+} strains are protected from the activity of reactive nitrogen species [34]. Other studies on PDIM have shown that this lipid and glycosylated forms of PDIM i.e., PGL are anti-inflammatory in nature [35]. Reed *et al.,* (2004) [7], showed that PGL was critical in HN878 dampening the cytokine

secretion in BMM. BMM infected with H37Rv$^{P1939/T605}$ without surface PGL significantly increased the secretion of cytokines by BMDM compared to HN878^{WT} that has surface PGL. Furthermore, the authors validated the phenotype by knocking out a gene in HN878^{WT} responsible for PGL metabolism and introducing the gene in H37Rv$^{P1939/T605}$ [7]. This resulted in the mutants of HN878 without PGL increasing cytokine secretion and the mutants of H37Rv with surface PGL dampening the cytokine response (Reed *et al.,* (2004). PDIM may have resulted in reduced induction of cytokines by EX30$^{Q1939/A605}$ by comparison to MRC16$^{P1939/A605}$. I could not find reports about the role of SL-1 in cytokine production modification in the literature, however, the glycolipid is implicated in other aspects of TB pathogenesis including cough induction [17] and increased survival in THP-1 cells [36]. In their experiments Sachdeva *et al.,* (2018) [18] showed that SL-1 was responsible for lysosome biogenesis, and they postulate that lysosome rewiring by *Mtb* lipids could help with adjustment of survival and trafficking within infected macrophages [18].

For the laboratory strains, overall H37Rv$^{P1939/T605}$ increased the secretion of CCL4 CXCL8, CXCL9, and IL-6 compared to controls more than HN878^{WT} and CDC151WT. I did not observe increased cytokines secretion by H37Rv$^{P1939/T605}$ compared to HN878^{WT}, however, there is a precedent for H37Rv$^{P1939/T605}$ increasing cytokines compared to HN878^{WT}. This was reported in experiments by [37] as well as in MBDM by [7] and PBMC [38]. These observations from literature affirm my observations that L4 clinical strains EX30$^{Q1939/A605}$ and MRC16$^{P1939/A605}$ results in more elevated cytokines compared to L2 EU111^{N1759} and EU40^{T1759} clinical strains.

Cytokine signalling in macrophages is critical for response against infection [39]. Cytokines signal through a variety of transcriptional factor (TF) pathways in macrophages [40] and some of these pathways are involved in promoting TF that are bind to the HIV-1 LTR and promote HIV-1 replication (Fig. 1.2). Some studies have shown a direct link between an increased cytokine milieu and increased HIV-1 replication IL-6, TNF and CCL2 in HIV-1 production in PBMC. [38, 41]. In my data I have observed that IL-6 is broadly significantly increased by infection with all *Mtb* strains relative to uninfected MDM (Table 3.2 – Table 3.4). It is also worth noting that MRC16$^{P1939/A605}$ significantly increased IL-6, TNF and CCL2 secretion more that EX30$^{Q1939/A605}$ infection (Table 3.3), this raises the chance that MRC16$^{P1939/A605}$ will result in high HIV-1 production. The laboratory strain H37Rv$^{P1939/T605}$ also significantly increased TNF and CCL2 relative compared to HN878^{WT} and CDC1551^{WT}, possibly signalling that co-

infection with this strain might increase HIV-1 production. *Mtb* infection which increased the production of HIV-1 LTR binding TF was shown to increase HIV-1 production *in vitro* [38] [42] and in BaL fluid from HIV-1/*Mtb* co-infected patients [41]. Therefore, the differential cytokine secretion observed between MDM infected with different strains (Table 3.2 – Table 3.3) raises the possibility of increased HIV-1 replication and production in the presence of these strains. Moreover, the increased cytokine secretion observed in MDM infected with MRC16$^{P1939/A605}$ over MDM infected with EX30$^{Q1939/A605}$ increases the chance that co-infection with MRC16$^{P1939/A605}$ will increase HIV-1 production more than EX30$^{Q1939/A605}$. The following chapter will analyse cytokine secretion in MDM co-infected with HIV-1 and the different strains on *Mtb* as well as investigate the effect of increased cytokine production on HIV-1 production and replication.

3.4. Conclusion

Three pairs of phylogenetically close strains of *Mtb* with SNP identified to be under selective pressure in lipid metabolising genes were investigated to identify *Mtb* strains of interest with potential impact on HIV-1 replication in human macrophages. I identified one pair of lineage 4 strains (EX30$^{Q1939/A605}$ and MRC16$^{P1939/A605}$) with extensive lipid profile differences to each other which both induce a large number of cytokines implicated in regulating HIV-1 replication during MDM infection. A second pair of lineage 2 strains (EU111^{N1759} and EU40^{T1759}) showed more subtle difference in lipid profile by TLC, one with a strong cording phenotype which also resulted in increased IL-6 production compared to its matched strain. The third pair of lineage 4 strains (EX86S12 and EU268R12) showed no cording and no lipid phenotype differences to each other and where not taken further for analysis. The difference in cytokine induction identified between the 2 strain pairs of interest may be attributed to the cell wall lipid differences identified and these will be taken forward to investigate their impact on HIV-1 replication during MDM co-infection in Chapter 4.

3.5. References

1. Niemann, S. and P. Supply, *Diversity and evolution of Mycobacterium tuberculosis: moving to whole-genome-based approaches.* Cold Spring Harb Perspect Med, 2014. **4**(12): p. a021188.
2. Gagneux, S., et al., *Variable host-pathogen compatibility in Mycobacterium tuberculosis.* Proc Natl Acad Sci U S A, 2006. **103**(8): p. 2869-73.

3. Comas, I., et al., *Out-of-Africa migration and Neolithic coexpansion of Mycobacterium tuberculosis with modern humans.* Nat Genet, 2013. **45**(10): p. 1176-82.
4. Brennan, P.J., *Structure, function, and biogenesis of the cell wall of Mycobacterium tuberculosis.* Tuberculosis (Edinb), 2003. **83**(1-3): p. 91-7.
5. Gago, G., L. Diacovich, and H. Gramajo, *Lipid metabolism and its implication in mycobacteria-host interaction.* Curr Opin Microbiol, 2018. **41**: p. 36-42.
6. Yang, L., et al., *Changes in the major cell envelope components of Mycobacterium tuberculosis during in vitro growth.* Glycobiology, 2013. **23**(8): p. 926-34.
7. Reed, M.B., et al., *A glycolipid of hypervirulent tuberculosis strains that inhibits the innate immune response.* Nature, 2004. **431**(7004): p. 84-7.
8. Queiroz, A. and L.W. Riley, *Bacterial immunostat: Mycobacterium tuberculosis lipids and their role in the host immune response.* Rev Soc Bras Med Trop, 2017. **50**(1): p. 9-18.
9. Stamm, C.E., A.C. Collins, and M.U. Shiloh, *Sensing of Mycobacterium tuberculosis and consequences to both host and bacillus.* Immunol Rev, 2015. **264**(1): p. 204-19.
10. Demento, S.L., et al., *Pathogen-associated molecular patterns on biomaterials: a paradigm for engineering new vaccines.* Trends Biotechnol, 2011. **29**(6): p. 294-306.
11. Middlebrook, G., R.J. Dubos, and C. Pierce, *Virulence and Morphological Characteristics of Mammalian Tubercle Bacilli.* J Exp Med, 1947. **86**(2): p. 175-84.
12. Leisching, G., et al., *The Host Response to a Clinical MDR Mycobacterial Strain Cultured in a Detergent-Free Environment: A Global Transcriptomics Approach.* PLoS One, 2016. **11**(4): p. e0153079.
13. Hunter, R.L., N. Venkataprasad, and M.R. Olsen, *The role of trehalose dimycolate (cord factor) on morphology of virulent M. tuberculosis in vitro.* Tuberculosis (Edinb), 2006. **86**(5): p. 349-56.
14. Indrigo, J., R.L. Hunter, and J.K. Actor, *Cord factor trehalose 6,6'-dimycolate (TDM) mediates trafficking events during mycobacterial infection of murine macrophages.* Microbiology (Reading), 2003. **149**(Pt 8): p. 2049-2059.
15. Glickman, M.S., J.S. Cox, and W.R. Jacobs, Jr., *A novel mycolic acid cyclopropane synthetase is required for cording, persistence, and virulence of Mycobacterium tuberculosis.* Mol Cell, 2000. **5**(4): p. 717-27.
16. Trivedi, A., et al., *Thiol reductive stress induces cellulose-anchored biofilm formation in Mycobacterium tuberculosis.* Nat Commun, 2016. **7**: p. 11392.
17. Ruhl, C.R., et al., *Mycobacterium tuberculosis Sulfolipid-1 Activates Nociceptive Neurons and Induces Cough.* Cell, 2020. **181**(2): p. 293-305 e11.

18. Sachdeva, K., et al., *Mycobacterium tuberculosis (Mtb) lipid mediated lysosomal rewiring in infected macrophages modulates intracellular Mtb trafficking and survival.* J Biol Chem, 2020. **295**(27): p. 9192-9210.
19. Siegrist, M.S. and C.R. Bertozzi, *Mycobacterial lipid logic.* Cell Host Microbe, 2014. **15**(1): p. 1-2.
20. Domenech, P. and M.B. Reed, *Rapid and spontaneous loss of phthiocerol dimycocerosate (PDIM) from Mycobacterium tuberculosis grown in vitro: implications for virulence studies.* Microbiology (Reading), 2009. **155**(Pt 11): p. 3532-3543.
21. Cambier, C.J., et al., *Mycobacteria manipulate macrophage recruitment through coordinated use of membrane lipids.* Nature, 2014. **505**(7482): p. 218-22.
22. Kirksey, M.A., et al., *Spontaneous phthiocerol dimycocerosate-deficient variants of Mycobacterium tuberculosis are susceptible to gamma interferon-mediated immunity.* Infect Immun, 2011. **79**(7): p. 2829-38.
23. Korf, J., et al., *The Mycobacterium tuberculosis cell wall component mycolic acid elicits pathogen-associated host innate immune responses.* Eur J Immunol, 2005. **35**(3): p. 890-900.
24. Kim, J., et al., *Low-dielectric-constant polyimide aerogel composite films with low water uptake.* Polymer Journal, 2016. **48**(7): p. 829-834.
25. Wilburn, K.M., R.A. Fieweger, and B.C. VanderVen, *Cholesterol and fatty acids grease the wheels of Mycobacterium tuberculosis pathogenesis.* Pathog Dis, 2018. **76**(2).
26. Ojha, A.K., et al., *Growth of Mycobacterium tuberculosis biofilms containing free mycolic acids and harbouring drug-tolerant bacteria.* Mol Microbiol, 2008. **69**(1): p. 164-74.
27. 27. Batt, S.M., D.E. Minnikin, and G.S. Besra, *The thick waxy coat of mycobacteria, a protective layer against antibiotics and the host's immune system.* Biochem J, 2020. **477**(10): p. 1983-2006.
28. Koch, A.S., et al., *The Influence of HIV on the Evolution of Mycobacterium tuberculosis.* Mol Biol Evol, 2017. **34**(7): p. 1654-1668.
29. Sirakova, T.D., et al., *The Mycobacterium tuberculosis pks2 gene encodes the synthase for the hepta- and octamethyl-branched fatty acids required for sulfolipid synthesis.* J Biol Chem, 2001. **276**(20): p. 16833-9.
30. Simeone, R., et al., *Functional characterisation of three o-methyltransferases involved in the biosynthesis of phenolglycolipids in Mycobacterium tuberculosis.* PLoS One, 2013. **8**(3): p. e58954.

31. Lescoat, A., et al., *Distinct Properties of Human M-CSF and GM-CSF Monocyte-Derived Macrophages to Simulate Pathological Lung Conditions In Vitro: Application to Systemic and Inflammatory Disorders with Pulmonary Involvement.* Int J Mol Sci, 2018. **19**(3).
32. Jolliffe, I.T. and J. Cadima, *Principal component analysis: a review and recent developments.* Philos Trans A Math Phys Eng Sci, 2016. **374**(2065): p. 20150202.
33. Day, T.A., et al., *Mycobacterium tuberculosis strains lacking surface lipid phthiocerol dimycocerosate are susceptible to killing by an early innate host response.* Infect Immun, 2014. **82**(12): p. 5214-22.
34. Rousseau, C., et al., *Production of phthiocerol dimycocerosates protects Mycobacterium tuberculosis from the cidal activity of reactive nitrogen intermediates produced by macrophages and modulates the early immune response to infection.* Cell Microbiol, 2004. **6**(3): p. 277-87.
35. Augenstreich, J., et al., *Phthiocerol Dimycocerosates from Mycobacterium tuberculosis Increase the Membrane Activity of Bacterial Effectors and Host Receptors.* Front Cell Infect Microbiol, 2020. **10**: p. 420.
36. Gilmore, S.A., et al., *Sulfolipid-1 biosynthesis restricts Mycobacterium tuberculosis growth in human macrophages.* ACS Chem Biol, 2012. **7**(5): p. 863-70.
37. Portevin, D., et al., *Human macrophage responses to clinical isolates from the Mycobacterium tuberculosis complex discriminate between ancient and modern lineages.* PLoS Pathog, 2011. **7**(3): p. e1001307.
38. Sandberg, J.K., et al., *HIV-1 Replication Is Differentially Regulated by Distinct Clinical Strains of Mycobacterium tuberculosis.* PLoS ONE, 2009. **4**(7).
39. Arango Duque, G. and A. Descoteaux, *Macrophage cytokines: involvement in immunity and infectious diseases.* Front Immunol, 2014. **5**: p. 491.
40. Leonard, W.J. and J.X. Lin, *Cytokine receptor signaling pathways.* J Allergy Clin Immunol, 2000. **105**(5): p. 877-88.
41. Hoshino, Y., et al., *Maximal HIV-1 replication in alveolar macrophages during tuberculosis requires both lymphocyte contact and cytokines.* J Exp Med, 2002. **195**(4): p. 495-505.
42. Henderson, A.J. and K.L. Calame, *CCAAT/enhancer binding protein (C/EBP) sites are required for HIV-1 replication in primary macrophages but not CD4(+) T cells.* Proc Natl Acad Sci U S A, 1997. **94**(16): p. 8714-9.
43. Zarini, S. Barkley, R.M. and Murphy, R.C. *Overview of lipid mass spectrometry and lipidomics*. (2019). In: D'Alessandro, A. (eds) High throughout metabolomics. Methods in molecular biology vol 1978.

3.6. Supplementary material

The following tables are supplementary data that form part of chapter 3. The supplementary material contains four tables cytokine secretion by MDM infected with different laboratory and clinical strains and constitutive cytokine secretion by uninfected. The cytokines were measured from SN harvested at both 24-hours post-infection and 96-hours post infection and analysed by Luminex assay. Luminex data was analysed using GraphPad prism.

Supplementary Table 3.1. Cytokine secretion from uninfected MDM and MDM infected with laboratory strains of *Mtb* 24-hours post-infection

	Median level of cytokine secretion with Interquartile range (pg/ml)			
Analyte	H37Rv$^{P1939/T605}$ **Infection**	CDC1551^{WT} **Infection**	HN878^{WT} **Infection**	**No infection**
CCL11	22.63 (11.78 - 33.48)	11.78 (4.51 - 33.48)	11.78 (4.51 - 33.48)	11.78 (4.51 - 33.48)
CCL2	5379 (2667 - 8983)	4006 (339 - 17500)	1184 (196.7 - 2806)	1767 (379.1 - 2806)
CCL3	1194 (697.2 - 2424)	2349 (783.4 - 5014)	250.1 (152.4 - 961.2)	181.7 (152.4 - 961.2)
CCL4	2288 (1987 - 5162)	3052 (411.4 - 8626)	207.2 (56.02 - 522.1)	115.8 (56.02 - 522.1)
CCL5	1744 (947.8 – 2540)	947.8 (32.64 - 2540)	947.8 (32.64 - 2540)	947.8 (32.64 - 2540)
CXCL10	43.44 (33.82 - 75.82)	37.13 (17.24 - 84.25)	18.25 (17.24 - 20.85)	18.25 (17.24 - 20.85)
CXCL8	10906 (6742 - 17052)	11933 (705.5 - 22255)	414.4 (304.6 - 880.2)	551.6 (304.6 - 880.2)
CXCL9	75.27 (34.78 - 115.8)	111.5 (101.3 - 223.8)	111.5 (34.78 - 115.8)	113.6 (34.78 - 115.8)
GM-CSF	17.14 (9.02 - 27.05)	10.83 (8.02 - 41.25)	8.02 (7.6 - 9.02)	8.52 (7.6 - 9.02)
IFN-α	195.3 (97.02 - 369.3)	130.9 9 (53.28 - 434.3)	53.28 (33.69 - 146.9)	100.1 (33.69 - 146.9)
IFN-γ	10.58 (10.39 - 20.69)	10.58 (9.97 - 25.25)	9.97 (3.8 - 10.58)	10.28 (3.8 - 10.58)
IL-10	15.13 (4.39 - 29.71)	80.1 (42.07 - 121.7)	10.96 (3.56 - 13.56)	5.985 (3.56 - 10.71)
IL-12	406 (107.2 - 567.4)	512.9 (21.16 - 1338)	36.29 (21.16 - 69.63)	36.29 (21.16 - 69.63)
IL-13	138.3 (105.4 - 200.6)	113.2 (35.24 - 297.1)	65.09 (35.24 - 171.3)	118.2 (35.24 - 171.3)

IL-15	5379 (2667 – 8983)	4006 (339 – 17500)	1184 (196.7 – 2806)	312.6 (19.32 – 522.1)
IL-17	66.46 (48.01 - 84.9)	57.15 (44 - 129.9)	44 (11.94 - 84.9)	64.45 (11.94 - 84.9)
IL-1RA	7301 (4569 - 8329)	8447 (5814 - 10396)	7420 (2562 - 16307)	6442 (2562 - 16307)
IL-1β	77.92 (31.82 - 98.68)	81.96 (57.62 - 158.1)	86.44 (6.17 - 317.2)	23.89 (11.77 - 31.82)
IL-2	45.16 (43.88 - 46.43)	54.76 (33.52 - 104.9)	19.72 (10.52 - 46.43)	35.83 (10.52 - 46.43)
IL-2R	274.4 (159 - 331.2)	323.9 (68.41 - 797.1)	86.27 (68.41 - 331.2)	208.7 (68.41 - 331.2)
IL-4	192.6 (158.5 - 231)	226.6 (74.68 - 393.6)	58.18 (34.8 - 74.68)	58.18 (34.8 - 74.68)
IL-5	43.71 (23.09 - 64.32)	36.07 (23.09 64.32)	34.02 (13.13 - 64.32)	49.17 (13.13 - 64.32)
IL-6	358.3 (190.3 - 514.2)	567 (21.01 - 1066)	16.65 (9.9 - 20.87)	16.65(15.41 - 20.87)
IL-7	144.9 (44.51 - 210.8)	91.68 (35.88 - 262.9)	35.88 (12.2 - 210.8)	123.3 (12.2 - 210.8)
TNF	18.34 (11.8 - 26.07)	21.96 (11.65 - 48.27)	10.37 (0.56 - 11.71)	4.82 (0.56 - 11.71)

Median cytokine secretion levels with interquartile range. values for n = 6 for $HN878^{WT}$ and n = donors for $CDC1551^{WT}$ and $H37Rv^{P1939/T605}$.

Supplementary Table 3.2. Median cytokine secretion level with interquartile range from uninfected MDM and MDM infected with laboratory strains of *Mtb* 96-hours post-infection

Median level of cytokine secretion with Interquartile range (pg/ml)				
Analyte	**H37Rv$^{P1939/T605}$ Infection**	CDC1551^{WT} **Infection**	HN878^{WT} **Infection**	**No infection**
CCL11	5.705 (0.98 - 15.42)	3.38 (0.28 - 33.48)	8.415 (0.99 - 33.48)	7.075 (0.28 - 33.48)
CCL2	2898 (765.8 - 10535)	2390 (517.9 - 13034)	2371 (583.8 - 17853)	572.6 (205.8 - 8328)
CCL3	803.4 (152.2 - 5097)	289.4 (49.87 - 555.3)	328.6 (49.87 - 971)	172.8 (10.74 - 924.7)
CCL4	1506 (247.1 - 6683)	452.3 (167.1 - 978)	490.8 (279.3 - 1177)	112.4 (22.4 - 699.7)
CCL5	107.9 (0.21 - 1018)	18.51 (0.21 - 2540)	32.64 (0.21 - 2540)	23.45 (0.21 - 2540)
CXCL10	4.05 (1.75 - 28.55)	3.35 (1.17 - 70.97)	10.38 (1.9 - 59.18)	10.03 (0.61 - 20.85)
CXCL8	13815 (3561 - 24048)	7974 (2159 - 18813)	7791 (847.3 - 19466)	443.4 (69.8 - 4413)
CXCL9	115.8 (66.65 - 209.1)	66.65 (30.7 - 171.1)	96.96 (30.7 - 223.8)	66.65 (30.7 - 115.8)
GM-CSF	7.595 (0.25 - 22.61)	1.2 (0.36 - 9.02)	5.055 (0.25 - 12.75)	3.895 (0.01 - 9.02)
IFN-α	61.51 (24.07 - 285.8)	44.42 (22.78 - 285.8)	51.51 (28.43 - 434.3)	40.86 (5.86 - 146.9)
IFN-γ	10.58 (7.88 - 63.16)	8.68 (1.55 - 26.25)	10.58 (2.9 - 32.05)	8.82 (0.21 - 32.05)
IL-10	2.29 (0.14 - 13.56)	0.89 (0.01 - 11.94)	2.685 (0.14 - 16.31)	2.15 (0.01 - 11.94)
IL-12	181.7 (36.29 - 603.1)	176.3 (36.29 - 518.5)	249.8 (21.16 - 747.6)	23.83 (3.85 - 69.63)
IL-13	20.51 (5.26 - 171.3)	14.56 (4.01 - 224.6)	27.22 (5.26 - 297.1)	22.16 (1.03 - 171.3)
IL-15	142.4 (61.85 - 522.1)	99.42 (39.92 - 522.1)	89.24 (19.32 - 522.1)	49.79 (18.1 - 522.1)
IL-17	11.35 (2.96 - 84.9)	9.6 (2.33 - 84.9)	22.9 (2.33 - 84.9)	14.8 (1 - 84.9)
IL-1RA	8295 (505.2 - 18272)	5374 (140.1 - 21156)	7140 (172.5 - 22536)	7128 (136.2 - 15459)
IL-1β	49.92 (14.46 - 124.9)	17.69 (2.05 - 98.68)	26.53 (6.86 - 182.7)	7.395 (2.05 - 28.3)
IL-2	12.51 (3.8 - 46.94)	8.885 (2.55 - 46.43)	12.35 (3.8 - 88.57)	10.19 (0.09 - 46.43)
IL-2R	285.6 (69.59 - 598.4)	99.47 (26.27 - 331.2)	135.1 (46.78 - 331.2)	68.41 (10.86 - 331.2)

IL-4	65.42 (20.22 - 186.6)	42 (5.85 - 231)	64.29 (13.1 - 316.9)	31.79 (0.4 - 74.68)
IL-5	10.42 (0.41 - 64.32)	3.965 (0.41 - 64.32)	15.18 (0.41 - 64.32)	13.47 (0.41 - 64.32)
IL-6	82.88 (48.73 - 1336)	103.7 (26.05 - 277.6)	145.2 (21.01 – 677.5)	7.085 (1.24 – 23.1)
IL-7	124.7 (50.74 - 210.8)	44.54 (12.2 - 234.7)	59.92 (32.55 - 262.9)	33.28 (5.12 - 210.8)
TNF	2.09 (0.34 - 19.2)	1.53 (0.05 - 11.8)	7.15 (0.34 - 19.43)	0.56 (0.05 - 11.71)

Median cytokine secretion levels with interquartile range. values for n = 6 for $HN878^{WT}$ and n = donors for $CDC1551^{WT}$ and $H37Rv^{P1939/T605}$.

Supplementary Table 3.3. Cytokine secretion levels from uninfected MDM and MDM infected with *Mtb* clinical strains 24-hours post-infection.

	Median level of cytokine secretion with Interquartile range (pg/ml)			
Analyte	EX30$^{Q1939/A605}$ **Infection**	**MRC16$^{P1939/A605}$ Infection**	*EU111^{N1759}* **Infection**	EU40^{T1759} **Infection**
CCL11	11.78 (4.51 - 33.48)	46.2 (38.25 - 104.8)	11.78 (4.51 - 33.48)	11.78 (4.51 - 33.48)
CCL2	3924 (1443 - 15580)	10212 (4228 - 21527)	3133 (613.9 - 14374)	2126 (583.8 - 6329)
CCL3	2479 (994.7 - 7086)	34807 (19403 - 42426)	1384 (802.6 - 9042)	666.3 (431.6 - 1458)
CCL4	2424 (1945 - 11242)	21469 (3430 - 42191)	1935 (773.3 - 10858)	1516 (744.3 - 2735)
CCL5	947.8 (32.64 - 2540)	7754 (3199 - 11858)	947.8 (32.64 - 2540)	947.8 (32.64 - 2540)
CXCL10	37.50 (17.24 - 146.6)	289.2 (216.8 - 4205)	34.99 (17.24 - 109.3)	22.35 (17.24 - 40.9)
CXCL8	11690 (7758 - 24933)	26614 (11933 - 28460)	8142 (2181 - 2478337)	492 (1951 - 12448)
CXCL9	111.5 (34.78 - 532.6)	822.2 (485.8 - 20945)	111.5 (34.78 - 391.6)	111.5 (34.78 - 115.8)
GM-CSF	24.07 (17.08 - 28.49)	236.9 (151.7 - 720.8)	12.73 (8.02 - 30.35)	10.83 (8.02 - 18.85)
IFN-α	126.6 (118.9 - 513.8)	529 (325.2 - 1362)	110.3 (53.28 - 434.3)	101.5 (88.34 - 146.9)
IFN-γ	19.30 (9.97 - 45.61)	268.5 (165.3 - 514.3)	13.19 (9.97 - 17.91)	10.28 (3.8 - 15.8)
IL-10	15.13 (4.39 - 29.71)	80.1 (42.07 - 121.7)	10.96 (3.56 - 13.56)	10.71 (3.56 - 13.56)
IL-12	345.5 (128.9 - 2146)	13815 (485.3 - 40483)	309.2 (21.16 - 2644)	109.7 (21.16 - 235.1)
IL-13	116.2 (95.54 - 375.2)	267.9 (175.8 - 506.8)	91.95 (35.24 - 325.8)	95.54 (35.24 - 224.6)
IL-15	342.8 (195.2 - 995.6)	1608 (1161 - 3574)	229.4 (19.32 - 995.6)	280.9 (19.32 - 522.1)
IL-17	52.14 (30.13 - 164.6)	180.5 (129.6 - 380.8)	52.14 (36.79 - 129.9)	44 (22.4 - 184.9)

IL-1RA	9940 (6819 - 14296)	20285 (14028 - 66894)	8591 (6655 - 13023)	8588 (5770 - 10196)
IL-1β	78.39 (48.89 - 474.7)	255.5 (199.3 - 565.3)	72.07 (31.82 - 448.7)	57.24 (31.82 - 170.7)
IL-2	45.41 (33.52 - 145.8)	206.3 (163.8 - 515.8)	39.65 (33.52 - 145.8)	34.47 (25.2 - 46.43)
IL-2R	457.1 (189.4 - 1309)	2751 (1647 - 5682)	188.3 (136.8 - 1309)	147.9 (86.27 - 331.2)
IL-4	191.6 (140.7 - 530.5)	806.3 (547.4 - 1689)	171.1 (74.68 - 497.9)	145.6 (74.68 - 182.4)
IL-5	36.07 (23.09 - 64.32)	207.2 (105.3 - 253)	34.02 (23.09 - 64.32)	34.02 (13.13 - 64.32)
IL-6	376.6 (141.3 - 1816)	14579 (8317 - 38549)	311.5 (28.96 - 1398)	165 (54.48 - 275.1)
IL-7	137.2 (44.51 - 457.4)	563.1 (295.6 - 985)	49.79 (12.2 - 457.4)	35.88 (12.2 - 210.8)
TNF	22.99 (18.39 - 57.98)	685.9 (311.3 - 1334)	19.79 (11.65 - 48.27)	14.01 (11.65 - 26.07)

Median cytokine secretion levels with interquartile range. values for n = 6 for $HN878^{WT}$ and n = donors for $CDC1551^{WT}$ and $H37Rv^{P1939/T605}$.

Supplementary Table 3.4. Median cytokine secretion level with interquartile range from uninfected MDM and MDM infected with *Mtb* clinical strains 96-hours post-infection

Median level of cytokine secretion with Interquartile range (pg/ml)				
Analyte	EX30$^{Q1939/A605}$ **Infection**	**MRC16$^{P1939/A605}$ Infection**	*EU111^{N1759}* **Infection**	EU40^{T1759} **Infection**
CCL11	8.745 (0.28 - 33.48)	24.52 (10.94 - 44.26)	8.415 (0.28 - 33.48)	8.08 (0.28 - 33.48)
CCL2	3297 (517.9 - 22078)	12091 (3454 - 37404)	1293 (335.6 - 21278)	1421 (537.2 - 10934)
CCL3	579.1 (49.87 - 4258)	8010 (1977 - 37826)	312.6 (22.82 - 929.2)	354 (86.97 - 1674)
CCL4	814.9 (268.4 - 4876)	6508 (950 - 21469)	353.4 (145.7 - 1301)	453 (181.1 - 2008)
CCL5	59.75 (0.21 - 2540)	1258 (120.4 - 9865)	23.45 (0.21 - 2540)	23.45 (0.21 - 2540)
CXCL10	11.07 (0.92 - 204.5)	84.36 (36.91 - 1112)	10.38 (0.61 - 151.6)	10.38 (1.17 - 116.8)
CXCL8	11360 (2050 - 31409)	24816 (11933 - 61681)	3703 (1106 - 22063)	7226 (3236 - 17043)
CXCL9	120.3 (30.7 - 391.6)	1312 (406.7 - 23258)	89.05 (30.7 - 223.8)	102.6 (30.7 - 130.4)
GM-CSF	4.545 (0.36 - 22.88)	171.4 (10.97 - 750.7)	4.255 (0.19 - 9.02)	4.35 (0.19 - 9.02)
IFN-α	86.16 (15.96 - 489.1)	246.8 (97.2 - 811.4)	47.7 (5.86 - 489.1)	47.67 (15.96 - 146.9)
IFN-γ	10.58 (1.55 - 38.63)	101.4 (13.84 - 294.9)	10.18 (0.21 - 32.05)	10.58 (0.21 - 32.05)
IL-10	2.53 (0.01 - 16.31)	24.31 (4.04 - 93.67)	2.53 (0.01 - 16.31)	2.075 (0.01 - 841)
IL-12	187.7 (70.48 - 866)	712.5 (485.3 - 26764)	75.55 (21.16 - 1084)	89.41 (36.29 - 488.2)
IL-13	42.14 (4.01 - 297.1)	103.3 (19.19 – 437.2)	25.73 (1.03 - 297.1)	24.92 (4.01 - 224.6)
IL-15	183.3 (30.8 - 522.1)	814.7 (224.5 - 2194)	115.1 (19.32 - 665.9)	92.65 (19.32 - 522.1)
IL-17	18.02 (1.11 - 87.99)	77.51 (11.35 - 267.4)	11.07 (1 - 84.9)	15.71 (1.1 - 84.9)
IL-1RA	11155 (167.3 - 28437)	19016 (584.8 - 69261)	7460 (142 - 23612)	8291 (182.5 - 25177)
IL-1β	38.75 (4.64 - 205.3)	213.3 (22.39 - 1466)	30.04 (4.64 - 283.1)	35.97 (6.86 - 98.68)
IL-2	19.87 (2.55 - 104.9)	97.62 (15.49 - 278.9)	18.36 (1.18 - 88.57)	17.85 (2.55 - 46.94)
IL-2R	153.6 (26.27 - 682.4)	1339 (369.7 - 3033)	102.6 (26.27 - 587.8)	113.5 (46.78 - 331.2)

IL-4	103.8 (8.34 - 356.2)	376.3 (87.65 - 1023)	63.27 (3.26 - 393.6)	61.21 (9.55 - 182.4)
IL-5	13.59 (0.41 - 64.32)	62.66 (16.07 - 227)	13.47 (0.41 - 64.32)	13.47 (0.41 - 64.32)
IL-6	185.7 (21.21 - 837.4)	7670 (2834 - 49607)	57.85 (6.82 - 650)	69.44 (16.12 - 174.8)
IL-7	107.5 (12.2 - 262.9)	329.3 (89.28 - 682.8)	38.6 (12.2 - 308.5)	47.65 (12.2 - 215.3)
TNF	7.18 (0.42 - 37.78)	168.5 (5.26 - 1847)	6.775 (0.05 - 37.78)	6.495 (0.42 - 19.2)

Median cytokine secretion levels with interquartile range. values for n = 6 for $HN878^{WT}$ and n = donors for $CDC1551^{WT}$ and $H37Rv^{P1939/T605}$.

Chapter 4. Direct *Mtb* co-infection and cytokine bystander effects on HIV-1 replication dynamics to a panel of *Mtb* clinical isolates

4.1. Introduction

HIV-1 is an obligate intracellular parasite, which relies completely on the host to continue its life cycle [1, 2]. The life cycle of HIV-1 is such that it requires a perpetual inflow of HIV-1 inducing human transcriptional factors to stimulate HIV-1 replication [45]. A study showed that HIV-1 replication was increased according to the magnitude of cytokines induced by co-infecting *Mtb* strains in a PBMC environment [38]. Equipped with the above information it would not be a stretch to postulate that HIV-1 might influence the evolution of co-infecting pathogens to select for genotypes that would bring infection and replication advantages to HIV-1. In fact, the study by Koch *et al.* (2017) [28], which found that *Mtb* strains have SNP under HIV-1 positive directional may point to HIV-1 selecting for strains that are advantageous to the virus. HIV-1/*Mtb* co-infection of the same host creates space for HIV-1 and *Mtb* to occupy the same niche in co-infected hosts. The lungs are the primary site of *Mtb* infection [46], and, as described by Costiniuk and Jenabian (2014) [47], the lungs are an ideal environment for HIV-1 persistence, with millions of alveoli in close proximity for easy cell-to-cell spread. Moreover, *Mtb* and HIV-1 could possibly be found sharing the same cells as, for example, both pathogens infect macrophages [47, 48].

In this chapter, I address Aim 1C: to assess whether differential cytokine induction by *Mtb* strains with different lipid phenotypes correlates with changes in HIV-1 replication and productive infection in MDM, as well as whether the presence of HIV-1 co-infection influences these cytokine profiles. The strains that were taken forward for these experiments are $EX30^{Q1939/A605}$ and the phylogenetically matched $MRC16^{P1939/A605}$ strains; and the $EU111^{N1759}$ and $EU40^{T1759}$ pair. The $MRC16^{P1939/A605}$ and $EX30^{Q1939/A605}$ pair was included because there were significant differences in the induction of cytokine secretion by $MRC16^{P1939/A605}$ compared to $EX30^{Q1939/A605}$, as well as observed lipid differences between the two (Chapter 3; Table 3.3). These strains were taken forward with their lineage matched laboratory strains H37Rv and CDC1551. $EU111^{N1759}$ and $EU40^{T1759}$ were included for deeper evaluation of their phenotype in the presence of HIV-1 co-infection because IL-6 was the only cytokine that was differentially secreted by MDM infected with $EU111^{N1759}$ compared to $EU40^{T1759}$ (chapter 3;

Table 3.4), but it has a known role in regulating HIV-1 transcription. These strains were taken forward with the lineage matched laboratory strain HN878.

The SN collected from MDM infected with different strains of *Mtb* was divided into SN that was used for analysis by Luminex in Chapter 3, while the remaining volume was for co-incubating TZM-bl cells and MDM to determine the effect of secreted soluble factors on HIV-1 replication. Firstly, I assessed the regulation of HIV-1 LTR transcriptional activity in TZM-bl cells by the cytokine milieu induced during MDM infection with *Mtb* clinical and laboratory strains characterised in Chapter 3. I also used the SN to incubate M2 MDM infected with HIV-1. These experiments would inform the effect that the *Mtb* microenvironment has on HIV-1 infection and replication in bystander cells. I then co-infected MDM with HIV-1 and the different strains of *Mtb* to study the effect conferred by these *Mtb* strains on cytokine production during direct HIV-1 co-infection and the consequences of altered cytokine production on HIV-1 productive infection by measuring HIVp24 in culture supernatants during co-infection.

4.2. Results

4.2.1. Assessing regulation of HIV-1 replication by measuring LTR activity in TZM-bl cells

Quantification of HIV-1 Gag p24 in culture supernatants measures specifically assembled and budded viruses. That is not a good representation of HIV-1 replication, partly because a large part of transcripts during replication may be defective at the sequence level to produce functional viral protein(s) and infectious particles [49], which could lead to a gap in resolving the true rate of replication. I used TZM-bl cells which have a luciferase reporter under the control of the HIV-1 LTR promoter (see chapter 2.2.11 for detailed description) to measure the transcriptional activity of the HIV-1 LTR. I used this to infer the impact of co-culturing these cells in SN with *Mtb*-induced cytokines on HIV-1 replication.

To measure LTR activity, I used SN harvested 24 hours and 96 hours post-infection of MDM with the panel of *Mtb* strains (See Section 3.2.4-7). The SN was used to incubate TZM-bl cells 24 hours before infection with HIV-1 (Fig. 4.1) to assess whether the SN would affect the uptake of HIV-1 and subsequent replication in TZM-bl cells. The SN was also used to incubate TZM-bl cells 6 hours after the cells were infected with HIV-1 (Fig. 4.1), to assess the effect of the SN on LTR activity but not initial uptake of HIV-1 by TZM-bl cells. In both experimental

set-ups, TZM-bl cells were incubated for 48 hours post HIV-infection and then lysed and the Bright Glo assay used to measure luciferase activity as a readout of LTR activity (Fig. 4.1).

When the SN was added before HIV-1 infection I postulated that soluble factors could prime the cells for HIV-1 to be taken up quickly into TZM-bl cells, and therefore the LTR activity would be significantly increased in relation to controls. Alternatively, HIV-1 receptor antagonistic cytokines might inhibit or slow the uptake of HIV-1 into TZM-bl cells, and the LTR activity would therefore be significantly decreased relative to controls. The experimental wells contained HIV-1 infected TZM-bl cells with SN from the different strain, while the controls were HIV-1 infected TZM-bl cells incubated with DMEM/ 10 % FBS media (media control) or incubated with SN from uninfected MDM.

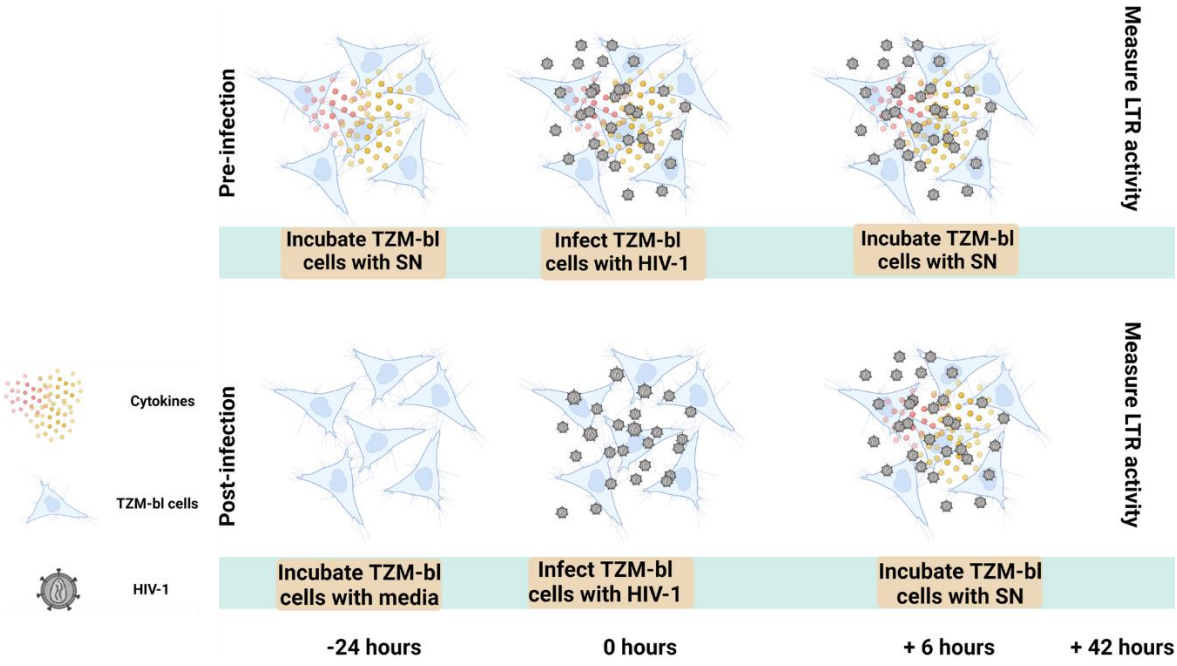

Figure 4.1. A schematic that shows the flow of how TZM-bl cells were used as a model for HIV-1 replication in the presence of *Mtb* induced SN.
TZM- bl cells were cultured until 80 % confluent. TZM-bl cells were plated in a 96-well plate and SN harvested 24 or 96 h post infection of MDM with a panel of Mtb strains was used to incubate TZM-bl cells. The SN from Mtb infected MDM was added to TZM-bl cells 24 h before infection with HIV-1 or 6 h after infection with HIV-1. HIV-1 infection was allowed to continue for 48 h. HIV-1 infected TZM-bl cells were harvested and LTR activity in TZM-bl cells was measured using the Bright Glo assay (Promega).

4.2.1.1. *Impact of pre-incubation and post-incubation with Mtb-induced conditioned media on HIV-1 LTR activity*

Firstly, I compared the LTR activity in both the pre-infection and post-infection models of TZM-bl cells incubated with media only (RPMI/DMEM) or incubated with SN from uninfected MDM. Here, I wanted to assess whether baseline cytokine secretion by uninfected MDM had any effect on HIV-1 LTR activity. To do this, I incubated TZM-bl cells with media containing both RPMI/DMEM media only or with SN from uninfected MDM, before or after HIV-1 infection (see Fig. 4.1). Data from TZM-bl cells infected with HIV-1 before and after incubation with SN from MDM harvested 24 hours and 96 hours post-infection (relative to *Mtb* and not HIV-1 infection) was compared with data from TZM-bl cells infected with HIV-1 and incubated with media only. This was used to establish effect of SN from MDM in the absence of infection. There was no difference in LTR activity as it relates to the uptake of HIV-1 into TZM-bl cells (pre-incubation) between TZM-bl cells incubated with media only and TZM-bl cells incubated with SN harvested from uninfected MDM 24 hours or 96 hours from uninfected MDM (Fig. 4.2A&C). Similarly, there was no significant difference in LTR activity between TZM-bl cells incubated with media only or TZM-bl cells incubated with SN from uninfected MDM for both the 24-hour (Fig. 4.2B) or the 96-hour time point (Fig. 4.2D). With these data in mind, the LTR activity from TZM-bl cells incubated with SN from uninfected MDM was used as control for all subsequent analyses.

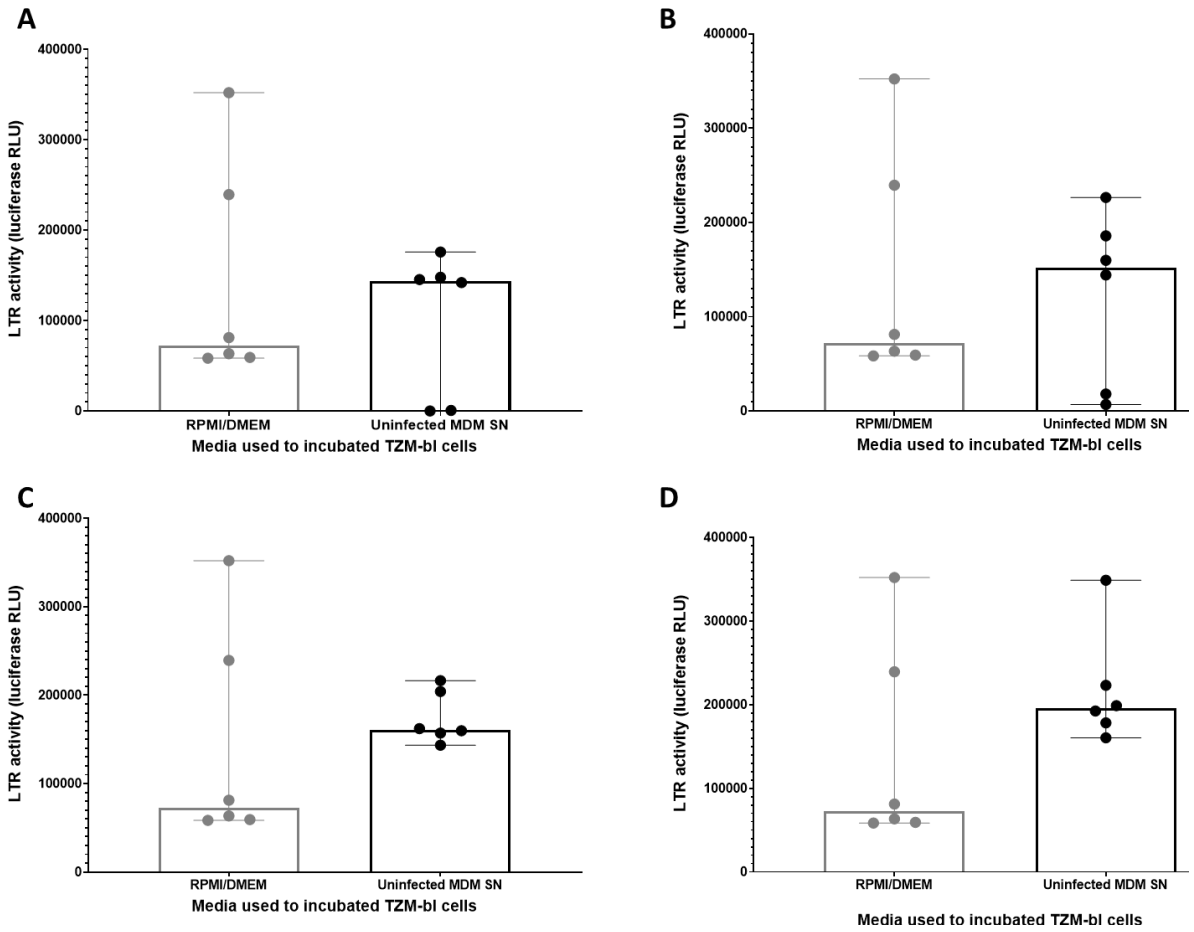

Figure 4.2. Analysis of LTR activity in TZM-bl cells infected with HIV-1 pre and post incubation with SN harvested from uninfected MDM or media only.
TZM-bl cells were infected with HIV-1 and incubated with media only for 48 hours or incubated with SN from uninfected MDM 24-hours before or 6-hours post-infection with HIV-1. LTR activity was measured 48 hours post-infection with HIV-1 in all experimental set-ups. The LTR activity was measured using the Bright Glo assay (Promega). Luminescence data was analysed by Graph Pad prism. Graphs show LTR activity in TZM-bl cells incubated with (**A**) SN from uninfected MDM (that correspond to 24-hours post-infection with *Mtb*) before HIV-1 infection, **(B)** SN from uninfected MDM (that correspond to 24-hours post-infection with *Mtb*) after HIV-1 infection, (**C**) SN from uninfected MDM (that correspond to 96-hours post-infection) before HIV-1 infection, **(D)** SN from uninfected MDM (that correspond to 96-hours post-infection) after HIV-1 infection. Median with IQR for n=6 donors or 6 replicates. Statistics were measured with Mann-Whitney T test. Significance regarded as $p<0.05$.

4.2.1.2. There is variability in LTR activity in TZM-bl cells pre- and post-incubated with 24- and 96-hour SN from MDM infected with *Mtb* clinical and laboratory strains

Next, I analysed LTR activity in TZM-bl cells infected with HIV-1 before co-culture with SN harvested 24-hours post-infection with the panel of clinical and laboratory strains. To do this, I incubated TZM-bl cells with SN harvested 24-hours post-infection with the panel of *Mtb* strains or with SN from uninfected MDM, before HIV-1 infection (see Fig. 4.1). I observed no significant increase in LTR activity in TZM-bl cells incubated with SN harvested 24-hours after infection with CDC1551^{WT} or H37Rv$^{P1939/T605}$ (Fig. 4.3A). There was a significant

increase in LTR activity in TZM-bl cells pre-incubated with SN from MDM infected with HN878 ($p = 0.0160$) (Fig. 4.3A). These data suggest that the 24-hour SN from CDC1551^{WT} or H37Rv$^{P1939/T605}$ strains did not affect the uptake of HIV-1 into the TZM-bl cells. The increase in LTR activity in TZM-bl cells pre-incubated with SN from HN878^{WT} infected MDM signals soluble factors in this SN may increase the uptake of HIV-1 (Fig. 4.3A).

TZM-bl cells incubated with SN harvested 24-hours post-infection with EX30$^{Q1939/A605}$ and MRC16$^{P1939/A605}$ clinical strains showed increased uptake of HIV-1 (Fig. 4.3B). I observed that SN harvested 24 hours post-infection from MDM infected with EX30$^{Q1939/A605}$ and MRC16$^{P1939/A605}$ significantly increased the HIV-1 LTR activity in TZM-bl cells ($p = 0.0062$ and 0.0062, respectively; Fig. 4.3B) compared to LTR activity in TZM-bl cells incubated with SN from uninfected MDM. Furthermore, SN MRC16$^{P1939/A605}$ also increased the uptake of HIV-1 into TZM-bl cells compared to SN from H37Rv$^{P1939/T605}$ (Fig. 4.3B). These results suggest that EX30$^{Q1939/A605}$ and MRC16$^{P1939/A605}$ infection of MDM induced factors early that increase the LTR activity, some of which may also prime the TZM-bl cells for rapid uptake of HIV-1.

Finally, I proceeded to analyse the effect of EU111^{N1759} and EU40^{T1759} SN on HIV-1 infection of TZM-bl cells. Similarly, to EX30$^{Q1939/A605}$ and MRC16$^{P1939/A605}$, there was a significant increase in HIV-1 LTR activity in TZM-bl cells by pre-incubation in SN harvested 24-hours following infection with EU111^{N1759} ($p = 0.0238$) and EU40^{T1759} ($p = 0.0016$) compared to SN from uninfected MDM (Fig. 4.3C). This data suggests that EU111^{N1759} and EU40^{T1759} infection produces soluble factors that prime TZM-bl cells and increase the uptake of HIV-1.

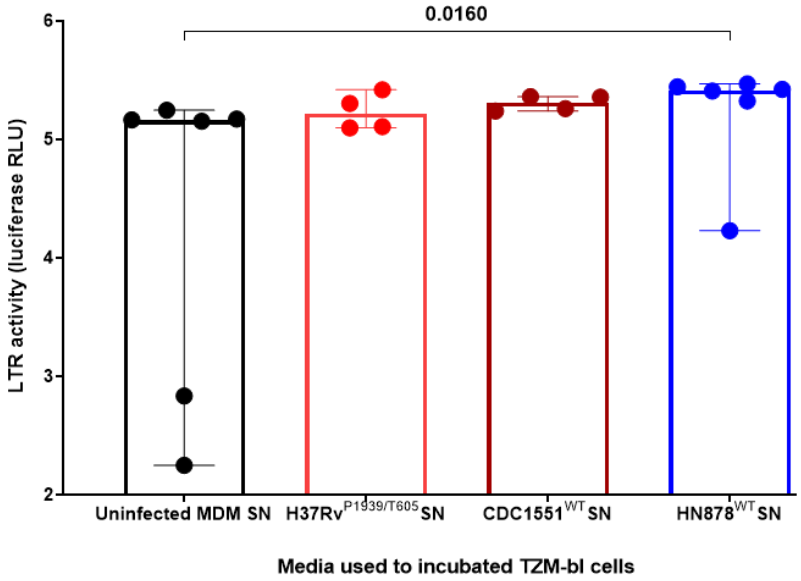
0.0160
LTR activity (luciferase RLU)
Uninfected MDM SN
H37Rv P1939/T605 SN
CDC1551 WT SN
HN878 WT SN
Media used to incubated TZM-bl cells

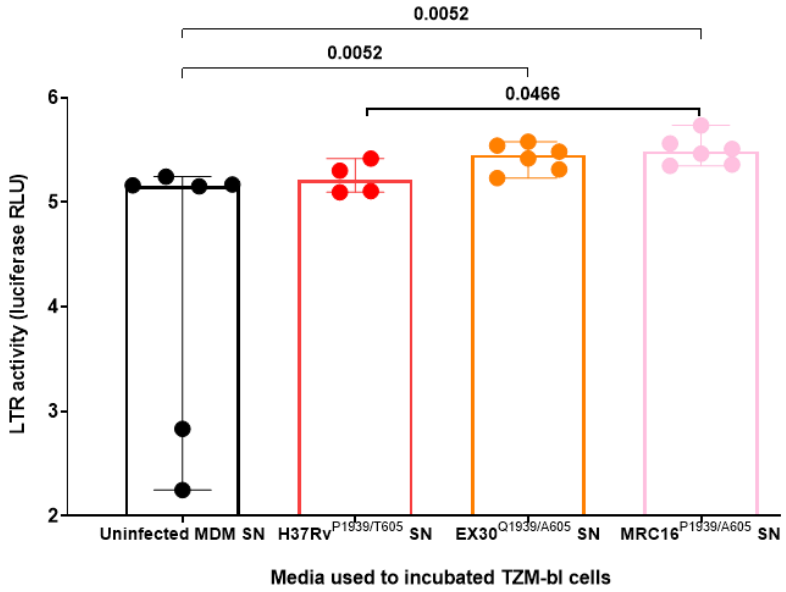
0.0052
0.0052
0.0466
LTR activity (luciferase RLU)
Uninfected MDM SN
H37Rv P1939/T605 SN
EX30 Q1939/A605 SN
MRC16 P1939/A605 SN
Media used to incubated TZM-bl cells

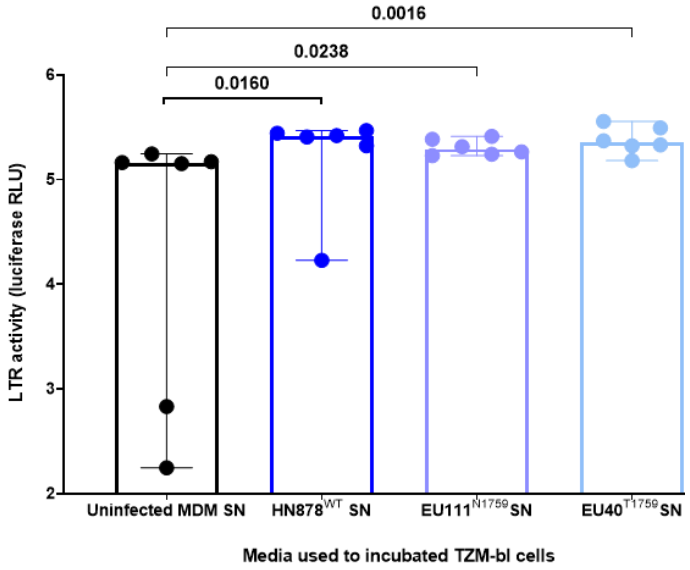
0.0016
0.0238
0.0160
LTR activity (luciferase RLU)
Uninfected MDM SN
HN878 WT SN
EU111 N1759 SN
EU40 T1759 SN
Media used to incubated TZM-bl cells

Figure 4.3. Analysis of TZM-bl cells infection with HIV-1 pre incubation with harvested 24-hours post-infection from MDM infected with from MDM infected with laboratory strains.
TZM-bl cells were incubated with SN from *Mtb* infected MDM 24-hours before infection with HIV-1. LTR activity was measured 48 hours post-infection with HIV-1, using the Bright Glo assay (Promega). Luminescence data was analysed by Graph Pad prism. Graphs show LTR activity in TZM-bl cells incubated with SN harvested 24-hours after infection of MDM with (**A**) $H37Rv^{P1939/T605}$ or $CDC1551^{WT}$ or $HN878^{WT}$ infected MDM, (**B**) $EX30^{Q1939/A605}$ or $MRC16^{P1939/A605}$ infected MDM, and (**D**) SN from MDM infected with $EU111^{N1579}$ or $EU40^{T1579}$. Median with IQR for n=6 donors or 4 donors of SN. Statistics were measured with Friedman's or Kruskallis-Wallis multiple comparison test. Significance was analysed by a two-stage linear step-up procedure of Benjamini, Krieger and Yekutieli was used to control for multiple comparison false discovery rate. P<0.05 are shown in graph.

I went on to complete similar co-culture experiments using SN that harvested 96-hours post-infection. Contrary to the SN harvested 24-hours post-infection, the LTR activity was increased in TZM-bl co-culture with SN harvested 96-hours post-infection from MDM infected with $CDC1551^{WT}$ ($p = 0.0221$) and $HN878^{WT}$ ($p = 0.0044$) induced SN also continued to result in high LTR activity (Fig. 4.4A). Of the laboratory strain $H37Rv^{P1939/T605}$ SN was the only one that did not result in increased LTR activity with both 24- and 96-hour SN (Fig. 3.3A – 3.4A). This data suggests that in the SN harvested 96-hours post-infection with $CDC1551^{WT}$ and $HN878^{WT}$, there are soluble factors that are induced by the strains that increase the activation of the HIV-1 LTR compared to soluble factors produced in uninfected MDM. The fact that the LTR activity was increased in TZM-bl cells that were co-cultured with SN before HIV-1 infection suggests there might be increased uptake of HIV-1 into TZM-bl cells in the presence of the SN from $CDC1551^{WT}$ and $HN878^{WT}$ (Fig. 4.4A).

Surprisingly, there was no modification of LTR activity in TZM-bl cells pre-incubated with SN harvested 96-hour post-infection with $EX30^{Q1939/A605}$ ($p = 0.7728$) and $MRC16^{P1939/A605}$ ($p = 0.248$, Fig. 4.4B). Taken together, this data suggests that the factors induced early (24-hours) from $EX30^{Q1939/A605}$ and $MRC16^{P1939/A605}$ infected MDM which increased the LTR activity and – potentially may lead to rapid uptake of HIV-1, may not be present in the 96-hour SN.

By comparison there was significant effect of SN isolated 96-hours post-infection from either $EU111^{N1759}$ ($p = 0.0238$) or $EU40^{T1759}$ ($p = 0.0230$) compared to SN from uninfected MDM (Fig. 4.4C) on the uptake of HIV-1 into TZM-bl cells (pre-incubation). $HN878^{WT}$ SN also resulted in increased LTR activity in TZM-bl cells compared to LTR activity induced by SN from $EU111^{N1759}$ ($p = 0.0230$) (Fig. 4.4C). This data shows that early and late induced soluble factors from lineage 2 strains, $EU111^{N1759}$, $EU40^{T1759}$ and $HN878^{WT}$ increase the LTR activity in HIV-1 infected TZM-bl cells, and that may be due to increased priming of TZM-bl cells and thus increased uptake of HIV-1.

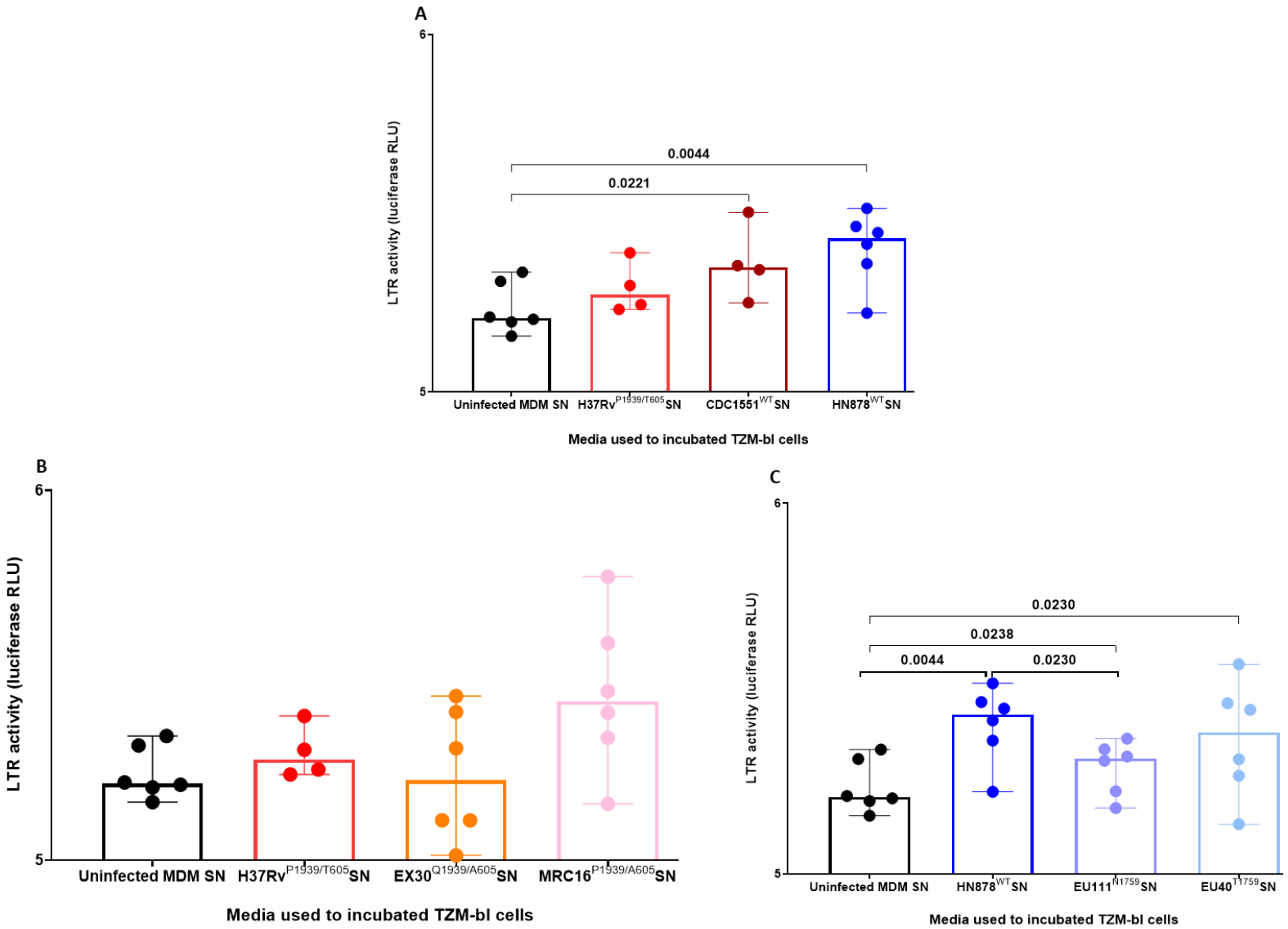
A
6
5
LTR activity (luciferase RLU)
0.0044
0.0221
Uninfected MDM SN
H37Rv P1939/T605 SN
CDC1551 WT SN
HN878 WT SN
Media used to incubated TZM-bl cells
B
6
5
LTR activity (luciferase RLU)
Uninfected MDM SN
H37Rv P1939/T605 SN
EX30 Q1939/A605 SN
MRC16 P1939/A605 SN
Media used to incubated TZM-bl cells
C
6
5
LTR activity (luciferase RLU)
0.0230
0.0238
0.0044
0.0230
Uninfected MDM SN
HN878 WT SN
EU111 N1759 SN
EU40 T1759 SN
Media used to incubated TZM-bl cells

Figure 4.4. Analysis of TZM-bl cells infection with HIV-1 pre-incubation with SN harvested 96-hours post-infection from MDM infected with clinical and laboratory strains.
TZM-bl cells were incubated with SN from *Mtb* infected MDM 24-hours before infection with HIV-1. LTR activity was measured 48 hours post-infection with HIV-1 in both experimental set-ups. The LTR activity was measured using the Bright Glo assay (Promega). Luminescence data was analysed by Graph Pad prism. Graphs show LTR activity in TZM-bl cells incubated with SN harvested 96-hours after infection of MDM. TZM-bl cells were 24-hours before HIV-1 infection with SN from (**A**) $H37Rv^{P1939/T605}$ or $CDC1551^{WT}$ or $HN878^{WT}$ infected MDM, (**B**) $EX30^{Q1939/A605}$ or $MRC16^{P1939/A605}$ infected MDM, and (**C**) SN from MDM infected with $EU111^{N1579}$ or $EU40^{T1579}$. Median with IQR for n=6 donors or 4 donors of SN. Statistics were measured with Kruskallis-Wallis multiple comparison test. Significance was analysed by a two-stage linear step-up procedure of Benjamini, Krieger and Yekutieli was used to control for multiple comparison false discovery rate. P<0.05 are shown in graph.

I went further to analyse the LTR activity in TZM-bl cells infected with HIV-1 and then co-cultured with SN harvested 24-hours post-infection with the panel of clinical and laboratory strains. To do this, I infected TZM-bl cells with HIV-1 for 6-hours and used the SN harvested 24-hours post-infection from *Mtb* strains or SN from uninfected MDM to co-culture the TZM-bl cells (see Fig. 3.1). In this data I observed a significant increase in LTR activity in TZM-bl cells incubated with SN from $CDC1551^{WT}$ (p = 0.0233) and $HN878^{WT}$ (p =0.0233) harvested 24-hours post-infection (Fig. 4.5A). Like with pre-incubation $H37Rv^{P1939/T605}$ did not have any effect on LTR activity in TZM-bl cells (Fig. 4.5A). These data indicate that soluble factors induced by $CDC1551^{WT}$ or $HN878^{WT}$ increase the LTR activity post-viral entry into TZM-bl cells.

When I analysed TZM-bl cells incubated with SN harvested 24-hours post-infection with $EX30^{Q1939/A605}$ and $MRC16^{P1939/A605}$ clinical strains, I observed that SN harvested 24-hours post-infection from MDM infected with $EX30^{Q1939/A605}$ significantly increased LTR activity (p = 0.0476) compared to TZM-bl cells incubated with SN from uninfected MDM (Fig. 4.5B). There was also a significant increase in LTR activity by SN from $EX30^{Q1939/A605}$ infected MDM compared to LTR activity induced by SN from $H37Rv^{P1939/T605}$ infected MDM (Fig. 3.5B). SN from the clinical strain $MRC16^{P1939/A605}$ increased the LTR activity compared to SN from uninfected MDM, but this increase was not significant at alpha 0.05 (FDR = 0.0819; p = 0.1489) and showed a trend to increasing LTR activity compared to SN from $H37Rv^{P1939/T605}$ (p = 0.0675; FDR<0.1) (Fig. 4.5B). These results suggest that $EX30^{Q1939/A605}$ induced factors early that increase the LTR activity and the effect maybe modest when using SN from $MRC16^{P1939/A605}$.

Finally, I proceeded to analyse the effect of $EU111^{N1759}$ and $EU40^{T1759}$ SN on HIV-1 LTR activity in TZM-bl cells. There was no significant effect on LTR activity in TZM-bl cells incubated with the 24-hour SN from both $EU111^{N1759}$ and $EU40^{T1759}$ (Fig. 4.5C). This data

suggests that factors induced early (24-hours) by $EU111^{N1759}$ and $EU40^{T1759}$ may be better at priming TZM-bl cells for rapid uptake of HIV-1 compared to activating the LTR activity post-viral infection.

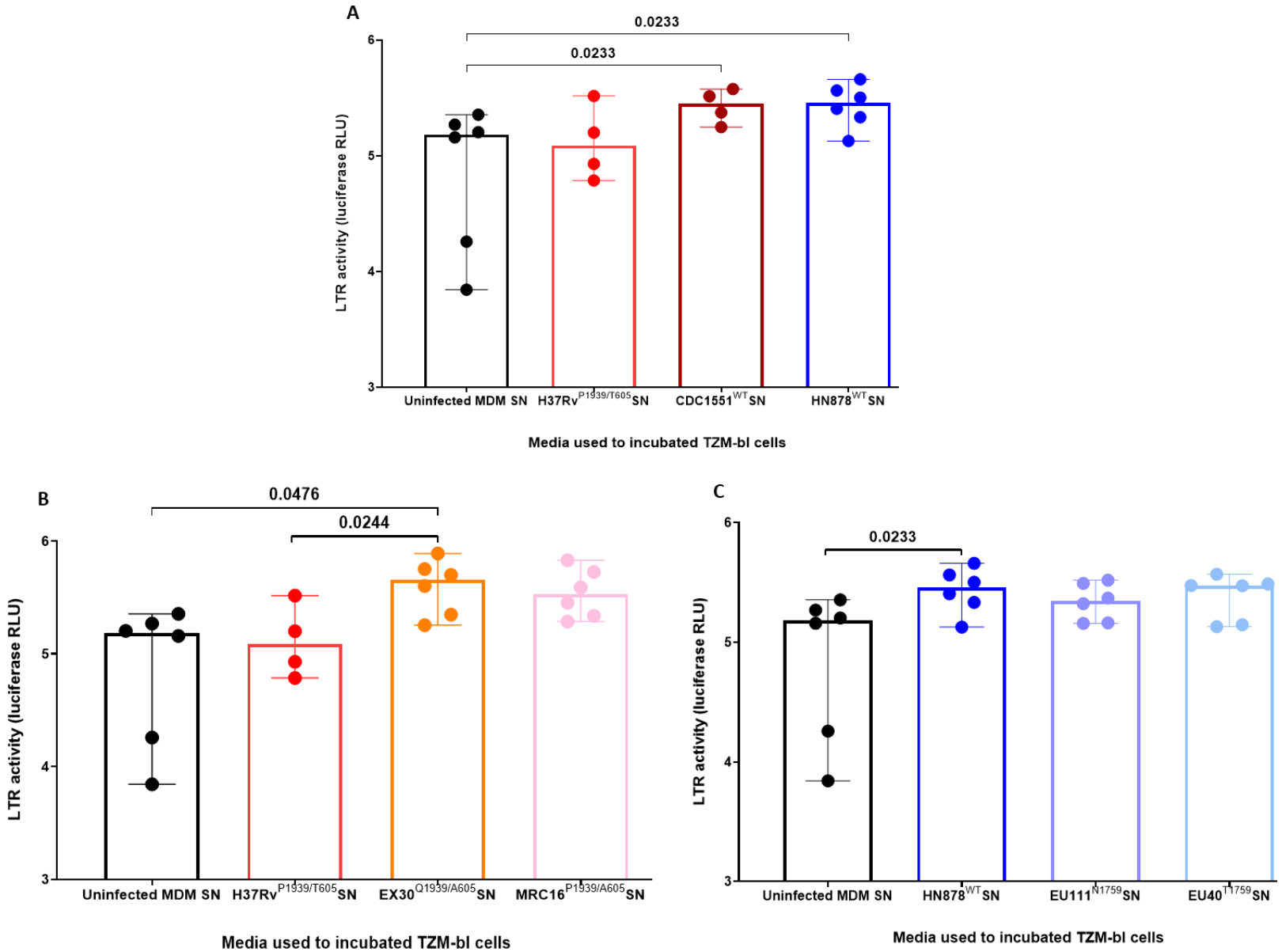
A
0.0233
0.0233
LTR activity (luciferase RLU)
6
5
4
3
Uninfected MDM SN
H37Rv P1939/T605 SN
CDC1551 WT SN
HN878 WT SN
Media used to incubated TZM-bl cells
B
0.0476
0.0244
LTR activity (luciferase RLU)
6
5
4
3
Uninfected MDM SN
H37Rv P1939/T605 SN
EX30 Q1939/A605 SN
MRC16 P1939/A605 SN
Media used to incubated TZM-bl cells
C
0.0233
LTR activity (luciferase RLU)
6
5
4
3
Uninfected MDM SN
HN878 WT SN
EU111 N1759 SN
EU40 T1759 SN
Media used to incubated TZM-bl cells

Figure 4.5. Analysis of HIV-1 LTR activity in TZM-bl cells incubated with SN harvested 24-hours post-infection of MDM infected with clinical and laboratory strains.
TZM-bl cells were incubated with SN from *Mtb* infected MDM 6-hours post-infection with HIV-1. LTR activity was measured 48 hours post-infection with HIV-1 in both experimental set-ups. The LTR activity was measured using the Bright Glo assay (Promega). Luminescence data was analysed by Graph Pad prism. Graphs show LTR activity in TZM-bl cells incubated with SN harvested 24-hours after infection of MDM. TZM-bl cells were 24-hours before HIV-1 infection with SN from (**A**) $H37Rv^{P1939/T605}$ or $CDC1551^{WT}$ or $HN878^{WT}$ infected MDM, (**B**) $EX30^{Q1939/A605}$ or $MRC16^{P1939/A605}$ infected MDM, and (**C**) SN from MDM infected with $EU111^{N1579}$ or $EU40^{T1579}$. Median with IQR for n=6 donors or 4 donors of SN. Statistics were measured with Kruskallis-Wallis multiple comparison test. Significance was analysed by a two-stage linear step-up procedure of Benjamini, Krieger and Yekutieli was used to control for multiple comparison false discovery rate. P<0.05 are shown in graph.

Finally, I analysed the effect of incubating TZM-bl that were infected with HIV-1 for 6-hours with SN harvested from MDM infected with clinical and laboratory strains for 96-hours. SN harvested 96-hours post-infection from MDM infected with either $CDC1551^{WT}$ (p = 0.0088) or SN from $HN878^{WT}$ (0.0088) increased LTR activity in TZM-bl cells when added 6-hours post-infection (Fig. 5.6A). Which means that factors that increased LTR activity in SN induced by both $CDC1551^{WT}$ and $HN878^{WT}$ are maintained at both 24-hours and 96-hours.
Unlike, the pre-incubation, LTR activity was significantly increased in TZM-bl cells incubated with SN harvested 96-hours post-infection with $EX30^{Q1939/A605}$ (p =0.0230) or $MRC16^{P1939/A605}$ (p = 0.0238, Fig. 4.6B) when the SN is added after HIV-1 infection. Taken together, this data suggests soluble factors from $MRC16^{P1939/A605}$ infected MDM and SN from MDM infected with $EX30^{Q1939/A605}$ increase LTR activity in HIV-1 infected TZM-bl cells.

By comparison both $EU111^{N1759}$ and $EU40^{T1759}$ induced SN increased LTR activity, although this was not significant relative to SN from uninfected MDM (Fig. 4.6C). This further solidifies that $EU111^{N1759}$ and $EU40^{T1759}$ induces factors that may aid with priming TZM-bl cells more than influencing the LTR activity post-viral entry.

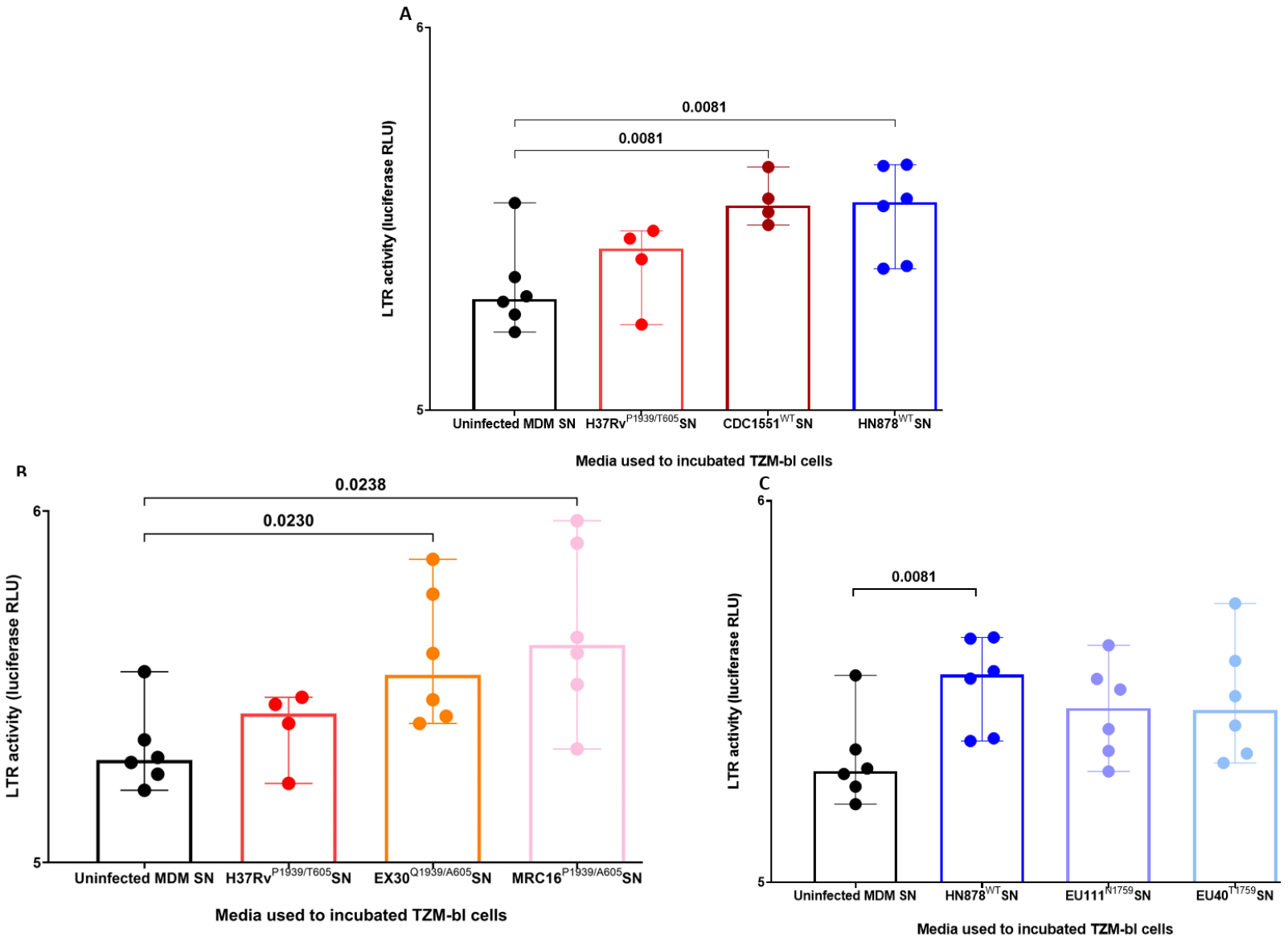
A
6
5
LTR activity (luciferase RLU)
0.0081
0.0081
Uninfected MDM SN
H37Rv P1939/T605 SN
CDC1551 WT SN
HN878 WT SN
Media used to incubated TZM-bl cells
B
6
5
LTR activity (luciferase RLU)
0.0238
0.0230
Uninfected MDM SN
H37Rv P1939/T605 SN
EX30 Q1939/A605 SN
MRC16 P1939/A605 SN
Media used to incubated TZM-bl cells
C
6
5
LTR activity (luciferase RLU)
0.0081
Uninfected MDM SN
HN878 WT SN
EU111 N1759 SN
EU40 T1759 SN
Media used to incubated TZM-bl cells

Figure 4.6. Analysis of HIV-1 LTR activity in TZM-bl cells incubated with SN harvested 96-hours post-infection of MDM infected with clinical and laboratory strains.
TZM-bl cells were incubated with SN from *Mtb* infected MDM 6-hours post-infection with HIV-1. LTR activity was measured 48 hours post-infection with HIV-1 in both experimental set-ups. The LTR activity was measured using the Bright Glo assay (Promega). Luminescence data was analysed by Graph Pad prism. Graphs show LTR activity in TZM-bl cells incubated with SN harvested 96-hours after infection of MDM. TZM-bl cells were 24-hours before HIV-1 infection with SN from (**A**) $H37Rv^{P1939/T605}$ or $CDC1551^{WT}$ or $HN878^{WT}$ infected MDM, (**B**) $EX30^{Q1939/A605}$ or $MRC16^{P1939/A605}$ infected MDM, and (**C**) SN from MDM infected with $EU111^{N1579}$ or $EU40^{T1579}$. Median with IQR for n=6 donors or 4 donors of SN. Statistics were measured with Kruskallis-Wallis multiple comparison test. Significance was analysed by a two-stage linear step-up procedure of Benjamini, Krieger and Yekutieli was used to control for multiple comparison false discovery rate. $P<0.05$ are shown in graph.

4.2.2. Impact of *Mtb*-induced cytokines on productive HIV-1 infection

In the next phase of analysis, I wanted to measure whether cytokines secreted by MDM infected with different strains of *Mtb* would have differential regulatory effects on HIV-1 productive infection in neighbouring cells, in the absence of direct co-infection. The SN that was used here was from *Mtb* infected MDM as described in Chapter 3. Analysis of cytokine secretion (Fig. 3.11) showed that cytokine secretion by MDM phenotype clustered together – indicating that for cytokines measured in these experiments, secretion was comparable between M1 and M2 MDM. This indicated that MDM phenotype has minimal contribution to observed variation in the data. With that in mind, I combined SN harvested from M1 and M2 MDM of the same donors, to create a combined M1 and M2 SN. Furthermore, analysis of contribution by donor variation on cytokine secretion also showed that differences between donors was not a major contributor of variation to cytokine secretion. Therefore, following combining M1 and M2 MDM for each strain used, I combined the M1 and M2 SN mixture from different donors, to have a SN that is mixture of M1 and M2 of all donors for each strain. This also enabled sufficient volume of a homogenous SN to be available to co-culture MDM from multiple new donors. The homogenous SN was taken to represent the mean cytokines induced across donors and MDM types, for each of the *Mtb* strains. To measure the impact of cytokine exposure on viral production during an established HIV-1 infection, I infected M2 MDM with HIV-1 for 18 hours. After 18 hours, I removed the media from MDM and added the combined SN from different donors and incubated the cells for 72 hours. I harvested the SN from the cells and used the SN to measured HIV-1 p24 secretion by Luminex assay (Fig. 4.5).

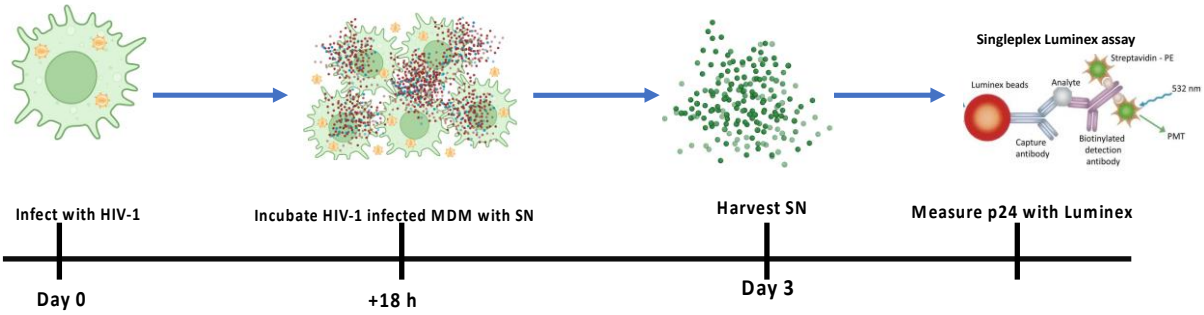

Figure 4.7. A schematic that shows the flow of incubating HIV-1 infected M2 MDM with SN harvested from *Mtb* infected MDM and analysis of secreted p24 antigen.
M2 MDM polarised MDM were infected with HIV-1 and incubated for 18 hours. The media was discarded from the MDM replaced with combined SN; SN from each strain were pooled to make a donor heterologous SN, consisting of SN from both M1 and M2 MDM. The MDM with SN were incubated for a further 54 hours. The SN was harvested and used to measure p24 antigen with Luminex assay.

I analysed HIV-1 production by measuring HIV-1 p24 in the SN of MDM that were infected with HIV-1 and then incubated with SN from the different laboratory strains. To achieve this, I used the combined SN to incubate M2 MDM 18-hours after HIV-1 infection. The overall data shows that MDM incubated with SN from different laboratory strains 18-hours post-infection with HIV-1 did not significantly alter HIV-1 production compared to MDM that were infected with HIV-1 and allowed to incubate in media only (Fig. 4.8A). Also, there was no difference in HIV-1 production between MDM incubated with SN from uninfected MDM compared to SN from HN878^{WT} ($p = 0.8270$), CDC1551^{WT} ($p = 0.8270$) and H37Rv$^{P1939/T605}$ ($p = 0.2265$, Fig. 4.8A). There was also no difference in HIV-1 production comparing SN harvested between the strains: HN878^{WT} and CDC1551^{WT} ($p = 0.8270$), CDC1551^{WT} and H37Rv$^{P1939/T605}$ ($p = 0.3397$), and HN878^{WT} compared to H37Rv$^{P1939/T605}$ ($p = 0.3397$, Fig. 4.8A). These data indicate that there was no effect on p24 production (as proxy for HIV-1 production) by the SN from the laboratory strains in MDM. I proceeded to measure HIV-1 productive infection in MDM infected with HIV-1 and then incubated with SN from EX30$^{Q1939/A605}$ or MRC16$^{P1939/A605}$ (Fig 4.8B). The data shows a surprising significant decrease in p24 production in the presence of EX30$^{Q1939/A605}$-induced SN compared to media only and uninfected SN controls ($p \leq 0.0148$, Fig. 4.8B), and only a decreased trend for MRC16$^{P1939/A605}$-induced SN ($p \geq 0.2201$, Fig. 4.8B). Furthermore, SN the lineage matched laboratory strain resulted in significantly more HIV-1 production compared to EX30$^{Q1939/A605}$ ($p = 0.0295$; Fig. 5.8B). This indicates a potentially powerful effect of *Mtb* strains on HIV-1 p24 production in neighbouring cells, suggesting that there may be soluble factors induced in response to EX30$^{Q1939/A605}$ and MRC16$^{P1939/A605}$ that inhibit HIV-1 productive infection.

Finally, I looked at the effect of $EU111^{N1759}$ and $EU40^{T1759}$ induced SN on HIV-production. I did not observe a significant influence on p24 secretion by MDM incubated with SN from either $EU111^{N1759}$ or $EU40^{T1759}$ (Fig. 4.4C).

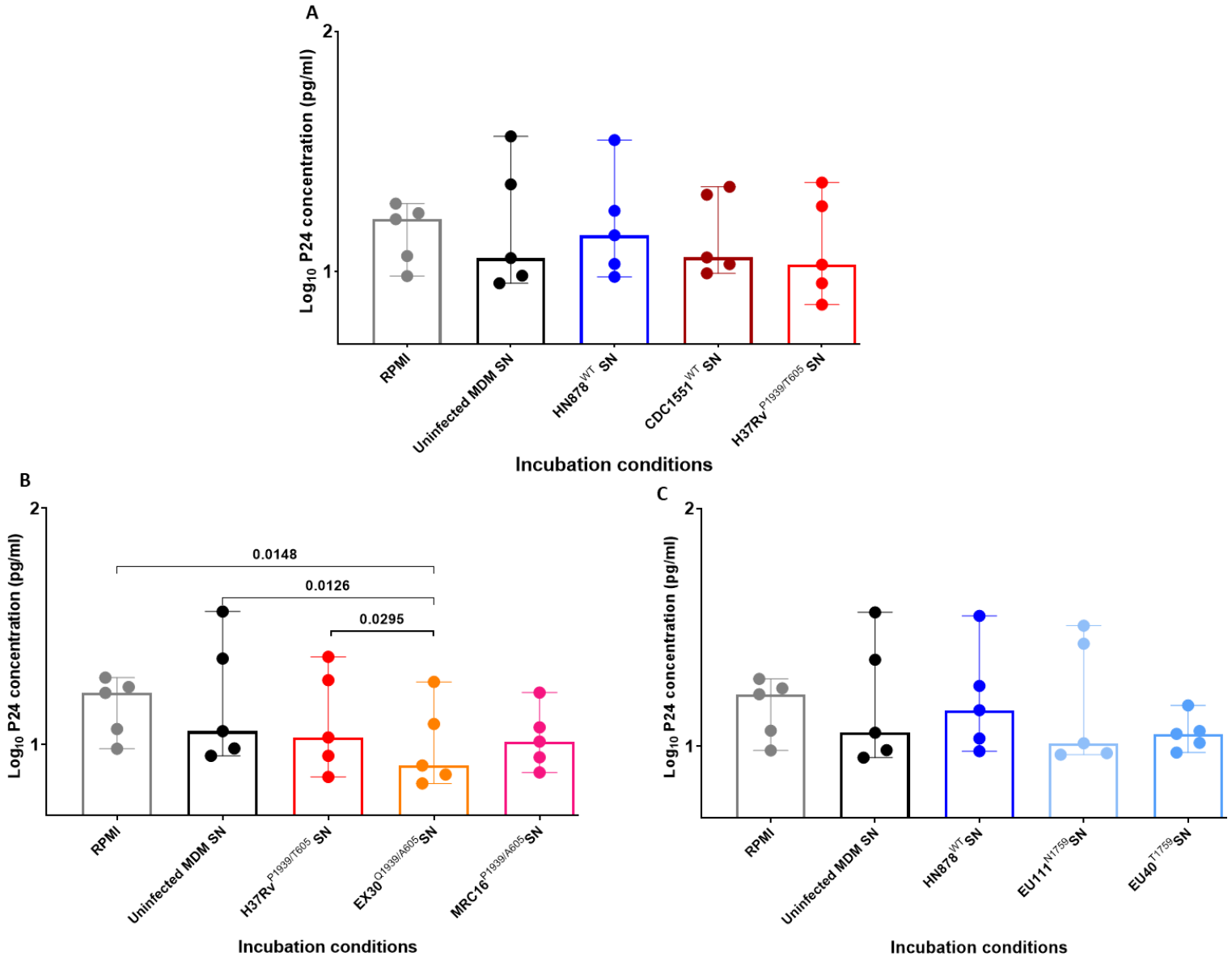
A
Log10 P24 concentration (pg/ml)
2
1
RPMI
Uninfected MDM SN
HN878 WT SN
CDC1551 WT SN
H37Rv P1939/T605 SN
Incubation conditions
B
Log10 P24 concentration (pg/ml)
0.0148
0.0126
0.0295
RPMI
Uninfected MDM SN
H37Rv P1939/T605 SN
EX30 Q1939/A605 SN
MRC16 P1939/A605 SN
Incubation conditions
C
Log10 P24 concentration (pg/ml)
RPMI
Uninfected MDM SN
HN878 WT SN
EU111 N1759 SN
EU40 T1759 SN
Incubation conditions

Figure 4.8. Secretion of HIV-1 p24 by MDM incubated with laboratory strain induced SN.
Monocytes from 6 donors were polarised M2 MDM. The MDM were infected with HIV-1 for 18-hours and the co-incubated with SN from MDM infected with a panel of *Mtb* strains. The MDM was harvested 72-hours post-infection HIV-1 and p24 was analysed by Luminex assay. Luminex data analysed by GraphPad Prism. The graphs represent p24 production in MDM incubated with SN from (**A**) $H37Rv^{P1939/T605}$, $CDC1551^{WT}$, $HN878^{WT}$ MDM, (**B**) $H37Rv^{P1939/T605}$ or $EX30^{Q1939/A605}$ or $MRC16^{P1939/A605}$ MDM and (C) $HN878^{WT}$ or $EU111^{N1759}$ or $EU40^{T1759}$. n=6 donors. Friedman's multiple comparison test with a significance cut off 0.05. A two-stage linear step-up procedure of Benjamini, Krieger and Yekutieli was used to control for multiple comparison false discovery rate with a cut of 0.1.

4.2.3. Analysis of cytokines from M1 and M2 polarised MDM co-infected with HIV-1 and a panel of *Mtb* strains

In the following experiments I analysed the effect of co-infection of MDM with HIV-1 on cytokine secretion and consequently HIV-1 production. I used M1 and M2 MDM in these experiments and first established confluent HIV-1 infection for 7 days before subsequent infection with the panel of *Mtb* strains I had selected. PMBC from six donors were used to polarise M1 and M2. Co-infected MDM were incubated for 24-hours, and SN was harvested. Fresh media was added to the cell culture, and after 96-hours, SN was harvested again and stored for cytokine secretion analysis by Luminex assay (Fig. 4.9).

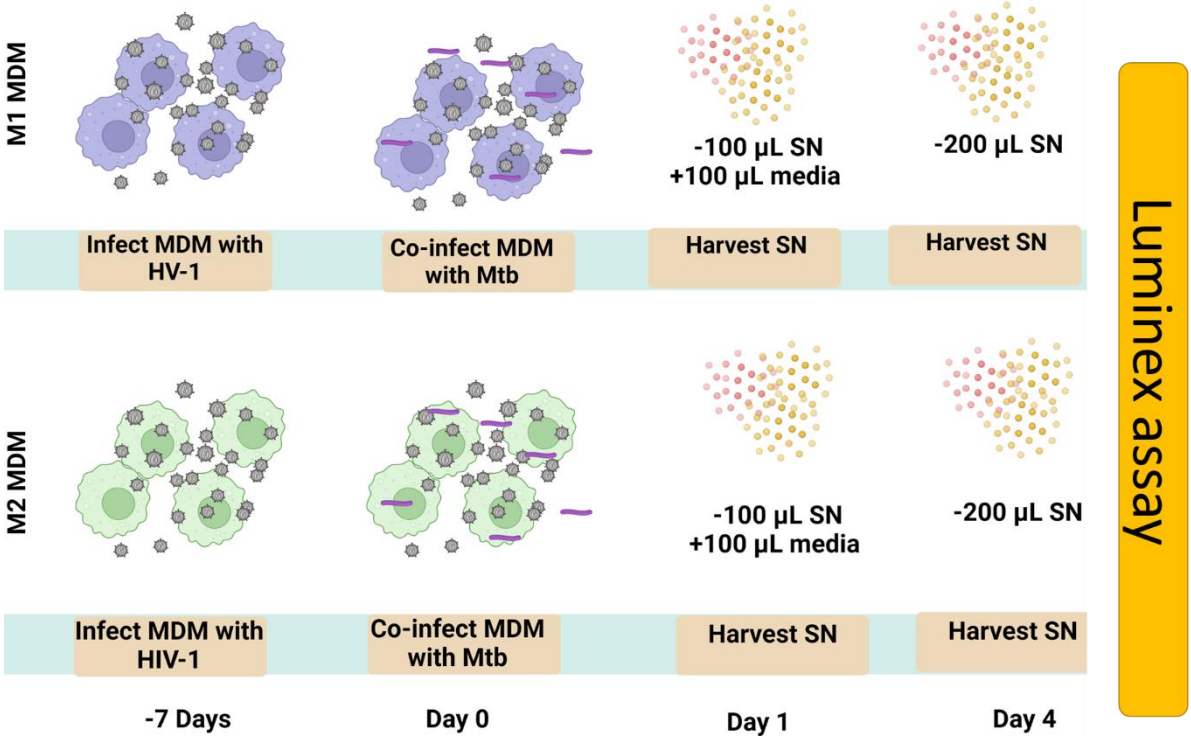

Figure 4.9. A simple schematic that shows the flow of the co-infection experiments performed and analysis of SN with Luminex assay.
M1 and M2 MDM polarised MDM were infected with HIV-1 this land incubated for 7 days, with the media replaced every 3rd day. Seven days post HIV-1 infection, MDM were coinfected with a panel of *Mtb* and further incubated. SN was harvested 24 h and 96 h post-infection and stored or for cytokine analysis by Luminex assay

I analysed cytokine secretion by M1 and M2 MDM co-infected with HIV-1/*Mtb* via Luminex (chapter 2; section 2.6) and I analysed the data via PCA using Qlucore omics statistical software. I selected PCA as an analysis method because the data is complex and there could be a variety of sources contributing to variation in the data including MDM phenotype, donor variability and *Mtb* strain used for infection. PCA analysis allows for resolution of patterns within the data and provides information around the primary sources of variation within complex datasets. Firstly, I analysed how much MDM phenotype contributed to the variation of cytokine production that was observed (Fig. 4.10A). This analysis revealed that there were subtle differential patterns of clustering between M1 and M2 MDM (Fig. 4.10A), more than had been seen when performing MD*M* infection with *Mtb* only (see chapter 3.2.3). This data shows that in the presence of co-infection with HIV-1 there are more (however, subtle) differences in cytokine secretion between M1 and M2. In the next phase of analysis, I stratified the PCA plot by donors and the strains of *Mtb* used for co-infection. Co-infection exposes variability of responses between donors (Fig. 4.10B-C). MDM donors have distinct clusters, such as donor two, three and four (Fig. 4.10B), which suggests these donors have distinct cytokine secretion phenotypes and that some of the variability observed could be related to inter-donor differences. It is worth mentioning that infection of donors 1-3 and donors 4-6 were completed on different days, however, the differences observed in cytokine secretion is not due to the batch effect. Because although they were completed in the same batch there are big difference between donor two and three, these have little overlap between each other, which clearly suggest big difference in cytokine secretion. While donors one, five and six cluster together in the PCA (Fig. 4.10B) - an outcome that indicates these donors have similar cytokine secretion patterns following infection with HIV-1 and *Mtb*.

I also stratified the PCA by co-infection with the different strains of *Mtb* and looked at HIV-1 only infection. The PCA shows that co-infection contributes to the variability observed in the data. Because HIV-1 only infection separates from co-infection with *Mtb* strains (Fig. 4.10C), particularly in relation to H37Rv and MRC16$^{P1939/A605}$ (Fig. 4.10C) two of the lineage 4 strains. This data indicates that during HIV-1/*Mtb* co-infection, the difference between donors (Fig. 4.10A) and the differences between the *Mtb* strains (Fig. 4.10C) used for co- infections account for most of the variation in cytokine production observed.

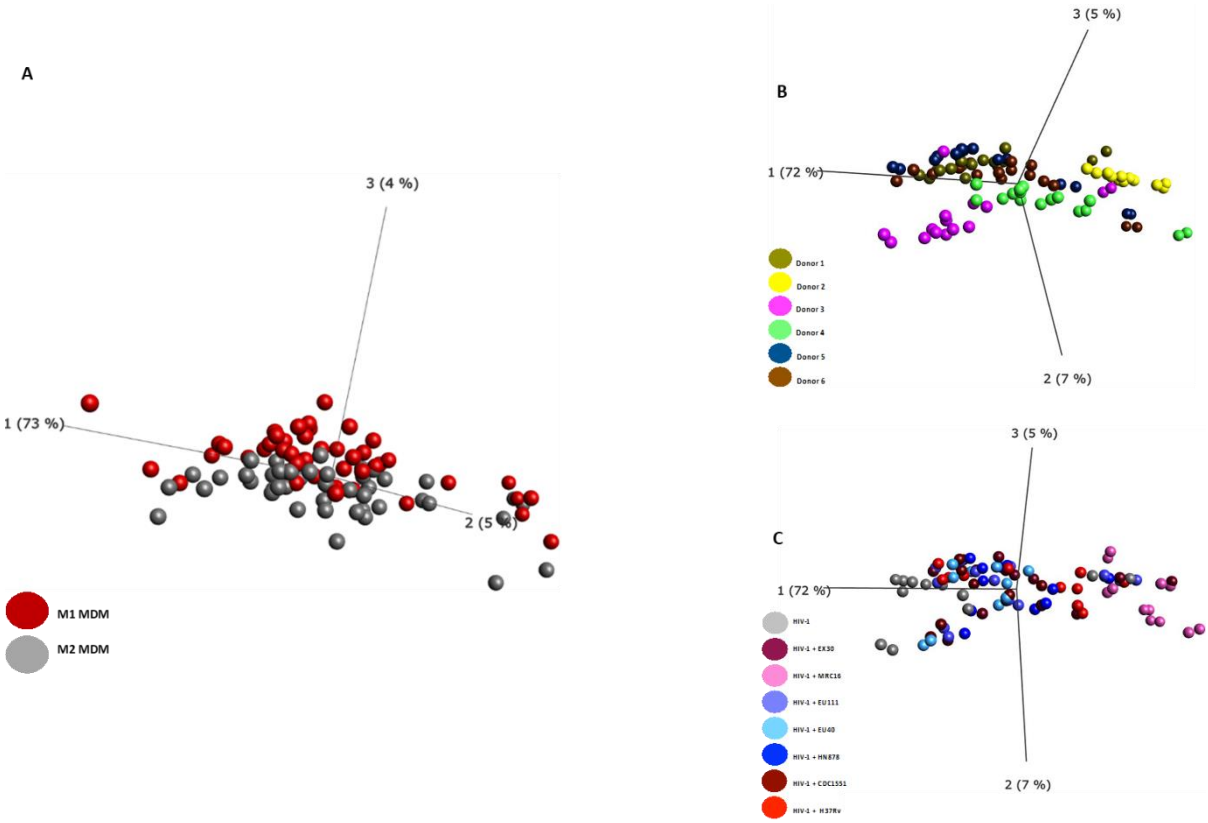

Figure 4.10. Principal component analysis of cytokine secretion 96 hours after HIV *Mtb* co-infection. Dates stratified by (A) MDM phenotype, (B) donor and (C) HIV-1 co-infected *Mtb* strain.
Monocytes from 6 donors were polarised to M1 and M2 MDM. MDM were infected with different with HIV-1 for 7-days. The HIV-1 co-infected MDM were infected with *Mtb* strains and incubated for 96 h. The SN was harvested and used for quantifying 25 cytokines by Luminex assay. Data was analysed by Qlucore omics explorer, each dot represents a single sample.

4.2.4. Analysis of individual cytokine secretion by MDM co-infected with HIV-1 and the different strains of *Mtb*

I measured the magnitude of cytokine induction by MDM that were infected with HIV-1 for seven days and the co-infected with the laboratory strains. Cytokines that had a significant fold change differences in at least one comparison are listed in the tables below. Where there was no significant fold change difference the value is not indicated, and the p-value is marked with ns. Raw data, including interquartile ranges are in supplementary tables at the end of this section.

There were no differences observed in cytokine secretion by MDM co-infected with the different laboratory strains (Table 4.1). However, there was a difference relative to the HIV-1 only control for some cytokines at 96-hours post-infection. HN878^{WT} and H37Rv$^{P1939/T605}$ co-infection significantly increased the production of IL-6, IL-12, CCL4 and CXCL8 relative to

the baseline control of HIV-1 only (Table 4.1). The laboratory strain CDC1551^{WT} did not significantly increase cytokine secretion relative to baseline HIV-1 infection.

Table 4.1. Comparison of cytokine secretion induced by the laboratory strains in HIV-1 co-infected MDM 24-hours and 96-hours

Cytokines harvested 96 hours post infection						
	H37Rv$^{P1939/T605}$/ HIV-1 v HIV-1		CDC1551^{WT}/ HIV-1 v HIV-1		HN878^{WT}/ HIV-1 v HIV-1	
Analyte	**Fold change**	**p-value**	**Fold change**	**p-value**	**Fold change**	**p-value**
IL-6	1.07	0.0055	-	ns	1.15	0.0006
CCL4	1.49	0.0022	-	ns	1.15	0.0034
CXCL8	2.76	0.0017	-	ns	2.65	0.0017
IL-12	1.2	0.0096	-	ns	1.2	0.0004

Kruskal-Wallis s multiple comparison test with Two-stage linear step-up procedure of Benjamini, Krieger and Yekutieli False discovery rate (FDR): with a cut off 0.1. Mean fold change between compared groups. p-value of comparison with FDR of <0.1. Fold change of non-significant (ns) value is not shown

I went on to compare cytokine secretion in MDM that were co-infected with HIV-1/EX30$^{Q1939/A605}$ or HIV-1/MRC16$^{P1939/A605}$ or H37Rv$^{P1939/T605}$. In these experiments I measured cytokines from SN harvested 24- and 96-hours post-co-infection using a Luminex assay. I observed that secretion of many cytokines was increased during co-infection with both EX30$^{Q1939/A605}$ and MRC16$^{P1939/A605}$, as compared to the HIV-1 only baseline control (Table 4.2). As seen during *Mtb* mono-infection (Table 3.3), most cytokines that were measured were secreted in significantly higher levels by MDM co-infected with MRC16$^{P1939/A605}$, compared to EX30$^{Q1939/A605}$ and this is true for both 24- and 96-hours post-infection (Table 4.2). There was significantly more IL-2R, IL-5 and IL-10 in MDM co-infected with HIV-1/MRC16$^{P1939/A605}$ compared to MDM co-infected with HIV-1/EX30$^{Q1939/A605}$ at 24-hours post-infection (Table 4.2). HIV-1/MRC16$^{P1939/A605}$ co-infection also resulted in significant increases of cytokines compared to the lineage matched laboratory strain H37Rv$^{P1939/T605}$ (Table 4.2). Interestingly, only IL-10 overlaps with cytokines significantly increased compared to HIV-1/EX30$^{Q1939/A605}$, other cytokines including IL-4, IL-6, CXCL10, TNF, IL-2, CCL11, IL-7 and CCL5 are uniquely different between HIV-1/H37Rv$^{P1939/T605}$ and HIV-1/MRC16$^{P1939/A605}$ co-infection at the 24-hour time point. There were no cytokines that were significantly different between MDM co-infected with HIV-1/EX30$^{Q1939/A605}$ compared to MDM co-infected with HIV-1/H37Rv$^{P1939/T605}$ at both time points (Table 4.2). There substantially more cytokines increased in by MDM co-infected with HIV-1/MRC16$^{P1939/A605}$ in at 96-hours compared to both HIV-1/EX30$^{Q1939/A605}$ and HIV-1/H37Rv$^{P1939/T605}$ co-infection (Table 4.2). In fact, CCL2

was the only cytokines that was comparably induced between HIV-1/MRC16$^{P1939/A605}$ and HIV-1/EX30$^{Q1939/A605}$, (Table 4.2), while this list included CXCL8, CCL11, CCL4, CXCL10, IL-13, IL-1RA and CCL2 when compared to HIV-1/H37Rv$^{P1939/T605}$ (Table 4.2). These data show that MRC16$^{P1939/A605}$ co-infection of HIV-1 infected MDM increases cytokines secretion beyond co-infection with HIV-1 with EX30$^{Q1939/A605}$ or H37Rv$^{P1939/T605}$. But there is no comparable difference in the induction of cytokines between EX30$^{Q1939/A605}$ and H37Rv$^{P1939/T605}$ co-infection conditions.

Table 4.2. Comparison of cytokines secretion induced by *Mtb* $EX30^{Q1939/A605}$ and $MRC16^{P1939/A605}$ in HIV-1 co-infected MDM

	Cytokines harvested 24-hours post infection									
	$EX30^{Q1939/A605}$/HIV-1 v $MRC16^{P1939/A605}$/HIV-1		$EX30^{Q1939/A605}$/HIV-1 v $H37Rv^{P1939/T605}$/HIV-1		$MRC16^{P1939/A605}$/HIV-1 v $H37Rv^{P1939/T605}$/HIV-1		$EX30^{Q1939/A605}$/HIV-1 v HIV-1		$MRC16^{P1939/A605}$/HIV-1 v HIV-1	
Analyte	**Fold change**	**p-value**	**Fold change**	**p-value**	**Fold change**	**p-value**	**Fold change**	**p-value**	**Fold change**	**p-value**
IL-10	-3.28	0.0433	-	ns	3.21	0.0223	-	ns	4.17	0.0015
IL-2R	-2.76	0.0433	-	ns	-	ns	-	ns	3.58	0.0015
IL-5	-2.13	0.0433	-	ns	-	ns	-	ns	2.38	0.0015
IL-1β	-	ns	-	ns	-	ns	2.49	0.0433	2.78	0.0209
IL-4	-	ns	-	ns	2.52	0.0368	1.74	0.0433	3.92	0.0015
IL-13	-	ns	-	ns	-	ns	1.43	0.0433	2	0.0015
IL-6	-	ns	-	ns	3.28	0.0368	1.32	0.0433	4.95	0.0015
CCL3	-	ns	-	ns	-	ns	1.30	0.0433	2.83	0.0209
CXCL9	-	ns	-	ns	19.27	0.0078	-	ns	22.31	0.0009
TNF	-	ns	-	ns	2.95	0.0278	-	ns	5.83	0.0005
IL-12	-	ns	-	ns	-	ns	-	ns	4.84	0.0094
IFN-γ	-	ns	-	ns	-	ns	-	ns	4.25	0.0009
GM-CSF	-	ns	-	ns	-	ns	-	ns	3.31	0.0005
IL-2	-	ns	-	ns	2.92	0.0260	-	ns	3.87	0.0005
IL-15	-	ns	-	ns	-	ns	-	ns	3.39	0.0009
CCL11	-	ns	-	ns	2.83	0.0163	-	ns	2.31	0.0141
IFNα	-	ns	-	ns			-	ns	3.43	0.0005
IL-7	-	ns	-	ns	1.84	0.0303	-	ns	2.72	0.0005
IL-17	-	ns	-	ns	-	ns	-	ns	2.89	0.0009
CXCL10	-	ns	-	ns			-	ns	8.06	0.0094
CCL4	-	ns	-	ns	-	ns	-	ns	3.66	0.0039
IL-1RA	-	ns	-	ns	-	ns	-	ns	3.40	0.0209

CCL2	-	ns	-	ns	-	ns	-	ns	3.09	0.0094
CCL5	-	ns	-	ns	2.63	0.0373	-	ns	-	ns
Cytokines harvested 96-hours post infection										
	$EX30^{Q1939/A605}$/HIV-1 v $MRC16^{P1939/A605}$/HIV-1		$EX30^{Q1939/A605}$/HIV-1 v $H37Rv^{P1939/T605}$/HIV-1		$MRC16^{P1939/A605}$/HIV-1 v $H37Rv^{P1939/T605}$/HIV-1		$EX30^{Q1939/A605}$/HIV-1 v HIV-1		$MRC16^{P1939/A605}$/HIV-1 v HIV-1	
Analyte	**Fold change**	**p-value**	**Fold change**	**p-value**	**Fold change**	**p-value**	**Fold change**	**p-value**	**Fold change**	**p-value**
CXCL9	-11.90	0.0004	-	ns	14.23	0.0004	1.88	ns	22.39	<0.0001
TNF	-7.69	0.0194	-	ns	25.2	0.0024	-	ns	26.84	0.0006
IL-7	-5.88	0.0109	-	ns	1.92	0.0408	-	ns	11.23	0.0015
IL-6	-5.88	0.0124	-	ns	10.43	0.0015	1.94	0.081	11.23	<0.0001
IL-12	-4	0.0312	-	ns	4.44	0.0063	1.44	0.0585	5.75	<0.0001
IL-10	-3.12	0.0307	-	ns	4.42	0.0042	-	ns	4.30	0.0028
CCL3	-2.85	0.0124	-	ns	3.01	0.0096	1.43	0.2694	4	0.0003
IL-2	-2.38	0.0408	-	ns	3.22	0.0171	-	ns	4.01	0.0023
CXCL8	-2.27	0.1462	-	ns	-	ns	2.71	0.0146	6	<0.0001
CCL11	-2.22	0.0109	-	ns	-	ns	-	ns	2.37	0.0048
IL-4	-2.17	0.0656	-	ns	3.05	0.0178	-	ns	3.64	0.0019
CCL4	-2.08	0.1483	-	ns	-	ns	1.45	0.0347	3	0.0004
IFNα	-1.96	0.0808	-	ns	2.33	0.0441	-	ns	2.892	0.0043
CXCL10	-1.85	0.0587	-	ns	-	ns	-	ns	1.96	0.0114
IL-1β	-1.17	0.1251	-	ns	7.27	0.0123	6.52	0.0516	7.59	0.0006
IFN-γ	-1.53	0.0573	-	ns	3.33	0.0153	2.44	0.1353	3.74	0.0007
IL-13	-1.42	0.0247	-	ns	-	ns	1.47	0.0247	2.10	<0.0001
IL-17	-2.06	0.0143	-	ns	2.23	0.0443	1.28	0.0662	2.63	<0.0001
GM-CSF	-3.57	0.0247	-	ns	9.57	0.0041	2.78	0.0247	9.93	<0.0001
IL-15	-2.43	0.0143	-	ns	2.86	0.0232	-	ns	3.57	<0.0001
IL-5	-1.87	0.0022	-	ns	2.34	0.0357	-	ns	2.21	<0.0001
IL-1RA	-1.59	0.0080	-	ns	-	ns	1.31	0.0412	2.10	<0.0001

IL-2R	-2.5	0.0247	-	ns	2.99	0.0084	1.55	0.0247	3.89	<0.0001
CCL2	-	ns	-	ns	-	ns	-	ns	2.87	0.0046

Friedman's multiple comparison test with Two-stage linear step-up procedure of Benjamini, Krieger and Yekutieli False discovery rate (FDR): with a cut off 0.1. Mean fold change between compared groups. p-value of comparison with FDR of <0.1. Fold change of non-significant (ns) value is not shown.

Next, I measured the secretion of cytokines in MDM co-infected with HIV-1 and *EU111*^{N1759} or EU40^{T1759} or HN878^{WT}. In these experiments, I observed when comparing between cytokines secreted by MDM infected with HIV-1 and then co-infected with *EU111*^{N1759} or EU40^{T1759}, there was minimal differences (Table 4.3). HIV-1/*EU111*^{N1759} co-infection increased the secretion of IL-13 ($p = 0.0423$), TNF (0.0061) and IL-2 ($p = 0.0209$) only compared to HIV-1/EU40^{T1759} at 24-hours post-infection, but the secretion of all cytokines was comparable at 96-hours post-infection (Table 4.3). A big difference between the two conditions was that EU111^{N1759} co-infection increased more cytokine secretion relative to HIV-1 only infection compared to co-infection with EU40^{T1759} (Table 4.3) at both time points. Interestingly, the lineage matched laboratory strain HIV-1/HN878^{WT} induces the secretion of cytokines including TNF ($p= 0024$), IL-6 ($p = 0.0039$), CCL4 ($p = 0.0094$), CCL3 ($p = 0.0209$) and CCL2 ($p = 0.0209$) compared to HIV-1/EU40^{T1759} co-infection (Table 4.3) at 24-hours post-infection. At the same time point I did not observe a difference in cytokines between HIV-1/EU111^{N1759} and HIV-1/HN878^{WT} co-infection. At 96-hours post-co-infection, co-infection with HN878^{WT} significantly increased the secretion of even more cytokines compared to co-infection with EU40^{T1759} (Table 4.3) and increased cytokines secretion compared to EU111^{N1759} co-infection (Table 4.3). MDM co-infected with HIV-1/HN878^{WT} significantly secreted more CXCL8, IL-4, IFNα, IL-12, GM-CSF, CCL4, CCL2 and CXCL10 compared to MDM co-infected with HIV-1/EU111^{N1759} or HIV-1/EU40^{T1759} (Table 4.3). There was an increase in the number of cytokines secreted in MDM co-infected with the clinical strain at 96-hours compared to cytokines secreted at 24-hours post-co-infection (Table 4.3). This data suggests that the SNP observed in EU111^{N1759} (Table 3.1), may not alter the cytokine induction phenotype observed between the strains. While these strains result in increased cytokine induction relative to baseline for some cytokines, the overall magnitude of secretion is lower compared to the lineage matched laboratory strain HN878^{WT}.

Table 4.3. Comparison of cytokine secretion induced by $EU111^{N1759}$ and $EU40^{T1759}$ in HIV-1 co-infected MDM

Cytokines harvested 24-hours post infection										
	$EU111^{N1759}$/HIV-1 v $EU40^{T1759}$/HIV-1		$EU111^{N1759}$/HIV-1 v $HN878^{WT}$/HIV-1		$EU40^{T1759}$/HIV-1 v $HN878^{WT}$/HIV-1		$EU111^{N1759}$/HIV-1 v HIV-1		$EU40^{T1759}$/HIV-1 v HIV-1	
Analyte	**Fold change**	**p-value**	**Fold change**	**p-value**	**Fold change**	**p-value**	**Fold change**	**p-value**	**Fold change**	**p-value**
TNF	1.42	0.0061	-	ns	-1.38	0.0024	-	ns	-	ns
IL-13	1.19	0.0433	-	ns	-	ns	-	ns	-	ns
IL-2	1.31	0.0209	-	ns	-1.35	0.0094	1.24	0.0433	-	ns
IL-6	-	ns	-	ns	-1.74	0.0039	-1.12	0.0094	-	ns
CCL4	-	ns	-	ns	-1.35	0.0094	1.4	0.0094	-	ns
CCL3	-	ns	-	ns	-1.21	0.0209	1.16	0.0094	-	ns
IL-4	-	ns	-	ns	-1.36	0.0209	1.54	0.0094	-	ns
IL-1β	-	ns	-	ns	-	ns	-	ns	-	ns
IL-12	-	ns	-	ns	-1.24	0.0039	-	ns	-	ns
GM-CSF	-	ns	-	ns	-1.25	0.0141	-	ns	-	ns
CCL2	-	ns	-	ns	-1.72	0.0209	-	ns	-	ns
IFN-γ	-	ns	-	ns	-1.18	0.0141	-	ns	-	ns
IFNα	-	ns	-	ns	-1.53	0.0433	-	ns	-	ns
CXCL10	-	ns	-	ns	-6.82	0.0039	2.82	0.0304	-	ns
IL-2R	-	ns	-	ns	-1.37	0.0024	-	ns	-	ns
CXCL8	-	ns	-	ns	-1.51	0.0209	-	ns	-	ns
Cytokines harvested 96-hours post infection										
	$EU111^{N1759}$/HIV-1 v $EU40^{T1759}$/HIV-1		$EU111^{N1759}$/HIV-1 v $HN878^{WT}$/HIV-1		$EU40^{T1759}$/HIV-1 v $HN878^{WT}$/HIV-1		$EU111^{N1759}$/HIV-1 v HIV-1		$EU40^{T1759}$/HIV-1 v HIV-1	
Analyte	**Fold change**	**p-value**	**Fold change**	**p-value**	**Fold change**	**p-value**	**Fold change**	**p-value**	**Fold change**	**p-value**
CXCL8	-	ns	-1.17	0.0080	-1.25	0.0043	2.27	0.0022	2.12	0.0022

TNF	-	ns	-	ns	-1.3	0.0412	1.42	0.0143	-	ns
IL-4	-	ns	-1.09	0.0107	-1.25	0.0080	1.39	0.0004	1.21	0.0016
IL-2	-	ns	-	ns	-	ns	1.36	0.0080	1.21	0.0016
IL-13	-	ns	-	ns	-	ns	1.34	0.0107	1.07	0.0189
IFNα	-	ns	-1.06	0.0107	-1.14	0.0031	1.30	0.0107	1.20	0.0031
IL-15	-	ns	-	ns	-	ns	1.24	0.0059	1.11	0.0321
IL-1RA	-	ns	1.19	0.0143	-	ns	1.22	0.0143	1.08	0.0143
IL-12	-	ns	-1.1	0.0247	-1.26	0.0011	1.12	0.0031	-	ns
IL-17	-	ns	-	ns	-	ns	1.16	0.0107	-	ns
CCL3	-	ns	-	ns	-	ns	1.08	0.0022	1.02	0.0143
GM-CSF	-	ns	1.01	0.0107	-1.1	0.0412	1.07	0.0412	-1.02	0.0247
CCL4	-	ns	-1	0.0412	-1.18	0.0247	-	ns	-	ns
CCL2	-	ns	-1.96	0.0022	-3.09	0.0022	-	ns	-	ns
CXCL10	-	ns	-1.03	0.0247	-1.16	0.0412	-1.04	0.0412	1.01	0.0043

Friedman's multiple comparison test with Two-stage linear step-up procedure of Benjamini, Krieger and Yekutieli False discovery rate (FDR): with a cut off 0.1. Mean fold change between compared groups. p-value of comparison with FDR of <0.1. Fold change of non-significant (ns) value is not shown.

4.2.5. Analysis of HIV-1 productive infection

Finally, to determine whether direct infection with different *Mtb* differentially regulated HIV-1 productive infection in MDM, I measured secreted HIV-1 p24 by Luminex assay, in the same SN in which cytokines were measured above (Fig. 4.6).

4.2.6. Analysis of HIV-1 production in MDM co-infected with different strains of *Mtb*

To further understand the effect of *Mtb* co-infection on HIV-1 productive infection, I analysed p24 secretion between the panel of *Mtb* used for HIV-1 co-infection. Firstly, I analysed HIV-1 productive infection in MDM co-infected with the laboratory strains. Co-infection with the laboratory strains did not modify HIV-1 productive infection in both the M1 and M2 MDM (Fig. 4.11A). Despite similar cytokine induction response in MDM (Table 4.1), there is a median high HIV-1 production in MDM that are co-infected with HN878 (2.24-fold) compared to H37Rv co-infected MDM (Fig. 4.11). H37Rv also resulted in low median HIV-1 production compared to CDC1551 co-infection (2.19-fold lower) and compared to HIV-1 only infected MDM (1.77-fold) (Fig. 4.11A), despite a higher cytokine induction phenotype (Table 4.1). This data points to a strain which induces a higher proinflammatory cytokine phenotype resulting in decreased HIV-1 production.

I went on to analyse p24 secretion in MDM co-infected with HIV-1 and *Mtb* clinical strains EX30$^{Q1939/A605}$ or MRC16$^{P1939/A605}$. I observed no difference in p24 secretion by MDM co-infected with either EX30$^{Q1939/A605}$ or MRC16$^{P1939/A605}$ (Fig. 4.11B). Here the phenotype that strains which induced higher cytokines results in a median low HIV-1 production persists. Because interestingly, the strain with the SNP under HIV-1 Furthermore, HIV-1/EX30$^{Q1939/A605}$ co-infected MDM increased the production of HIV-1 by a median fold of 2.4 ($p = 0.0525$) compared to HIV-1/MRC16$^{P1939/A605}$ co-infection, which shows trend to significance. MDM co-infected with HIV-1/MRC16$^{P1939/A605}$ resulted in, albeit not significant ($p = 0.1530$), low median HIV-1 production compared to MDM co-infected with HIV-1 only. The data once again pointing to negative regulation of HIV-1 production by strains that induce a high pro-inflammatory phenotype. Finally, when comparing the impact on HIV-1 secretion in MDM co-infected with EU111^{N1759} or EU40^{T1759}, the magnitude of secreted p24 observed in EU111^{N1759} and EU40^{T1759} co-infected MDM was comparable to that seen with HIV-1 alone (Fig. 4.11C). Thus, in line with the limited impact of EU111^{N1759} and EU40^{T1759} co-infection on MDM cytokine production, they had no impact of HIV-1 viral production during direct co-infection

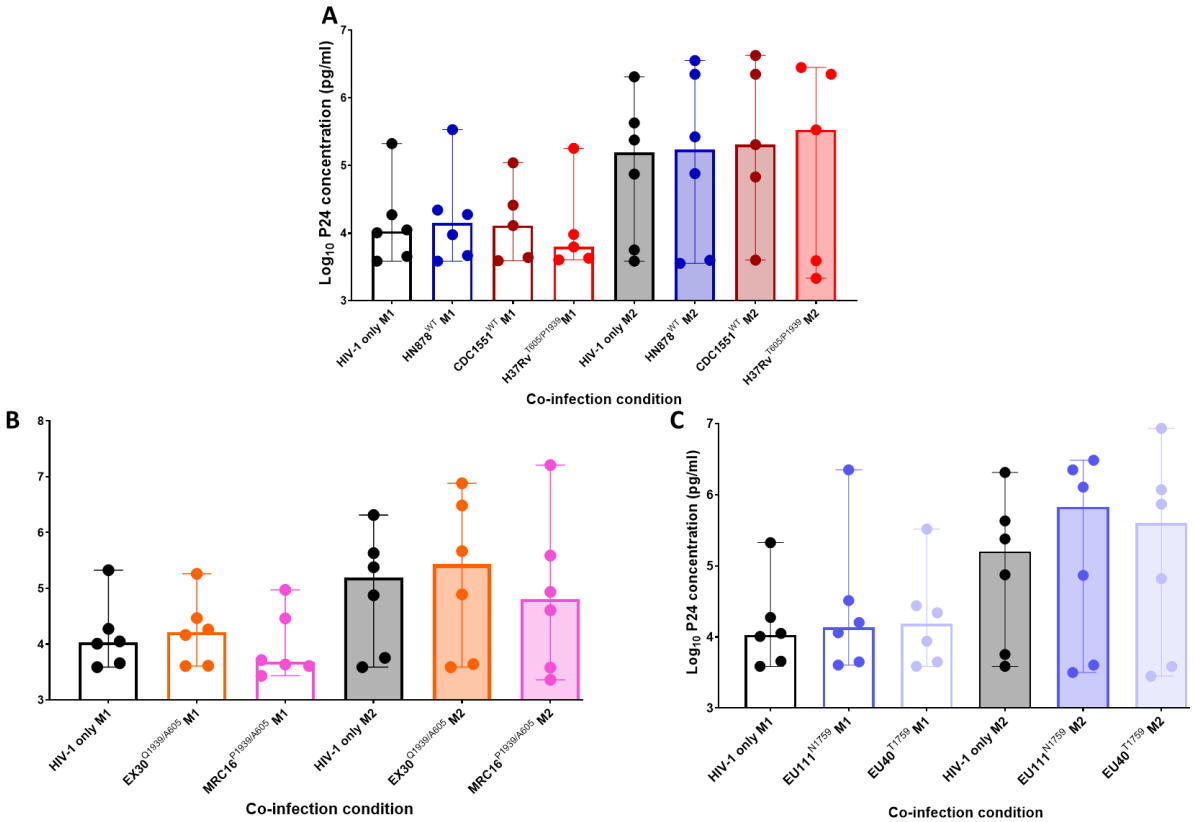

Figure 4.11. HIV-1 production from MDM co-infected with different clinical and laboratory strains.
Monocytes from 6 donors were polarised to M1 and M2 MDM. The MDM were infected with HIV-1 and SN was harvested and used for quantifying HIV-1 p24 by Luminex assay. **A)** p24 analysed from MDM donors co-infected with HIV-1 and the laboratory strains, **B)** $EX30^{Q1939/A605}$ and $MRC16^{P1939/A605}$ and **C)** $EU111^{N1759}$ and $EU40^{T1759}$. Luminex data was analysed by GraphPad prism, each dot represents p24 from each donor.

4.3. Discussion

In this chapter I wanted to answer whether differences observed in cytokine induction by the different strains of *Mtb* (chapter 3; Table 3.2 – 3.4), would result in differential production and replication of HIV-1. Concurrently, I wanted to understand whether there were differences in cytokine secretion due to co-infection of the same macrophages by HIV-1 and *Mtb* and whether that has an impact on HIV-1 production. Soluble factors from *Mtb* infected macrophages increased the infection of TZM-bl cells by HIV-1 (Fig. 4.3 – Fig. 4.4) and the soluble factors also increased the LTR activity of HIV-1 in TZM-bl cells (Fig. 4.5 – Fig. 4.6). There was no effect on HIV-1 production by soluble factors from *Mtb* infected MDM (Fig. 4.8). There was increased secretion of cytokines in MDM co-infected with HIV-1 and *Mtb* strains, but the major contributor of the variation was inter-donor variability (Fig. 4.11B), as was co-infecting strain (Fig. 4.10C). There were no statistically significant alterations to HIV-1 production in MDM that were co-infected with HIV-1 and *Mtb* strains (Fig. 4.11). There appears to be a reduction of HIV-1 production in MDM that induce more cytokines.

Productive infection measures packaged and secreted mature viral particles. It does not provide a record of HIV-1 replication in the cells. HIV-1 replication produces a host of defective viral genome which are not packaged and secreted to the SN. It is for this reason that secreted p24 antigen cannot be used to infer HIV-1 replication. To analyse HIV-1 replication I used the TZM-bl cells with the HIV-1 LTR linked to a luciferase reporter. This allowed is a direct measure of the HIV-1 promoter activity and thus can be used to infer HIV-1 replication. Soluble factors can aid or hinder the uptake of HIV-1 into cells. Some soluble factors prime cells for uptake of HIV-1 by increasing the expression of surface HIV-1 co-receptors [53], while other soluble factors such as CCL4 and CCL5 physiologically bind to HIV-1 co-receptors limiting the uptake of HIV-1 into cells [50]. Post uptake and integration soluble factors can activate the HIV-1 LTR by stimulating the production of hTF that bind to and activate the activity of the HIV-1 LTR [45].

Table 4.4. A summary table of the effect of SN from the different strains on LTR activity in TZM-bl cells

HIV-1 replication in TZM-bl cells incubated with *Mtb* induced SN				
	Pre-infection		Post-infection	
	24-hour SN	96-hour SN	24-hour SN	96-hour SN
H37Rv$^{P1939/T605}$	=	=	=	=
HN878^{WT}	+	=	+	+
CDC1551^{WT}	=	+	+	+
EX30$^{Q1939/A605}$	+	=	+	+
MRC16$^{P1939/A605}$	+	=	+	+
EU111^{N1759}	+	+	=	=
EU40^{T1759}	+	+	=	=

= shows where SN had no effect on HIV-1 LTR activity, + shows where SN increased HIV-1 LTR activity

TZM-bl cells were incubated with SN from *Mtb* infected MDM 24-hours or 96-hours post-infection, 24-hours before or 6-hours after infecting the TZM-bl cells with HIV-1. There was an increase in HIV-1 LTR activity whether the SN was added before or after HIV-1 infection for some strains. The increased LTR activity observed in TZM-bl cells incubated with SN before infection with HIV-1, points to the SN priming the TZM-bl cells for HIV-1 uptake. This means soluble factors from the SN of HN878, CDC1551, the clinical pair EX30$^{Q1939/A605}$ and MRC16$^{P1939/A605}$ and the clinical pairs EU111^{N1759} and EU40^{T1759} all primed TZM-bl cells for HIV-1 infection (Fig. 4.3; Table 4.4). It is surprising that H37Rv SN, despite increased average cytokine induction compared to CDC1551 (chapter 3; Table 3.2), did not significantly affect LTR activity in TZM-bl cells (Fig. 4.3; Table 4.4).

The priming of TZM-bl cells for rapid uptake of HIV-1 is likely due to a combination of cytokines induced early following infection with the clinical strains. However, I observed that IL-6 was consistently upregulated in the 24-hour SN of the strains which resulted in increased LTR pre-infection compared to uninfected MDM (Chapter 3; Table 3.2 – Table 3.4). Although IL-6 is also increased early in CDC1551^{WT}, the SN from this strain did not significantly increase LTR activity in the pre-infection model – but a compelling trend was observed with a p-value of 0.0847 at FDR<0.1. I propose that it is likely that the presence of some cytokines from SN of MDM infected with the clinical and laboratory strains increased HIV-1 entry co-receptors in TZM-bl cells, thus providing an environment that is highly permissive to infection by HIV-1.

Also worth noting, the 96-hour SN from EX30$^{Q1939/A605}$ and MRC16$^{P1939/A605}$ clinical strains as well as H37Rv$^{P1939/T605}$ laboratory strain did not significantly increase LTR activity when TZM-bl cells were incubated with the SN before HIV-1 infection (Fig. 4.4; Table 4.4). At the same time the 96-hour SN from EU111^{N1759}, EU40^{T1759}, HN878^{WT} and CDC1551^{WT} increased the LTR activity. While it is unlikely, that a single cytokine may be responsible for the overall observed phenotype, it may however, be contributing. In this case, CXCL9 was the only cytokine that was increased by H37Rv$^{P1939/T605}$, EX30$^{Q1939/A605}$ and MRC16$^{P1939/A605}$ at the 96-hour time point, relative to uninfected MDM (Chapter 3; Table 3. 3). This cytokine was not affected by HN878^{WT}, CDC1551^{WT}, EU111^{N1759} and EU40^{T1759} relative to uninfected MDM (Chapter 3; Table 3.2 – 3.4.). It does not appear that HIV-1 uptake is blocked by SN from H37Rv$^{P1939/T605}$, EX30$^{Q1939/A605}$ and MRC16$^{P1939/A605}$, because the LTR activity is comparable to LTR activity in TZM-bl cells incubated with SN from uninfected control (and by proxy TZM-bl cells in media only) (Fig 4.4B; Table 4.4). This means that SN from HN878^{WT}, CDC1551^{WT}, EU111^{N1759} and EU40^{T1759} likely increase HIV-1 entry co-receptors or speed up a post-HIV-1 entry mechanism in the TZM-bl cells. This data suggests that the L4 clinical strains EX30$^{Q1939/A605}$, and MRC16$^{P1939/A605}$ induced SN early (24-hours) that increased the uptake into TZM-bl cells. The L2 clinical strains EU111^{N1759} and EU40^{T1759} appear to induce factors at both 24-hours and 96-hours post-infection. It is difficult understand which cytokines play the most critical role in increasing HIV-1 uptake because in the larger picture, EX30$^{Q1939/A605}$ and MRC16$^{P1939/A605}$, induce the same cytokines and more than EU111^{N1759} and EU40^{T1759} with respect to uninfected MDM. Yet, TZM-bl cells incubated with 96-hour from EX30$^{Q1939/A605}$ and MRC16$^{P1939/A605}$ appears to be limited in HIV-1 uptake compared to SN induced by EU111^{N1759} and EU40^{T1759} at the same time point.

TZM-bl cells are highly permissive to HIV-1 infection due to high expression of co-receptors including CD4 and CCR5. It's therefore projected that when the *Mtb*-induced SN is added 6-hours after infection a substantial number of HIV-1 particles are already taken up into TZM-bl cells and hence the cytokine impact will have a greater influence on HIV-1 LTR post integration, reducing the impact on HIV-1 uptake. Increased LTR activity was observed in TZM-bl cells incubated with both the 24-hour and 96-hours SN from MDM infected with EX30$^{Q1939/A605}$, HN878^{WT} and CDC1551^{WT} (Fig. 4.5; Table 4.4). It was surprising that MRC16$^{P1939/A605}$-induced SN only increased LTR activity with the 96-hour SN and had no effect with the 24-hour SN. given that this strain induces more cytokines that EX30$^{Q1939/A605}$ at both time points (Chapter 3; Table 3.3). It is difficult to recognise the precise factor(s) involved

with increasing LTR activity in the SN EX30$^{Q1939/A605}$, but not in MRC16$^{P1939/A605}$ SN. Perhaps the overabundance of cytokines induced by MRC16$^{P1939/A605}$ may have a negative effect on LTR activity. This can be supported by the observation that at the 24-hour time point the levels of cytokines induced by MRC16$^{P1939/A605}$ relative to uninfected MDM are highly elevated compared to levels the strain induces at 96-hours post-infection relative to uninfected MDM. Furthermore, using the 96-hour SN with relatively the same cytokine profile – but in less quantities compared to 24-hour SN (comparing only cytokines analysed in this project), resulted in significantly high LTR activity (Fig. 4.5 – Fig. 4.6; Table 4.4). This data may be indicating that although cytokines may increase LTR activity in TZM-bl, an overabundance of cytokines may also serve to limit the LTR activity. Additionally, HIV-1 replication may be influenced differently under different conditions. For example, the SN of H37Rv$^{P1939/T605}$ with comparably higher cytokine magnitude than SN from lineage matched CDC1551^{WT} had no effect of HIV-1 LTR activity with the 96-hour SN. On the other hand, with EU111^{N1759} and EU40^{T1759}-induced SN resulted in increased LTR activity when the SN was added before infection and had no effect post-infection, which means these strains likely induce mainly factors that prime TZM-bl cells and have less impact LTR activation post-integration.

Table 4.5. A summary table of the effect of SN from the different strains on LTR activity in TZM-bl cells

Summary of HIV-1 production in MDM incubated with *Mtb* induced SN	
	96-hours SN
H37Rv$^{P1939/T605}$	=
HN878^{WT}	=
CDC1551^{WT}	=
EX30$^{Q1939/A605}$	-
MRC16$^{P1939/A605}$	=
EU111^{N1759}	=
EU40^{T1759}	=

= shows where SN had no effect on HIV-1 LTR activity, + shows where SN increased HIV-1 LTR activity

HIV-1 and *Mtb* may not always be co-infecting the same cell but might share the same close environment which may still give a chance for *Mtb* to influence HIV-1 via the cytokine milieu. This phenomenon is called the bystander cell effect. Here I measured the bystander effect by infecting M2 MDM with HIV-1 and incubating the HIV-1 infected MDM with *Mtb*-induced SN (Fig. 4.7; Table 4.5). Surprisingly, the *Mtb*-induce SN from the laboratory strains and clinical pair EU111^{N1759} and EU40^{T1759} did not affect HIV-1 productive infection, whilst it was

significantly decreased by the clinical pair EX30$^{Q1939/A605}$ and decreased but not significantly by MRC16$^{P1939/A605}$ (Fig. 4.8; Table 4.5). Productive infection is also increased in MDM that were incubated with SN from H37Rv$^{P1939/T605}$ compared to productive infection in MDM incubated with EX30$^{Q1939/A605}$ SN (Fig. 4.8; Table 4.5). I propose that, rather than this phenotype being increased production of HIV-1 in the presence of H37Rv$^{P1939/T605}$ SN but is rather an impeding of production in the presence of SN from EX30$^{Q1939/A605}$. There is prior evidence which supports that *Mtb*-induced soluble factors increase HIV-1 replication and productive infection in PBMC [38]. So, it was a surprise to observe that EX30$^{Q1939/A605}$ and MRC16$^{P1939/A605}$-induced SN significantly decreased HIV-1 productive infection compared to SN from unstimulated MDM and HIV-1 only infected MDM. However, there is precedent for *Mtb* induced soluble factors leading to a decrease in HIV-1 productive infection during co-infection. Similar findings have been observed in earlier studies on the effect of *Mtb* co-infection on HIV-1 replication, that either reported inhibition or no effect on HIV-1 replication and productive infection in MDM when co-infected with *Mtb* [54-56]. Shattock *et al.,* (1994) [54], showed that MDM infected with H37Rv had a greater than 50 % reduction in the LTR activity using an reverse transcriptase assay [54]. Although the authors did not measure the effect of infection on viral release by MDM, they suggest that the assay they used could also be extended to productive infection [54]. Mancino *et al.,* (1994) [55], reported that infecting MDM with *Mtb* and then HIV-1 results in increased HIV-1 productive infection, as measured by p24 in the SN. However, when the authors either simultaneously infected MDM with HIV-1 and *Mtb* or co-infected HIV-1 infected MDM with *Mtb* they observed no difference in HIV-1 productive infection [55]. It is estimated that a single round of infection for HIV-1 in macrophages is 48-hours [57]. In my experiments the SN was added 18-hours post HIV-1 infection, possibly even before all the HIV-1 is taken up into MDM. This increases the likelihood that HIV-1 receptor antagonists such as CCL3, CCL4 and CCL5 inhibited the uptake of HIV-1 into MDM and affected subsequent infection rounds with HIV-1 hence the low p24 in the presence of EX30$^{Q1939/A605}$- and MRC16$^{P1939/A605}$-induced SN.

The investigation into the effect of differential cytokine induction on HIV-1 productive infection was completed with M1 and M2 MDM. I found no significant modification of HIV-1 productive infection between MDM co-infected with experimental strains and the controls strains. It is worthy to note that the samples used were harvested 11 days post HIV-1 infection and four days post *Mtb* co-infection and cell death was not analysed in these experiments. Cell death is a practical reason why productive infection would be similar between the models

despite differences in HIV-1 replication. As mentioned earlier that HIV-1 is an obligate intracellular parasite that is completely reliant on the host for replication. MRC16$^{P1939/A605}$ which significantly increases cytokine production compared to EX30$^{Q1939/A605}$ was expected to increase HIV-1 production as well. However, if there was increased cell death due to MRC16$^{P1939/A605}$ co-infection, that would give a reasonable explanation for the similar HIV-1 production levels between EX30$^{Q1939/A605}$ and MRC16$^{P1939/A605}$.

4.4. Conclusion

Two pairs of phylogenetically close strains of *Mtb* belonging to L2 and L4, with a SNP predicted to be under HIV-1 selection in a lipid metabolising gene were tested for their capacity to induce HIV-1 replication and production. I observed that soluble factors induced by these strains in MDM increased the HIV-1 LTR activity (as a proxy for HIV- replication) in TZM-bl using SN harvested 24-hours and 96-hours post-infection. The SN from the strains also primed the TZM-bl cells, increasing infection with HIV-1, however, this was only noticed with SN harvested 24-hours post-infection for the L4 clinical strains, pointing to soluble factors that are produced early. The L2 clinical strains induced primed TZM-bl cells with both 24-hour and 96-hour SN, pointing that factors involved in priming are produced at both time points for these strains. There was no differential modification of HIV-1 production by L2 clinical pairs EU111^{N1759} and EU40^{T1759}, also these strains had a minimal effect on cytokine secretion in co-infected MDM. There was a significant difference in cytokine secretion between MDM co-infected with clinical strain EX30$^{Q1939/A605}$ and clinical pair MRC16$^{P1939/A605}$. However, this difference did not translate to differences in HIV-1 production during co-infection. However, co-incubation with SN from EX30$^{Q1939/A605}$ clinical strain resulted in significantly decreased HIV-1 production in MDM. The clinical pair EX30$^{Q1939/A605}$ and MRC16$^{P1939/A605}$ were taken forward for genetic engineering in Chapter 5, after which analysis of the role of the SNP observed in EX30$^{Q1939/A605}$ on the difference in cytokine secretion and whether this would influence HIV-1 production either during direct infection or via a bystander effect is analysed in Chapter 6.

4.5. References

1. Niemann, S. and P. Supply, *Diversity and evolution of Mycobacterium tuberculosis: moving to whole-genome-based approaches.* Cold Spring Harb Perspect Med, 2014. **4**(12): p. a021188.
2. Gagneux, S., et al., *Variable host-pathogen compatibility in Mycobacterium tuberculosis.* Proc Natl Acad Sci U S A, 2006. **103**(8): p. 2869-73.
3. Comas, I., et al., *Out-of-Africa migration and Neolithic coexpansion of Mycobacterium tuberculosis with modern humans.* Nat Genet, 2013. **45**(10): p. 1176-82.
4. Brennan, P.J., *Structure, function, and biogenesis of the cell wall of Mycobacterium tuberculosis.* Tuberculosis (Edinb), 2003. **83**(1-3): p. 91-7.
5. Gago, G., L. Diacovich, and H. Gramajo, *Lipid metabolism and its implication in mycobacteria-host interaction.* Curr Opin Microbiol, 2018. **41**: p. 36-42.
6. Yang, L., et al., *Changes in the major cell envelope components of Mycobacterium tuberculosis during in vitro growth.* Glycobiology, 2013. **23**(8): p. 926-34.
7. Reed, M.B., et al., *A glycolipid of hypervirulent tuberculosis strains that inhibits the innate immune response.* Nature, 2004. **431**(7004): p. 84-7.
8. Queiroz, A. and L.W. Riley, *Bacterial immunostat: Mycobacterium tuberculosis lipids and their role in the host immune response.* Rev Soc Bras Med Trop, 2017. **50**(1): p. 9-18.
9. Stamm, C.E., A.C. Collins, and M.U. Shiloh, *Sensing of Mycobacterium tuberculosis and consequences to both host and bacillus.* Immunol Rev, 2015. **264**(1): p. 204-19.
10. Demento, S.L., et al., *Pathogen-associated molecular patterns on biomaterials: a paradigm for engineering new vaccines.* Trends Biotechnol, 2011. **29**(6): p. 294-306.
11. Middlebrook, G., R.J. Dubos, and C. Pierce, *Virulence and Morphological Characteristics of Mammalian Tubercle Bacilli.* J Exp Med, 1947. **86**(2): p. 175-84.
12. Leisching, G., et al., *The Host Response to a Clinical MDR Mycobacterial Strain Cultured in a Detergent-Free Environment: A Global Transcriptomics Approach.* PLoS One, 2016. **11**(4): p. e0153079.
13. Hunter, R.L., N. Venkataprasad, and M.R. Olsen, *The role of trehalose dimycolate (cord factor) on morphology of virulent M. tuberculosis in vitro.* Tuberculosis (Edinb), 2006. **86**(5): p. 349-56.
14. Indrigo, J., R.L. Hunter, and J.K. Actor, *Cord factor trehalose 6,6'-dimycolate (TDM) mediates trafficking events during mycobacterial infection of murine macrophages.* Microbiology (Reading), 2003. **149**(Pt 8): p. 2049-2059.

15. Glickman, M.S., J.S. Cox, and W.R. Jacobs, Jr., *A novel mycolic acid cyclopropane synthetase is required for cording, persistence, and virulence of Mycobacterium tuberculosis.* Mol Cell, 2000. **5**(4): p. 717-27.
16. Trivedi, A., et al., *Thiol reductive stress induces cellulose-anchored biofilm formation in Mycobacterium tuberculosis.* Nat Commun, 2016. **7**: p. 11392.
17. Ruhl, C.R., et al., *Mycobacterium tuberculosis Sulfolipid-1 Activates Nociceptive Neurons and Induces Cough.* Cell, 2020. **181**(2): p. 293-305 e11.
18. Sachdeva, K., et al., *Mycobacterium tuberculosis (Mtb) lipid mediated lysosomal rewiring in infected macrophages modulates intracellular Mtb trafficking and survival.* J Biol Chem, 2020. **295**(27): p. 9192-9210.
19. Siegrist, M.S. and C.R. Bertozzi, *Mycobacterial lipid logic.* Cell Host Microbe, 2014. **15**(1): p. 1-2.
20. Domenech, P. and M.B. Reed, *Rapid and spontaneous loss of phthiocerol dimycocerosate (PDIM) from Mycobacterium tuberculosis grown in vitro: implications for virulence studies.* Microbiology (Reading), 2009. **155**(Pt 11): p. 3532-3543.
21. Cambier, C.J., et al., *Mycobacteria manipulate macrophage recruitment through coordinated use of membrane lipids.* Nature, 2014. **505**(7482): p. 218-22.
22. Kirksey, M.A., et al., *Spontaneous phthiocerol dimycocerosate-deficient variants of Mycobacterium tuberculosis are susceptible to gamma interferon-mediated immunity.* Infect Immun, 2011. **79**(7): p. 2829-38.
23. Korf, J., et al., *The Mycobacterium tuberculosis cell wall component mycolic acid elicits pathogen-associated host innate immune responses.* Eur J Immunol, 2005. **35**(3): p. 890-900.
24. Kim, J., et al., *Low-dielectric-constant polyimide aerogel composite films with low water uptake.* Polymer Journal, 2016. **48**(7): p. 829-834.
25. Wilburn, K.M., R.A. Fieweger, and B.C. VanderVen, *Cholesterol and fatty acids grease the wheels of Mycobacterium tuberculosis pathogenesis.* Pathog Dis, 2018. **76**(2).
26. Ojha, A.K., et al., *Growth of Mycobacterium tuberculosis biofilms containing free mycolic acids and harbouring drug-tolerant bacteria.* Mol Microbiol, 2008. **69**(1): p. 164-74.
27. Batt, S.M., D.E. Minnikin, and G.S. Besra, *The thick waxy coat of mycobacteria, a protective layer against antibiotics and the host's immune system.* Biochem J, 2020. **477**(10): p. 1983-2006.
28. Koch, A.S., et al., *The Influence of HIV on the Evolution of Mycobacterium tuberculosis.* Mol Biol Evol, 2017. **34**(7): p. 1654-1668.

29. Sirakova, T.D., et al., *The Mycobacterium tuberculosis pks2 gene encodes the synthase for the hepta- and octamethyl-branched fatty acids required for sulfolipid synthesis.* J Biol Chem, 2001. **276**(20): p. 16833-9.
30. Simeone, R., et al., *Functional characterisation of three o-methyltransferases involved in the biosynthesis of phenolglycolipids in Mycobacterium tuberculosis.* PLoS One, 2013. **8**(3): p. e58954.
31. Lescoat, A., et al., *Distinct Properties of Human M-CSF and GM-CSF Monocyte-Derived Macrophages to Simulate Pathological Lung Conditions In Vitro: Application to Systemic and Inflammatory Disorders with Pulmonary Involvement.* Int J Mol Sci, 2018. **19**(3).
32. Jolliffe, I.T. and J. Cadima, *Principal component analysis: a review and recent developments.* Philos Trans A Math Phys Eng Sci, 2016. **374**(2065): p. 20150202.
33. Day, T.A., et al., *Mycobacterium tuberculosis strains lacking surface lipid phthiocerol dimycocerosate are susceptible to killing by an early innate host response.* Infect Immun, 2014. **82**(12): p. 5214-22.
34. Rousseau, C., et al., *Production of phthiocerol dimycocerosates protects Mycobacterium tuberculosis from the cidal activity of reactive nitrogen intermediates produced by macrophages and modulates the early immune response to infection.* Cell Microbiol, 2004. **6**(3): p. 277-87.
35. Augenstreich, J., et al., *Phthiocerol Dimycocerosates From Mycobacterium tuberculosis Increase the Membrane Activity of Bacterial Effectors and Host Receptors.* Front Cell Infect Microbiol, 2020. **10**: p. 420.
36. Gilmore, S.A., et al., *Sulfolipid-1 biosynthesis restricts Mycobacterium tuberculosis growth in human macrophages.* ACS Chem Biol, 2012. **7**(5): p. 863-70.
37. Portevin, D., et al., *Human macrophage responses to clinical isolates from the Mycobacterium tuberculosis complex discriminate between ancient and modern lineages.* PLoS Pathog, 2011. **7**(3): p. e1001307.
38. Sandberg, J.K., et al., *HIV-1 Replication Is Differentially Regulated by Distinct Clinical Strains of Mycobacterium tuberculosis.* PLoS ONE, 2009. **4**(7).
39. Arango Duque, G. and A. Descoteaux, *Macrophage cytokines: involvement in immunity and infectious diseases.* Front Immunol, 2014. **5**: p. 491.
40. Leonard, W.J. and J.X. Lin, *Cytokine receptor signaling pathways.* J Allergy Clin Immunol, 2000. **105**(5): p. 877-88.

41. Hoshino, Y., et al., *Maximal HIV-1 replication in alveolar macrophages during tuberculosis requires both lymphocyte contact and cytokines.* J Exp Med, 2002. **195**(4): p. 495-505.
42. Henderson, A.J. and K.L. Calame, *CCAAT/enhancer binding protein (C/EBP) sites are required for HIV-1 replication in primary macrophages but not CD4(+) T cells.* Proc Natl Acad Sci U S A, 1997. **94**(16): p. 8714-9.
43. Summers, W.C., *Virus infection.* Viruses, 2009. **1**: p. 546 - 552.
44. Eisenreich, W., et al., *How Viral and Intracellular Bacterial Pathogens Reprogram the Metabolism of Host Cells to Allow Their Intracellular Replication.* Front Cell Infect Microbiol, 2019. **9**: p. 42.
45. Falvo, J.V., et al., *Arc of a vicious circle: pathways activated by Mycobacterium tuberculosis that target the HIV-1 long terminal repeat.* Am J Respir Cell Mol Biol, 2011. **45**(6): p. 1116-24.
46. Nakata, K., et al., *Mycobacterium tuberculosis enhances human immunodeficiency virus-1 replication in the lung.* Am J Respir Crit Care Med, 1997. **155**(3): p. 996-1003.
47. Costiniuk, C.T. and M.A. Jenabian, *The lungs as anatomical reservoirs of HIV infection.* Rev Med Virol, 2014. **24**(1): p. 35-54.
48. Guirado, E., L.S. Schlesinger, and G. Kaplan, *Macrophages in tuberculosis: friend or foe.* Semin Immunopathol, 2013. **35**(5): p. 563-83.
49. Pasternak, A.O. and B. Berkhout, *What do we measure when we measure cell-associated HIV RNA.* Retrovirology, 2018. **15**(1): p. 13.
50. Kedzierska, K. and S.M. Crowe, *Cytokines and HIV-1: interactions and clinical implications.* Antivir Chem Chemother, 2001. **12**(3): p. 133-50.
51. Herbein, G. and A. Varin, *The macrophage in HIV-1 infection: from activation to deactivation?* Retrovirology, 2010. **7**: p. 33.
52. Pauls, E., et al., *Restriction of HIV-1 replication in primary macrophages by IL-12 and IL-18 through the upregulation of SAMHD1.* J Immunol, 2013. **190**(9): p. 4736-41.
53. Sozzani, S., et al., *Interleukin 10 increases CCR5 expression and HIV infection in human monocytes.* J Exp Med, 1998. **187**(3): p. 439-44.
54. Shattock, R.J., J.S. Friedland, and G.E. Griffin, *Phagocytosis of Mycobacterium tuberculosis modulates human immunodeficiency virus replication in human monocytic cells.* J Gen Virol, 1994. **75 (Pt 4)**: p. 849-56.

55. Mancino, G., et al., *Infection of human monocytes with Mycobacterium tuberculosis enhances human immunodeficiency virus type 1 replication and transmission to T cells.* J Infect Dis, 1997. **175**(6): p. 1531-5.
56. Goletti, D., et al., *Inhibition of HIV-1 replication in monocyte-derived macrophages by Mycobacterium tuberculosis.* J Infect Dis, 2004. **189**(4): p. 624-33.
57. Cassol, E., et al., *M1 and M2a polarization of human monocyte-derived macrophages inhibits HIV-1 replication by distinct mechanisms.* J Immunol, 2009. **182**(10): p. 6237-46.

4.6. Supplementary material

The following supplementary data provides raw cytokine secretion level. The material contains four tables of cytokine secretion by MDM infected with HIV-1 and MDM co-infected with HIV-1 and different laboratory and clinical strains and constitutive cytokine secretion by uninfected. The cytokines were measured from SN harvested at both 24-hours post-infection and 96-hours post infection and analysed by Luminex assay. Luminex data was analysed using GraphPad prism.

Supplementary Table 4.1. Cytokine secretion level with interquartile range from HIV-1 infected MDM and MDM co-infected with HIV-1/*Mtb* laboratory strains 24-hours post-infection with *Mtb*

	Median level of cytokine secretion with Interquartile range (pg/ml)			
Analyte	H37Rv$^{P1939/T605}$ Infection	CDC1551^{WT} Infection	HN878^{WT} Infection	HIV-1 infection
CCL11	14.51 (11.78 - 43.25)	22.63 (11.78 – 33.48)	28.48 (11.78 - 33.48)	28.48 (11.78 - 40.17)
CCL2	4395 (3249 - 12877)	6520 (2531 - 16708)	4580 (3644 - 22925)	3329 (421.9 - 10708)
CCL3	14153 (623.9 - 33823)	1518 (1074 - 2748)	4773 (3069 - 32150)	435.9 (152.4 - 34508)
CCL4	6727 (1691 - 21469)	2825 (1847 - 4214)	6280 (3063 - 21469)	335.2 (56.02 - 21469)
CCL5	1575 (947.8 - 8792)	1744 (947.8 - 2540)	2540 (947.8 - 6434)	2540 (947.8 - 8663)
CXCL10	134 (18.25 - 1202)	222.8 (29.6 - 860.5)	115.2 1.93 - 590.9)	53.97 (18.25 - 569.5)
CXCL8	16864 (6925 - 26684)	10549 (5885 - 15652)	20966 (11933 - 26799)	955.7 (315.6 - 27329)
CXCL9	119.3 (115.8 - 485.8)	75.27 (34.78 - 115.8)	169.8 (34.78 - 429.6)	115.8 (34.78 - 485.8)
GM-CSF	129.3 (9.02 - 1073)	18.04 (9.02 - 36.15)	52.72 (9.02 - 436.3)	9.02 (7.6 - 727.4)
IFN-α	337.9 (146.9 - 530.5)	125.9 (104.9 - 434.3)	342.7 (125.5 - 489.1)	216.3 (33.69 - 505)
IFN-γ	71.91 (10.58 - 303.5)	10.49 (10.39 - 10.58)	22.61 (10.58 - 237.6)	10.58 (3.8 - 273.1)
IL-10	16.3 (3.56 - 64.72)	6.89 (3.56 - 11.94)	13.6 (3.56 - 47.52)	8.41 (3.56 - 58.39)
IL-12	2065 (36.29 - 13815)	238.2 (199.9 - 365.9)	664.9 (475.3 - 12126)	69.63 (36.29 - 13815)
IL-13	188.8 (171.3 - 286.4)	160.1 (83.21 - 224.6)	239.6 (105.4 - 297.1)	171.3 (65.09 - 264.3)
IL-15	643.1 (522.1 - 1744)	392.9 (195.2 - 522.1)	522.1 (321.6 - 1337)	522.1 (103.1 - 1466)
IL-17	103.4 (84.9 - 173.2)	60.85 (22.41 - 84.9)	84.9 (48.01 - 149.3)	84.9 (11.94 - 173.2)
IL-1RA	11973 (7726 - 16253)	7450 (3309 – 16801)	9284 (4248 - 17754)	9659 (841 - 16715)
IL-1β	88.16 (23.89 - 354.5)	85.22 (39.73 - 130.7)	247.2 (65.24 - 325.3)	40.4 (11.77 - 448.4)
IL-2	73.77 (46.43 - 194.8)	45.16 (35.41 - 46.43)	85.47 (43.88 - 163.6)	46.43 (10.52 - 194.8)

IL-2R	994.6 (331.2 - 2961)	274.4 (217.7 - 331.2)	692.5 (360.6 - 2698)	331.2 (86.27 - 2717)
IL-4	317.8 (127.3 - 803.1)	190.8 (150.6 - 231)	356.2 (213.4 - 645.9)	58.18 (34.8 - 803.1)
IL-5	97.75 (64.32 - 200.3)	43.71 (23.09 - 64.32)	64.32 (38.12 - 185.6)	64.32 (13.13 - 200.3)
IL-6	1640 (120.3 - 17373)	251.6 (190.6 - 402.5)	731.4 (474.4 - 8836)	29.32 (20.87 - 15854)
IL-7	271.3 (210.8 - 594.9)	137.2 (44.51 - 210.8)	205.2 (104.3 - 511.5)	210.8 (12.2 - 552.2)
TNF	51.39 (0.56 - 1111)	21.19 (11.71 - 26.07)	37.78 (20.38 - 250.4)	11.8 (11.71 - 742)

Median cytokine secretion levels with interquartile range. values for n = 6 for $HN878^{WT}$ and n = donors for $CDC1551^{WT}$ and $H37Rv^{P1939/T605}$.

Supplementary Table 4.2. Median cytokine secretion level with interquartile range from HIV-1 infected MDM and MDM co-infected with HIV-1/*Mtb* laboratory strains 96-hours post-infection with *Mtb*

	Median level of cytokine secretion with Interquartile range (pg/ml)			
Analyte	H37Rv$^{P1939/T605}$ Infection	CDC1551^{WT} Infection	HN878^{WT} Infection	No infection
CCL11	14.51 (11.78 - 43.25)	6.7 (0.51 - 32.43)	8.415 (2.978 - 31.92)	7.075 (0.51 - 33.48)
CCL2	4561 (430 - 22632)	1797 (513.9 - 27713)	5355 (903.3 - 27199)	797 (167.5 - 24192)
CCL3	1857 (103.3 - 28211)	423.4 (65.94 - 1153)	812.6 (161.8 - 1087)	306.9 (13.9 - 27753)
CCL4	1110 (275.9 - 21469)	606.7 (253.6 - 2223)	1089 (379.6 - 1970)	168.4 (47.23 - 21469)
CCL5	1575 (947.8 - 8792)	491.8 (0.21 - 5109)	543.5 (29.3 - 5109)	481 (0.21 - 5194)
CXCL10	4.575 (1.59 - 513.7)	2.915 (1.23 - 627.6)	15.2 (1.5 - 626.3)	11.83 (0.17 - 440.7)
CXCL8	14126 (2819 - 27559)	8026 (3108 - 15921)	14688 (3638 - 12813)	771.6 (108.7 - 27208)
CXCL9	144.5 (66.65 - 659.1)	87.62 (34.78 - 659.1)	108.5 (58.68 - 624.3)	76 (34.78 - 391.6)
GM-CSF	7.73 (0.25 - 253.8)	1.115 (0.25 - 12.75)	5.665 (0.57 - 12.5)	3.925 (0.01 - 303.4)
IFN-α	67.47 (24.07 - 489.1)	38.73 (24.07 - 580.5)	90.64 (31.04 - 556.4)	31.06 (14.71 - 489.1)
IFN-γ	10.58 (4.55 - 219.4)	6.64 (0.75 - 23.49)	13.19 (1.545 - 22.74)	7.19 (0.75 - 219.4)
IL-10	2.13 (0.14 - 47.52)	0.365 (0.14 - 10.22)	2.375 (0.14 - 10.08)	2.075 (0.01 - 49.73)
IL-12	302.7 (36.29 - 10228)	160 (59.05 - 496.2)	273.5 (107.3 - 437.2)	31.39 (8.15 - 9851)
IL-13	21.28 (1.03 - 260.5)	15.41 (1.03 - 264.2)	49.71 (1.03 - 263.2)	28.85 (1.03 - 252.5)
IL-15	154.3 (61.85 - 1156)	85.82 (43.08 - 522.1)	187.9 (57.16 - 479.1)	90.99 (18.1 - 1202)
IL-17	11.35 (1 - 140.7)	7.495 (1 - 84.9)	23.49 (1.998 - 83.9)	7.965 (1 - 149.3)
IL-1RA	9079 (702.5 - 27676)	4958 (188.4 - 31910)	7093 (566.6 - 31722)	7148 (182.9 - 31948)
IL-1β	29.11 (12.72 - 206.7)	19.23 (8.62 - 98.68)	39.41 (10.8 - 283.1)	11.77 (0.46 - 241.9)
IL-2	13.02 (2.16 - 140.7)	8.865 (2.16 - 46.43)	22.94 (4.925 - 44.27)	8.335 (0.09 - 140.7)

IL-2R	300.2 (43.91 - 2125)	116.9 (43.91 - 331.2)	181.8 (69.59 - 287.3)	86.27 (10.86 - 2400)
IL-4	66.46 (14.3 - 668.2)	37.84 (11.14 - 231)	105.3 (14.3 - 219.8)	32.87 (3.96 - 707.5)
IL-5	10.48 (0.41 - 169.5)	3.965 (0.41 - 64.32)	11.81 (0.41 - 63.91)	13.47 (0.41 - 169.5)
IL-6	149.4 (24.1 - 9691)	86.34 (34.83 - 220.6)	307.8 (45.26 - 185.8)	12.16 (0.42 - 12059)
IL-7	210.8 (75.07 - 437.3)	91.78 (12.2 - 225.6)	203.1 (46.9 - 213.4)	132.5 (12.2 - 478)
TNF	2.425 (0.34 - 90.98)	1.345 (0.34 - 11.8)	6.99 (0.34 - 11.46)	0.675 (0.14 - 105)

Median cytokine secretion levels with interquartile range. values for n = 6 for $HN878^{WT}$ and n = donors for $CDC1551^{WT}$ and $H37Rv^{P1939/T605}$.

Supplementary Table 4.3. Median cytokine secretion level with interquartile range from HIV-1 infected MDM and MDM co-infected with HIV-1/*Mtb* clinical strains 24-hours post-infection with *Mtb*

	Median level of cytokine secretion with Interquartile range (pg/ml)			
Analyte	EX30$^{Q1939/A605}$ Co-infection	MRC16$^{P1939/A605}$ Co-infection	*EU111*^{N1759} Co-infection	EU40^{T1759} Co-infection
CCL11	30.51 (11.78 - 43.25)	46.23 (33.48 - 98.22)	28.83 (11.78 - 35.85)	27.76 (11.78 - 33.59)
CCL2	4893 (4131 – 19798)	6389 (4917 – 29466)	3988 (3489 – 17328)	3852 (2055 – 10235)
CCL3	6408 (1553 – 36106)	33583 (18809 – 41393)	4217 (1510 – 32832)	868.8 (646.7 – 32205)
CCL4	7230 (2096 – 21469)	21469 (3430 – 43621)	5499 (2024 – 21469)	1805 (1327 – 21469)
CCL5	2540 (947.8 – 9318)	8773 (2540 – 15910)	2540 (947.8 – 6875)	2540 (947.8 – 6286)
CXCL10	105.5 (29.6 - 800.3)	193.5 (174 – 4422)	34.99 (17.24 - 109.3)	22.35 (17.24 - 40.9)
CXCL8	22332 (7353 – 27327)	26448 (11933 – 28076)	20109 (6205 – 26523)	9010 (3257 – 27213)
CXCL9	296.2 (34.78 - 538.5)	775.2 (538.5 – 16676)	208.4 (34.78 - 391.6)	115.8 (34.78 - 368.7)
GM-CSF	37.75 (17.08 - 747.7)	410.6 (229.1 – 1364)	43.01 (9.02 - 480.4)	22.95 (9.02 - 411.3)
IFN-α	381.8 (119 - 580.5)	528.3 (307.1 – 1432)	231.5 (104.9 - 537.2)	146.9 (88.34 - 399.4)
IFN-γ	30.71 (10.39 - 288.4)	294.9 (148.9 - 549.2)	10.58 (10.39 - 246.6)	10.58 (3.8 - 219.4)
IL-10	10.71 (3.56 - 66.81)	71.98 (39.65 - 143.4)	10.22 (3.56 - 56.24)	10.18 (3.56 - 45.29)
IL-12	905.4 (245.6 – 13815)	13815 (485.3 – 37610)	611.6 (250.7 – 12817)	142 (36.29 – 11655)
IL-13	271.4 (95.54 - 325.8)	282.8 (167.8 - 530.4)	232.2 (95.54 - 297.1)	198 (65.09 - 256.5)
IL-15	739.7 (263.7 – 1687)	1696 (1056 – 3574)	522.1 (195.2 – 1248)	522.1 (103.1 – 1248)
IL-17	129.9 (48.01 - 187.7)	184.1 (124.3 - 380.8)	84.9 (36.79 - 165.5)	84.9 (22.41 - 149.3)
IL-1RA	11350 (4478 – 21644)	17030 (13569 – 69070)	10733 (4518 – 18749)	10278 (3537 – 13460)
IL-1β	263.4 (49.24 - 684.5)	326.8 (159.1 – 679)	226.5 (49.24 - 331.9)	98.68 (39.73 – 252)
IL-2	104.1 (35.41 - 199.7)	209.3 (150.6 - 494.6)	88.57 (35.41 - 163.6)	46.43 (25.22 - 152.4)

IL-2R	982.1 (269.4 – 2774)	2896 (1524 – 5645)	578.8 (217.7 – 2441)	331.2 (86.27 – 2338)
IL-4	420.7 (165.8 – 835)	817.1 (518.6 – 1630)	373.2 (132.9 - 720.3)	154.9 (110.6 – 677)
IL-5	64.32 (23.09 - 214.1)	220.5 (97.4 - 281.4)	64.32 (23.09 - 200.3)	64.32 (23.09 - 185.6)
IL-6	1071 (228.5 – 17538)	16879 (11969 – 22015)	659.4 (212.9 – 11509)	179.9 (123.3 – 8339)
IL-7	329.2 (44.51 - 594.9)	579.4 (275.1 – 1023)	105.6 (44.51 - 525.4)	210.8 (12.2 – 458)
TNF	48.27 (16.3 - 827.3)	950.8 (400.1 – 1346)	31.93 (14.09 - 320.5)	11.8 (9.08 - 218.7)

Median cytokine secretion levels with interquartile range. values for n = 6 for $HN878^{WT}$ and n = donors for $CDC1551^{WT}$ and $H37Rv^{P1939/T605}$.

Supplementary Table 4.4. Median cytokine secretion level with interquartile range from HIV-1 infected MDM and MDM co-infected with HIV-1/*Mtb* clinical strains 96-hours post-infection with *Mtb*

	Median level of cytokine secretion with Interquartile range (pg/ml)			
Analyte	$EX30^{Q1939/A605}$ Co-infection	$MRC16^{P1939/A605}$ Co-infection	$EU111^{N1759}$ Co-infection	$EU40^{T1759}$ Co-infection
CCL11	9.735 (0.51 – 51.96)	29.92 (15.89 – 56.25)	8.08 (0.51 – 33.48)	8.08 (0.51 – 33.48)
CCL2	7310 (457.3 – 39117)	12456 (3454 – 49098)	1293 (335.6 – 21278)	1421 (537.2 – 10934)
CCL3	736.1 (49.99 – 36031)	18002 (3741 – 36855)	425.9 (49.99 – 28085)	432.9 (127.7 – 24940)
CCL4	1268 (183.3 – 21469)	6389 (950 – 21469)	635.8 (156.8 – 19814)	577.2 (312.6 – 16439)
CCL5	676.8 (0.21 – 11039)	1185 (136.9 – 11025)	481 (0.21 – 4636)	481 (0.21 – 3875)
CXCL10	18.74 (0.81 – 493.2)	68.44 (22.93 – 787.1)	12.19 (1.23 – 494.1)	12.19 (1.59 – 548.7)
CXCL8	14484 (1773 – 27300)	22760 (11933 – 123091)	10354 (1279 – 26981)	9497 (2396 – 27120)
CXCL9	115.8 (34.78 – 886)	1083 (376.2 – 20093)	87.62 (34.78 – 886)	100.5 (34.78 – 659.1)
GM-CSF	4.35 (0.47 – 1165)	296.8 (13.59 – 1237)	4.78 (0.01 – 306.3)	4.655 (0.36 – 262.8)
IFN-α	104.5 (14.71 – 723)	277.3 (115.2 – 1063)	75.48 (14.71 - 691.2)	65.23 (14.71 – 620.1)
IFN-γ	22.61 (2.76 – 391.2)	120.2 (20.13 – 682.8)	9.23 (0.75 – 251)	10.03 (0.75 – 205.6)
IL-10	2.375 (0.14 – 64.72)	25.42 (4.73 – 108)	2.225 (0.14 – 56.24)	2.075 (0.01 – 47.52)
IL-12	201.6 (59.92 – 13815)	821.9 (485.3 – 27064)	144.5 (42.97 – 10290)	108.1 (21.62 – 9118)
IL-13	51.91 (1.03 – 325.8)	105.3 (18.84 – 473.5)	41.41 (1.03 – 325.8)	38.09 (1.03 – 256.5)
IL-15	188.8 (18.1 – 2001)	818.7 (249.1 – 2194)	153.7 (18.1 – 1293)	97.9 (18.1 – 1108)
IL-17	18.02 (1 – 201.5)	71.63 (11.57 – 267.4)	16.3 (1 – 157.6)	9.87 (1 – 149.3)
IL-1RA	11584 (277.3 – 33316)	19299 (702.5 – 54779)	7780 (182.9 – 36457)	7881 (235.2 – 31492)
IL-1β	56.47 (10.8 – 859.5)	354 (26.68 – 2384)	28.63 (5.92 – 505.6)	26.1 (10.8 – 252)
IL-2	20.36 (1.23 – 236.9)	91.7 (21.18 – 294.3)	10.5 (0.09 – 152.4)	17.85 (2.16 – 143.7)

IL-2R	176.9 (10.86 – 3350)	1380 (526.7 – 3295)	113.9 (10.86 – 2296)	113.1 (43.91 – 1805)
IL-4	93.38 (7.75 – 920.1)	357.4 (110.8 – 1187)	76.04 (7.75 – 737.2)	59.09 (14.3 – 685.8)
IL-5	10.2 (0.41 – 227)	66.61 (16.07 – 227)	15.18 (0.41 – 214.1)	13.47 (0.41 – 185.6)
IL-6	171.5 (13.51 – 23698)	8226 (3558 – 51810)	102.3 (8.53 – 13311)	69.06 (15.61 – 9581)
IL-7	140 (12.2 – 654.7)	336.8 (134.2 – 754.5)	132.5 (12.2 – 516.2)	160.2 (12.2 – 487.8)
TNF	7.27 (0.14 – 848.4)	218.2 (7.53 – 1675)	6.62 (0.14 – 118.3)	6.435 (0.34 – 85.52)

Median cytokine secretion levels with interquartile range. values for n = 6 for $HN878^{WT}$ and n = donors for $CDC1551^{WT}$ and $H37Rv^{P1939/T605}$.

Chapter 5. Genetic engineering of SNP in *pks2* of *Mycobacterium tuberculosis* clinical and laboratory strains: reverting clinical strain SNP to wildtype and introducing clinical variant SNP into wildtype laboratory strain

5.1. Introduction

Genetic engineering is a powerful tool for studying gene function and the potential effect(s) of mutations. A number of techniques are available for genetic engineering in *Mtb* that can accomplish mutagenesis or allelic exchange [1]. In this project I used the allelic exchange method of recombineering [2] as a tool for generating single base pair changes in *Mtb* clinical and laboratory strains of interest. Recombineering was best suited for use in my experiments because it avoids the use of a suicide vector, which is integrated into the genome of the host cells to introduce the mutation of interest [1]. Mutagenesis using a suicide vector requires that the full-length gene with the mutation be cloned into a plasmid that contains an antibiotic resistance marker [3]. The plasmid with the gene of interest is used to transform *Mtb* where it integrates via homologous recombineering into the genome of *Mtb* [3], While unmarked mutants can be generated using a suicide vector, this approach requires several rounds of culture and selection. Given that I was working with clinical strains, I wanted to keep passage to a minimum and therefore chose the recombineering approach [2]. Recombineering takes advantage of homologous recombination proteins found in mycobacteriophages (Fig 5.1). The protein gp61 from the mycobacteriophage Che9c facilitates homologous recombination in recombineering of *Mtb* (Fig. 5.1) [2]. A key study by van Kessel and Hatful, (2008) [2] defined parameters for successful recombineering. The authors showed that recombineering with ssDNA yielded a better result than using dsDNA and that it was over 10 000-times more efficient when using ssDNA designed to bind to the lagging strand compared ssDNA designed to bind to the leading strand [2]. These principles were followed when designing the recombineering strategy designed here.

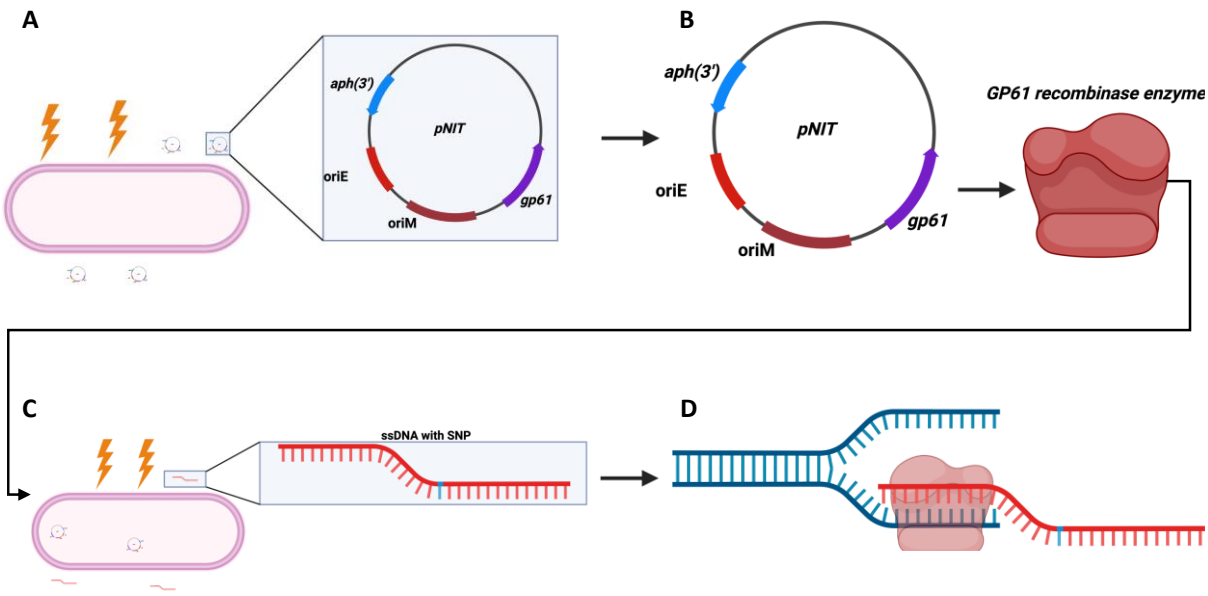

Figure 5.1. Simplified schematic of recombineering.
(**A)** *Mtb* strains are electroporated in the presence of pNIT plasmid that contains a gene for GP61 recombinase enzyme and *aph*(3') gene that confers resistance to kanamycin, (**B**) Strains transformed with pNIT are cultured and the production of GP61 recombinase enzyme is induced with IVN, (**C**) following induction bacterial are further electroporated in the presence of ssDNA substrate with the SNP of choice and (**D**) the GP61 enzyme facilitates homologous recombination between genomic DNA and the ssDNA during replication and consequently the insertion of the SNP of choice in the genomic DNA.

This chapter describes attempts to genetically engineer SNP in lipid metabolising *Mtb* genes that were observed in clinical *Mtb* strains predicted to be under HIV-1 positive directional selection [4], to establish a clear genotype-phenotype link between SNP in lipid metabolism genes, cytokine production and, consequently, HIV-1 replication. In this work, I attempted to revert the SNP observed in the clinical strains to the wildtype H37Rv$^{P1939/T605}$ sequence, and to introduce the SNP found in the clinical strains into wildtype H37Rv$^{P1939/T605}$.

Given the technical challenges around genetic engineering of clinical *Mtb* strains, only one pair of clinical isolates was taken forward for recombineering. I selected MRC16$^{P1939/A605}$ and EX30$^{Q1939/A605}$ based on their cording and lipid phenotypes (Chapter 3). These data showed that although both strains exhibited an intensive cording phenotype in media without detergent supplementation, MRC16$^{P1939/A605}$ showed higher levels of cording compared to EX30$^{Q1939/A605}$ (chapter 3; Fig. 3.4). Moreover, TLC data revealed differences in cell wall lipids between the strains (chapter 3; Fig. 3.6 – 3.9). When the strains were used to infect MDM in the presence (chapter 4; Table 4.3) and absence of HIV-1 co-infections (chapter 3; Table 3.2), there was significantly more cytokines induce by MDM infected or co-infected with MRC16$^{P1939/A605}$ compared to EX30$^{Q1939/A605}$. These phenotypic differences guided the selection of strains to be

taken, forward for genetic engineering to definitively link the observed SNP to the phenotypes observed in previous chapters phenotypes.

5.2. Results

5.2.1. Protein modelling to predict functional consequence of the two pks2 mutations in clinical strains.

I used a predicted model of the protein Pks2 from *Mtb* to analyse the potential impact of SNP 5817, which confers the change from proline to glutamine is position 1939 (P1939Q), and SNP 1815, which confers the amino acid change from threonine 605 to an alanine (T605A) (Table 3.1). To do this, I used the protein fold recognition server, Phyre2 (http://www.sbg.bio.ic.ac.uk) [5], to predict a 3D structure of Pks2 from *Mtb*. Although predicted protein structures can be used to draw inferences about the protein, it should be noted, however, that some regions of the modelled structure may be predicted with low confidence, which can, in turn, impact the final predicted spatial position of the amino acid in the protein.

The first mutation of interest is a proline-glutamine change at position1939 (P1939Q) found in $EX30^{Q1939/A605}$ (Fig. 5.2A). The original amino acid P1939 has a ring-shaped side chain and occupies a pocket of space in the 3D structure that is created by surrounding amino acids. In the mutagenesis predictive model, the amino acid replacing P1939, glutamine-1939 (Q1939) has a long side chain and appears to protrude outside of the pocket of space originally occupied by P1939 (Fig. 5.2B) suggesting potentially significant implications for the protein's structure and function.

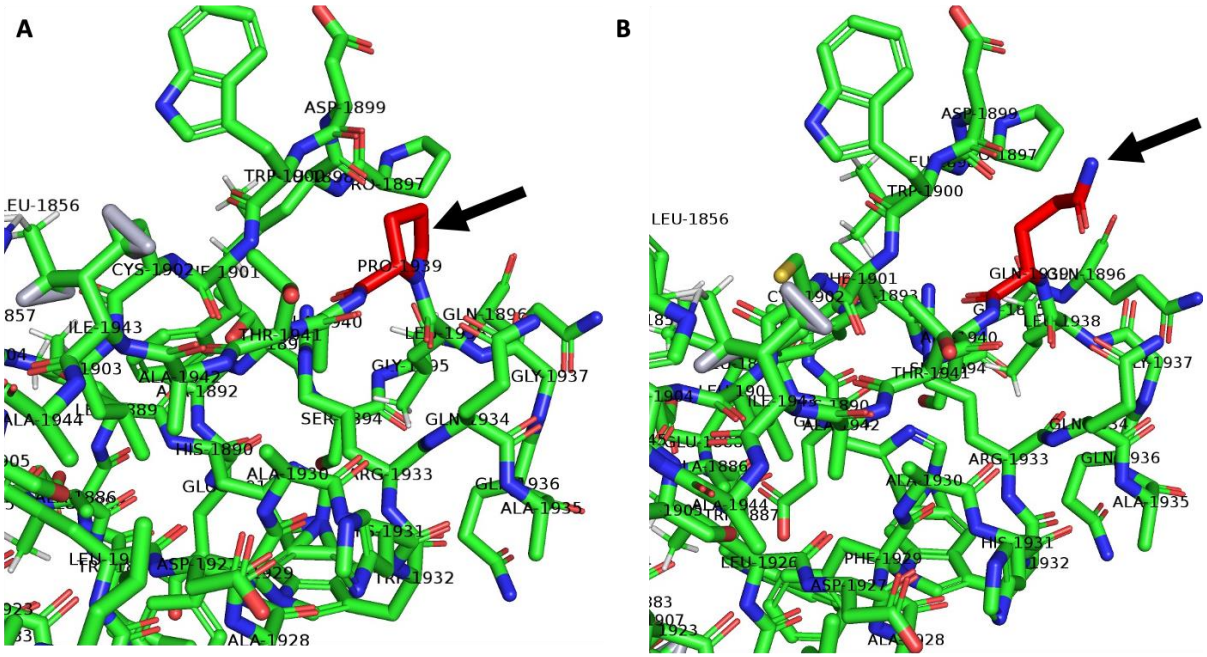

Figure 5.2. A computer-generated model of pks2 protein from *Mycobacterium tuberculosis* showing proline in position 1939.
The protein structure was generated using an amino acid sequence from mycobrowser (https://mycobrowser.epfl.ch). The model was generated using Protein Fold Recognition Server (Phyre2) (http://www.sbg.bio.ic.ac.uk). The final 3D structure was analysed using the molecular visualisation software Pymol. (**A)** shows the position of proline-1939 (arrow); an amino acid found in EX30$^{Q1939/A605}$, (**B)** in silico mutation of proline to glutamine (arrow), to match amino acid found in H37Rv.

The second amino acid of interest is found in both EX30$^{Q1939/A605}$ and MRC16$^{P1939/A605}$: threonine-605, (T605). This amino acid is found on the surface Pks2 in a region looped. The original amino acid in that position a threonine at position 605 has a long non-polar side chain (Fig. 5.3A) and is replaced by a smaller polar amino acid, alanine (Fig. 5.3b). According to the predictive model and mutagenesis the orientation of the side chain does not change and still protrudes outwards, which suggests this mutation may have a minor impact on protein secondary structure and function. Given that this mutation is found in both strains and is predicted to have limited impact on protein structure, it is unlikely that this amino acid change has a major phenotypic consequence in this context.

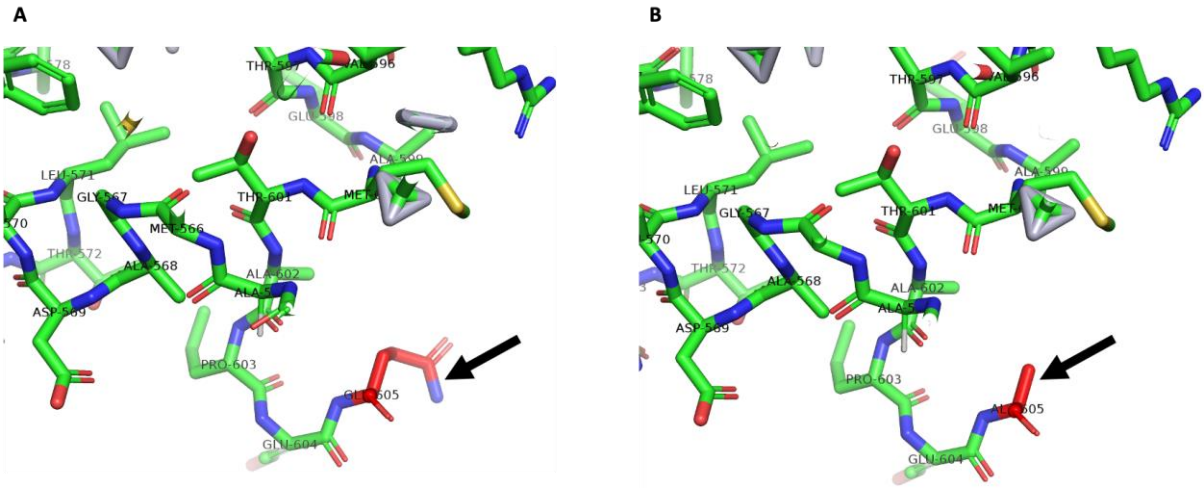

Figure 5.3. A computer-generated model of pks2 protein from *Mycobacterium tuberculosis* showing threonine in position 605.
The protein structure was generated using an amino acid sequence from mycobrowser (https://mycobrowser.epfl.ch). The model was generated using Protein Fold Recognition Server (Phyre2) (http://www.sbg.bio.ic.ac.uk). The final 3D structure was analysed using the molecular visualisation software Pymol. **A)** shows the position of threonine-605 (arrow); an amino acid found in *EX30*$^{Q1939/A605}$ and *MRC16*$^{P1939/A605}$, **(B)** in silico mutation of proline to alanine (arrow), to match amino acid found in H37Rv.

5.2.2. Recombineering of *pks2* in EX30$^{Q1939/A605}$, MRC16$^{P1939/A605}$ and H37Rv$^{P1939/T605}$

5.2.2.1. Transformation of strains with pNIT plasmid containing the gene for the gp61 recombinase enzyme

The first step of recombineering is introduction of the pNIT [2], plasmid containing the mycobacteriophage-derived proteins required for successful homologous recombination [2]. The experimental flow applied to do this is presented in Fig. 5.3 with water used as a negative control and the episomal pOLYG plasmid [6] as a positive transformation control.

The growth of colonies on 7H10 media supplemented with kanamycin (kan 25 ug/ml) was indicative of successful transformation with pNIT. *Mtb* doesn't contain a gene that confers resistance to kan and therefore growth in the presence of kan suggests that cells have taken up the plasmid and should be further screened for successful transformation. I observed 3x104 and 1x104 CFU for EX30$^{Q1939/A605}$ and MRC16$^{P1939/A605}$, respectively on kan containing plates (Table 5.1) indicating successful uptake of pNIT. For all dilutions, the H37Rv strain electroporated with pNIT displayed a lawn and therefore it was not possible to determine a colony count for this strain (Table 5.1). Controls provided expected results: the negative control of *Mtb* electroporated in the presence of water only and plated in media with kan did not produce colonies, yet an aliquot of the same sample of *Mtb* strains grew on antibiotic-free media (Table 5.1) confirming that cells were still viable. The strains were also electroporated

in the presence of pOLYG as a positive control for transformation and that produced colonies that were too numerous to count (TNTC).

Table 5.1. Colony counts of *Mtb* strains electroporated following electroporation to insert pNIT plasmid.

Strain	Sample	Experiment/control	Antibiotic	CFU/mL
EX30$^{Q1939/A605}$ colony counts				
EX30$^{Q1939/A605}$	pNIT plasmid	pNIT electroporation experiment	kanamycin	3 X10^4
EX30$^{Q1939/A605}$	Water/No DNA	Negative growth control	kanamycin	0
EX30$^{Q1939/A605}$	Water/No DNA	Positive growth control	No antibiotic	1.12 X10^9
MRC16$^{P1939/A605}$ colony counts				
MRC16$^{P1939/A605}$	pNIT	pNIT electroporation experiment	kanamycin	1 X10^4
MRC16$^{P1939/A605}$	Water/No DNA	Negative growth control	kanamycin	0
MRC16$^{P1939/A605}$	Water/No DNA	Positive growth control	No antibiotic	8.21 X10^8
H37Rv colony counts				
H37Rv$^{P1939/T605}$	pNIT plasmid	pNIT electroporation experiment	kanamycin	TNTC
H37Rv$^{P1939/T605}$	Water/No DNA	Negative growth control	kanamycin	0
H37Rv$^{P1939/T605}$	Water/No DNA	Positive growth control	No antibiotic	TNTC

I selected single colonies that were growing on kan containing media and applied colony PCR to detect the *aph3'*gene. Colony PCR was performed by picking single colonies and resuspending in TE buffer. Part of the resuspended colony was plated on a 7H10 media plate and the rest was heat killed for colony PCR. Five colonies from the EX30$^{Q1939/A605}$ electroporation and one colony displayed the correctly sized band for the *aph3'* gene (Fig. 5.4:

lane 4) and was taken forward for recombineering. Three MRC16$^{P1939/A605}$ colonies that were growing on kan were picked and tested for the presence of *aph3'* via PCR. Amplification of *aph3'* was also only observed one of the colonies. A total of eight colonies for H37Rv$^{P1939/T605}$ were picked and tested for the presence of the gene, and again amplification was successful from one colony. Electrophoresis gels for MRC16$^{P1939/A605}$ and H37Rv$^{P1939/T605}$ are not shown in the data, however, they resemble that of EX30$^{Q1939/A605}$ (Fig. 5.4). The growth of the strains in media supplemented with kan and the PCR results were taken as confirmation of a successful transformation, the amplicons were not sequenced.

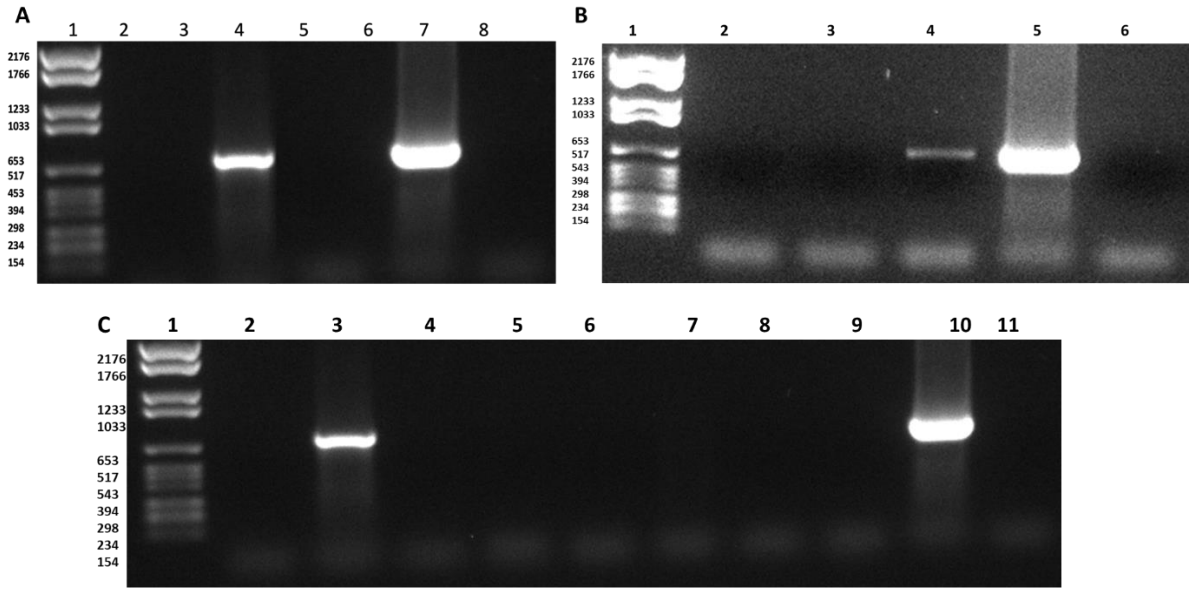

Figure 5.4. Agarose gel of APH(3') gene amplified from a colony of EX30$^{Q1939/A605}$:pNIT.
Multiple single colonies were picked and resuspended in TE buffer. Colony samples were boiled 80 °C for 1 h, boiled samples were used for PCR to amplify the *aph(3')* gene using the Roche FastStart Taq kit. PCR products were analysed using gel electrophoresis with the Sigma-Aldrich DNA molecular ladder VI and reference. The gels represents amplification of a 764 bp fragment of the *aph(3')* gene from single colonies and amplification of *aph(3')* gene from pNIT isolated from *E. coli* used a positive control. The first lane is always the molecular weight ladder, the second last lane is always the positive control, and the final lane is always the negative control for all gels. **A)** amplification from *EX30$^{Q1939/A605}$* single colonies lane 2, 3, 5 and 6 represent failed amplification from colonies and lane 4 represents a successful amplification of *aph(3')* gene, **B**) amplification from MRC16$^{P1939/A605}$ single colonies lane 2, and 3 represent failed amplification from colonies and lane 4 represents a successful amplification of *aph(3')* gene, **C**) amplification from H37Rv$^{P1939/T605}$ single colonies lane 2, 4, 5, 6, 7, 8, and 9 represent failed amplification from colonies and lane 3 represents a successful amplification of *aph(3')* gene.

5.2.2.2. Confirmation of stable production of GP61

Before electroporation to introduce the ssDNA substrate into *Mtb*, I tested whether the *gp61* gene was expressed and the GP61 recombinase protein was stably produced by the transformed *Mtb* strains. This test was only completed in the *gp61* gene in the pNIT plasmid is under the control of an isovaleronitrile inducible promoter, which is activated by the addition of IVN.

EX30$^{Q1939/A605}$:pNIT was grown until an OD600 of 0.8 and induced with 0.1 mM of IVN, and samples were collected before induction (0 h), 8 hours post-induction, and 24 hours post-induction for analysis with SDS-PAGE. (Fig. 5.4). This testing stable protein production was boy completed in EX30$^{Q1939/A605}$ and the data was inferred for MRC16$^{P1939/A605}$ and H37Rv$^{P1939/T605}$.

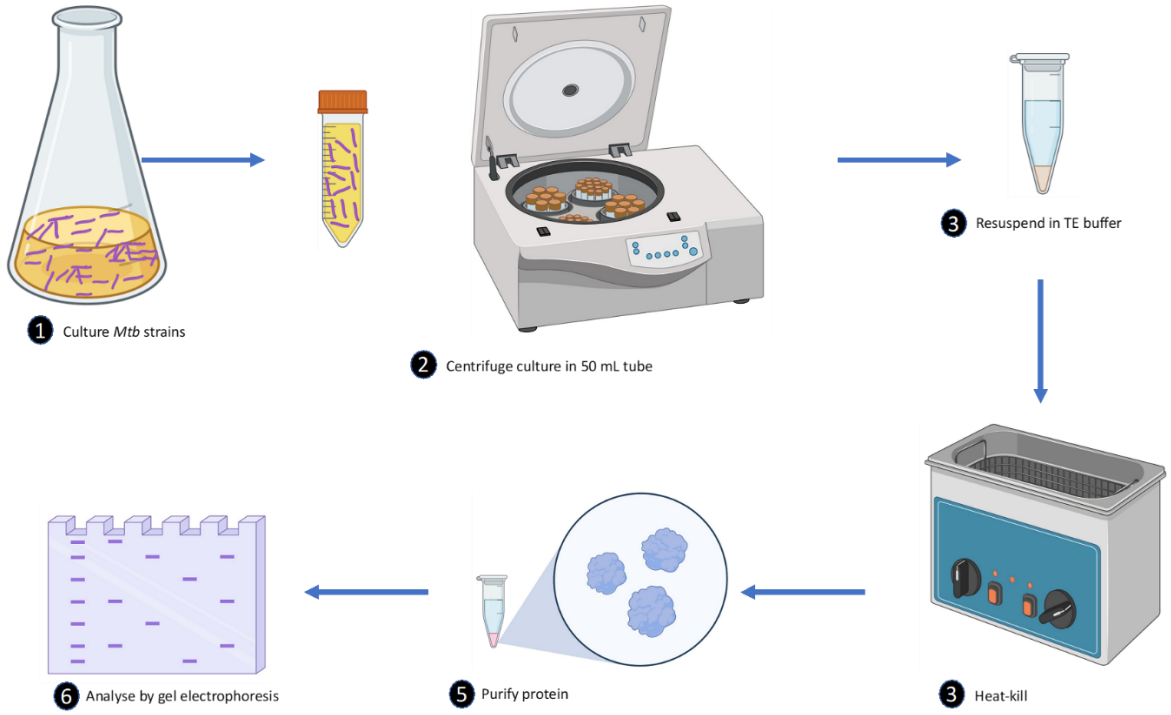

Figure 5.5. Schematic of protein analysis in *Mtb* strains following induction with IVN.
Mtb culture was grown in media and induced with INV. The culture was harvested by centrifugation and heat killed. Heat-killed culture was used to purify protein. The protein was analysed using SDS-PAGE.

I assessed the production of GP61 recombinase enzyme in EX30$^{Q1939/A605}$:pNIT by analysing protein production via SDS-PAGE. SDS-PAGE is not a quantitative method, however, by observing an increase in the size of a protein band at an expected molecular weight over time, differences in the scale of protein production can be inferred. Here I observed an increase in the size of the protein band at 72 kilodaltons (kDa) (Fig. 5.6), which is the expected molecular weight of GP61 protein, which suggests that more of the protein is being produced over time. A small band of protein was observed at 0 hours (lane 2) (Fig. 5.6), before induction, which points to a leaky promoter, leading to production of small protein quantities in the absence of IVN treatment. However, the protein band increases substantially in size 8 hours after induction and further increases 24 hours after induction. This evidence can be taken to infer that IVN induced the production of GP61 and importantly these data confirm that the pNIT plasmid is functional in EX30$^{Q1939/A605}$::pNIT.

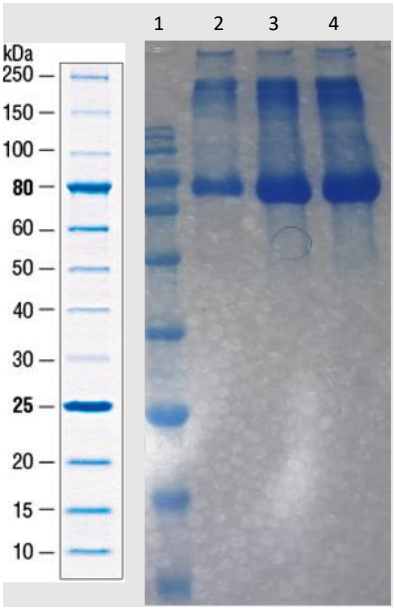

Figure 5.6. SDS-PAGE of gp61 protein induced in *EX30*$^{Q1939/A605}$::pNIT using IVN.
EX30$^{Q1939/A605}$::pNIT was cultured in 5 mL of 7H9 media supplemented with kanamycin until the an OD600 of 0.6. – 0.8. 1 mL of the culture was harvested. 1 mM of IVN was added to the remaining culture. 2 mL of media was harvested after 8 h and 24 h post induction. The cells were heat killed and protein was harvested. The protein was analysed using a 15 % SDS-PAGE. An unstained Protein Ladder, Broad Range (New England BioLabs) was used as a marker. (1) molecular weight marker, (2) 0 h before induction, (3) production of protein after 8 h of inducing, (4) protein produced 24 h post induction.

5.2.2.3. Co-electroporation of ssDNA with pOLYG to decrease the number of colonies to be screened in search of mutants.

The final step of recombineering involves transforming *Mtb* (containing the recombinase expressing pNIT plasmid) with ssDNA substrates to insert the desired mutation. The ssDNA substrates were designed to introduce SNP in two *pks2* positions: SNP-5817 (aa1939) and SNP-1815 (aa605) (Table 2.5). The ssDNA substrates were designed to be homologous to these regions except for the one nucleotide change that confers the mutation. Effective recombination at the region of interest would result in the incorporation of the desired single base change into the strains genome [2]. The final step in recombineering is completed without a positive selective marker, to create unmarked transformants [2]. The lack of a positive selective markers makes screening for the successfully transformed mutant challenging. Therefore, I used a co-electroporation approach to minimize the number of colonies that would need to be screened. To do this, I co-electroporated strains with ssDNA together with the episomal pOLYG [6] plasmid. This plasmid has a gene that confers resistance to hyg in the backbone, meaning that only colonies which take up pOLYG would grow in the presence of hyg supplementation in the media plates. Transformed samples could then be selected on hyg and colonies that grow would indicate that DNA had been taken up during electroporation. Although uptake of

pOLYG does not necessarily correlate with uptake of the ssDNA substrate, this approach was taken to reduce the number of transformants that would need to be screened by PCR to identify successful incorporation of the SNP (via homologous recombination of ssDNA). Following identification of positive recombinants, the pOLYG plasmid could be lost from strains by successive rounds of subculturing in antibiotic-free media. The pNIT+ strains were prepared for electroporation by culturing as previously stated (Chapter 2.3.3). Details of electroporation conditions are described in table 5.2.

Table 5.2. Colony counts of *Mtb* strains electroporated following electroporation to insert pNIT plasmid**.**

DNA used for electroporation	Media conditions for selection	Purpose
No DNA (water)	Antibiotic free	Provides an indication of the number of cells that survived the electroporation.
No DNA (water)	hyg	Would indicate whether cells were contaminated with a hyg resistant strain or whether spontaneous mutations with hyg resistance were occurring.
pOLYG only	hyg	Provides an indication efficiency of DNA uptake during electroporation.
pOLYG + ssDNA	hyg	Would generate ssDNA transformed cells. The inclusion of pOLYG in the electroporation allows for the use of hyg for selection.
ssDNA only	Antibiotic free	Would generate ssDNA transformed cells.

CFU counts for H37Rv$^{P1939/T605}$ following electroporation to modify SNP-1815 (T605A) and SNP-5817 (P1939Q) are represented in Fig. 5.7A and Fig. 5.7B, respectively. The CFU count for all three strains were roughly similar at about 1x10^6 cfu/ml following electroporation with pOLYG only and plating in media supplemented with hyg (clear plots) (Fig. 5.7A). The cfu

for EX30$^{Q1939/A605}$ and H37Rv$^{P1939/T605}$ electroporated with water and plated on antibiotic free media, were also similar at about 1.3x10^6 and 1.2x10^6 cfu/ml, while the cfu counts for MRC16$^{P1939/A605}$ were the highest at 1x10^7 cfu/ml (Fig. 5.7A). The clinical strain cfu decreased when electroporated in the presence of pOLYG only, this was more evident in with MRC16$^{P1939/A605}$ (Fig. 5.7A).

The cfu count dropped considerably in both EX30$^{Q1939/A605}$ and MRC16$^{P1939/A605}$ when the strains were electroporated in the presence of both ssDNA and pOLYG, then plated on media with hyg (Fig. 5.7B&C). The number of EX30$^{Q1939/A605}$ colonies (electroporated with pOLYG and either ssDNA) that grew in the presence of hyg was 3-4 logs lower (Fig. 5.7A-C) as compared to colonies for the positive growth control (electroporated in the presence of water and plated on antibiotic-free media). Similar to EX30$^{Q1939/A605}$, MRC16$^{P1939/A605}$ samples electroporated with ssDNA + pOLYG that were plated on media containing hyg displayed 5-log less colonies compared to colonies that were plated in media without antibiotic (Fig. 5.7A-C). This suggests that inclusion of ssDNA in the co-electroporation results in lower survival of the clinical strains. This was not observed in the cfu counts for H37Rv$^{P1939/T605}$ transformed in the presence of ssDNA and/or pOLYG, in which the cfu remained roughly 1x10^{6}CFU/mL (Fig. 5.7B&C). This cfu count is similar to positive control (H37Rv$^{P1939/T605}$ electroporated in the presence of water and plated without hyg) for all the electroporation conditions (Fig. 5.7A and Fig. 5.7B). This data indicates that pOLYG is easily taken up by the strain, which then become hyg resistant and that electroporation efficiency of H37Rv$^{P1939/T605}$ was high.

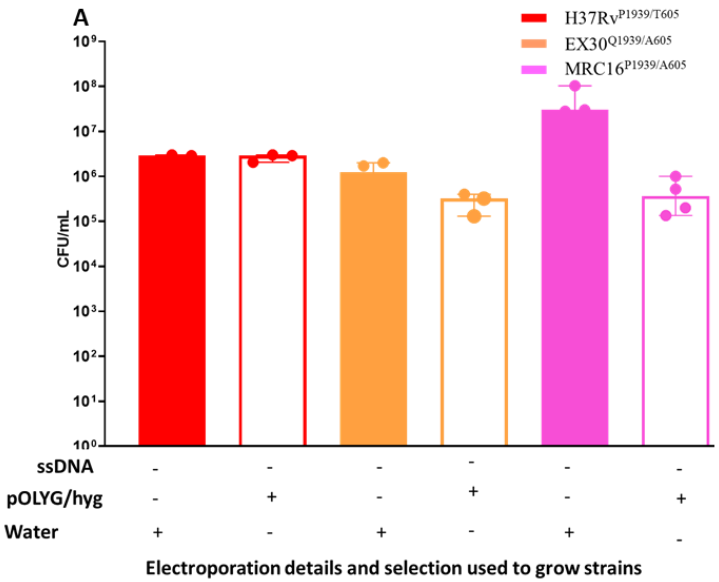
A
H37Rv^P1939/T605
EX30^Q1939/A605
MRC16^P1939/A605
CFU/mL
ssDNA
pOLYG/hyg
Water
Electroporation details and selection used to grow strains

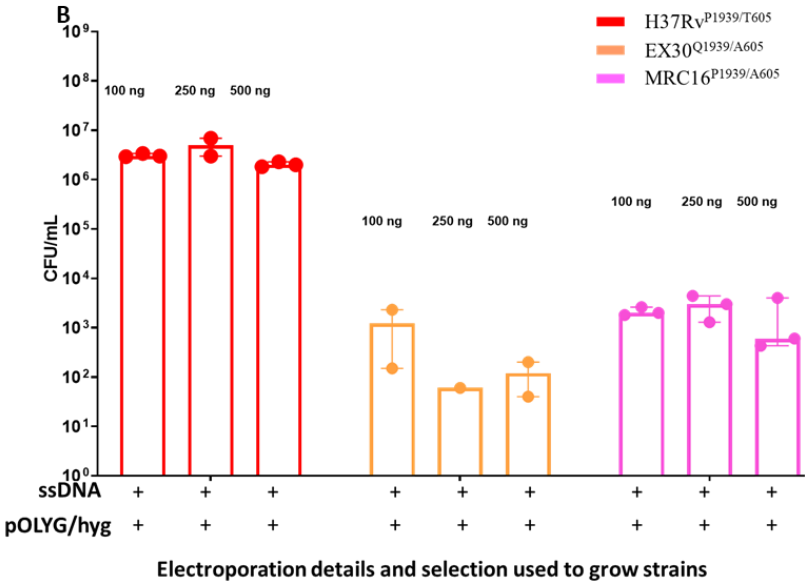
B
H37Rv^P1939/T605
EX30^Q1939/A605
MRC16^P1939/A605
100 ng
250 ng
500 ng
CFU/mL
ssDNA
pOLYG/hyg
Electroporation details and selection used to grow strains

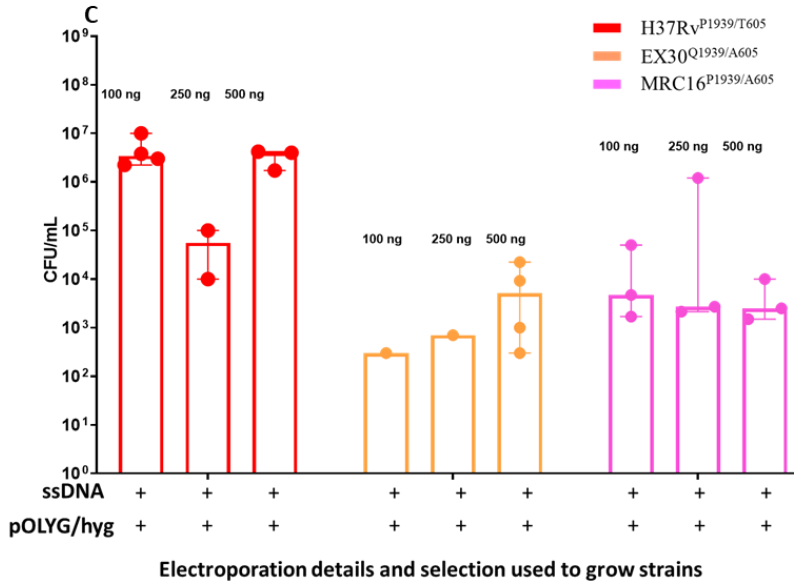
C
H37Rv^P1939/T605
EX30^Q1939/A605
MRC16^P1939/A605
100 ng
250 ng
500 ng
CFU/mL
ssDNA
pOLYG/hyg
Electroporation details and selection used to grow strains

Figure 5.7. Average CFU following electroporation in the presence of ssDNA and/or pOLYG to change two SNP in *pks2*.
H37Rv$^{P1939/T605}$: pNIT, EX30$^{Q1939/A605}$:pNIT and MRC16$^{P1939/A605}$:pNIT were electroporated in the presence of water or 500 ng pOLYG or three different concentration of each ssDNA substrate (100 ng, 250 ng and 500ng) with or without 500 ng of pOLYG. The electroporation samples were plated in the solid media supplemented or not supplemented with Hygromycin. Plates were incubated and colonies were counted 2 – 3 weeks later. Each dot represents number of colonies counted for each dilution factor in each concentration of ssDNA. **(A)** transformation with pOLYG only **(B)** transformation with ssDNA substrates specific for SNP-1815 changing amino acid T605 to A605 (ssDNA-T605A) for all strains and (**C**) transformation with ssDNA substrates specific for base 5817 changing amino acid Q1939 to P1939 for all strains.

5.2.3. Mutation confirmation: SNP-1817 is more amenable to change than SNP-5817

Sanger sequencing was used to confirm successful introduction of the desired mutation following electroporation. Colonies growing on hyg were subjected to a colony boil and each region of interest within *pks2* was amplified, and correctly sized products were submitted for Sanger sequencing. A representative sequencing chromatogram for SNP-1815 indicates the successful change of **g**cc to **a**cc (A605T) in the genome of the EX30$^{Q1939/A605}$::pNIT strain (Fig. 5.10).

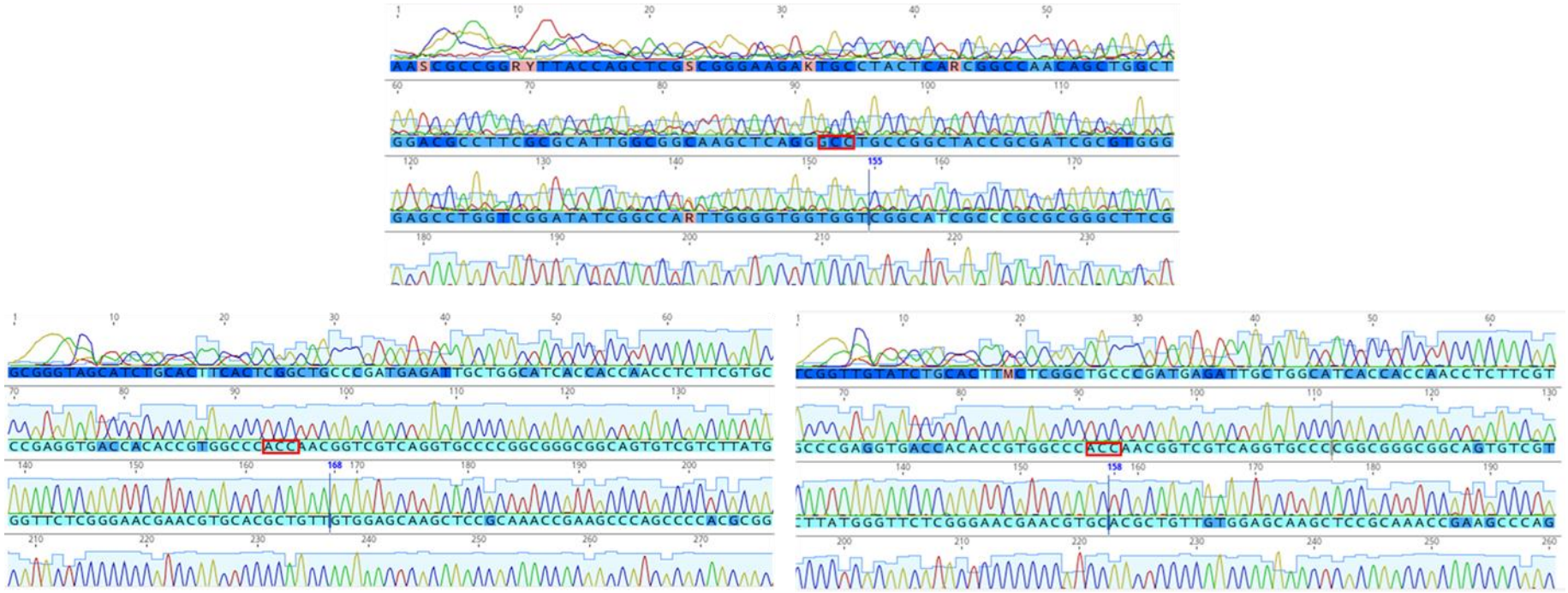

Figure 5.8. Sanger sequencing data representation of base modification at amino acid position 605.
Colonies of EX30$^{Q1939/A605}$::pNIT, MRC16$^{P1939/A605}$::pNIT and H37Rv$^{P1939/T605}$::pNIT, respectively, were resuspended in TE buffer and heat killed. PCR was performed on the colony boils to amplify a region of *pks2* spanning position SNP-1815, aa605. The PCR amplicons were sent for sequencing at the Central Analytic Facility at Stellenbosch University. The images represents position 605 where (**A**) **acc** in H37Rv$^{P1939/T605}$ was changed to **gcc**, (**B) gcc** in EX30$^{Q1939/A605}$ was changed to **acc and (C**) **gcc** in MRC16$^{P1939/A605}$ was changed to **acc.**. Data was analysed using the genius prime software (Biomatters).

Table 5.3 shows the number of colonies for which *pks2* was successfully amplified together with the percentage of colonies that contained the desired mutation. For EX30$^{Q1939/A605}$ and MRC16$^{P1939/A605}$ all the colonies that were screened for the SNP-1815 modification (A605T) showed the correct base change at that site, indicating a 100 % success screening success rate for the A605T mutation. Surprising H37Rv$^{P1939/T605}$ was less amenable to the change in that position, but with only a 4.16 % success rate. Given that H37Rv$^{P1939/T605}$ is a well characterised strain, that has been passaged numerous times, it was expected to be more permissive to electroporation compared to the clinical strains. However, I observed that the recovered H37Rv$^{P1939/T605}$ bacteria when electroporated with ssDNA and pOLYG (Fig. 5.7) was similar to pOLYG only, whereas electroporation in the presence of ssDNA and pOLYG for the clinical strains reduced bacterial viability (Fig. 5.8 – Fig. 5.9). This could mean that H37Rv$^{P1939/T605}$ was efficient in uptaking pOLYG and less efficient in uptaking the ssDNA. Alternatively, the lower rate of induced mutation in H37Rv$^{P1939/T605}$ is that there are other mutations in this strain that would negatively interact with the 605 mutations (i.e. epistatic effects), however further investigation of this potential reason was beyond the scope of this work and successfully generated mutants were taken forward for phenotyping (Table 5.4)

Table 5.3. The rate of positive mutants in the number of screened colonies for the *Mtb* strains

		***Pks2*:605**			***Pks2*:1939**	
Strains	**Colonies screened by PCR**	**PCR$^+$ colonies sequenced**	**Colonies with SNP change**	**Total colonies screened. by PCR**	**PCR$^+$ colonies sequenced**	**Colonies with SNP change**
EX30$^{Q1939/A605}$: pNIT	19	14	14 (100%)	70	46	0
MRC16$^{P1939/A605}$: pNIT	12	11	11 (100%)	63	56	0
H37Rv$^{P1939/T605}$:pNIT	37	24	1 (4.16 %)	84	52	0
Total screened	68	49	25 (51 %)	217	210	0

While electroporation experiments to introduce the SNP-1815 mutation was successful for all strains, after screening a total of 68 colonies, strains containing a mutation at SNP-5817 (aa1939) could not be found (Table 5.4). To generate these strains, the electroporation was repeated (this time only using the pOLYG co-electroporation strategy because contamination was prevalent when using ssDNA alone in previous assays) and plated in media supplemented with hyg. Two different electroporation experiments were completed for each strain and after screening a total of 217 colonies from both experiments, no colonies that contained a mutation at the desired position were identified for all three strains (Table 5.4). The mutation at aa1939 seems to be less amenable to induced genetic change, which might point to that position being critical for the protein and changing it affects the integrity of the protein.

Table 5.4 indicates the panel of mutant strains that were generated via the genetic engineering strategy presented above and taken forward for further characterisation via immunological and lipid assays to establish genotype-phenotype relationships. The mutant MRC16$^{P1939/A605T}$ strain carries the same allele combination as wildtype H37Rv, whereas the mutant H37Rv$^{P1939/T605A}$ has the *pks2* allele combination of wildtype MRC16. Wildtype EX30$^{Q1939/A605}$ and mutant EX30Q1939/A605T contain unique combinations that are not present in the other 4 strains.

Table 5.4. The combination of wildtype and their mutant strains that were successfully created with genetic engineering.

Original Strains	1st SNP details	Amino acid	2nd SNP details	Amino acid	Mutant strain
EX30$^{Q1939/A605}$	nt: C5817	Q1939	nt: G1815	A605	EX30Q1939/A605T
MRC16$^{P1939/A605}$	nt: A5817	P1939	nt: G1815	A605	MRC16$^{P1939/A605T}$
H37Rv	nt: A5817	P1939	nt: A1815	T605	H37Rv P1939/T605A

5.2.4. Analysis of wild-type and mutant *Mtb* strain lipid profiles by TLC

To understand whether there were differences in cell wall lipids between WT and mutants' strains of *Mtb*, both WT and mutant strains were sent for TLC analysis. These strains presumed

to have lost the pOLYG plasmid since there was no growth observed in media supplemented with hyg. Strains were prepared as in Chapter 3 (section 3.3.1, methods: 2.2.4) for analysis with TLC. Due to delays over COVID-19 lock-downs, the full repertoire of lipids characterised in Chapter 3 (Fig. 3.6 – 3.9) could not be completed for mutants but will be done as future work. Only characterisation of TDM, TMM, and PE, CL and PIM lipids are reported in Figure 5.11. The TLC data shows that whilst the loading of the same amount of extract was performed similar density for all strains was not observed, the mutant H37Rv$^{P1939/T605A}$ has the faintest lipid profile of all strains. Compared to wildtype H37Rv, H37Rv$^{P1939/T605A}$ has a relative decrease in TMM, and CL compared to TDM and PE and a loss of the two lower PE bands. It is also missing PI and PIMs, although these are the faintest in wildtype and thus their absence could be due to the overall lower lipid staining for the mutant. Comparing EX30$^{Q1939/A605}$ and EX30Q$^{1939/A605T}$ they were near identical expect for a faint lower PE band that was present in the mutant EX30$^{Q1939/A605T}$ and not wildtype they also have a relatively higher abundance of PI as compared to H37Rv. Both these strains are missing TMM in their cell wall lipid extract (Fig. 5.11). I also observed only subtle differences in the lipids measured for MRC16$^{P1939/A605}$ and MRC16$^{P1939/A605T}$. Both strains were missing TMM and PIMs in their cell wall lipid extract, and both also have the fainter lower PE band which was also present in mutant EX30$^{Q1939/A605T,}$ and this was also relatively brighter in mutant MRC16$^{P1939/A605T}$ compared to wildtype MRC16 (Fig. 5.11). PI was also barely detectable in wildtype MRC16 and absent in mutant MRC16$^{P1939/A605T}$. Unfortunately, SL-1 our primary lipid of interest regulated by pks2 is not clearly represented in these TLC.

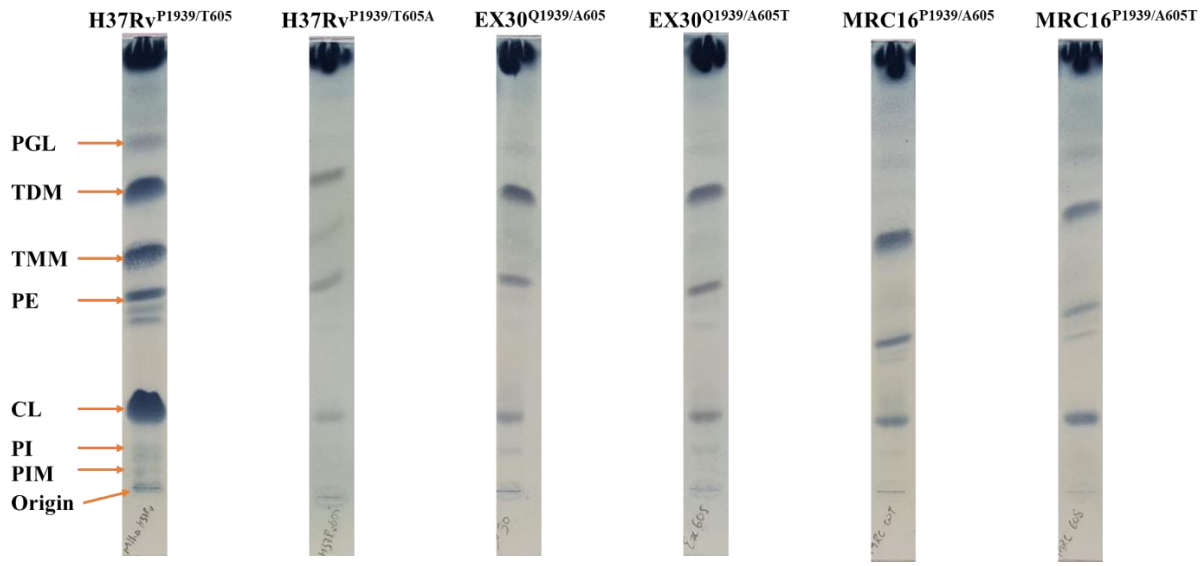

Figure 5.9. Thin layer chromatography analysis of apolar cell wall lipids from *Mtb* WT and mutant strains.

All the strains were cultured media without Tween 80. The strains were allowed to grow for 10 days. The cultures were centrifuged, and the media discarded, and the pellet was heat-killed at 80 °C for 1 h. The pellet was used to extract polar and apolar lipids, which were analysed by TLC. The TLC represent lipids from $H37Rv^{P1939/T605}$ (P1939/T605), $H37Rv^{P1939/T605A}$ (P1939/T605A), $EX30^{Q1939/A605}$ (Q1939/A605), $EX30^{Q1939/A605T}$ (Q1939/A605T), $MRC16^{P1939/A605}$ (P1939/A605) and $MRC16^{P1939/A605T}$ (P1939/A605T). Lipids represent: TDM (Trehalose di-mycolate), TMM (Trehalose mono-mycolate), PE (phosphatidylethanolamine), CL (cardiolipin) and PIM (phosphatidylinositol mannosides). Arrow points to lipid difference between wildtype and mutant strains.

5.3. Discussion

To address the question of whether the clinical strain phenotype differences I observed in Chapter 3 and Chapter 4 are attributable to the SNP in *pks2*, the two *Mtb* clinical strains $EX30^{Q1939/A605}$ and $MRC16^{P1939/A605}$ and one lineage matched laboratory strain H37Rv were taken forward for genetic engineering. $EX30^{Q1939/A605}$ and $MRC16^{P1939/A605}$ clinical strains were chosen for genetic engineering because I observed differences in cording phenotypes (Fig. 3.4), differences in cell wall lipid production (Chapter 3; Fig 3.6 -3.9), and differences in cytokine secretion in the absence (Table 3. 3) and presence of HIV-1 co-infection (Table 4.2) between these strains. There were two SNP identified in *pks2* of $EX30^{Q1939/A605}$, the first SNP in position 5817 was identified by Koch *et al.,* (2017) [4] to be under HIV-1 positive directional selection and changes a proline to a glutamine (P1939Q). A second SNP in position 1815, was chosen after analysis of *pks2* sequences in both $EX30^{Q1939/A605}$ and $MRC16^{P1939/A605}$ (Table 2.3). The SNP was chosen because it occurs in the same gene as the SNP under positive directional selection and it only occurs in the clinical strains and not the lab strain. The SNP is a non-synonymous SNP changing a threonine to an alanine (T605A) and I predicted the SNP may work in tandem with the SNP 5817 (P1939Q). I successfully generated single-base mutations at SNP-1815 in all three strains but could not generate mutations at SNP-5817 in any strain.

A search of the protein data bank (PDB) did not yield results of know structure of the Pks2 protein from *Mtb*. Bordoli *et al.,* (2009) [7], stated that the number of determined protein structures is less than 1 % of the know protein sequences [7]. However, proteins can be classified into families with similar sequences and similar fold and function [8], and such similarities form basis for protein structure prediction via the sequence [7]. I used an online tool Phyre2 [5] to predict the structure of Pks2 from the amino acid sequence (Fig. 5.2 – Fig. 5.3). The amino acid sequence of a protein can be used to predict with high accuracy the 3D structure of proteins. *Pks2* encodes a synthase involved in the metabolism of SL-1 [9], and if mutations occur in the active site it is conceivable that they could affect the functioning of the synthase, and therefore possibly SL-1 production in these strains. The SNP responsible for

P1939Q is observed in a region that does not appear to correspond to the active site and the proline assumes a slightly buried spatial distribution in the protein. Proline is a ring shaped bulky amino acid which can occupy a small pocket of space, due to the ring-shaped structure, but glutamine has a longer side chain (Fig 5.2). When glutamine replaces an amino acid like proline its long side chain may cause steric clashes with adjacent amino acids, disrupting forces responsible for holding the protein structure intact [10]. This information shows the possible effects amino acid changes may have on protein structure and consequently function (Fig 5.2). However, further studies are required to confirm whether any phenotypic changes result from the difference in amino acids and by extension the SNP.

The second SNP responsible for T605A mutation occurs in an alpha helix that makes up a loop on the surface of protein and this position is unlikely to be in the active site of the protein (Fig 5.3). However, since the change is from a long-chained, polar amino acid (threonine) to a smaller, non-polar amino acid (alanine), this may serve to have a destructive effect on the stability of the protein. The protein structure achieves stability by burying the non-polar side chains. In fact in a given protein structure, 75 % of the non-polar side chains are buried [11].
To determine genotype-phenotype relationships, recombineering was applied to introduce SNP of interest into EX30$^{Q1939/A605}$, MRC16$^{P1939/A605}$ and H37Rv (Chapter 2; Table 2.4). The first step of recombineering requires the introduction of the pNIT plasmid into strains to facilitate expression of recombineering proteins. Strains transformed with pNIT were easily identified by antibiotic selection because of the *aph3'* gene on pNIT, which confers kan resistance [12]. The second step of recombineering involves introducing ssDNA containing the179utateon of interest into the pNIT-transformed strains. To facilitate more efficient screening of this second step of recombineering, I modified the original protocol for recombineering slightly [2]. During the second round of electroporation to insert the ssDNA substrate, I included a plasmid pOLYG [6], which has a hyg resistance sequence in the backbone. The inclusion of this plasmid allowed more efficient selection of transformants for screening because bacteria which take up pOLYG would be selected on plates supplemented with hyg. Even though transformation with pOLYG does not translate to transformation with ssDNA or homologous recombination in transformed bacteria, it does lower the number of colonies to be screened. The pOLYG plasmid would be subsequently lost in the strains following culture in media without hyg supplementation.

The SNP responsible for T605A, was amenable to mutation in the clinical strains as indicated by 100% success rate of screening via Sanger sequencing were positive for the mutation (Table

5.3). H37Rv appeared to be less amenable to genetic change because only a single colony out of 24 was positive for the introduced mutation. SNP-5817 responsible for P1939Q found in $EX30^{Q1939/A605}$ and predicted to be HIV-1 positive directional selection could not be mutated via recombineering in this work. Without significantly more work, it is difficult to provide a conclusive reason for why this SNP could not be changed. It is possible that the P1939Q mutation changes the protein structure too significantly and requires other mutations within the genome to allow for effective protein folding.

Although I was not able to successfully make the change at SNP-5817 in $EX30^{Q1939/A605}$, I was able to make a new mutant combination with the change in SNP-1815 that changes T605 to A605 in $EX30^{Q1939/A605T}$ and $MRC16^{P1939/A605T}$; the MRC16 mutant resembles wildtype H37Rv whilst $EX30^{Q1939/A605T}$ contains a new unique *pks2* allele combination. The mutation of SNP-1815 in $H37Rv^{P1939/T605A}$ created a mutant strain which resembles wildtype $MRC16^{P1939/A605}$. From the limited data that is available on lipid production between the mutant and WT strains, SL-1 could not be assessed, and only subtle changes in PE were seen between the clinical wildtype and mutants. By contrast $H37Rv^{P1939/T605A}$ showed dramatic relative loss of TMM and CL/PG compared to TDM and PE. Due to the large number of lipid changes observed in the mutant $H37Rv^{P1928/T650A}$ compared to wildtype $H37Rv^{P1939/T605}$ these may be due to other SNP introduced into $H37Rv^{P1939/T605A}$. The effects electroporation on global lipid production in the strains and more specifically the effect on the lipid of interest if critical to analyse. While attempts were made to measure the same lipid species for the strains before and after electroporation, this was not possible. To understand this effect whole genome sequencing of the strains to compare any differences in genes responsible for the metabolism of the lipids that differ between the wild-type and mutant strains.

It must be noted that much work remains to be completed to look at the full repertoire of lipids measured initially to conclude the effect of the mutation on cell wall lipid production. This includes the critical SL-1 lipid, which is regulated by the *pks2* gene, which is the primary gene of interest in these strains. Without the TLC analysis of TLC in the mutant strains to understand the effect of the mutation, this work remains incomplete. An important future experiment is the analysis of the mutant strains with lipid mass-spectrometry to see the effect of the mutations on cells wall lipids, especially in the critical SL-1. Nevertheless, genetic engineering of clinical *Mtb* strains to establish genotype-phenotype relationships are not often undertaken and the partial success of this strategy represents a significant technical achievement. Lastly, for both

EX30$^{Q1939/A605}$ and MRC16$^{P1939/A605}$, selection on hyg after co-electroporation with pOLYG+ssDNA resulted in fewer colonies, than when cells were electroporated with ssDNA-only and plated on antibiotic-free media. These data show that my modification of the conventional protocol to include co-electroporation of a plasmid containing an antibiotic marker to allow selection of electroporated bacteria successfully reduced the overall number of colonies to be screened for SNP validation.

5.4. Conclusion

I was able to use recombineering to successfully make unmarked mutants in clinical *Mtb* strains, which as mentioned above has not often been attempted nor accomplished often in the field. Mutation efficiency appears to be site specific in *Mtb* because SNP-1815 responsible for T605A was easily changeable back to A605T in the clinical strains or T605A in the lab strain to match the clinical strain SNP. However, I was unable to successfully change SNP-5817, responsible for P1939Q in EX30 predicted to be under HIV-1 selection pressure. Mutants generated in this section were taken forward along with WT strains to infect MDM in the presence of HIV-1 co-infection to examine the role (if any) that is played by the SNP observed in position 1815 (T605A) on P1939Q related immunological phenotypes.

Supplementary Figure 5.1. thin layer chromatography analysis of lipids from different strains of *Mtb*

The TLC runs by Dr Apoorva Bhatt were conducted simultaneously with other lipids from different projects in our lab. As such, the TLC runs for the strains sent for this project were not completed chronologically and for this reason the TLC gels shown here are from two different gels that were modified to put matching strains next to each other. The following

picture shows the original TL

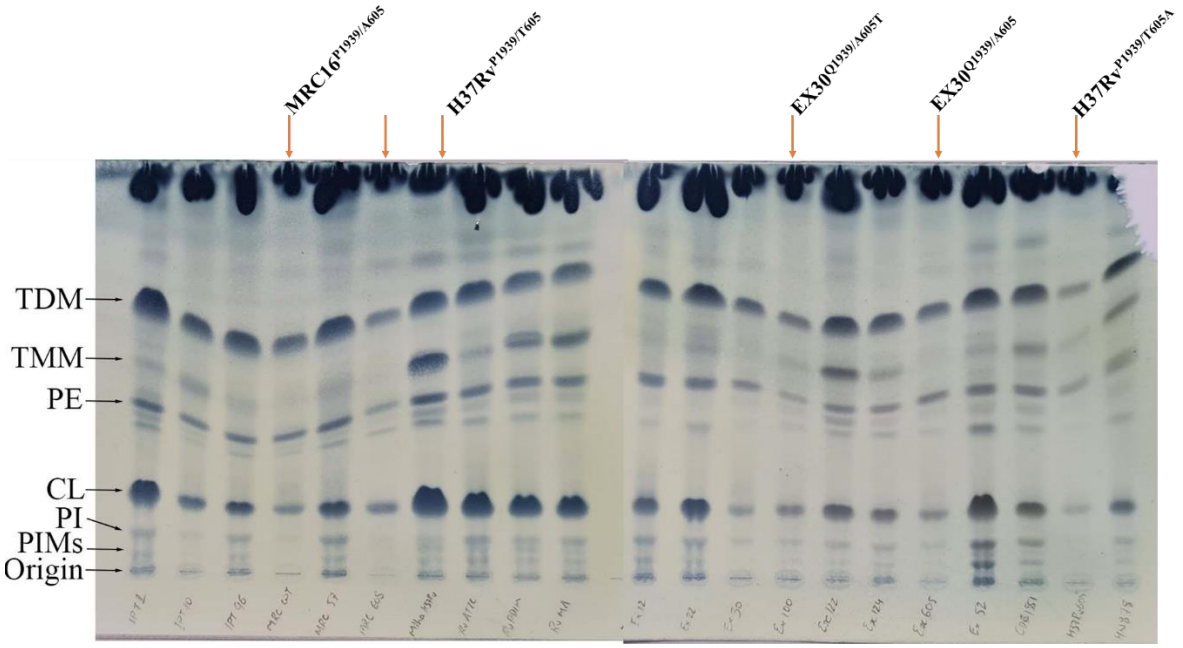

Figure 5.10. Thin layer chromatography analysis of apolar cell wall lipids from *Mtb* WT and mutant strains.
All the strains were cultured media without Tween 80. The strains were allowed to grow for 10 days. The cultures were centrifuged, and the media discarded, and the pellet was heat-killed at 80 °C for 1 h. The pellet was used to extract polar and apolar lipids, which were analysed by TLC. The TLC represent lipids from different strains on *Mtb*. Lipids represent: TDM (Trehalose di-mycolate), TMM (Trehalose mono-mycolate), PE (phosphatidylethanolamine), CL (cardiolipin) and PIM (phosphatidylinositol mannosides). Arrow points to lipid difference between wildtype and mutant strains.

5.5. References

1. Lamrabet, O. and M. Drancourt, *Genetic engineering of Mycobacterium tuberculosis: a review.* Tuberculosis (Edinb), 2012. **92**(5): p. 365-76.
2. van Kessel, J.C. and G.F. Hatfull, *Efficient point mutagenesis in mycobacteria using single-stranded DNA recombineering: characterization of antimycobacterial drug targets.* Mol Microbiol, 2008. **67**(5): p. 1094-107.
3. Boshoff, H.I. and V. Mizrahi, *Expression of Mycobacterium smegmatis pyrazinamidase in Mycobacterium tuberculosis confers hypersensitivity to pyrazinamide and related amides.* J Bacteriol, 2000. **182**(19): p. 5479-85.
4. Koch, A.S., et al., *The Influence of HIV on the Evolution of Mycobacterium tuberculosis.* Mol Biol Evol, 2017. **34**(7): p. 1654-1668.
5. Kelley, L.A., et al., *The Phyre2 web portal for protein modeling, prediction and analysis.* Nat Protoc, 2015. **10**(6): p. 845-58.

6. Garbe, T.R., et al., *Transformation of mycobacterial species using hygromycin resistance as selectable marker.* Microbiology (Reading), 1994. **140 (Pt 1)**: p. 133-8.
7. Bordoli, L., et al., *Protein structure homology modeling using SWISS-MODEL workspace.* Nat Protoc, 2009. **4**(1): p. 1-13.
8. Chothia, C., *Proteins. One thousand families for the molecular biologist.* Nature, 1992. **357**(6379): p. 543-4.
9. Sirakova, T.D., et al., *The Mycobacterium tuberculosis pks2 gene encodes the synthase for the hepta- and octamethyl-branched fatty acids required for sulfolipid synthesis.* J Biol Chem, 2001. **276**(20): p. 16833-9.
10. Fitzkee, N.C. and G.D. Rose, *Reassessing random-coil statistics in unfolded proteins.* Proc Natl Acad Sci U S A, 2004. **101**(34): p. 12497-502.
11. Patki, A.U., A.C. Hausrath, and M.H. Cordes, *High polar content of long buried blocks of sequence in protein domains suggests selection against amyloidogenic non-polar sequences.* J Mol Biol, 2006. **362**(4): p. 800-9.
12. Murphy, K.C., K. Papavinasasundaram, and C.M. Sassetti, *Mycobacterial recombineering.* Methods Mol Biol, 2015. **1285**: p. 177-99.

Chapter 6. Linking *Mtb pks2* genotype to cytokine and HIV-1 phenotype in co-infected human macrophages

6.1. Introduction

Mtb co-infection affects HIV-1 replication by two mechanisms: (1) *Mtb* lipids bind to host PRR and stimulate HIV-1 activating hTF [1], (2) *Mtb* lipids stimulate cytokines which also induce HIV-1 activating human transcriptional factors (hTF) and thereby increase HIV-1 replication [1]. Cytokines also influence HIV-1 infection dynamics by increasing the expression of HIV-1 entry co-receptor or blocking access to HIV-1 co-receptors [2]. The outcome of *Mtb* infection varies between different strains [3]. This difference in phenotype was documented in differential cytokine production between HN878 and H37Rv [4]. In fact, Reed and colleagues [4], showed that H37Rv increased cytokine production compared to HN878 because it lacked a cell wall lipid that modifies cytokine secretion. Using this data, Ranjbar *et al.,* (2009) [5], showed that increased production of cytokines by CDC1551 compared to HN878 accounted for the observed increase in HIV-1 p24 antigen of PBMC co-infected with CDC1551 compared to HN878 [5]. This data demonstrates that underlying genetic variation in *Mtb* strains and consequent diversity in cytokine responses may influence HIV-1 infection in disease sites. The outcome of HIV-1 infection is also determined by the biology of the infected host [6]. A study by Trachtenberg *et al.,* (2003) [7], found that individuals who were homozygous for two of the three HLA class I alleles progressed more rapidly to AIDS compared to individuals who were heterozygous for all three alleles [7]. While a different study showed slow disease progression in individuals with isoleucine-80 in *HLA-B* compared to individuals with threonine in position 80 [8]. The observations in these studies underly the question of the effect of different inflammatory environments on HIV-1 replication.

As described in Chapter 5, several phenotypic differences between the phylogenetically close MRC16$^{P1939/A605}$ and EX30$^{Q1939/A605}$ strains, including differences in lipid (chapter 3; Figs 3.6 – 3.9) and cytokine production in the absence (chapter 3; Table 3.3) and presence of HIV-1 co-infection (chapter 4; Tabl3 4.2) were observed. Phenotypic differences were not as profound between EU111^{N1759} and EU40^{T1759}, therefore only MRC16$^{P1939/A605}$ and EX30$^{Q1939/A605}$ were taken forward for genetic engineering. The data presented in the sections that follow describe in-depth immunological characterisation of engineered strains generated in Chapter 5, together with their wildtype strains, to investigate the impact that single base pair changes in *pks2* have

on cytokine production and HIV-1 replication during *Mtb*-HIV-1 coinfection of human macrophages.

6.2. Results

6.2.1. Trans-well assay set-up to monitor direct co-infection and bystander effects of *Mtb* infection on HIV-1 production.

The *Mtb*/HIV-1 co-infection experiments used to assess the impact of SNP engineering on strain-induced phenotypes were carried out using a trans-well assay. The trans-well plate is a good model to mimic simultaneous co-infection in the top chamber and bystander cell effect in the bottom chamber. The top chamber of the trans-well plate has a membrane with pores that are 0.4 μm in size (Fig. 6.1). These pores sizes allowed the movement of HIV-1 particles between the top and bottom chamber - HIV-1 particle sizes are between 100 to 120 nm in diameter [9] - while restricting the movement of *Mtb* bacteria from the top to the bottom chamber, as *Mtb* rods are an average 2-4 μm in size [10]. Due to the number of conditions and strains to be tested, I only used M2 MDM for infection with both HIV-1 and *Mtb* strains. In Chapter 3 and Chapter 4, I observed that there were limited differences in cytokine secretion between M1 and M2 polarised MDM during co-infection with *Mtb* and HIV-1. Although I did not observe any differences in HIV-1 production between M1 and M2 MDM, there is precedent in the literature for increased HIV-1 production in M2 MDM compared to M1 [11, 12], therefore I chose M2 polarised MDM for these experiments. I used seeded M2 MDM in the top and the bottom well. I infected both the top and bottom wells with HIV-1 and allowed the infection to continue for seven days without mixing the two wells, while refreshing 50% of the media every three days. After seven days, I co-infected the top well only with *Mtb* for 4 hours and then combined the top and the bottom well to allow cytokines to mix. I harvested the SN in co-infected MDM (top chamber) and the bystander MDM (bottom chamber) 24- and 96-hours post-infection with *Mtb* and used Luminex to measure p24.

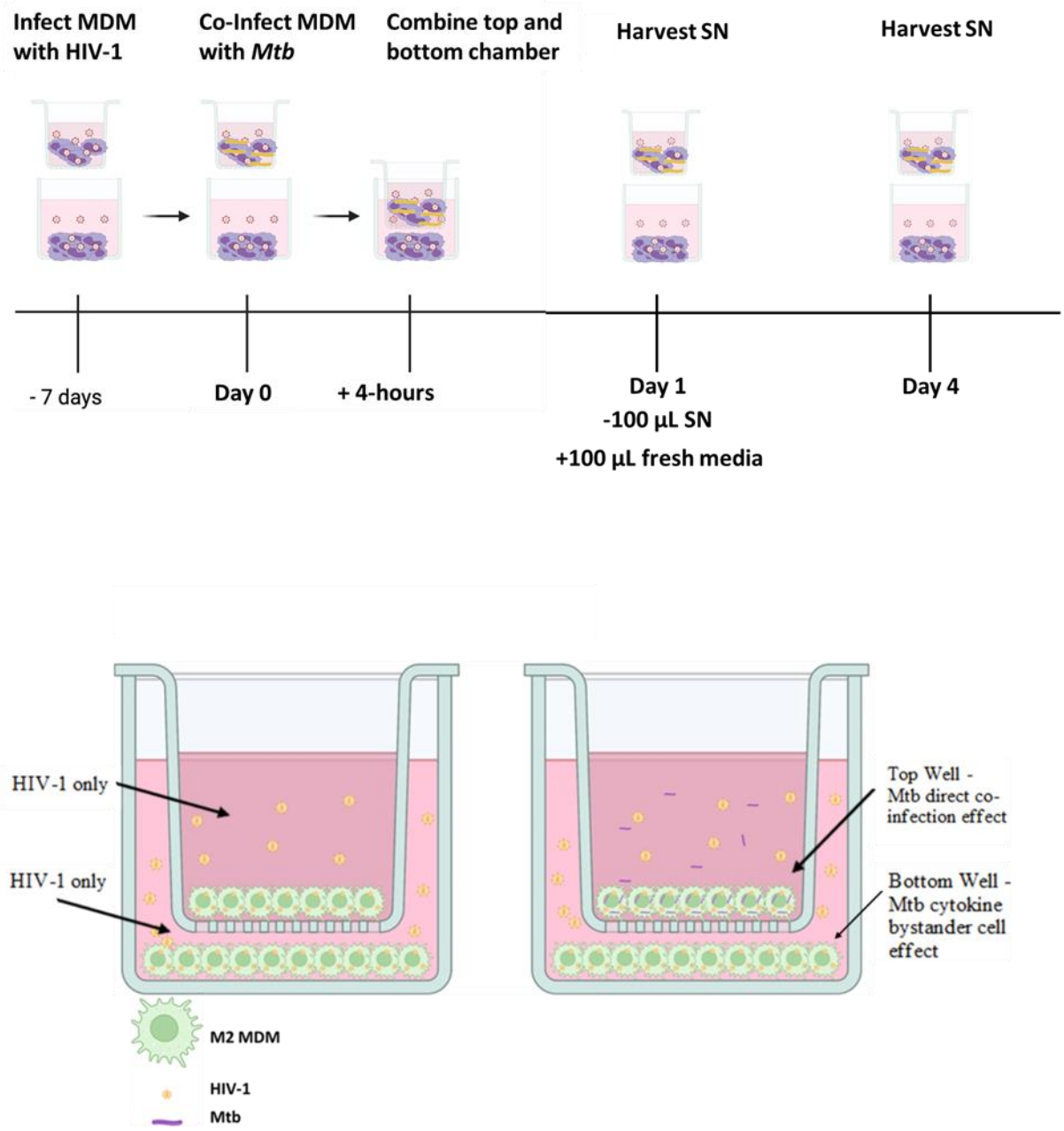

Figure 6.1. Schematic trans-well plate infectin conditions used to assess the impact of *Mtb* strains on HIV-1 replication in co-infected and bystander cells.
The schematic shows **(A)** top chamber and bottom chamber of the trans-well plate with MDM infected with HIV-1 only, **(B)** top and bottom chamber of the trans-well plate with top chamber co-infected with *Mtb* and HIV-1 and the bottom chamber infected with HIV-1 only.

6.2.2. Trans-well baseline parameters: HIV-1 migration is similar between the top and the bottom chamber.

One of the caveats to this trans-well assay is the pore size of the membrane separating the top and the bottom chamber. Ideally, a trans-well membrane that excludes both HIV-1 and *Mtb*

from moving between the chambers (Fig. 6.1), while allowing cytokines and chemokines to move freely, would have been best to use. In that case, phenotypes observed in each chamber would be resulting from the infection carried out in that chamber and the cytokine milieu only. However, a trans-well plate with this membrane was not available to use and there one that was used in these experiments had pores which allowed the movement of HIV-1 as well as cytokines between the top and the bottom chambers and this might influence the analysis of HIV-1 production measured by SN HIVp24. It was, therefore, important to understand the movement of HIV-1 from the top chamber to the bottom chamber and from the bottom chamber to the top chamber in the absence of co-infection. That would help to understand the contribution of migrating HIV-1 to the observed HIV-1 phenotype in the chamber being analysed. To achieve this, I set up three control wells where there was: (1) HIV-1 infection of the top chamber only, (2) HIV-1 infection occurred in both the top and bottom chamber, and (3) HIV-1 infection only in the bottom chamber. I then analysed HIV-1 production in the top and bottom chambers for each condition to understand how HIV-1 moved to an uninfected chamber from an infected chamber. All chambers were seeded with the same amount of MDM and infected with the same MOI of HIV-1.

Firstly, I analysed the production of HIV-1 p24 in the top chamber only of all three experimental conditions (Table 6.1; Fig 6. 2A). The data here shows a statistically significant difference in p24 (as a proxy for HIV-1) in the top chamber when there is infection in that chamber (Table 6.1; Fig 6. 2A). The amount of HIV-1 harvested in the top chamber when both the top and the bottom chamber are infected is 65-fold higher ($p = 0.0016$) compared to HIV-1 harvested in the top chamber when only the bottom chamber is infected (Table 6.1; Fig 6. 2A). Moreover, there was 57.6-fold more HIV-1 ($p = 0.0238$) in the top chamber when only the top chamber was infected compared to HIV-1 harvested in the top chamber when only the bottom chamber was infected (Table 6.1; Fig 6. 2A) There was no statistically significant difference in HIV-1 production in the top chamber when the bottom chamber was also infected ($p = 0.2448$) (Table 6.1; Fig 6. 2A). This data shows that, although HIV-1 was recovered in the top chamber when there was no direct top chamber infection, which proves migration from the bottom to the top chamber, the amount of HIV-1 was not enough to influence analysis of HIV-1 production in the top chamber.

Then, I went on to measure the amount of HIV-1 recovered in the bottom chamber from all three experimental conditions (Table 6.1; Fig. 6.2B). Analysis of HIV-1 from the bottom

chamber shows that HIV-1 was 10.1-fold higher in the bottom chamber when both the top and the bottom chamber are infected compared to when only the top chamber is HIV-1 infected (p = 0.0016) (Table 6.1; Fig. 6.2B). The bottom chamber also had 5.6-fold higher HIV-1 in the SN (p = 0.0238), when only the bottom chamber was infected compared to when only in the top chamber was infected (Table 6.1; Fig. 6.2B). Importantly, there was no statically significant difference in HIV-1 production between having infection in both the top and the bottom chamber compared to having infection in the bottom chamber only (p = 0.2448) (Table 6.1; Fig 6. 2B). This data indicates that although there was more movement of HIV-1 from the top to the bottom chamber, than bottom to top, this was not significant to influence HIV-1 production analysis in the bottom chamber.

Table 6.1. Analysis of HIV-1 p24 production by MDM in the trans-well plate

HIV-1 harvested in top chamber						
	Infection Both chambers v infection Top chamber		**Infection Both chambers v infection bottom chamber**		**Infection top chamber v infection bottom chamber**	
Analyte	Fold change	p-value	Fold change	p-value	Fold change	p-value
HIV-1 p24	**-**	**ns**	**65.01**	**0.0016**	**57.62**	**0.0238**
HIV-1 harvested in bottom chamber						
	Infection Both chambers v infection Top chamber		**Infection Both chambers v infection bottom chamber**		**Infection bottom chamber v infection top chamber**	
Analyte	Fold change	p-value	Fold change	p-value	Fold change	p-value
HIV-1 p24	**10.12**	**0.0016**	**-**	**ns**	**5.65**	**0.0238**

Statistics: Kruskal-Wallis multiple comparison test with Two-stage linear step-up procedure of Benjamin, Krieger and Yekutieli False discovery rate (FDR): with a cut off 0.1. Mean fold change between compared groups. P-value of comparison with FDR of <0.1. Fold change of non-significant (ns) value is not shown.

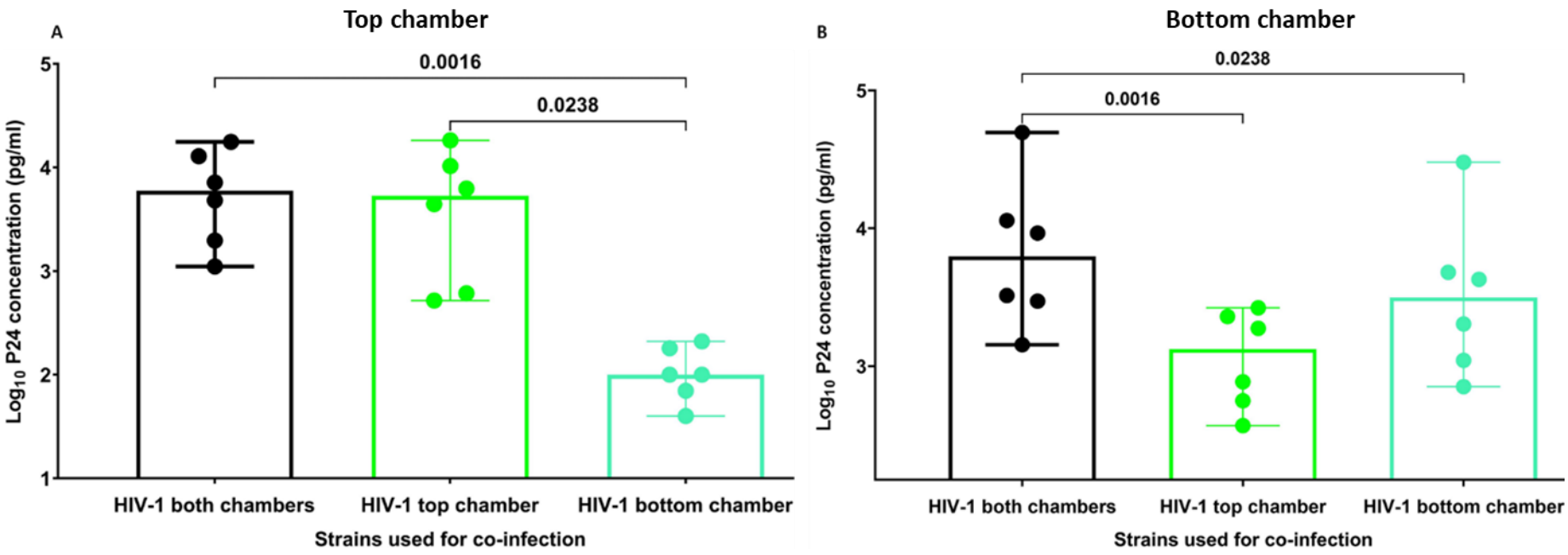

Figure 6.2. Secretion of p24 by MDM infected with HIV-1.
Monocytes from 6 donors were polarised to M2. The MDM were infected with HIV-1 for 7 days. Seven days post-infection the media replaced (equivalent to co-infection). SN that was used for p24 analysis was harvested after 96-hours. Secretion of p24 was measured by Luminex assay **A)** from the top chamber only and **B)** from the bottom chamber only. Statistics: Kruskal-Wallis multiple comparison test with Two-stage linear step-up procedure of Benjamin, Krieger and Yekutieli False discovery rate (FDR): with a cut off 0.1. Mean fold change between compared groups. P-value of comparison with FDR of <0.1. Fold change of non-significant (ns) value is not shown.

6.2.3. Cytokine secretion is influenced differently between top and bottom chamber

The bottom well in this trans-well assay will not be co-infected with *Mtb*. The HIV-1 production in the bottom chamber will be influenced by cytokines that are secreted in the bottom chamber and well as cytokines secreted in the top chamber that migrate to the bottom chamber. It was therefore also important to understand the dynamics of cytokine movement between the top and the bottom chamber, in the absence of *Mtb* co-infection. I compared cytokines migration using three controls: (1) HIV-1 infection in both the top and the bottom chamber, (2) HIV-1 only infection in the top chamber only, (3) HIV-1 infection in the bottom chamber only. In these experiments there are two conditions: (1) two wells received HIV-1 infection in one chamber (top or bottom) which allow me to understand the dynamics of cytokines secretion in each chamber independently. The second condition is the well with infection in both the top and the bottom chamber, this condition resembles the condition of the co-infection and will allow the analysis of cytokine movement between the chambers when both chambers are infected. In this chapter, only 13 of the original 25 cytokines were analysed (Supplementary Table 6.1 – 6.2), these cytokines were selected based on whether they are involved in HIV-1 regulation according to literature, and their secretion patterns during *Mtb* infection (Chapter 3) and co-infection (Chapter 4).

Analysis of cytokine secretion in the top chamber showed no difference in 12 of the 13 cytokines measured in the top chamber (Table 6.2). This includes comparison between the well infected in the top chamber only compared to the well with infection in the bottom chamber only. This means that the HIV-1 infected bottom well resulted in sufficient movement and stimulation of cytokine secretion to result in comparable cytokine secretion between the wells. The well with infection in both the top and bottom chamber increased the secretion of CCL2 compared to infection in either only the top or bottom chambers ($p \leq 0.0433$). This data suggests that HIV-1 infection increases CCL2 secretion because the increased CCL2 observed possibly results from secretion in the top well augmented by migrated CCL2 from the bottom well.

I observed a slightly different dynamic of cytokine induction in the bottom chamber compared to the top chamber. In the bottom chamber, there was significantly higher TNF ($p = 0.0009$), IL-1β (0.0209) and IL-8 (0.0209) in the infected bottom chamber compared to the well with infection in the top chamber only (Table 6.2), indicating these are cytokines induced by directly

HIV-infected cells. I also observed that CCL2 and CCL4 are increased in the bottom chamber when the top chamber is also infected (Table 6.2).Taken together, this data indicates that during HIV-1 infection when only a few cytokines are induced, cytokines do move between the top and bottom chambers, confirming that this assay will allow the evaluation of *Mtb*-induced cytokines from the top chamber on HIV replication in the HIV-only infected bottom chamber.

Table 6.2. The comparison of cytokine secretion between the top and the bottom chamber of trans-well infected with HIV-1

Cytokines harvested in top chamber						
Top infection v Bottom infection			**Both infection vs Top infection**		**Both infection vs Bottom infection**	
Analyte	Fold change	p-value	Fold change	p-value	Fold change	p-value
CCL2	-	ns	1.37	0.0015	1.20	0.0433

Cytokines harvested in bottom chamber						
Bottom chamber v Top chamber			**Both chamber vs Top chamber**		**Both chamber vs Bottom chamber**	
Analyte	Fold change	p-value	Fold change	p-value	Fold change	p-value
TNF	2.277	0.0009	-	ns	-	ns
IL-1β	1.832	0.0209	-	ns	-	ns
IL-8	1.607	0.0209	-	ns	-	ns
CCL4	-	ns	1.367	0.0433	1.313	0.0209
CCL2	-	ns	1.36	0.0015	1.14	0.0433

Kruskalis-Wallis multiple comparison test with Two-stage linear step-up procedure of Benjamin, Krieger and Yekutieli False discovery rate (FDR): with a cut off 0.1. Mean fold change between compared groups. P-value of comparison with FDR of <0.1. Fold change of non-significant (ns) value is not shown.

6.2.4. Analysis of p24 secretion in MDM co-infected with different strains of *Mtb* in the presence of HIV-1 co-infection

I used SN to measure the secretion of p24 (as proxy for HIV-1 production) in MDM co-infected with the different strains of *Mtb*. I measured whether mutating the SNP in H37Rv$^{P1939/T605}$ to match the SNP found in the clinical strains or reverting the SNP in the clinical strains to match H37Rv$^{P1939/T605}$ would have an effect in HIV-1 modulation.

Firstly, I analysed HIV-1 p24 in the SN harvested 24-hours post-co-infection. I did not observe any significant modification of HIV-1 p24 production for all the strains in both co-infection and bystander cells compared to HIV-1 only infected MDM (Fig. 6.3A-B). There was a trend towards decreased p24 production observed in MDM co-infected with both $H37Rv^{P1939/T605}$ ($p = 0.0304$; FDR 0.10093) and $MRC16^{P1939/A605T}$ ($p = 0.0833$; FDR 0.1374) (Fig. 6.3A). These strains match each other in the position of interest, both have a threonine in the position of interest (Fig. 6.3A). There was no significant modification of p24 production in MDM co-infected with $EX30^{Q1939/A605}$ or $EX30^{Q1939/A60T}$ 24-hours post-co-infection (Fig. 6.3A). In the bystander cells $EX30^{Q1939/A605T}$ environment showed a trend towards decreased p24 production ($p = 0.0433$; FDR 0.1429) (Fig. 6.3B). These data suggests that co-infection with strains of *Mtb* that having a threonine in position-605 potentially plays a role in decreased p24 production early following co-infection (Fig. 6.3A) or exposure to HIV-1/*Mtb* co-infected environment (Fig. 6.3B).

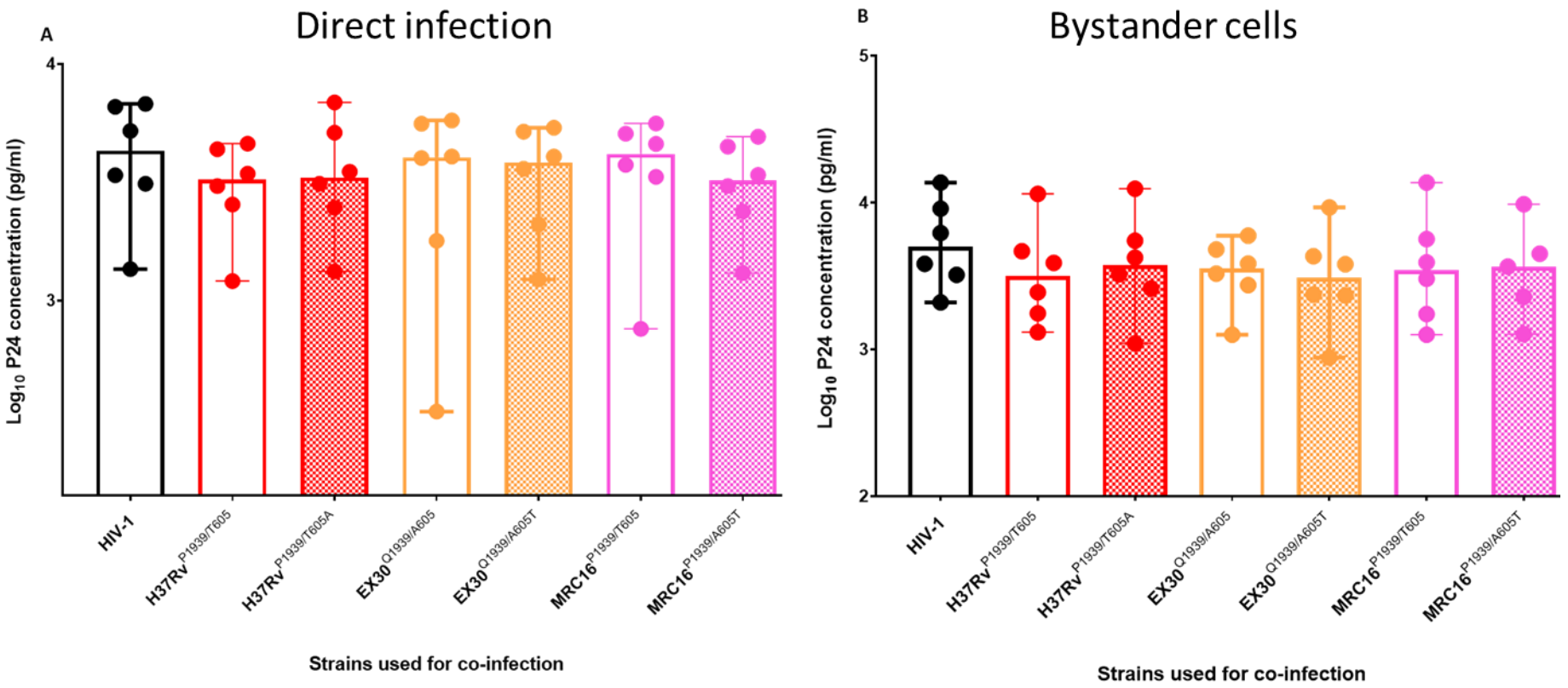

Figure 6.3. Secretion of p24 by MDM infected with HIV-1 and a panel of *Mtb* strains and p24 from bystander cells exposed to HIV-1/*Mtb* co-infection environment 24-hours after *Mtb* infection.

Monocytes from 6 donors were polarised to M2. The MDM were infected with HIV-1 and later co-infected with the different strain of *Mtb*. SN from co-infected MDM was harvested 24-hours post-co-infection with *Mtb* and used for p24 analysis by Luminex assay. Secretion of p24 was measured 24-hours post co-infection in **A)** direct co-infection (top chamber) and **B)** bystander cells (bottom chamber). Friedman's multiple comparison or Kruskalis-Wallis multiple comparison test with two-stage linear step-up procedure of Benjamin, Krieger and Yekutieli False discovery rate (FDR): with a cut off 0.1. Values are considered significant at FDR of ≤0.1 and p≤ 0.05.

I proceeded to measure the production of p24 in MDM that were co-infected for 96-hours or bystander MDM that were exposed to HIV-1/*Mtb* co-infection for 96-hours. In these experiments, I observed a uniform decrease in p24 production in during co-infection with *Mtb* strains compared to MDM infected with HIV-1 only (Fig. 6.4A). This decrease was not significant but showed a trend in MDM co-infected with either MRC16$^{P1939/A605}$ ($p = 0.0833$; FDR 0.1374) or MRC16$^{P1939/A60T}$ ($p = 0.0833$; FDR 0.1374) (Fig. 6.4A). HIV-1 p24 production was significantly low in MDM co-infected with EX30$^{Q1939/A605}$ ($p = 0.0016$), EX30$^{Q1939/A605T}$ ($p = 0.0238$), H37Rv$^{P1939/T605}$ ($p = 0.0230$) and H37Rv$^{P1939/T605A}$ ($p = 0.0238$) (Fig. 6.4A) compared to MDM infected with HIV-1 only (Fig. 6.4A). MDM co-infected with EX30$^{Q1939/A605}$ resulted less p24 production compared to MDM co-infected with EX30$^{Q1939/A605T}$, although this decrease was not significant ($p = 0.2484$; FDR 0.0910) (Fig. 6.4A). This data shows that p24 production is lowered by co-infection with *Mtb* strains in MDM. The data also shows that changing the SNP-605 EX30$^{Q1939/A605}$ potentially results in altered HIV-1 regulation phenotype during co-infection.

The production of p24 was not significantly altered in bystander MDM exposed to HIV-1/MRC16$^{P1939/A605}$, HIV-1/MRC16$^{P1939/A60T}$, HIV-1/H37Rv$^{P1939/T605}$ or HIV-1/H37Rv$^{P1939/T605A}$ compared to MDM exposed to HIV-1 only environment (Fig. 6.4B). The environment of the HIV-1/EX30$^{Q1939/A605T}$ also did not significantly alter p24 production in bystander MDM (Fig. 6.4B). However, similar to MDM exposed to 96-hour SN of EX30$^{Q1939/A605}$ (Chapter 4; Fig. 4.8B), bystander MDM exposed to EX30$^{Q1939/A605}$ here resulted in significantly less p24 production ($p = 0.0460$), compared to MDM exposed to HIV-1 only environment (Fig. 6.4B). This data confirms that EX30$^{Q1939/A605}$ infection produces factors that lead to lowered production of p24 in MDM, and that could be linked to SNP-605 because this phenotype is removed in the EX30$^{Q1939/A605T}$ strain (Fig. 6.4B).

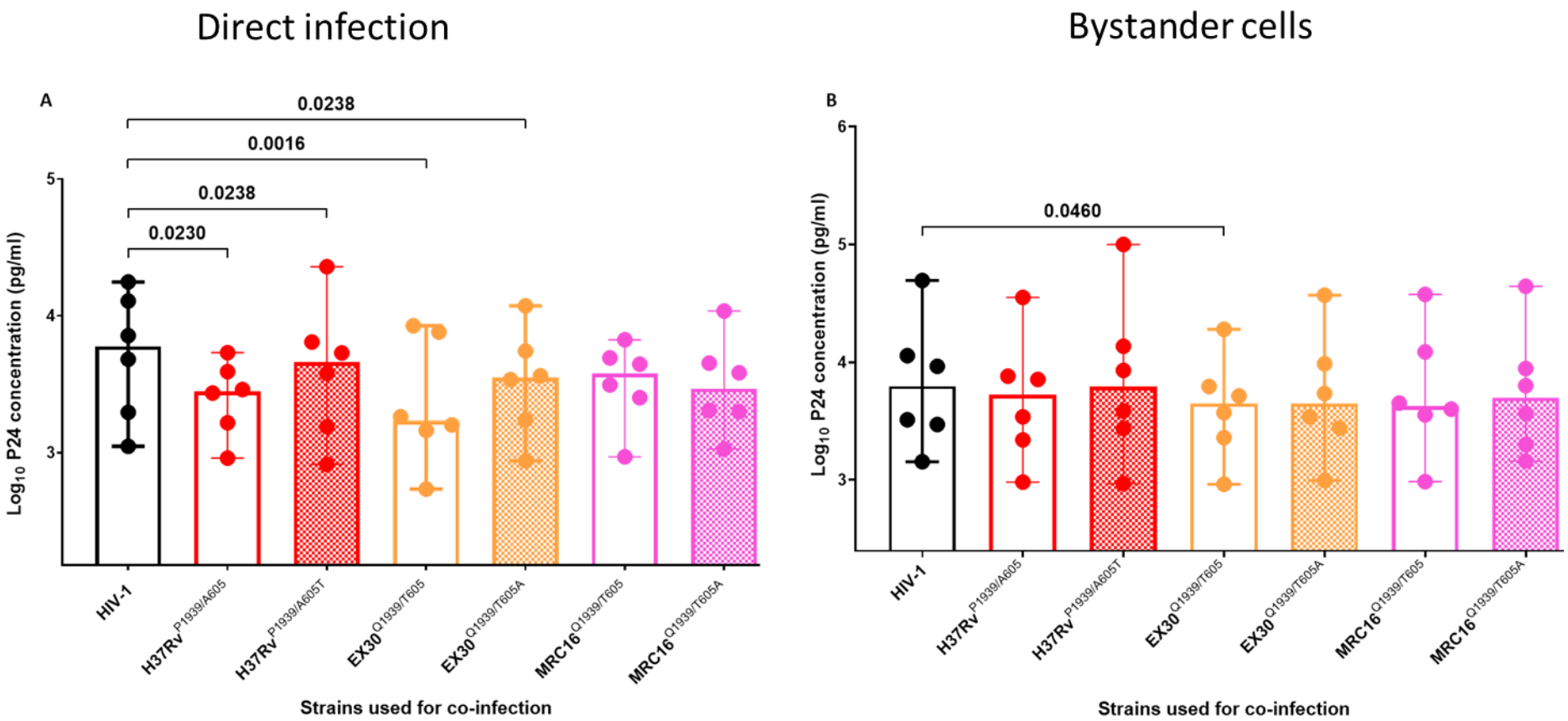

Figure 6.4. Secretion of p24 by MDM infected with HIV-1 or bystander cells exposed to HIV-1/*Mtb* co-infection environment 96-hours after *Mtb* infection. Monocytes from 6 donors were polarised to M2. The MDM were infected with HIV-1 and later co-infected with the different strain of *Mtb*. SN from co-infected MDM was harvested 24-hours post-co-infection with *Mtb* and used for p24 analysis by Luminex assay. Secretion of p24 was measured 96-hours post co-infection in **A)** direct co-infection (top chamber) and **B)** bystander cells (bottom chamber). Friedman's multiple comparison or Kruskalis-Wallis multiple comparison test with two-stage linear step-up procedure of Benjamin, Krieger and Yekutieli False discovery rate (FDR): with a cut off 0.1. Values are considered significant at FDR of ≤0.1 and p≤ 0.05.

6.2.5. Analysis of cytokine secretion in MDM directly infected with *Mtb* in the presence of HIV-1 co-infection

I used the same in SN in (section 6.3) above to measure the secretion of cytokines in MDM co-infected with the different strains of *Mtb* to understand how cytokine modulation may impact HIV-1 production during co-infection. Using a 13-plex Luminex assay I analysed cytokine/chemokine levels in SN harvested from the co-infected MDM (top chamber) and the bystander MDM (bottom chamber) 96-hours post-infection with *Mtb* and analysed sample clustering by PCA (Fig. 6.5). Here, I analysed whether there were differences in the cytokine production patterns between MDM which were directly co-infected with *Mtb* and bystander MDM. This data shows cytokine production patterns stratified by co-infection or bystander cells, fig 6.5A or infection fig 6.5B. The PCA plot in Fig 6.5A shows that even though there is a degree of overlap in clustering patterns, the global differences in clustering patterns are clear between direct co-infection and bystander conditions. Analysing Fig 6.5A&B simultaneously shows that the differences in clustering patterns arise from the addition of *Mtb*, which triggers the separation in clustering between co-infection and bystander conditions. Because these differences are less distinct in the HIV-1 only infection or uninfected conditions, Fig 6.5A&B, which confirms that co-infection and the bystander cell effect have different biological phenotypes. Taking this into account analyses of both co-infection and bystander cells were treated differently.

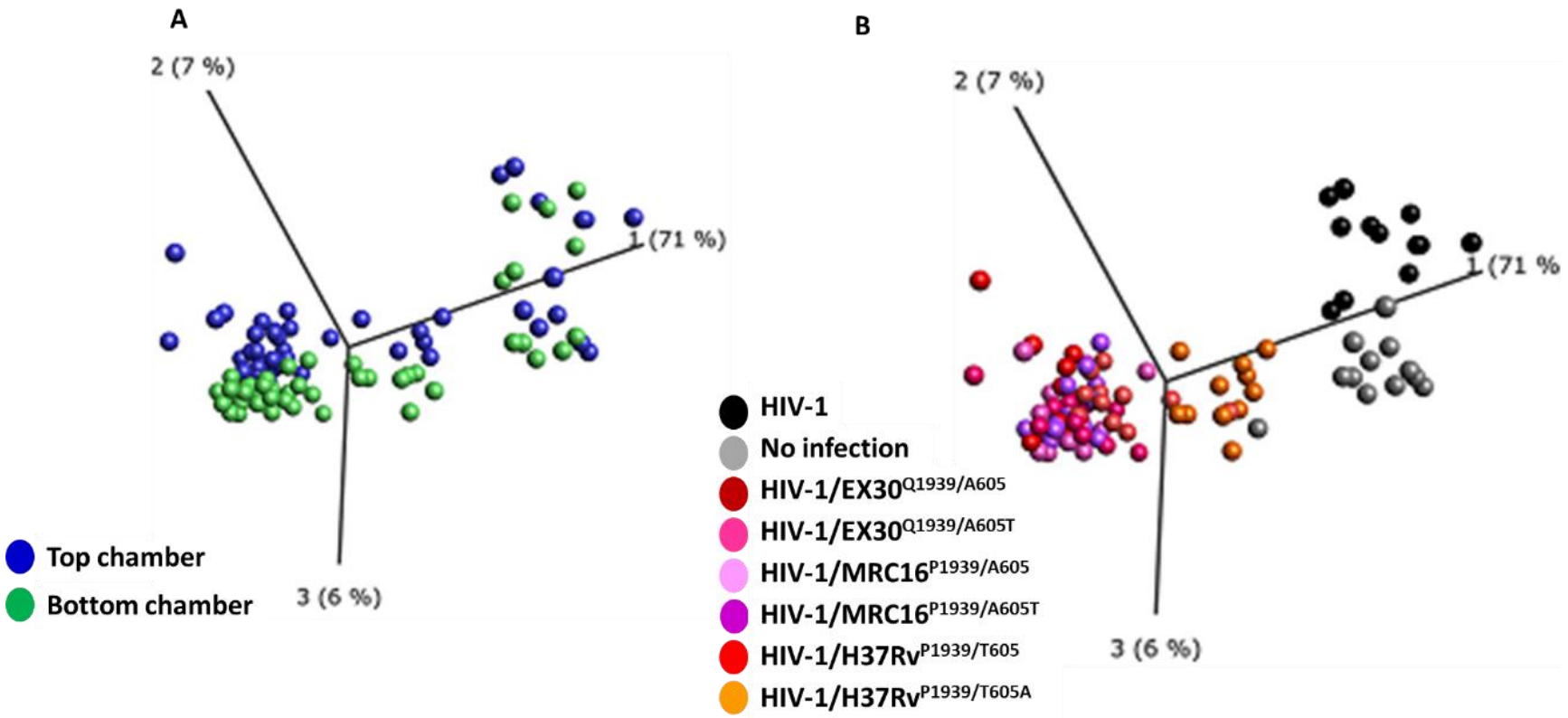

Figure 6.5. PCA analysis showing differences in cytokines production by MDM seeded in the top chamber and the bottom chamber of a trans-well plate. Monocytes from 6 donors were polarised to M2 MDM. MDM were seeded in top and bottom well of a trans-well plate. The trans-wells were kept separately (not allowed to mix) and infected with HIV-1 in either both top and bottom chamber (matching well), top well only or bottom well only or left uninfected with HIV-1 in both chambers for seven days. The top well was co-infected with *Mtb* strains for 4 h. Both wells were washed and replaced with fresh media. The top and bottom wells were connected to allow mixing between wells. The SN was harvested 4 days post mixing and used to measure cytokines with Luminex assay. SN was harvested from n=6 donors. Data was analysed by Qlucore omics explorer, each dot represents a single sample.

To compare the effect of the mutation on cytokine production by MDM, firstly, I compared cytokine secretion induced during co-infection with either $EX30^{Q1939/A605}$ or EX30Q1939/A605T, $H37Rv^{P1939/T605}$ or $H37Rv^{P1939/T605A}$ and $MRC16^{P1939/A605}$ or $MRC16^{P1939/A605T}$. Changing the SNP in position-605 in $H37Rv^{P1939/T605}$ to $H37Rv^{P1939/T605A}$ resulted in a strain that induced significantly lower secretion of IL-6, IL-8, TNF, CXCL10, IL-1β, CCL5, GM-CSF, CCL3, CCL4, IL-10, and IFN-γ when co-infecting 24-hours post-co-infection (Table 6.3). There were no significant differences in the production of cytokines in MDM that were co-infected with either $EX30^{Q1939/A605}$ or EX30Q1939/A605T (Table 6.3), this was also the same for MDM co-infected with $MRC16^{P1939/A605}$ or $MRC16^{P1939/A605T}$ (Table 6.3). Bystander MDM exposed to HIV-1/$H37Rv^{P1939/T605A}$, similarly had decreased cytokines (Table 6.3). The mutation in position-605 mutation in $EX30^{Q1939/A605}$ resulted in increased secretion of CCL2 (-1.52 Folds; $p = 0.0017$) compared to the original strain without the mutation (Table 6.3). I did not observe any difference in cytokine secretion at 96-hours between $MRC16^{P1939/A605}$ and $MRC16^{P1939/A605T}$. These data suggest that a mutation at position 605 in *pks2* in the $H37Rv^{P1939/T605}$ background attenuates inflammatory cytokine production during direct co-infection. This data is surprising given that $H37Rv^{P1939/T605A}$ has a similar genetic background to $MRC16^{P1939/A605}$ in the positions of interest.

Table 6.3. Comparison of cytokines secreted in HIV-1 infected bystander MDM exposed to cytokines from HIV-1/H37Rv$^{P1939/T605}$ or HIV-1/H37Rv$^{P1939/T605A}$ 96-hours after *Mtb* infection

Cytokines secreted from MDM co-infected with HIV-1/*Mtb*						
	H37Rv$^{P1939/T605}$ v H37Rv$^{P1939/T605A}$		EX30$^{Q1939/A605}$ v EX30$^{Q1939/A605T}$		MRC16$^{P1939/A605}$ v MRC16$^{P1939/A605T}$	
Analyte	Fold change	p-value	Fold change	p-value	Fold change	p-value
IL-6	22.19	0.0038	-	ns	-	ns
IL-8	12.88	0.0008	-	ns	-	ns
TNF	12.81	0.0006	-	ns	-	ns
CXCL10	6.2	0.0107	-	ns	-	ns
IL-1β	5.38	0.0136	-	ns	-	ns
CCL5	4.99	0.0087	-	ns	-	ns
GM-CSF	4.63	0.0272	-	ns	-	ns
CCL3	4.09	0.0135	-	ns	-	ns
CCL4	3.18	0.0057	-	ns	-	ns
IL-10	2.66	0.0100	-	ns	-	ns
IFN-γ	2.25	0.0170	-	ns	-	ns

Cytokines secreted from MDM exposed to environment of HIV-1/*Mtb* co-infection			
H37Rv$^{P1939/T605}$ v H37Rv$^{P1939/T605A}$	EX30$^{Q1939/A605}$ v EX30$^{Q1939/A605T}$	MRC16$^{P1939/A605}$ v MRC16$^{P1939/A605T}$

Analyte	Fold change	p-value	Fold change	p-value	Fold change	p-value
CCL2	-	ns	-1.52	0.0017	-	ns
IL-6	27.24	0.0003	-	ns	-	ns
IL-8	8.63	0.0001	-	ns	-	ns
TNF	9.19	0.0003	-	ns	-	ns
CXCL10	7.97	0.0139	-	ns	-	ns
IL-1β	9.05	<0.0001	-	ns	-	ns
CCL5	3.22	0.0008	-	ns	-	ns
GM-CSF	4.34	0.0017	-	ns	-	ns
CCL3	3.3	0.0037	-	ns	-	ns
CCL4	4.43	0.0003	-	ns	-	ns
IL-10	2.66	0.0037	-	ns	-	ns
IFN-γ	2	0.0012	-	ns	-	ns
CCL11	2.84	0.0052	-	ns	-	ns

Statistics: Friedmans multiple comparison test with Two-stage linear step-up procedure of Benjamini, Krieger and Yekutieli False discovery rate (FDR): with a cut off 0.1. Mean fold change between compared groups. P-value of comparison with FDR of <0.1. Fold change of non-significant (ns) value is not shown.

6.2.6. HIV-1 production correlated with cytokine secretion

Given I had observed a large variation in the amount of HIV-1 p24 in SN within each infection condition, to understand the role played by the inflammatory environment on HIV-1 production, I next analysed whether there were any correlations between cytokine secretion and HIV-1 production in co-infected and bystander MDM. The interpretation of the relationship between cytokine secretion and p24 secretion are contained in Table 6.4. To assess the association between cytokine secretion and p24 secretion in MDM, I performed a non-linear regression plot analysis with all 13 cytokines against p24 antigen harvested from the same infection condition and interpreted the degree of correlation according to the correlation coefficient thresholds in Table 6.4.

Table 6.4. Cytokines secreted by MDM co-infected with HIV-1/MRC16$^{P1939/A605}$ or HIV-1/MRC16$^{P1939/A605T}$

Correlation coefficient (R^2)	Interpretation
0.00 – 0.29	Negligible correlation
0.3 – 0.49	Weak correlation
0.5 – 0.69	Moderate correlation
0.7 – 1.00	Strong correlation

Firstly, I performed a Two-way Anova to determine the source of variation observed in HIV-1 production in MDM. To do this I plotted the HIV-1 production data in Graph-Pad prism using the column graph option, where each donor was stratified by column and each strain was stratified by rows and analysed the data using a Two-way Anova analysis on the data (Table 6.5). This analysis was done for both the co-infection data and the HIV-1 produced in bystander cells (Table 6.5). Surprisingly, there was no significant contribution by the different strains to the variation observed in the data (Table 6.5) in both co-infection and in the bystander cells. This means that for these infections, the differences between the strains were not the major contributor to differences observed in HIV-1 production. Conversely, HIV-1 production was significantly influenced by donor variation (Table 6.5.), in both co-infection and bystander cells. Much of the variation (58.25 %; p = <0.0001) in HIV-1 production in MDM co-infected with HIV-1 and different strains of *Mtb* resulted from donor variation. A similar phenotype was observed for bystander cells, where 71.02 % (p = <0.0001) of the variation resulted from

donor variation. Using this data, I performed correlation analysis stratifying the data by the different donors.

Table 6.5. Analysis of the source of variation in HIV-1 production using a Two-way Anova

Source of variation in HIV-1 production by co-infected MDM			
Source of Variation	**% Of total variation**	**P-value**	**Significant**
Strains	8.764	0.2846	No
Donors	58.25	<0.0001	Yes
Source of variation in HIV-1 production by bystander cells			
Strains	6.013	0.2921	No
Donors	71.02	<0.0001	Yes

I went on to analyse the correlation of p24 production with cytokine secretion between the different donors. There were only two cytokines that had a correlation with a R^2 of 0.3 or higher (regarded as a correlation of interest, Table 6.4) with HIV-1 p24 levels. There was a moderate positive association between the secretion of CCL2 and the production of p24 in co-infected MDM of different donors ($R^2 = 0.6739$, $p < 0.0001$) (Fig. 6.4A). There was also a negative association between the secretion of IL-1β secretion and the production of p24 in these MDM ($R^2 = -0.53$, $p = <0.0001$) (Fig. 6.6B). The correlation plots in Fig. 6.6, show the contribution of each donor shown in a specific colour, with each dot representing a different infection or uninfected condition. Whilst data points do vary for each donor, given the effect of different infection conditions, the dots from each donor are more tightly clustered together.

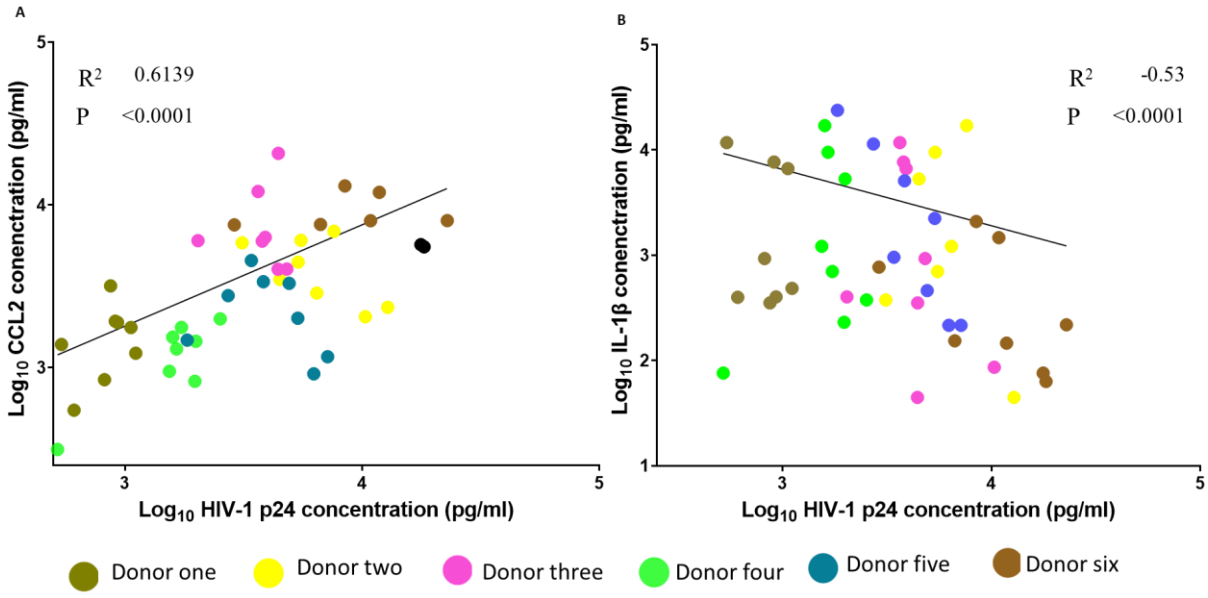

Figure 6.6. A correlation plot for the association of cytokine secretion and the production of HIV-1 in MDM. Monocytes from 6 donors were polarised to M2. The MDM were infected with HIV-1 and later co-infected with $MRC16^{P1939/A605}$ or $MRC16^{P1939/A605T}$. Co-infected MDM were harvested 96 hours post-co-infection and the secretion of cytokines and HIV-1 production were measured by Luminex assay. Correlation of HIV-1 production was compared with secretion of **A)** CCL2 and **B)** IL-1β.

I went on to do correlation analysis between cytokines in the bystander cell wells and the production of HIV-1 in those wells. I observed that there were two cytokines in the bystander wells that correlated with the production of cytokines (Fig. 6.7A-B). Similar to the co-infection, CCL2 had a moderate positive correlation with the production of HIV-1 (Fig. 6.7A) (R^2 = 0.6139, p = <0.0001) and this time IL-8 was negatively correlated with production HIV-1 in bystander cells (R^2 = 0.6649, p = 0.0011).

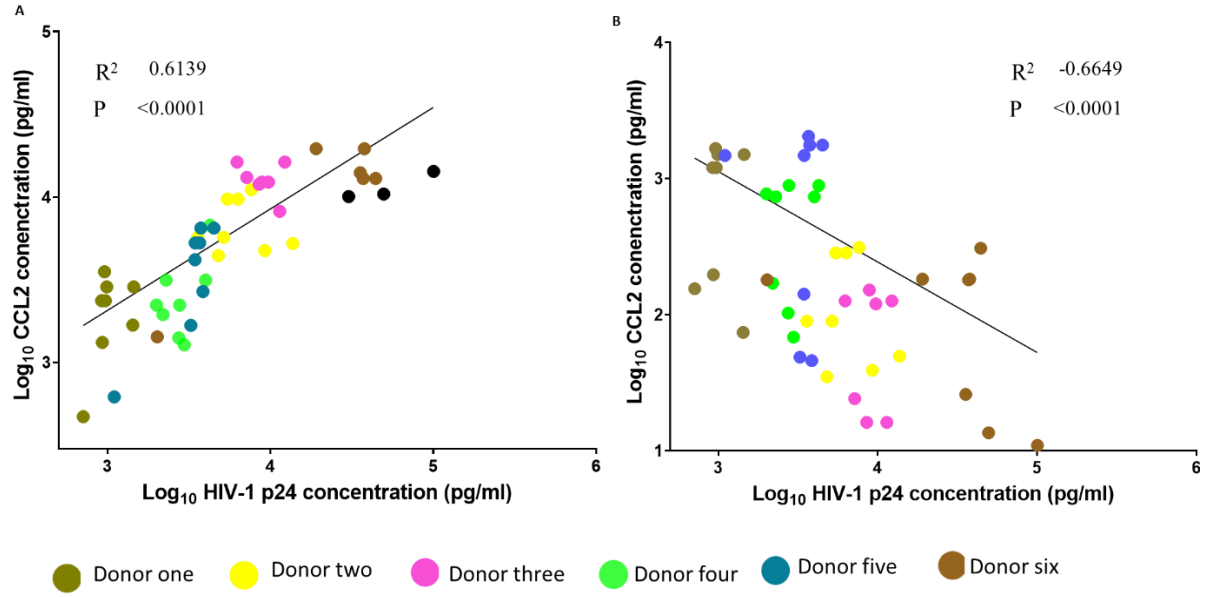

Figure 6.7. A correlation plot for the association of cytokine secretion and the production of HIV-1 in MDM.

Monocytes from 6 donors were polarised to M2. The MDM were infected with HIV-1 and later co-infected with MRC16$^{P1939/A605}$ or MRC16$^{P1939/A605T}$. Co-infected MDM were harvested 96 hours post-co-infection and the secretion of cytokines and HIV-1 production were measured by Luminex assay. Correlation of HIV-1 production was compared with secretion of **A)** CCL2 and **B)** IL-8.

6.3. Discussion

In this chapter I aimed to determine whether the SNP observed in EX30$^{Q1939/A605}$ and MRC16$^{P1939/A605}$ could be attributed to the differences in cytokine induction by the strains observed in Chapter 3. I also aimed to understand the contributions of the SNPs to the HIV-1 production phenotype observed in Chapter 4. I used the mutant strains generated in Chapter 5, along with their wild-type strains to infect MDM in a trans-well assay. One of the major limitations to this trans-well assay used for these experiments was the pore size which was not sufficient to exclude the movement of HIV-1 between the top and the bottom chamber. I determined that there was not sufficient HIV-1 migrating between chambers to influence observed HIV-1 replication phenotypes (Table 6.1; Fig. 6.2). This is because, although HIV-1 is observed in a chamber originally not infected (which shows migration), the amount of HIV-1 observed in the well was still significantly less than compared to HIV-1 observed in the well when directly infected (Table 6.1; Fig. 6.2). Moreover, the control with HIV-1 infection on both the top and the bottom chamber did not have significantly increased HIV-1 production in the top chamber compared to the well infected in the top chamber only or significantly higher HIV-1 in the bottom chamber compared to well infected in the bottom chamber only (Table 6.1; Fig. 6.2). This means that despite this control having HIV-1 infection in both top and bottom chamber there was not enough movement of HIV-1 to result in one chamber having significantly higher HIV-1.

Here, I show that a single nucleotide change was not sufficient to result in difference in cytokine induction by the clinical strains EX30$^{Q1939/A605}$ to EX30$^{Q1939/A605T}$ or MRC16$^{P1939/A605}$ or MRC16$^{P1939/A605T}$, however, there were striking differential cytokine capacities between H37Rv$^{P1939/T605}$ and H37Rv$^{P1939/T605A}$. This data indicates that the mutation of T605A back to A605T in the clinical strains does not affect cytokine secretion induction but, changing H37Rv$^{P1939/T605}$ to resemble the clinical strains in that position resulted in an attenuated H37Rv$^{P1939/T605A}$ strain relative H37Rv$^{P1939/T605}$. There were more cytokines that were significantly induced by H37Rv$^{P1939/T605}$ co-infection relative to HIV-1 only infection compared to cytokines significantly induced by HIV-1/H37Rv$^{P1939/T605A}$ co-infection. The amount of p24 production in MDM that are co-infected is decreased relative to MDM that are infected with HIV-1 only (Fig. 6.4A) at 96-hours post-co-infection. The decreased p24

observed was significant in MDM that were co-infected with all the strains, apart from MRC16$^{P1939/A605}$ and MRC16$^{P1939/A605T}$ (Fig. 6.3 – 6.4). In the bystander cells, only environment induced by EX30$^{Q1939/A605}$ significantly (Fig. 6.4B).

The data in (Fig. 6.3 – Fig. 6.4) affirms that there is a degree of decreased HIV-1 production in MDM that are infected with HIV-1 and later co-infected with *Mtb*. Furthermore, there is evidence that the SNP in position-605 may play a role in HIV-1 modification. However, the effects of the modification are likely enhanced at a later time-point (96-hours and beyond post-co-infection) and in concert with the SNP in position-1939. This is because although both MRC16$^{P1939/A605T}$ and H37Rv$^{P1939/T605}$ modified HIV-1 production 24-hours post-co-infection, this modification did not reach significance (Fig. 6.3A). This data leaves the question about how far the modification would have proceeded if SNP P1939 was modified to Q1939 in these strains. In similar conditions, EX30$^{Q1939/A605T}$, which differs by Q1939 from these strains did not affect HIV-1 production in direct co-infection (Fig. 6.3A). But the environment induced by HIV-1/EX30$^{Q1939/A605T}$ co-infection, showed a trend to decreased HIV-1 production 24-hours post-co-infection (Fig. 6.3B) and this is the only condition with that phenotype. These data suggest a role for T605 to decreased HIV-1 regulation, a phenotype which is observed in with the P1939 background in direct co-infection and in bystander cells in the background of Q1939.

In previous experiments (Chapter 4; Fig. 4.13), I reported that co-infection with the different strains did not regulate HIV-1 production 96-hours post-co-infection. In the trans-well assay, I observed a significant decrease in HIV-1 production in the presence of several strains of *Mtb* (Fig. 6.4A) 96-hours post-co-infection. This data makes it hard to discern the critical role players in the observed phenotype. This is because HIV-1 production was decreased in MDM whether co-infected with a strain with P1939/T605, P1939/A605, Q1939/T605 or Q1939/A605 background for EX30 and H37Rv based strains (Fig. 6.4A). But at the same time MRC16$^{P1939/A605}$ and MRC16$^{P1939/A605T}$ did not significantly decrease HIV-1 production but only showed a trend to decreased HIV-1 at 96-hours post-co-infection (Fig. 6.4A). A possible reason for this phenotype might be that direct co-infection HIV-1 regulation of HIV-1 will be contingent on both the cytokine milieu and the *Mtb* cell wall components. This increases the need for a deeper analysis of the lipids of the strain used in these experiments to check whether there could have contributed to the observed phenotype.

Analysis of HIV-1 production by bystander cells revealed that MDM exposed to HIV-1/EX30$^{Q1939/A605}$ environment had decreased HIV-1 production 96-hours post-exposure, compared to MDM infected with HIV-1 only (Fig. 6.4B). This phenotype is persistent in this strain because in MDM incubated with EX30$^{Q1939/A605}$-induced SN resulted in decreased HIV-1 production (Chapter 4; Fig. 4.8). The fact that this phenotype is abrogated in MDM exposed to HIV-1/EX30$^{Q1939/A605T}$ environment (Fig. 6.4B), suggests that these two SNP may work in concert to modify HIV-1 production 96-hours post-co-infection. It is interesting that EX30$^{Q1939/A605}$, the strain with the SNP that was predicted to be under HIV-1 positive directional selection, has a persistent phenotype of low HIV-1 production, both during co-infection and in bystander. The strains that did not have the Q1939 mutations did not modify HIV-1 production in bystander cells, both in the co-incubation experiment (Chapter 4; Fig. 4.8) and the trans-well assay Fig. 6.3B and Fig. 6.4B.

Productive infection cannot be used a proxy for HIV-1 replication because p24 specifically looks at assembled and budded viruses. During HIV-1 replication large parts of transcripts may be defective at the sequence level and therefore viral protein and infectious particles would not be produced [14]. Early 24-hours and late 96-hour SN from EX30$^{Q1939/A605}$ SN increased HIV-1 LTR activity in TZM-bl cells (which can used to infer HIV-1 replication) compared to SN from uninfected MDM or media only (Chapter 4; Fig. 4.6). Taken together this data indicates that HIV-1 replication is not hindered by EX30$^{Q1939/A605}$ SN and possibly co-infection and that thus the decrease in released HIV-1 p24 during co-infection with EX30$^{Q1939/A605}$ suggests EX30$^{Q1939/A605}$ may also induced factors that delay the packaging and release of HIV-1 particles into the SN.

There was a striking difference in cytokine secretion between MDM co-infected with H37Rv$^{P1939/T605}$ or H37Rv$^{P1939/T605A}$ (Table 6.2). Exposure to H37Rv$^{P1939/T605}$ both in direct co-infection and in the bystander, cells induced an increased inflammatory phenotype compared to exposure to H37Rv$^{P1939/T605A}$ (Table 6.2). In fact, the SNP change in H37Rv$^{P1939/T605A}$ appears to have attenuated the strain's ability to induce a robust cytokine response like H37Rv$^{P1939/T605}$. The cytokine induction phenotype of H37Rv$^{P1939/T605A}$ is closer to HIV-1 only infected MDM in both co-infection and bystander cells.

Despite marked differences in cytokine induction between H37Rv$^{P1939/T605}$ and H37Rv$^{P1939/T605A}$ co-infection, I found no significant difference in cytokines secretion 96-hours

by mutating the clinical strains EX30$^{Q1939/A605}$ (Table 6.3) or MRC16$^{P1939/A605}$ (Table 6.4). When comparing cytokine induction between EX30$^{Q1939/A605}$ or EX30$^{Q1939/A605T}$, there was no significant difference between the strains (Table 6.3). However, there was on average higher levels of cytokines induced by EX30$^{Q1939/A605T}$ compared to HIV-1 only infected MDM than cytokine levels induced by EX30$^{Q1939/A605A}$ compared to HIV-1 only. Although EX30$^{Q1939/A605T}$ did not significantly change cytokine induction compared EX30$^{Q1939/A605}$, the dynamics of cytokine regulation by EX30$^{Q1939/A605T}$ were different compared to the EX30$^{Q1939/A605}$. For example, the observed increase in CCL5 secretion by MDM co-infected EX30Q1939/A605T compared to HIV-1 only infected MDM was 55.76-fold while the increased observed from MDM co-infected with EX30$^{Q1939/A605}$ was 28.94-fold, an almost two-fold difference in CCL5 secretion compared to HIV-1 only by the two strains. This data supports the hypothesis that mutation of the secondary *pks2* SNP in EX30$^{Q1939/A605}$ (T605A; 1815) will have a subtle effect on cytokine induction by this strain compared to the WT SNP and that changing the primary SNP (P1939Q; 5817) might have shown more differences between the strains. There were comparable cytokine secretion phenotypes between MRC16$^{P1939/A605}$ and MRC16$^{P1939/A605T}$ co-infected MDM (Table 6.5). For MRC16$^{P1939/A605}$ and MRC16$^{P1939/A605T}$ not only was there a comparable cytokine induction phenotype between conditions co-infected or exposed to both strains (Table 6.5), the degree to which the strains increased cytokine secretion beyond HIV-1 only infection was also comparable.

In the panel of cytokines that were measured the production of CCL2 was the most noticeable. CCL2 is the only cytokine that was consistently not different in production levels between HIV-1 only infected MDM and MDM co-infected with *Mtb* or bystander MDM exposed to *Mtb* induced cytokines. So, it was expected that the cytokine will be further elevated in the presence of *Mtb* co-infection. CCL2 was increased in MDM infected H37Rv (chapter 3; Table 3.2) by 2.38-folds, EX30$^{Q1939/A605}$ by 3.35-folds and MRC16$^{P1939/A605}$ by 9.28-folds (chapter 3; Table 3.3) in the absence of HIV-1 co-infection. However, only MRC16$^{P1939/A605}$ (chapter 4; Table 4.3) increased CCL2 by 2.87-folds in the presence of HIV-1 co-infection. This data shows a trend of decreased CCL2 secretion by MDM co-infected with HIV-1 and *Mtb* strains. This data was surprising given that CCL2 is increased by HIV-1 infection [15], and also in *Mtb* infection alone [16].

To understand whether cytokine secretion could be linked to HIV-1 production, I created correlation plots of HIV-1 production against the cytokines measured here. But, firstly, since

both the differences between strain and the differences between donors is a potential source of variation in HIV-1 production, I needed to understand the greatest source of variation. The Two-way Anova analysis showed that differences between strains was responsible for a small percentage of the variation observed in HIV-1 production, whilst differences between donors accounted for most of the variation observed in HIV-1 production. With this data in mind, the analysis of correlation was stratified by donors and the differences between strains were ignored.

CCL2 was observed to be consistently positively correlating with HIV-1 production in both co-infection and bystander cells. CCL2 is a β-chemokine that is induced in HIV-1 infection and in patients plasma levels of CCL2 correlate with plasma viremia [17]. In *Mtb* infection the chemokine is associated with protection and granuloma formation [18, 19], however, there is also association of CCL2 with severe systemic inflammation and worsened TB outcome [20]. The data showed that donors with increased productive HIV-1 infection are also donors with elevated levels of CCL2 secretion in their SN. Studies by Fantuzzi *et al.,* (2003) [21] and Sabbatucci *et al.,* (2015) [15], have demonstrated that neutralisation of CCL2 in MDM drastically reduced the amount of p24 detected in the SN. Furthermore, Sabbatucci *et al.,* (2015) [15] showed that the CCL2 did not affect viral entry into MDM but associated with viral productive infection in a post-entry mechanism. The experiments by Fantuzzi *et al.,* (2003) [21], also showed that blocking CCL2 drastically reduced the release of p24 antigen from the cells, but there was a significant accumulation of cell-associated p24 antigen, which was backed up by another study in 2019 [22]. These experiments clearly show the association of CCL2 and p24 secretion. My experiments agree with literature in that increased CCL2 secretion was associated with increased viral load as measured by secreted p24 antigen. But importantly that individual door variation in baseline CCL2 levels positively correlates with the *in vitro* level of HIV-1 infection.

HIV-1 p24 was also negatively associated with IL-1β secretion, such that donors with high secretion of IL-1β had low HIV-1 p24 levels in the SN. IL-1β is a well-known pro-inflammatory cytokine which is significant for host defence responses against infection and injury [23]. However, the release of IL-1β particularly in macrophages is associated with a form of cell death named pyroptosis [23]. Pyroptosis is a caspase-1 and caspase-4/5 dependent inflammation inducing cell death [24]. Pyroptosis is mechanistically and phenotypically distinct from apoptosis, by inducing a pro-inflammatory phenotype, which is actively inhibited

during apoptosis [24]. Pyroptosis occurs through the assembly of NOD-, LRR- and pyrin domain- containing protein 3 (NLRP3) inflammasome [25]. The NLRP3 inflammasome complex mediates caspase-1 activation which proteolytically activates IL-1β and the pyroptosis pore-inducing gasdermin-D (GSDMD) [25]. Experiments showed that in a RAW-asc line which the GSDMD gene is knocked-out the IL-1β production is almost eliminated and the cells are resistant to pyroptosis [26]. Furthermore, Semino *et al.,* (2018) [27], showed that cells undergoing apoptosis have been associated with low release of IL-1β, but cells undergoing pyroptosis hyper-secreted IL-1β [27]. Thus, decreased productive infection in the donors with high IL-1β secretion may be a result of increased cell death in these donors, limiting the source of cells for ongoing HIV-1 replication. Further, given that this correlation was only observed in the co-infected cells and not the bystander cells, thus giving credence to the fact that HIV-1 production was decreased in donors with high IL-1β potentially due to increased cell death of directly co-infected cells.

I have also found that IL-8 secretion negatively associates with p24 secretion in bystander MDM exposed to HIV-1/*Mtb* co-infection SN (Fig. 6.7B). There are contrasting role for IL-8 on HIV-1 replication and production in literature. IL-8 is a chemoattractant cytokine that is produced by amongst other immune cells macrophages [28]. IL-8 is a chemotactic peptide produced by macrophages that may be involved in the recruitment of inflammatory cells [29]. In the context of HIV-1 studies almost collectively associate IL-8 with increased HIV-1. A 2001 study found that the addition of exogenous IL-8 in HIV-1 infected MDM increased HIV-1 replication [30]. Another study found that production and secretion of IL-8 is increased in presence of HIV-1 infection [31] and IL-8 correspondingly decreased following ART viral suppression in children [32]. There are several studies that have related IL-8 with decreasing HIV-1 replication. A study of HIV-1 infection of using MAGIC5 cells (a HeLa derived cell line which stably produced CCR5) showed that IL-8 inhibited the infection of these cells via downregulation CCR5 [33]. Another study in MDM showed that addition of IL-8 to HIV-1 infected MDM resulted in significantly less HIV-1 replication compared to media only treated MDM [34]. IL-8 also inhibited the integration of HIV-1 DNA in peripheral blood lymphocytes in a dose dependent manner [35]. These data suggest that IL-8 may have an inhibitory effect in the early stages of HIV-1 infection, where it results in decreased CCR5 or decreased integration of HIV-1 into host genome. But the role of IL-8 may change to enhancement of HIV-1 replication post-integration. That IL-8 only negatively correlated with p24 in bystander

cells suggests that this cytokine may have been responsible for decreased HIV-1 production in donors with high IL-8 secretion.

While the trans-well assay was useful at measuring both co-infection and the bystander cell in the same system, there were also limitations to the assay. Ideally, it would have been better that migration HIV-1 between the chambers is prohibited, to allow production of HIV-1 exclusively in each well. This would allow only the contribution of cytokines to be considered for the phenotype of HIV-1 production.

In these experiments the use of HIV-1 RNA as a measure of replication in combination with p24 would have revealed greater detail. The use of p24 secretion to measure HIV-1 partially reveals the true rate of replication, because this measurement relies on mature virions that are packaged and then secreted. The ideal measurements are the RNA which would reveal the raw rate of HIV-1 replication without discriminating between defective and non-defective sequences. Moreover, measuring the amount of integrated HIV-1 DNA between the different conditions would reveal whether the rate of replication relative to the amount of integrated DNA across the different conditions.

6.4. Conclusion

Changes in a single base position in *pks2* in two clinical strains resulted in subtle differences in *Mtb*-induced cytokines and HIV-1 viral production during co-infection of human MDM. Modification of the same base in H37Rv$^{P1939/T605}$, by comparison, had dramatic attenuation of the inflammatory profile induced during HIV-1 co-infection and attenuated the reduction in HIV-1 production during co-infection. The modest changes in cytokine and HIV-1 production observed in the modified clinical strains were overshadowed by the differences in HIV-1 production because of donor variability in CCL2, IL-1β and IL-8 production. As such the level of HIV-1 production during co-infection is both modified by the infecting *Mtb* but the level of effect is primarily governed by the inflammatory background of the individual from which MDM were derived.

6.5. References

1. Falvo, J.V., et al., *Arc of a vicious circle: pathways activated by Mycobacterium tuberculosis that target the HIV-1 long terminal repeat.* Am J Respir Cell Mol Biol, 2011. **45**(6): p. 1116-24.

2. Kedzierska, K. and S.M. Crowe, *Cytokines and HIV-1: interactions and clinical implications.* Antivir Chem Chemother, 2001. **12**(3): p. 133-50.
3. Chacon-Salinas, R., et al., *Differential pattern of cytokine expression by macrophages infected in vitro with different Mycobacterium tuberculosis genotypes.* Clin Exp Immunol, 2005. **140**(3): p. 443-9.
4. Reed, M.B., et al., *A glycolipid of hypervirulent tuberculosis strains that inhibits the innate immune response.* Nature, 2004. **431**(7004): p. 84-7.
5. Sandberg, J.K., et al., *HIV-1 Replication Is Differentially Regulated by Distinct Clinical Strains of Mycobacterium tuberculosis.* PLoS ONE, 2009. **4**(7).
6. Martin, M.P. and M. Carrington, *Immunogenetics of HIV disease.* Immunol Rev, 2013. **254**(1): p. 245-64.
7. Trachtenberg, E., et al., *Advantage of rare HLA supertype in HIV disease progression.* Nat Med, 2003. **9**(7): p. 928-35.
8. Martin, M.P., et al., *Epistatic interaction between KIR3DS1 and HLA-B delays the progression to AIDS.* Nat Genet, 2002. **31**(4): p. 429-34.
9. Sakuragi, J., *Morphogenesis of the Infectious HIV-1 Virion.* Front Microbiol, 2011. **2**: p. 242.
10. Ufimtseva, E., et al., *Analysis of Mycobacterium tuberculosis Uptake by Alveolar Mcrophages after Ex vivo Expansion Indicates Processing Host Cells with Pathogen Actually from Lung Tissue of Patients with Pulmonary Tuberculosis.* Int J Mycobacteriol, 2020. **9**(2): p. 176-184.
11. Cassol, E., et al., *M1 and M2a polarization of human monocyte-derived macrophages inhibits HIV-1 replication by distinct mechanisms.* J Immunol, 2009. **182**(10): p. 6237-46.
12. Robinson, T.O., et al., *CD4 regulatory T cells augment HIV-1 expression of polarized M1 and M2 monocyte derived macrophages.* Virology, 2017. **504**: p. 79-87.
13. Koch, A.S., et al., *The Influence of HIV on the Evolution of Mycobacterium tuberculosis.* Mol Biol Evol, 2017. **34**(7): p. 1654-1668.
14. Pasternak, A.O. and B. Berkhout, *What do we measure when we measure cell-associated HIV RNA.* Retrovirology, 2018. **15**(1): p. 13.
15. Sabbatucci, M., et al., *Endogenous CCL2 neutralization restricts HIV-1 replication in primary human macrophages by inhibiting viral DNA accumulation.* Retrovirology, 2015. **12**: p. 4.

16. Ansari, A.W., D. Meyer-Olson, and R.E. Schmidt, *Selective expansion of pro-inflammatory chemokine CCL2-loaded CD14+CD16+ monocytes subset in HIV-infected therapy naive individuals.* J Clin Immunol, 2013. **33**(1): p. 302-6.
17. Weiss, L., et al., *Plasma levels of monocyte chemoattractant protein-1 but not those of macrophage inhibitory protein-1alpha and RANTES correlate with virus load in human immunodeficiency virus infection.* J Infect Dis, 1997. **176**(6): p. 1621-4.
18. Kipnis, A., et al., *Role of chemokine ligand 2 in the protective response to early murine pulmonary tuberculosis.* Immunology, 2003. **109**(4): p. 547-51.
19. Saunders, B.M. and W.J. Britton, *Life and death in the granuloma: immunopathology of tuberculosis.* Immunol Cell Biol, 2007. **85**(2): p. 103-11.
20. Hasan, Z., et al., *CCL2 responses to Mycobacterium tuberculosis are associated with disease severity in tuberculosis.* PLoS One, 2009. **4**(12): p. e8459.
21. Fantuzzi, L., et al., *Endogenous CCL2 (monocyte chemotactic protein-1) modulates human immunodeficiency virus type-1 replication and affects cytoskeleton organization in human monocyte-derived macrophages.* Blood, 2003. **102**(7): p. 2334-7.
22. Ajasin, D.O., et al., *CCL2 mobilizes ALIX to facilitate Gag-p6 mediated HIV-1 virion release.* Elife, 2019. **8**.
23. Lopez-Castejon, G. and D. Brough, *Understanding the mechanism of IL-1beta secretion.* Cytokine Growth Factor Rev, 2011. **22**(4): p. 189-95.
24. Fink, S.L. and B.T. Cookson, *Apoptosis, pyroptosis, and necrosis: mechanistic description of dead and dying eukaryotic cells.* Infect Immun, 2005. **73**(4): p. 1907-16.
25. Swanson, K.V., M. Deng, and J.P. Ting, *The NLRP3 inflammasome: molecular activation and regulation to therapeutics.* Nat Rev Immunol, 2019. **19**(8): p. 477-489.
26. He, W.T., et al., *Gasdermin D is an executor of pyroptosis and required for interleukin-1beta secretion.* Cell Res, 2015. **25**(12): p. 1285-98.
27. Semino, C., et al., *Progressive waves of IL-1beta release by primary human monocytes via sequential activation of vesicular and gasdermin D-mediated secretory pathways.* Cell Death Dis, 2018. **9**(11): p. 1088.
28. Koch, A.E., et al., *Interleukin-8 as a macrophage-derived mediator of angiogenesis.* Science, 1992. **258**(5089): p. 1798-801.
29. Apostolopoulos, J., P. Davenport, and P.G. Tipping, *Interleukin-8 production by macrophages from atheromatous plaques.* Arterioscler Thromb Vasc Biol, 1996. **16**(8): p. 1007-12.

30. Lane, B.R., et al., *Interleukin-8 stimulates human immunodeficiency virus type 1 replication and is a potential new target for antiretroviral therapy.* J Virol, 2001. **75**(17): p. 8195-202.
31. Nookala, A.R. and A. Kumar, *Molecular mechanisms involved in HIV-1 Tat-mediated induction of IL-6 and IL-8 in astrocytes.* J Neuroinflammation, 2014. **11**: p. 214.
32. Pananghat, A.N., et al., *IL-8 Alterations in HIV-1 Infected Children With Disease Progression.* Medicine (Baltimore), 2016. **95**(21): p. e3734.
33. Richardson, R.M., et al., *Interleukin-8-mediated heterologous receptor internalization provides resistance to HIV-1 infectivity. Role of signal strength and receptor desensitization.* J Biol Chem, 2003. **278**(18): p. 15867-73.
34. Csoma, E., et al., *Human herpesvirus 6A decreases the susceptibility of macrophages to R5 variants of human immunodeficiency virus 1: possible role of RANTES and IL-8.* Virus Res, 2006. **121**(2): p. 161-8.
35. Rollenhagen, C. and S.N. Asin, *IL-8 decreases HIV-1 transcription in peripheral blood lymphocytes and ectocervical tissue explants.* J Acquir Immune Defic Syndr, 2010. **54**(5): p. 463-9.

6.6. Supplementary material

The following supplementary data provides raw cytokine secretion level. The cytokines data was analysed from MDM seeded in the top and bottom chamber of trans-well assay (Fig. 6.1). MDM were infected with HIV-1 and co-infected with a panel of original clinical strains of *Mtb* and their matched single base mutants, alongside a lineage matched laboratory wild-type and mutant strain. The data also contains cytokines secretion data from MDM exposed to environments from the co-infection condition. The cytokines were measured from SN harvested at 96-hours post infection and analysed by Luminex assay. Luminex data was analysed using GraphPad prism.

Supplementary material 6.1. Cytokine secretion in MDM infected with HIV-1 or exposed to HIV-1 infected cytokine milieu

Median level of cytokine secretion with Interquartile range (pg/ml) in top chamber of trans-well plate				
Analyte	Both chambers	Top chamber	Bottom chamber	No infection
CCL2	1444 (211.8 – 4220)	928.5 (313.1 – 4335)	1784 (822.4 – 5699)	1483 (313.1 – 5522)
CCL4	205.2 (61.55 - 447.9)	280.2 (61.55 - 378.8)	195 (156.3 - 629.7)	181.4 (61.55 - 409.9)
CXCL10	5.57 (0.41 - 20.47)	2.775 (0.41 - 117.7)	7.76 (3.85 - 36.04)	9.055 (0.41 - 129.6)
GM-CSF	127.5 (85.03 - 179.5)	165.4 (26.62 - 240.6)	120.7 (71.3 - 208.6)	106.6 (75.25 - 160.9)
IL-8	41.86 (13.55 - 155.2)	41.17 (1.05 - 140.5)	42.53 (10.96 - 102.7)	30.9 (10.96 - 88.3)
IL-10	2.82 (1.01 - 4.21)	3.12 (1.01 - 14.45)	2.18 (1.01 - 6.93)	1.84 (1.01 - 15.04)
IL-1β	116.6 (44.58 - 300.8)	98.9 (44.58 - 359.6)	145.8 (44.58 - 484.2)	81.01 (44.58 - 397.9)
IL-6	0.7 (0.04 - 0.91)	0.9 (0.04 - 2.49)	0.475 (0.04 - 2.1)	0.475 (0.04 - 10.51)
TNF	3.145 (2.18 - 4.9)	5.57 (0.44 - 7.28)	4.235 (2.18 - 6.76)	3.83 (2.18 - 5.44)

Median cytokine secretion levels with interquartile range. values for n = 6 donors

Supplementary material 6.2. Cytokine secretion in MDM infected with HIV-1 or exposed to HIV-1 infected cytokine milieu

	Median level of cytokine secretion with Interquartile range (pg/ml) in the			
Analyte	Both chambers	Top chamber	Bottom chamber	No infection
CCL2	2919 (468.4 – 10046)	1695 (61.65 – 7051)	3207 (1275 – 10405)	2153 (457.8 – 8686)
CCL4	385.1 (268.3 - 837.5)	420.2 (115.8 - 628.4)	338.4 (203.5 - 988.9)	281.1 (115.8 - 614.1)
CCL3	5.065 (3.17 - 49.51)	6.65 (4.43 - 17.1)	4.75 (0.02 - 11.4)	4.43 (1.91 - 13.3)
CCL5	3.69 (2.91 - 959.8)	3.495 (2.91 - 6.76)	3.3 (2.13 - 4.46)	2.91 (2.91 - 3.69)
CXCL10	9.105 (0.16 - 28.79)	5.37 (0.16 - 187.6)	11.14 (5.65 - 81.45)	11.87 (0.16 - 136.6)
GM-CSF	258.9 (153.5 – 6899)	336.1 (235.5 - 385.3)	214.2 (197.9 - 716.6)	178.7 (138.2 - 268.1)
IL-8	18.78 (9.2 - 63.87)	16.12 (6.57 - 52.11)	16.05 (8.84 - 35.99)	10.61 (6.57 - 32.05)
IL-10	1.38 (0.91 - 3.95)	2.685 (0.42 - 9.76)	1.94 (0.67 - 6.34)	1.265 (0.91 - 7.5)
IL-1β	194.5 (52.2 – 840)	120.8 (36.32 - 698.8)	193.5 (36.32 - 840.4)	50.07 (36.32 - 573.2)
IL-6	3.125 (0.29 – 1640)	2.09 (0.29 - 155.2)	3.14 (0.29 – 140)	1.08 (0.29 - 16.67)
TNF	24.07 (14.85 - 51.76)	16.59 (10.37 - 21.14)	16.3 (10.37 - 22.54)	12.03 (7.57 - 13.97)

Median cytokine secretion levels with interquartile range. values for n = 6 donors

Supplementary material 6.3. Cytokine secretion in MDM co-infected with HIV-1/*Mtb* clinical strains 96-hours post-infection with *Mtb*

	Median level of cytokine secretion with Interquartile range (pg/ml) in top chamber of trans-well					
Analyte	H37Rv$^{P1939/T605A}$ co-infection	H37Rv$^{P1939/T605A}$ co-infection	EX30$^{Q1939/A605}$ co-infection	EX30$^{Q1939/A605T}$ co-infection	MRC16$^{P1939/A605}$ co-infection	MRC16$^{P1939/A605T}$ co-infection
CCL11	32.87 (24.11 - 40.79)	13.74 (7.09 - 13.74)	40.79 (32.87 - 48.13)	28.49 (24.11 - 40.79)	40.79 (32.87 - 48.13)	28.49 (24.11 - 40.79)
CCL2	7621 (1942 – 13998)	3953 (1317 – 14270)	6085 (2358 – 19580)	7482 (2217 – 12926)	6085 (2358 – 19580)	7482 (2217 – 12926)
CCL3	67.96 (57.14 - 86.42)	18.69 (10.76 - 37.43)	74.33 (59.05 - 97.25)	61.6 (48.87 - 85.79)	74.33 (59.05 - 97.25)	61.6 (48.87 - 85.79)
CCL4	5323 (2546 – 13231)	1154 (676.2 – 2965)	4055 (1119 – 13145)	3924 (2366 – 13382)	4055 (1119 – 13145)	3924 (2366 – 13382)
CCL5	38.01 (12.82 - 53.36)	12.44 (6.76 - 15.07)	41.67 (18.06 – 1572)	34.89 (15.44 - 49.72)	41.67 (18.06 – 1572)	34.89 (15.44 - 49.72)
CXCL10	746.1 (368.1 – 2133)	69.6 (26.43 – 339)	720.7 (8.68 – 1495)	689.1 (390.4 – 1318)	720.7 (8.68 – 1495)	689.1 (390.4 – 1318)
IL-8	542.1 (151.6 – 2043)	95.56 (24.16 - 196.8)	535.3 (89.5 – 1479)	509.3 (126.1 – 1762)	535.3 (89.5 – 1479)	509.3 (126.1 – 1762)
IFN-γ	105.8 (92.82 - 135.1)	56.43 (36.71 – 75)	110.1 (105.8 – 131)	110.1 (83.99 - 126.9)	110.1 (105.8 – 131)	110.1 (83.99 - 126.9)
IL-10	29.73 (22.34 - 43.49)	5.845 (3.74 - 18.72)	33.83 (3.33 - 39.98)	29.64 (22.85 - 38.69)	33.83 (3.33 - 39.98)	29.64 (22.85 - 38.69)
IL-1β	3661 (461.1 – 23753)	493.7 (145.9 – 2091)	3789 (352.2 – 11748)	3258 (375.8 – 17012)	3789 (352.2 – 11748)	3258 (375.8 – 17012)

IL-6	972.3 (289 – 1616)	35.87 (23.05 - 51.09)	1117 (347.2 – 3248)	843.6 (280.8 – 1610)	1117 (347.2 – 3248)	843.6 (280.8 – 1610)
TNF	556.4 (255.1 - 967.1)	52.82 (34.2 - 99.45)	485.4 (268.1 - 705.4)	429.3 (236.3 - 898.3)	485.4 (268.1 - 705.4)	429.3 (236.3 - 898.3)

Median cytokine secretion levels with interquartile range. values for n = 6 donors

Supplementary material 6.4. Cytokine secretion in MDM infected with HIV-1 and exposed to HIV-1/*Mtb* environment for 96-hours

	Median level of cytokine secretion with Interquartile range (pg/ml) in the bottom chamber of trans-well plate					
Analyte	$H37Rv^{P1939/T605A}$ Infection	$H37Rv^{P1939/T605A}$ Infection	$EX30^{Q1939/A605}$ Infection	$EX30^{Q1939/A605T}$ Infection	$MRC16^{P1939/A605}$ Infection	$MRC16^{P1939/A605T}$ Infection
CCL11	19.8 (8.7 - 28.13)	8.7 (8.7 - 8.7)	35.32 (28.13 - 41.83)	35.32 (28.13 - 44.9)	25.82 (8.7 - 41.83)	19.8 (8.7 - 28.13)
CCL2	3607 (1301 – 7537)	2440 (841.5 – 8010)	1537 (1386 – 13077)	5302 (1764 – 12082)	4568 (1894 – 20740)	3429 (1450 – 7998)
CCL3	65.85 (50.39 - 99.26)	8.63 (5.18 - 44.96)	74.9 (71.47 - 88.45)	82.56 (57.52 - 91.79)	76.17 (59.29 - 87.61)	69.75 (48.59 - 90.96)
CCL4	3484 (1992 – 7060)	1006 (861 – 2131)	3039 (1256 – 4255)	3292 (1948 – 8574)	3197 (1542 – 6898)	2822 (1969 – 7031)
CCL5	21.6 (6.79 - 38.12)	4.225 (0.5 - 12.05)	15.35 (5.53 - 532.7)	31.89 (6.17 - 460.7)	32.95 (8.6 - 373.7)	20.07 (7.4 - 37.19)
CXCL10	510.3 (258.5 – 1662)	58.46 (18.14 - 283.1)	477.5 (42.23 – 1009)	776.6 (90.15 - 936.8)	490.8 (1.75 – 1016)	482.3 (271.3 - 887.1)
IL-8	7021 (2457 – 22438)	715.3 (187.8 – 1456)	4941 (1658 – 12104)	5077 (1938 – 19657)	5775 (3011 – 16706)	5111 (2712 – 19927)
IFN-γ	38.55 (32.73 - 60.83)	17.44 (7.42 - 32.73)	38.55 (32.73 - 60.83)	52.61 (38.55 - 60.83)	38.49 (7.42 - 49.85)	35.64 (26.78 - 44.25)
IL-10	34.61 (26.3 - 48.82)	9.59 (5.18 - 26.3)	34.71 (9.23 - 45.8)	38.38 (11.64 - 46.52)	34.57 (3.12 - 48.12)	34.44 (26.3 - 46.7)
IL-1β	3018 (716.5 – 6452)	530 (194.9 – 1250)	2109 (736.7 – 3978)	2708 (610.1 – 5803)	2827 (793.5 – 7732)	2679 (665.4 – 5919)

IL-6	722.3	26.16	461.5	921.3	862.2	710.5
	(186.1 – 1379)	(18.44 - 77.58)	(260.6 – 2127)	(220.9 – 3479)	(297.4 – 3381)	(181 – 1061)
TNF	483.6	36.3	257.3	400.5	418.9	401.1
	(162.6 - 705.3)	(17.94 - 47.82)	(167.3 - 387.3)	(159.5 - 455.8)	(223.6 - 620.4)	(123.7 - 594.7)

Median cytokine secretion levels with interquartile range. values for n = 6 donors

Chapter 7. Discussion

7.1. Background and rationale for the study

Mtb is thought to have evolved and migrated with modern humans over 70 000 years ago [1]. HIV-1 was identified in the early 1980s, which is, by comparison, a relatively recent event [2]. Pathogens need to evolve and adapt with their host to become successful [3], this includes *Mtb* which would have needed to evolve to adapt within humans for survival [1]. In the context of *Mtb* evolution within the host, HIV-1 co-infection represents a new influence upon which *Mtb* evolution occurs [4]. Studies have investigated the impact of this new evolutionary landscape on *Mtb* evolution [5, 6] including how drug resistance could evolve in the context of HIV-1 co-infection [6] and more broadly genome wide site-by-site analysis of potential effects of HIV-1 on evolutionary selections of SNP [5]. SNP are an important source of diversity in MTBC [7] and therefore studying SNP becomes important to understanding the evolution of *Mtb*. Most studies around the functional consequences of *Mtb* SNP have focused mostly on drug resistance conferring SNP [7]. In the study presented here, I hypothesised that *Mtb* strains with SNP in genes involved in cell wall lipid metabolism could induce differential secretion of cytokines during infection of MDM. Furthermore, in the context of HIV-1 co-infection, the consequential change in cytokine milieu may modify HIV-1 replication dynamics. A key study around the subject focused on the presence or absence of a whole gene *polyketide synthase* (*pks15/1*) involved in the metabolism of PGL [8, 9]. Reed *et al.,* wherein pks, showed that in an HN878 strain in which *pks15/1* had been deleted did not produced PGL. These authors showed that PGL was involved in dampening pro-inflammatory cytokine secretion, the strain lacking PGL had a hyperinflammatory phenotype compared to the strain with PGL [8]. In another important study, Sandberg *et al.,* (2009) [9], they showed that the CDC1551 (without surface PGL) significantly increased HIV-1 production compared to HN878 (with surface PGL). However, CDC1551 and an HN878 *pks15/1* strain, without surface PGL induced similar levels of HIV-1 production in PBMC [9] which directly implicates PGL in the regulation of HIV-1 production. While these studies have contributed important understandings to the dynamics of clinical *Mtb* strain variation and its impact on the infection milieu, the work I have undertaken here is, to my knowledge, the first time a detailed assessment of the impact of a single SNP in *Mtb* on the dynamics of HIV-1 infection and replication dynamics.

I used a panel of *Mtb* strains for in which SNP had been previously predicted to be under HIV-1 positive directional selection by evolutionary models [5]. I specifically focussed on SNP in

lipid metabolising genes because the cell wall of *Mtb* is key for its pathobiology. The cell wall of *Mtb* is the first point of contact with the host immune system and lipids present in the cell wall are predicted to have crucial implications for the outcomes of host-pathogen interactions [10]. I therefore focused on understanding the functional impact of SNP on the host immune response to infection by these strains. As a control, I selected *Mtb* strains that were phylogenetically close to strains containing the SNP of interest to control for genetic variation, together with well-characterised laboratory strains from the same lineages. In Chapters 3 and 4 I used this panel of nine *Mtb* strains to investigate whether the strains (and by inference the phenotypic changes conferred by the SNP identified) differentially regulated cytokine production in MDM in the presence and absence of HIV-1 co-infection. Following this, in Chapter 4 I also evaluated the dynamics of HIV-1 productive infection between strains in co-infection models as well as in bystander cells exposed to SN from *Mtb* infected MDM. In Chapter 5, to establish genotype-phenotype relationships more conclusively for the role of the SNP on the observed phenotypes, I applied recombineering to genetically modify pairs of phylogenetically close *Mtb* strains with the strongest phenotype together with a lineage-matched laboratory strain. Genetic manipulation of clinical *Mtb* strains is technically challenging, however this kind of work is essential if the phenotypic consequences of SNP uncovered by WGS and computational models it to be better understood. Finally, in Chapter 6, the resultant mutant strains along with the original strains were used to co-infect HIV-1 infected MDM or expose HIV-1 infected MDM to *Mtb*-induced SN in the same experiment using a trans-well culture system, following which the effect of direct co-infection and bystander effect was assessed in relation to modification of HIV-1 productive infection and correlation with the induced inflammatory milieu.

7.2. Different *Mtb* strains with SNP in lipid metabolising genes have altered cell wall lipid profiles, and cording phenotypes.

The cell wall of *Mtb* is a critical structure for the survival the bacteria during infection [11], which is made up of complex lipids that confer *Mtb* with hydrophobicity (Fig. 1.3) [12, 13]. Cell wall lipids are critical to maintaining the integrity of the bacteria, because alterations of cell wall lipid compositions can affect cell wall lipid hydrophobicity and consequently cell wall integrity [14]. Given the importance of the cell wall lipid structure to the survival of *Mtb* from degradation by host derived enzymes [15], oxygen and nitrogen intermediates [16] and offering little permeability to antibiotics and toxic molecules [17], small changes to these lipids could

have immense consequences to *Mtb.* During invasion *Mtb* cell wall lipids including but not limited to, PIM, LM, LAM form the first point of contact with host cell receptors [18] and that invariably links them to the immune response against *Mtb*.

Sulfatides (SL) are sulphated trehalose esters on the cell wall of *Mtb* of which SL-1 is the most abundant [18]. The discovery by Middlebrook *et al.,* (1959) [37] that SL-1 was present only in pathogenic *Mtb* began an intense search for the role of SL-1 in pathogenesis of *Mtb*. Early researchers showed a correlation between the yields of SL-1 on the surface of *Mtb* cell wall fractions and virulence in *Mtb* [38] and the association of SL-1 with the prevention of phagosome-lysosome fusion [39]. A study in macrophages found that monocytes that were primed with lipopolysaccharide (LPS) and then treated with SL-1 showed reduced production of superoxide; which is deployed to control bacterial growth, compared to monocytes that were treated with other *Mtb* cell wall lipids such as TDM or muramyl dipeptide [40]. In fact, the authors assert that SL-1 inhibits the production of superoxide to levels resembling that of cells not primed with LPS [40].

The analysis of cell wall lipids, via TLC, in the strains used in this study revealed some differences in the cell wall lipids between the clinical strains (Fig. 3.6 – Fig. 3.9). For example, the clinical strains EX30$^{Q1939/A605}$, EX86^{S12} and EU268^{R12} were missing SL-1 in their lipid extract, whereas the lipid was present in all the laboratory strains as well as the clinical strains MRC16$^{P1939/A605}$, EU111^{N1759} and EU40^{T1759} (Fig. 3.6). Furthermore, MRC16$^{P1939/A605}$ lacked PDIM, which was present in phylogenetically close strain EX30$^{Q1939/A605}$ (Fig. 3.7). The implications in the infection phenotypes of the strains because of the differences in cell wall SL-1 and PDIM were of particular interest. The role of SL-1 in *Mtb* pathogenesis is not fully elucidated with links to controlling intracellular growth of the bacilli [19], to inducing coughing in a guinea pig model [20] and inhibiting the maturation of the phagolysosome [13]. But the SL-1 phenotype between the strains was fascinating because the metabolism of SL-1 involves *pks2,* the gene with the SNP of interested that is predicted to be under HIV-1 positive directional selection [5], and the secondary SNP predicted to augment the phenotype is also located in *pks2.* PDIM on the other hand is a major virulence factor of *Mtb* which is only found in pathogenic strains of *Mtb* [21]. PDIM plays a role in macrophage invasion by *Mtb* [22], the role of PDIM and its glycosylated form PGL also extends to immune modulation [8, 16, 23] and could possibly play a major role in differences in cytokine secretion induced by EX30$^{Q1939/A605}$ and MRC16$^{P1939/A605}$.

The panel of *Mtb* strains were also observed to have varying degrees of cording and clumping when grown in media without detergent (Fig. 3.2 – Fig. 3.3). Cording may have minimal effect on the outcome of these experiments because the strains used in subsequent immunological experiments were subjected to vigorous shaking with beads to make them into single cells prior to use in assays. Unless residual cording remained following the attempt to break the cords, the bacteria used were presumed to be planktonic. Nevertheless, an assessment of cording of the clinical strains was an important first step in phenotypic characterisation and a brief discussion of how cording may impact *Mtb* infection and disease progression is worthwhile. This is particularly important given that cording has been recorded *in vivo* [24, 25] and, should the strains reform cords following infection cording may have implications in the later time points. Cording is a virulence characteristic [26] observed in *Mtb*, that has been attributed to the cell wall lipid TDM [27]. Although the role of clumping in virulence of *Mtb* is yet to be clarified, the lipids that are associated with clumping PAT and DAT [28] are found exclusively in virulent strains of *Mtb* [21] and are associated with virulence [29]. The process of cording and clumping is likely a complex pathway that involves many steps and other lipids. This statement is validated by the data I produced, because all the strains I studied exhibited TDM and DAT in the cell wall lipid extracts, however, the degree of cording and clumping varied greatly between the strains. The laboratory strains along with clinical strains $EX86^{S12}$, $EU268^{R12}$ and $EU40^{T1759}$ exhibited clumping only, and no cording observed in these strains (Fig. 3.2 – Fig. 3.3). The differences in the level of clumping observed in these strains despite all strains containing DAT (PAT was not measured here), shows the diversity of cording phenotypes observed within *Mtb* strains. Differences in clumping were even observed between two lineage matched strains, $H37Rv^{P1939/T605}$ and $CDC1551^{WT}$ (Fig. 3.2). The clinical strains $EX30^{Q1939/A605}$, $MRC16^{P1939/A605}$ and $EU111^{N1759}$ exhibited both cording and clumping phenotypes to varying degrees as well (Fig. 3.3). Interestingly, the clinical strain $EU111^{N1759}$ and the phylogenetically close $EU40^{T1759}$ strain, exhibited similar cell wall lipid profiles for all lipids measured however had large differences in the cording phenotype. The quantities of the lipids produced by the different strains may be important to understanding why the observed cording was different between the strains. The most extensive cording amongst the strains was observed in $MRC16^{P1939/A605}$, which was also the most different strain in terms of cell wall lipid content compared to other strains as well as its clinical pair $EX30^{Q1939/A605}$. With reference to $EX30^{Q1939/A605}$ and $MRC16^{P1939/A605}$, the strains were different in the production of PDIM, AC2PMI6, and AC_2PMI_4 (Fig 3.9) which were only present in $EX30^{Q1939/A605}$.

As mentioned, cording may be influenced by the quantity of the lipids produced, rather than just the kind of lipids. However, without mass spectrometry analysis, it is difficult to determine the quantities of lipids in these strains and this could be an interesting avenue for future work. Mutants which lacked DAT, a lipid that according to Dubey *et al.,* (2002) [28], had a more severe clumping phenotype. It would therefore be worthwhile to measure this lipid in the strains to investigate the association with the severity of clumping. These kinds of differences in cell wall lipids can have major implications for cytokine induction. The data discussed above show that cell wall lipids may also play a role in *Mtb* cording and clumping phenotypes that are likely to impact pathogenesis. Cording involves a tight association of many bacteria which will likely increase the number of bacteria inhaled during exposure and could worsen the outcome of infection compared to exposure to planktonic bacteria [25]. Host responses to corded versus non-coded bacteria are also likely to be different, for example Kalsium *et al.,* (2018) [25], found that non-cording mycobacterial species were easily phagocytosed by MDM compared to corded bacteria. Clumping meanwhile, may aid *Mtb* against the toxic effects of drugs, Trivedi *et al.* (2016) [30] showed that *Mtb* in biofilm were metabolically active despite treatment with a 100X MIC of isoniazid [30]. These are natural phenomenon of *Mtb,* and I show here that genetically diverse clinical strains of *Mtb* greatly vary in degrees of cording and clumping. While cording is unlikely to have played a role in subsequent immunological assays due to infection stock generation involving bead beating, cording, and clumping can have important outcomes during *Mtb* infection and disease and was therefore an important phenotype to report.

7.3. Diverse *Mtb* strains with cell wall lipid differences differentially induce cytokines in mono-infected and HIV-1 co-infected MDM.

I went on to measure cytokine secretion induced by the different strains of *Mtb*. The strains used here have a SNP that was predicted to be under HIV-1 positive directional selection [5]. I measured the ability of the strains to induce a variety of pro-inflammatory cytokines and chemokines due to their role in inducing HIV-1 replication [9, 31], stimulation of HIV-1 in latently infected cells [32] and increasing the susceptibility of $CD4^+$ T cells to infection with HIV-1 [33]. Therefore, it is fair to postulate that the mechanism for HIV-1 related selection is to favour strains of *Mtb* that will provide HIV-1 with a perpetually inflamed environment for continued replication. The analysis I discuss below was focused on the regulation of cytokines

that are known to influence HIV-1 replication to investigate whether the SNP influences HIV-1 infection via differential cytokine production. Out of the six clinical strains initially selected for the project (Table 2.3), EX86^{S12} and EU268^{R12} were not taken forward for infection of MDM as they showed similar lipid profiles and clumping/cording phenotypes and were therefore not predicted to induce differential cytokines upon MDM infection.

7.3.1. Phylogenetically close *Mtb* strains with different SNP in lipid metabolising genes differentially induce the secretion of cytokines implicated in HIV-1 infection

The inhibition of macrophage infection by HIV-1 involves either the increased production of HIV-1 antagonistic chemokines, CCL4 (MIP-1β), CCL3 (MIP-1α) and CCL5 (RANTES). These chemokines are natural ligands for HIV-1 co-receptor CCR5 [34]. In other instances, there is an increased production of pro-inflammatory cytokines TNF and IL-1β which downregulate the surface expression of CD4 [35]. Two clinical strain pairs with a SNP that was predicted to be under HIV-1 positive directional selection in *pks2* identified by Koch *et al*., (2017) [5] and three lineage-matched laboratory strains were used to profile cytokine induction by these seven strains in MDM. Overall, the cytokine results described in Chapter 3 highlight the vast differences in infectious outcome between strains of *Mtb.* There was no difference in the secretion of cytokines between the laboratory strains, except for IL-6 secretion which was significantly upregulated by H37Rv$^{P1939/T605}$ compared to HN878^{WT} and CDC1551^{WT} (Table 3.2). This is despite documented differences in genetic background between the strains and that HN878^{WT} belongs to a different lineage than H37Rv$^{P1939/T605}$ and CDC1551^{WT}. On the other hand, although not surprising given their relatedness phylogenetically and lack of lipid profile differences, showing only a cording and clumping phenotype difference (Fig. 3.2), the clinical strain pair EU111^{N1759} and EU40^{T1759} did not differentially regulate the secretion of cytokines in MDM (Table 3.4).

By comparison, the clinical strain EX30$^{Q1939/A605}$ and its phylogenetically close paired strain, MRC16$^{P1939/A605}$, induced different secretion phenotypes of these cytokines in both the *Mtb* mono-infection and HIV-1 co-infection experiments (Chapter3; Chapter 4). MRC16$^{P1939/A605}$ displayed an increased capacity to induce secretion of cytokines both 24-hours and 96-hours post-infection. Of the 25 cytokines measured only CCL2, CXCL8, IL-2R were comparably induced by MRC16$^{P1939/A605}$ and EX30$^{Q1939/A605}$ 24-hour post-infection. By contrast only IL-13 and IL-1RA were comparably induced between the strains at 96-hours post-infection (Table

3.3). This phenotype may be linked to differences in the cell wall lipids between EX30$^{Q1939/A605}$ and MRC16$^{P1939/A605}$. It is reassuring that clinical pairs with the most differences observed in their cell wall lipids, exhibit the most differential induction of cytokines.

Studies have shown that SL-1, on top of decreasing the production of superoxide in monocytes as described above, increases the secretion of cytokines such as IL-1β and TNF [41]. Monocytes that were primed with LPS and then treated with SL-1 secreted increased levels of IL-1β and TNF [41]. More recent work has shown that SL-1 negatively regulates the growth of *Mtb in vivo* using THP-1 cells [19] a trait the authors say may serve to limit the growth of *Mtb* during the latent phase of infection [19]. In a Guinea pig model of infection other authors have shown that SL-1 induces cough [20]. This evidence from literature shows the many aspects of pathogenesis SL-1 may be involved in during infection including increased cytokine secretion. My data supports this literature because MRC16$^{P1939/A605}$, which contains SL-1 in the lipid extract, induces higher secretion of pro-inflammatory cytokines compared to EX30$^{Q1939/A605}$ that is missing SL-1. Also, worthy to mention EU111^{N1759} and EU40^{T1759} which both have SL-1 in their cell wall extract comparably induce the secretion of cytokines, which further solidifies the phenotype of SL-1.

One of the cell wall lipids that was different between the pairs is PDIM. This lipid, including the glycosylated form referred to as PGL, have long been implicated as anti-inflammatory lipids that can lead to dampening the secretion of pro-inflammatory cytokines [42]. An important study by Reed *et al.,* (2004) [8], showed that PGL was critical to dampen the cytokine secretion in BMDM infected with HN878. The authors infected BMDM with two strains: H37Rv that did not contain surface PGL and HN878 that did have surface PGL. The results showed that H37Rv significantly increased the secretion of cytokines by BMDM compared to HN878. Furthermore, the authors validated the phenotype by knocking out a gene in HN878 that is responsible for PGL metabolism and further, introducing this gene into H37Rv [8]. In my work, PDIM is missing in MRC16$^{P1939/A605}$ (Fig. 3.7), and this strain had a hyperinflammatory phenotype compared the phylogenetically close strain EX30$^{Q1939/A605}$ (Table 3.3). I propose that the difference in the cytokine induction between MRC16$^{P1939/A605}$ and EX30$^{Q1939/A605}$ is linked to the absence of PDIM in MRC16$^{P1939/A605}$ and the presence of SL-1. The presence of PDIM in EX30$^{Q1939/A605}$ may have caused this strain to have a tighter regulation on pro-inflammatory cytokines, whereas MRC16$^{P1939/A605}$ did not have this ability.

Taken together these data show support the hypothesis that variation in lipids on the cell wall of *Mtb* clinical strains can affect the cytokine response during infection. However, the scope of my work was not focussed on the effect of the presence or absence of whole lipid species. A central theme in my work was genotype-phenotype correlation, and as such my work investigated how a SNP in genes that code for enzymes involved in the lipid metabolism may modify *Mtb* lipid composition and further, how this SNP-induced lipid variation would impact cytokine secretion during MDM infection, and consequently HIV-1 replication and viral particle production. To that point, this is the first time that *pks2* has been artificially mutated to analyse the role that a single SNP may play in lipid metabolism and cytokine secretion in the context of HIV-1 infection. Having observed the differences in cytokine secretion and cell wall lipid production between strains that differ by a single SNP, below I discuss how the differences impacted to HIV-1 replication and production.

7.4. *Mtb*-induced soluble factors induce the transcription of HIV-1 LTR but do not increase active HIV-1 productive infection

HIV-1 viral load can be measured either by HIV-1 RNA or secreted p24 antigen. Using *in vitro* experiments, determination of intracellular RNA levels provides the best inference of replication, because secreted p24 specifically looks at assembled and budded viruses. Many transcripts generated during replication may be defective at the sequence level and therefore viral protein and infectious particles may not be produced [43]. Therefore, the true replication rate of HIV-1 could be underestimated by only measuring secreted p24 levels, even though some studies have found concordance between viral RNA copies and p24 antigen secretion in plasma of HIV-1 infected patients [44, 45]. I wanted to determine whether the strains of *Mtb* that contained a SNP predicted to be under HIV-1 positive directional selection impacted HIV-1 replication or productive infection. To measure how *Mtb* induced soluble factors affect HIV-1 replication, I measured LTR activity in TZM-bl cells infected with HIV-1 as a proxy for HIV-1 replication. TZM-bl cells are engineered to contain a gene for the firefly Luciferase protein under the control of HIV-1 LTR and therefore, the production of Luciferase protein can be used is a direct measure of HIV-1 LTR activity [46, 47]. In Chapter 4, TZM-bl cells were incubated with SN derived from the different strains of *Mtb*. I used SN harvested 24-hours and 96-hours post-infection of MDM with different *Mtb* strains. I assessed the effect of adding the SN on TZM-bl cells prior to infection on HIV-1 replication therefore, the data from these

experiments could represent altered uptake of HIV-1 into TZM-bl cells by the SN, as well as regulation of replication.

7.4.1. *Mtb*-induced soluble factors increase HIV-1 infection and replication into TZM-bl cells

To understand how an *Mtb*-induced inflammatory milieu impacted HIV-1 uptake and replication in TZM-bl cells, I first incubated TZM-bl with SN from MDM infected with different strains of *Mtb* for 24-hours and then infected the TZM-bl cells with HIV-1. I observed a general priming of TZM-bl cells by SN from MDM infected with different clinical strains of *Mtb* harvested 24-hours post-infection, this was observed by increased LTR activity in TZM-bl cells 48-hours post HIV-1 infection. The SN harvested 24-hours post-infection with all the strains significantly increased the uptake of HIV-1 into TZM-bl cells, except for SN from H37Rv$^{P1939/T605}$, while the SN from CDC1551^{WT} showed a strong trend ($p = 0.08487$) at FDR<0.1 (Chapter 4; Fig. 4.3). Analysis of the cytokine milieu of the SN from the different strains revealed that EX30$^{Q1939/A605}$ and CDC1551^{WT} showed a trend to increased CCL3, IL-4 and TNF, while these cytokines were significantly increased by MRC16$^{P1939/A605}$, EU111^{N1759} and EU40^{T1759} infection. These cytokines were not influenced by H37Rv$^{P1939/T605}$ infection of MDM. It was surprising to discover that SN harvested 96-hours post-infection with EX30$^{Q1939/A605}$ or MRC16$^{P1939/A605}$ clinical strains did not increase LTR activity. By contrast, LTR activity was increased by pre-treatment in SN from clinical pair strains EU111^{N1759} or EU40^{T1759} as well as laboratory stains CDC1551^{WT} or HN878^{WT} laboratory when harvested 96-hours post infection. Since there LTR activity in TZM-bl cells incubated with the 96-hour SN of EX30$^{Q1939/A605}$ or MRC16$^{P1939/A605}$ was comparable to LTR activity induced by the control, it does not appear that the SN decreased the uptake of HIV-1 into the TZM-bl cells or blocked the LTR activity. It emerges as though the factors that were produced early by these strains which led to increased HIV-1 uptake may not be present in the later time-point. The cytokine profile of induced by EX30$^{Q1939/A605}$ or MRC16$^{P1939/A605}$ 96-hours post-infection correspond with cytokines induced by the strains that increased the uptake of HIV-1, except for CXCL9 which is increased by EX30$^{Q1939/A605}$ and MRC16$^{P1939/A605}$ (Chapter 3; Table 3.2 – 3.4). CXCL9 is reported to positively correlated with HIV-1 viral load in literature [76] and in some cases lack of CXCL9 results in reduced HIV-1 replication [84]. Therefore, decreased LTR activity in SN with increased CXCL9 in opposite to what is reported in literature.

Having established that pre-treatment of TZM-bl cells in *Mtb*-induced SN increased LTR activity post-infection, I also analysed the effect of cytokines from MDM infected with the clinical strains when added post-HIV-1 infection. SN from the L2 clinical strains EU111^{N1759} or EU40^{T1759} appears to have factors that are dominant in priming the TZM-bl cells to take up HIV-1, less so in promoting LTR activity post-viral entry. This is because incubating TZM-bl cells 6-hours post-HIV-1 infection with either 24-hours or 96-hours SN from these strains does not affect the LTR activity (Chapter 4; Fig. 4.5 – 4.6). Contrary to SN from EX30$^{Q1939/A605}$ or MRC16$^{P1939/A605}$ which either show a trend or increase the LTR activity with both 24-hour or 96-hour SN. It was unexpected that the LTR activity is increased in EX30$^{Q1939/A605}$, HN878^{WT} and CDC1551^{WT} SN harvested 24-hours post-infection while it was not increased with SN from MRC16$^{P1939/A605}$. However, unsurprisingly the SN harvested 96-hours post-infection from all four of these strains increased the LTR activity when the SN is added after HIV-1 infection (Chapter 4; Fig. 4.6). I postulate that the overabundance of cytokines induced in response to MRC16$^{P1939/A605}$ in the 24-hour SN may have resulted in the SN from this strain only showing a trend to increased LTR activity and not a significant increase. This is because the 96-hour SN, which has the same cytokine profile as the 24-hour SN, but in less quantities, significantly increases the LTR activity.

It is not surprising that SN from *Mtb* infected MDM increases HIV-1 replication, previous studies have shown that cytokines increase HIV-1 replication in a variety of cell types (reviewed by [53]). A 2009 study, showed that CDC1551 induced greater cytokine secretion in PBMC compared to HN878, and that this resulted in increased HIV-1 production in CDC1551 co-infected PBMC compared to HN878 co-infected PBMC [9]. So, for these results I expected that the MRC16$^{P1939/A605}$ SN which had a higher concentration of the cytokines measured at both 24- and 96-hours compared to EX30$^{Q1939/A605}$ SN (Table 3.3) would significantly increase LTR activity. However, this data shows the regulation of HIV-1 replication maybe a complex pathway, because CDC1551^{WT}- and HN87^{WT}-induced SN significantly increased the LTR activity compared to H37Rv$^{P1939/T605}$ with similar cytokines concentrations. Even further, EU111^{N1759} and EU40^{T1759} induced SN did not increase LTR activity in HIV-1 infected TZM-bl cells at both 24-hour and 96-hour time-points compared to controls even though these strains significantly increased some cytokines, including IL-6 and IL-1β. The absence of consistency between which cytokines may regulate HIV-1 LTR activity adds a layer of complication to establishing which cytokines are critical to the phenotype.

Irrespective, these data show that culturing of cells in *Mtb*-induced inflammatory microenvironments either before or after HIV-1 infection increase the amount of replicating virus in TZM-bl cells following HIV-1 infection, in the absence of bacteria. It also confirms that different strains of *Mtb* have variable impact on the production of soluble factors that are associated with increased susceptibility to HIV-1 infection. Others have reported similar findings in other cell types. For example, Thayil *et al.,* (2012) [48], showed that $CD4^+$ T cells exposed to *Mtb* resulted in significantly increased infectivity with HIV-1 compared to unstimulated cells or cells stimulated with non-pathogenic mycobacterial species [48]. A study by Garrait *et al.* (1997) [49], showed that pleural fluid from *Mtb* was sufficient to activate CD4+ T cells for HIV-1 infection in a manner comparable to recombinant IL-2 activation. Furthermore, these authors showed that soluble factors in the *Mtb* pleural fluid could account for the activation, because there was a 60 % and 90 % reduction in secreted p24 with the blocking of IL-6 and TNF, using anti-IL-6 and anti-TNF respectively [49]. Another study found that macrophages pre-treated with pleural fluid from TB patients increased viral production by 6-fold compared to macrophages pre-treated with pleural fluid from non-TB patients [50]. Taking the literature into consideration, my data suggests that: (1) either the cytokines measured in these experiments are not expansive to cover all the cytokines that play a role in promoting the uptake of HIV-1 into TZM-bl cells or (2) in addition to cytokines there are strain specific intrinsic factors that promote the uptake into TZM-bl cells. Taken together, the phenotype of HIV-1 infection might be a strain specific phenotype.

7.4.2. HIV-1 productive infection in MDM was either decreased or unaffected in the presence of *Mtb*-induced soluble factors

Having observed the effect of the SN on LTR activity in TZM-bl cells, I went on to analyse whether increased LTR activity in TZM-bl cells would translate to increased productive HIV-1 replication in MDM. To investigate this, I infected MDM with HIV-1 for 18-hours and incubated the MDM with a fraction of the same SN used in the TZM-bl assay. I harvested SN from the MDM infected with HIV-1 72-hours post-incubation and measured secreted HIV-1 p24 using a Luminex assay (proxy for HIV-1 production). To my surprise, I observed decreased p24 secretion in the presence of SN from $EX30^{Q1939/A605}$ and not its close paired strain $MRC16^{P1939/A605}$, compared to SN from uninfected MDM (Fig. 4.6). It therefore seems that $EX30^{Q1939/A605}$ produces factors that are inhibitory to HIV-1 productive infection. This is surprising because $EX30^{Q1939/A605}$ SN increased the activity of LTR in TZM-bl cells, possibly

aiding in both accelerated uptake of HIV-1 into TZM-bl cells as well as increased replication of post-integrated HIV-1.

Similar findings have been reported in early studies on the effect of *Mtb* co-infection on HIV-1 replication that reported either inhibition or no effect on HIV-1 productive infection in MDM co-infected with *Mtb* [51, 52]. Mancino *et al.,* (1994) [51], reported that infecting MDM with *Mtb* for 4-days and then co-infecting with HIV-1 results in increased HIV-1 productive infection, as measured by p24 in the SN. However, when the authors either simultaneously infected MDM with HIV-1 and *Mtb* or co-infected HIV-1-infected MDM with *Mtb* they observed no difference in HIV-1 productive infection [51]. Furthermore, in an experiment with heat killed *Mtb,* Goletti *et al.,* (2004) showed inhibition of HIV-1 productive infection by MDM stimulated with heat killed *Mtb* [52]. Goletti and colleagues (2004), also described the inhibition of HIV-1 productive infection by MDM incubated with SN from live *Mtb,* which agrees with my observations (Fig. 4.10). These bodies of work support my observations.

Cytokines such IL-4 are associated with inhibition of HIV-1 in M2 MDM [35] and IFN-α in MDM [53]. These cytokines are not significantly increased by the laboratory strains or *EU111*^{N1759} and EU40^{T1759} compared to the controls. This provides an explanation for the decreased HIV-1 production in MDM co-cultured with SN from EX30$^{Q1939/A605}$. It is still puzzling though that the production of HIV-1 is not more inhibited by MRC16$^{P1939/A605}$ SN considering the high production of these cytokines by MRC16$^{P1939/A605}$ compared to EX30$^{Q1939/A605}$. However, the experiment was only allowed to continue for 72-hours which may not have been a sufficient time to fully see the phenotype in these experiments. Analysis of both the DNA to assess the effect of the SN on integration of the HIV-1 cDNA and the RNA to look at the rate of replication of HIV-1 would have provided a more comprehensive view of all the dynamics at play. If the integration or replication were affected by the soluble factors, then a better understanding of why the production was affected may have come to light.

7.5. HIV-1 production was not affected in MDM co-infected with different strains of *Mtb* despite elevated HIV-1 inducing cytokines

Co-culturing MDM with *Mtb*-induced SN gives information about the effect the *Mtb* environment on bystander cells. Yet, the effect of *Mtb* can be both from direct co-infection as well as the bystander effect [31]. LTR, the promoter of all HIV-1 genes, contains binding

motifs for a variety of hTF, including NF-κB, Sp, AP-1, NFAT, C-EBP and ATF [31]. In this context, *Mtb* lipids – which stimulate signalling pathways that increase these hTF (directly or increase the production of cytokines that stimulate these hTF) - will likely increase the stimulation of HIV-1 LTR, and thereby increase HIV-1 replication and possibly productive infection. However, in these experiments, I did not directly measure induction of hTF by the different *Mtb* strains. Instead, used a surrogate measurement of the cytokine secretion induced by these activated hTF. I measured the effect of co-infection in M1 and M2 MDM. To this end, I infected M1 and M2 polarised MDM with HIV-1 for seven days and then co-infected the MDM with the panel of different *Mtb* strains (Fig 4.7). I harvested the SN 96-hours post-co-infection with the *Mtb* strains and used the SN to measure secreted HIV-1 p24 using Luminex assays (Table 4.1 – 4.3).

Infecting of MDM with the HIV-1 for seven days and then co-infecting with the different strains, I observed that there were no differences in secreted p24 in the SN of MDM co-infected with the different strains of *Mtb* (Fig. 4.10) compared to HIV-1 only infected MDM. The analysis of HIV-1 production between $EX30^{Q1939/A605}$ and $MRC16^{P1939/A605}$ co-infected MDM showed a trend to increased HIV-1 production by $EX30^{Q1939/A605}$ compared to $MRC16^{P1939/A605}$ co-infection (Fig. 4.10B). This was not expected given the results of cytokines measured from MDM co-infected with the two strains. MDM co-infected with $MRC16^{P1939/A605}$ had significantly elevated cytokine secretion compared to MDM co-infected with $EX30^{Q1939/A605}$. There was an expectation that cytokines would then enhance HIV-1 replication, post-integration, by stimulating pro-HIV-1 hTF. For example, TNF induced pro-inflammatory pathway is regulated by NF-κB or MAPK pathways, TNF binds to two cell surface receptors TNFR1 and TNFR2, which through a cascade of downstream protein signal activates the NF-κB or MAPK pathways [54]. Likewise, the promoter of IL-1ß is controlled at the promoter level by a variety of hTF that also bind the HIV-1 LTR, including Ap-1, C/EBP and NF-κB [31]. In turn, the binding of IL-1ß to its cell surface receptor IL-1 receptor also stimulates the NF-κB pathway [55]. The stimulation of these cytokines by *Mtb* infection not only increases their secretion but increases the chances of stimulating HIV-1 LTR in co-infected cells. However, the same phenotype was persistent throughout all the co-infection conditions (Fig. 4.10). Both $EU111^{N1759}$ and $EU40^{T1759}$ did not differentially regulate p24 secretion compared to HIV-1 only infected MDM or compared to each other (Fig. 4.10C). Even the laboratory strains similarly regulated HIV-1 productive infection compared to each other and compared to the HIV-1 only infected condition (Fig. 4.10A).

This data was surprising because in literature, there are many records of cytokines increasing the production of HIV-1 in MDM, CCL2 [56], and IL-6 [57], IL-6 was also shown to increase HIV-1 production in PBMC [9]. IL-6 increases HIV-1 replication and productive infection either alone or in concert with TNF as measured by RNA and productive infection as measured by p24 secretion [57]. I found that IL-6 secretion is significantly increased during co-infection with all the strains excluding CDC1551 co-infection compared to HIV-1 only infected MDM (Table 4.1 – Table 4.3). Moreover, MRC16$^{P1939/A605}$ co-infection significantly increased IL-6 secretion compared to EX30$^{Q1939/A605}$ co-infection, yet my data shows a trend to increased HIV-1 production in EX30$^{Q1939/A605}$ co-infected MDM compared to MRC16$^{P1939/A605}$ co-infected MDM (Fig. 4.10B). It worth reporting though, the MDM used by Poli *et al.,* (1990) [57] for their experiments were not subjected to co-infection which could affect cell viability and hence showed increased HIV-1 productive infection.

CCL2 in my co-infection experiments was only elevated in MRC16$^{P1939/A605}$ co-infection compared to HIV-1 only infected MDM (Table 4.2). CCL2 has been shown to be important in HIV-1 budding from MDM [56] and infection of MDM with HIV-1 [58]. Therefore, comparable levels of CCL2 in my experiments could lead to similar levels of HIV-1 production in co-infection experiments. For example, despite showing increased CCL2 secretion in the mono-infection model (Table 3.3), MRC16$^{P1939/A605}$ co-infection did not significantly increase CCL2 compared to EX30$^{Q1939/A605}$ co-infection (Table 4.2). On the other hand, CCL2 is significantly elevated in MDM co-infected with MRC16$^{P1939/A605}$ compared to HIV-1 only infected MDM, which is expected to increase HIV-1 production, but this is not the phenotype that was observed (Fig. 4.18). Measurements of p24 were taken 4-days post-co-infection of the MDM with different strains of *Mtb* and 11-days post-infection with HIV-1 and cell death was not measured. MRC16$^{P1939/A605}$ was shown to have a hyper-inflammatory phenotype in MDM (Table 3.3), which could have resulted in cell death in the co-infection model. HIV-1 strictly requires host cells for replication and therefore if there were increased cell death, that would have affected HIV-1 production dynamics. Therefore, a measure of cell death along with HIV-1 production in these experiments would have provided more detailed understanding of the differences observed in cytokine secretion and HIV-1 production.

7.6. Engineering the *pks2* SNP in *Mtb* strains changed cytokine secretion in *Mtb* infected MDM

To assess whether the observed differences in cytokine induction by the different strains was the result of the SNP that were identified by WGS and evolutionary analysis, I applied recombineering to the clinical strains and a lineage matched laboratory strain. While $EU111^{N1759}$ and $EU40^{T1759}$ strain pair resulted in increased secretion of some cytokines compared to controls in both co-infection and mono-infection, there was no differences in cytokine induction between $EU111^{N1759}$ and $EU40^{T1759}$ (Table 3.4 and Table 4.3). There was also no difference in the production of cell wall lipids between strain $EU111^{N1759}$ and $EU40^{T1759}$ (Fig. 3.6 – Fig. 3.9). With this data in mind, I reasoned that there was no value in performing genetic engineering in $EU111^{N1759}$ and $EU40^{T1759}$.

Therefore, the clinical strains taken forward for genetic engineering were the $EX30^{Q1939/A605}$ and $MRC16^{P1939/A605}$ pair. I also included the $H37Rv^{P1939/T605}$ laboratory strain as it matched the lineage (L4) of the clinical strains and is known to be amenable to genetic manipulation. There were two SNP of interest observed in $EX30^{Q1939/A605}$, relative to the H37Rv genome. The first was the P1939Q mutation that was predicted to be under HIV-1 positive directional selection [5]. The second was the T605A mutation that was found in both $EX30^{Q1939/A605}$ and the clinical partner, $MRC16^{P1939/A605}$, and was selected for engineering because it also occurs in *pks2* and may augment the phenotype induced by P1939Q. The fact that this SNP was not found in $H37Rv^{P1939/T605}$ was an incentive to further investigate whether it could have a supplemental effect on a potential phenotype induced by P1939Q. I used recombineering [59] to introduce the two SNP observed in $EX30^{Q1939/A605}$ into $H37Rv^{P1939/T605}$ (thus attempting to create an $EX30^{Q1939/A605}$ *pks2* genotype in $H37Rv^{P1939/T605}$) and to change the position in $EX30^{Q1939/A605}$ to match the genotype of $H37Rv^{P1939/T605}$ at these sites. The $MRC16^{P1939/A605}$ strain was a mix between the $H37Rv^{P1939/T605}$ and $EX30^{Q1939/A605}$ genotypes: the original strain was the same as $H37Rv^{P1939/T605}$ in position 1939 (Q1939P) but had the second mutation at 605 (T605A) (Table 2.3). Therefore, the aim of recombineering in $MRC16^{P1939/A605}$ was to change position 1939 to match the $EX30^{Q1939/A605}$ genotype (P1939Q) and changing position 605 position to match $H37Rv^{P1939/T605}$ (A605T).

Recombineering was not successful for introducing the SNP predicted to be under HIV-1 directional selection (conferring the P1939Q amino acid change) in this project. However, I was able to engineer the secondary SNP (aa605) in all the strains (Table 5.4). While I was not

able to introduce the mutation that was predicted to be under HIV-1 positive directional selection, introduction of the secondary SNP represents an important accomplishment. Genetic engineering of clinical *Mtb* strains is not often accomplished due to the technical challenges of these kinds of experiments. Furthermore, the phenotypic role of the secondary SNP that was amenable to recombineering-based mutagenesis was carefully investigated via immunological models, presenting an important contribution to genotype-phenotype characterisation within the field. It was also predicted that any changes identified would be more subtle to that which would be achieved by modifying the primary SNP of interest at position 1939, or by completely knocking out *pks2*.

All the mutant strains generated here (Table 2.4), along with the original unmutated clinical strains (Table 2.3) were sent for lipid analysis using TLC. This was completed to test if there were any changes in the cell wall lipid production because of changing the amino acid at that site. PDIM and SL-1 which were different between MRC16$^{P1939/A605}$ and EX30$^{Q1939/A605}$ were of particular interest. Unfortunately, due to time constraints the specific TLC plates to generate these data could not be finalised in time to make this important comparison (Fig. 5.11) and this would represent a priority area for future research. The limited TLC data available showed limited differences in production of TDM, PE, CL, and PIM between EX30$^{Q1939/A605}$ and EX30$^{Q1939/A605T}$, with only the emergence of a band under PE observed in the mutant EX30$^{Q1939/A605T}$. It also appears that both strains are missing the TMM lipids from their fractions. There was also limited difference in the production of these lipids between MRC16$^{P1939/A605}$ compared to the mutated MRC16$^{P1939/A605T}$, with only a small change in the relative ratio of the same band under PE. Interestingly though, the mutation of H37Rv$^{P1939/T605}$ to H37Rv$^{P1939/T605A}$ appears to have changed the production of some lipids between the three strains. Firstly, H37Rv$^{P1939/T605A}$ is missing the PIM as having a decreased relative abundance of TMM, CL and some lipid species in the PE fraction compared to H37Rv$^{P1939/T605}$. The quantity of extracted lipids between the strains also appears to be different, although the same mass of bacteria was used to extract the lipid. TLC analysis to cover the full repertoire of lipids initially analysed in Fig. 3.6 – Fig. 3.9 needs to be completed to draw any conclusions around whether the mutations have any alterations on lipid production in the strains, in particular SL-1 which was not able to be assessed in the 1D TLC PNP055-22.

7.6.1. Genetically engineered *Mtb* strains modify HIV-1 productive infection compared to wildtype

Despite the P1939Q site not being amenable to genetic manipulation in all strains, the secondary mutation, T605A, that was found in $EX30^{Q1939/A605}$ and $MRC16^{P1939/A605}$ was successfully mutated in all strains. I used the strains generated including the wild-type strains to infect MDM using a trans-well assay. The trans-well assays facilitated a concurrent HIV-1/*Mtb* co-infection model in the top chamber, and a bystander cell effect model in the matching bottom chamber because *Mtb* bacteria were excluded from moving from the top chamber to the bottom (Fig. 6.1). SN were harvested from both the co-infection and bystander models respectively and used to measure p24 secretion using (as a proxy for productive infection) by Luminex assay.

Control experiments comparing well with HIV-1 infection only first established that there was not sufficient movement of HIV-1 from either the top chamber to the bottom chamber or the bottom chamber to the top chamber to influence the quantity of HIV-1 harvested when both chambers are HIV-1 infected, as occurs in the co-infection model (Chapter 6; Table 6.1). This suggests that quantification of HIV-1 in either the top or the bottom chamber can be generally inferred as coming from that chamber.

This data is consistent with previous reports that HIV-1 production ins decreased in MDM when the cells are infected with HIV-1 first and then *Mtb* later. But the trans-well experiments also showed that HIV-1 regulation can be different in closely related *Mtb* strains, and that single base alteration may affect the HIV-1 regulation phenotype. This was observed in MDM co-infected with $MRC16^{P1939/A605T}$ showing a trend to decreased HIV-1 production compared to MDM co-infected with $MRC16^{P1939/A605}$ (Chapter 6; Fig. 6.3A). $MRC16^{P1939/A605}$ and $H37Rv^{P1939/T605}$ co-infection showed a trend to decreased HIV-1 compared to MDM infected with HIV-1 only. Interestingly, this phenotype was observed in MDM that were infected with strains that have the P1939/T605 background (Chapter 6; Fig. 6.3A). The close parental strain ($MRC16^{P1939/A605}$) and the close mutant strain ($H37Rv^{P1939/T605A)}$ did not affect HIV-1 production. Antoher example of pottential infleunce by a single base change was observed when the HIV-1/$EX30^{Q1939/A605T}$ mutant strain showed a trend to decreased HIV-1 production in bystander cells exposed for 24-hours, but the phenotype is not retained with the parental $EX30^{Q1939/A605}$ co-infection environment (Chapter 6; Fig. 6.3).

The effects of decreased HIV-1 production are enhanced in the 96-hour time point. The fact that all the strains showed a consistent phenotype despite a different genetic backgrounds might be pointing to the role lipids also play in modulating HIV-1 production as well (Fig. 6.4A). Although an extensive study into the lipid phenotype is required for these strains, my previous data showed that H37Rv$^{P1939/T605}$ and EX30$^{Q1939/A605}$ showed lipid differences in to MRC16$^{P1939/A605}$ (Chapter 3; Fig. 3.6 -3.9). This may explain why MRC16$^{P1939/A605}$ only showed a trend to decreased HIV-1 production and while the original EX30$^{Q1939/A605}$, EX30$^{Q1939/A605T}$, H37Rv$^{P1939/T605}$ and H37Rv$^{P1939/T605A}$ all resulted in significantly low HIV-1 production.

HIV-1/EX30$^{Q1939/A605}$ exposed bystander MDM also resulted in significantly less HIV-1 production compared to HIV-1 only infected bystander MDM, which was not observed from the mutant EX30$^{Q1939/A605T}$. This data aligns with my previous observation in Chapter 4 (Fig. 4.10) where HIV-1 infected MDM co-cultured with SN harvested 96-hours post-infection of MDM with EX30$^{Q1939/A605}$ resulted in decreased production of HIV-1. These data strongly suggest that infection with EX30$^{Q1939/A605}$ results in the production of factors that inhibit HIV-1 productive infection. Interestingly, this may be linked to *pks2* since this phenotype is abrogated in the presence of HIV-1/EX30$^{Q1939/A605T}$ SN.

Taken together, these data indicate that HIV-1 production was affected by a mutation at position-605. However, I had initially predicted that this SNP would only augment the phenotype of the SNP at position 1939 (which was the one predicted to be under HIV-1 selection). It is difficult to conclusively assess what the role of the 1939 SNP might be, since after multiple attempts, it was not amenable to genetic engineering (Table 5.3). It possible that changing the SNP that was predicted to be under HIV-1 positive directional selection may have shown a stronger HIV-1 production differences between the wild-type and mutant strains. Similar experiments with other SNP predicted to be under HIV-1 selection or further attempts on this SNP will provide clear data in the future.

7.6.2. Secretion of p24 correlates with donor inflammatory phenotype

A study by Sandberg *et al.,* (2009) [9], showed that *Mtb* strains could result in specific modification of HIV-1 production in PBMC [9]. However, in another study, the degree of *in vitro* replication of HIV-1 in MDM is consistently a donor-linked phenotype [60]. While these

are two different mechanisms of action, they are not mutually exclusive. It is plausible that an *Mtb* strain could modify the donor immune response such that it favours HIV-1 replication. To understand which of these variables had a significant contribution to the variation in p24 production in the trans-well assay, I performed a Two-way Anova. The data I generated suggested that in both co-infection and bystander models, the difference between the strains was minimal in contrast to the major contribution to variation in HIV-1 production attributed to differences between donors (Table 6.5).

Given the above information, I sought to understand whether the donor-linked variation in HIV-1 production was correlated with individual donor variation in immune response. This is inspired by the understanding that, HIV-1 replication and productive infection are cytokine driven phenotypes [61-63]. To achieve this, I correlated the levels of secreted cytokines and secreted p24 in co-infected MDM and bystander MDM and coloured the correlation points by donor to determine the contribution of each donor to the observed data (Fig. 6.6 – Fig. 6.7).

I observed a clear donor dependent HIV-1 production phenotype in both directly co-infected and bystander cells. The amount of HIV-1 harvested from each donor during direct co-infection was positively correlated to the amount of CCL2 secreted by the donor. The donors that secreted low levels of CCL2, following co-infection, also had the lowest amount of HIV-1 in the SN. This phenotype is present in the bystander cell model as well. In the literature, CCL2 is connected with increased release of HIV-1 particles to the SN [56, 58, 64], and it therefore makes sense that donors with elevated CCL2 would also have increased p24 in the SN; while an absence of CCL2 significantly affects the release of HIV-1 particles in MDM [56, 64]. Fantuzzi *et al.,* (2003) [56] showed that it was not necessarily the replication of HIV-1 that was impaired by the lack of CCL2, but rather the release of HIV-1 particles. The authors reported an increase in cell associated p24, but not cell free virions in the absence of CCL2 [56]. This was validated in subsequent study which showed that in the absence of CCL2, a Clade B HIV-1 strain is impaired in its ability to recruit ESCRT complex proteins – a set of proteins that necessary for budding of viral particles [64]. My data combined with observations from literature show that donor's induction of CCL2 following infection with *Mtb* plays a critical role in determining the extent of HIV-1 viral production.

I also found a negative association of between secretion of IL-1β with p24 secretion in HIV-1 co-infection. In this case, the donors with low secretion of p24 showed high levels of IL-1β

(Fig. 6.6B). It is possible that the negative correlation of p24 secretion and IL-1β is due to pyroptosis, a pro-inflammatory form of necrotic cell death. Elevated release of IL-1β particularly in macrophages is associated with pyroptosis [65]. HIV-1 as an obligate intracellular parasite, relies completely on the host to continue its life cycle [66, 67]. The observed decreased productive infection in the donors with high IL-1β secretion may be a result of increased cell death in these donors, limiting the source of cells for ongoing HIV-1 replication. This explanation is strengthened by the fact p24 and IL-1β correlation is not observed in the bystander model, where cell death is presumed to be less than the co-infection model. This data here shows that different donors have varying susceptibility to HIV-1 – and some may have an increased capacity to die more rapidly following co-infection. While donors with high IL-1β in the SN have low HIV-1 production, which at first might appear to be a positive observation, since low HIV-1 production may be due to increased necrotic cell death, these donors are more vulnerable to inflammatory tissue damage during HIV-1 infection.

IL-8 was also negatively associated with p24 secretion however this was only found in the bystander model (Fig. 6.7B). IL-8 has a dual effect on HIV-1 during infection. Data from published literature suggests that post-integration, IL-8 may serve to enhance HIV-1 replication [68-72]. However, some studies have shown that IL-8 can have an inhibitory effect on HIV-1 replication, particularly during the early stages of infection [73-75]. The matching co-infection wells showed a negative correlation of IL-1β and p24, which I predict to be a result of cell death, I hypothesise that phenotype is not observed in the bystander cells because high IL-8 resulted in low levels of infection and integration and thus not susceptible to death similar the co-infected matched wells. It worthy to note the effect of IL-8 on infection and integration were not explored directly in this work and are only inferred from the data and the literature. Nevertheless, it does appear that increased IL-8 provides an avenue for limiting HIV-1 infection and viral DNA integration in susceptible hosts. Further studies are warranted to understand the mechanism by which IL-8 downregulates CCR5 and integration of HIV-1 viral DNA [74, 75].

These data presented here show that host underlying genetic differences play a crucial role in designing experiments to determine the role of cytokines in HIV-1 infection, replication and control, and overall susceptibility to HIV-1, and cytokines play an important role in HIV-1 infection, replication, and control. As this was highlighted in an important study by Jacobs *et al.,* (2017) [76] that showed that cytokines from elite controllers of HIV-1 could control HIV-

1 replication *in vitro* by up to 80 %. It is important to understand underlying host genetic differences that confer resistance or susceptibility to HIV-1 infection and potentially rapid AIDS progression. As I have shown here that production of HIV-1 is a host-linked phenotype. There are studied that have defined differences in human genotypes and how those influence infectiousness and disease progression [77, 78]. I have provided both experimental and evidence from the literature that *Mtb* co-infection increased susceptibility to infection with HIV-1. This is a mechanism for *Mtb* to exacerbate HIV-1 infection and possibly the spread of HIV-1. But according to the evidence host underlying genetic difference may play a considerable role on determining the fate of disease post-infection.

7.7. Limitations of the study

Researchers must accept that laboratory conditions used as models to study any phenotype of interest will always have caveats. While *in vitro* and *ex vivo* systems that are used in laboratory settings are good models to infer phenotypes, there are limitations, and these should be considered and acknowledged in thinking about the implications of one's data for the field. In this spirit, below I provide a brief description of the limitations of the work I have presented for my thesis.

7.7.1. *Mtb* culture

To complete infection of cell cultures using *Mtb,* the bacteria must be cultured under laboratory-controlled conditions. Although *Mtb* was cultured in the absence of detergent to ensure cell wall integrity, the natural cording phenotype of *Mtb* strains is disrupted by repeated bashing of the corded bacteria using silica beads to make single cells prior to MDM infection. Cording is a virulence characteristic of *Mtb* and the loss of natural cording significantly change the observed infection phenotypes. Increased cytokine production by corded bacteria (compared to non-corded bacteria) was reported in in studies in mice [79] a recent study has shown that different methods of preparing *Mtb* resulting significantly different outcome in cytokine secretion [80]. Importantly, the authors showed that the *Mtb* cell wall is affected by the type of method that is used to prepare cells infectious stock [80]. While these methods are necessary modifications to ensure that the correct MOI is used for infection, it may affect how they relate to the *in vivo* immune response when bacterial are cording and presents an important limitation to be aware of.

7.7.2. *In vitro* models of infection

Even though the use of genetically engineered cell lines and *in vitro* infection models can provide a great insight about mechanisms of action in infection, they do have limitations – several of which are mentioned below. During MDM cell culture, MDM are not replenished during *in vitro* study as would be the case in the body with newly migrating monocytes, which are a source of fresh cells for both HIV-1 and *Mtb* infection. Secondly, TZM-bl cells are genetically modified cells to allow for ease of HIV-1 infection. Therefore, HIV-1 infection of TZM-bl cells is biased which may not be informative about the role of cytokines in making cells susceptible to infection. Thirdly, macrophages are long-live reservoirs of HIV-1 less prone to cytopathic effects compared to T cells and support less replication than T cells [81]. Perhaps using a mixed T cell system of infection, such as PBMC, would have better reflected HIV-1 replication and productive infection, which could be done in future work. Co-culturing MDM with SN is a less dynamic set-up than what would be observed in the human body. Here, the cytokine concentrations are fixed and there would not be a gradient and the movement of cytokines as expected during natural infection. Moreover, the HIV-1 strain that was used for these experiments is not geographically represented of strains in the local settings - infections were carried out using HIV-1 BaL, whereas the majority of infections in the South African population involve the sub-type C strain [82]. Part of this work was informed by work done by Ranjbar *et al.*(200) [9], where they used dual tropic HIV-1 strains from subtype B, C and E. It is possible that infection with a sub-type C strain could have yielded different results in HIV-1 production and could form an important area for further study on this topic.

Critical experiments that are missing from the data include using RNA as a measure of HIV-1 replication in MDM. These experiments are key to providing insights around the rate of replication that is not completely discernible from p24 secretion because of defective RNA that are not packaged to a mature virion. An analysis of HIV-1 viral cDNA integration into host genome would also have been important to understand whether integration was affected by any of the experimental conditions and to allow a ratio of integrated HIV DNA relative to replicating viral RNA to be calculated.

7.7.3. Mutation and interpretation of results

To achieve genetic engineering, strains of *Mtb* need to go through two successive rounds of electroporation. Electroporation involves a harsh process of introducing high voltage to the *Mtb* bacteria to facilitate transformation. This has a potential to not only damage the cell wall

but may introduce more mutations to the DNA of the *Mtb*. DNA from strains which were subject to electroporation was sent for WGS to determine whether the electroporation process did not introduce any additional damage to the DNA. Unfortunately, the data from those experiments is not included in this work owing to time constraints but would be a necessity for any publication. The absence of the data limits absolute certainty on the role of SNP that was engineered without knowing the full genetic background of strains.

The primary SNP that was predicted by Koch *et al.,* (2017) [5] to be under HIV-1 positive directional selection could not be changed via recombineering in these experiments. Therefore, the phenotypes observed in these experiments are not reflective of the effect a SNP under HIV-1 positive directional selection on cytokine induction and HIV-1 production. As such, the phenotypes observed may be the more subtle of the phenotypes induced by a SNP predicted only to augment HIV-1 replication and production. A comprehensive TLC analysis of both the wild-type and mutant strains for comparison of the effect of mutation cell wall lipid production. Analysis of the same lipids between the strains would provide better comparisons and present a key experiment for future work, especially SL-1 since the gene of interest was involved in SL-1 metabolisms.

Finally, ssDNA substrates that were in these experiments were designed to bind the lagging strand, which work well for the secondary SNP (T605A), but not for the primary SNP (P1939Q), which might have been part of the reason this site could not be successfully mutated. More ssDNA substrates which bind the leading strand must be used in subsequent rounds of electroporation to see if efficiency will improve the generation of mutants for SNP-5817 (P1939Q).

7.8. Relevance of study in the field

Limitations as described above notwithstanding, the work I have presented above provides significant new knowledge and technical accomplishments in my field. In terms of evolutionary dynamics, disease progression and pathobiology, advances in genomic studies have increased our appreciation of the diversity of *Mtb* strains and how this might impact TB disease. However, the impact of HIV-1 co-infection on the evolution of *Mtb* strains has been studied thus far to a lesser degree and is important to understand for purposes of dynamics of HIV-1 virulence and the development of drug resistance in strains that infect and TB cause disease in co-infected patients – particularly, due to the very close association of these two

diseases where rates are high. Important for this study, is the feedback loop of how *Mtb* evolution will impact HIV-1 and AIDS progression, and how HIV-1 itself may impact the evolution of *Mtb*. Here, I looked at how a single nucleotide change in *Mtb*, that was predicted to be under HIV-1 positive directional selection [5], would influence cytokine production in MDM and potentially HIV-1 replication. There are many studies that have shown that *Mtb* lipids influence the immune response to infection and therefore I selected a SNP in a lipid metabolising gene as I predicted that disturbing the cell wall lipid phenotype in *Mtb* may have implications for the immune response to *Mtb* strains. The work focused on a single nucleotide, but the results could inform how HIV-1 may direct *Mtb* evolution to the benefit of HIV-1 production and replication.

This is the first time to my knowledge that a study attempts to understand whether a SNP in *Mtb* that is predicted to be under HIV-1 positive directional selection influences HIV-1 replication and production *in vitro*. In this work, I have demonstrated that different strains of *Mtb* can impact the immune environment, with several important phenotypic consequences.

Firstly, the data shows that different strains of *Mtb* assume different physical characteristics when grown in liquid media without detergent. Some strains, despite phylogenetic similarity can have diverse cording phenotype, as observe with $EU111^{N1759}$ and $EU40^{T1759}$ or diverse cell wall lipids as observed with $EX30^{Q1939/A605}$ and $MRC16^{P1939/A605}$. The data suggests that lipids are vital to immune induction by *Mtb* strains because the $EX30^{Q1939/A605}$ and $MRC16^{P1939/A605}$ clinical pair with the most differences in cell wall lipids also showed the most variation in cytokine induction for phylogenetically close strains. Given that both cording and cell wall lipids are implicated in virulence, future studies in the field must consider the effect of growing strains in the presence of detergent on cording and cell wall lipids. The effect of absence of these phenotypes may affect data interpretation.

The data showed that the immuno-environment induced by different strains of *Mtb* affected HIV-1 replication in TZM-bl cells. Firstly, it can be interpreted that *Mtb*-induced SN increased the susceptibility of TZM-bl cells to HIV-1 infection when the SN is added before HIV-1 infection. Furthermore, *Mtb*-induced SN also resulted in increased LTR activity; a proxy for HIV-1 replication, compared to TZM-bl cells incubated with SN from uninfected MDM or media only. Granted the phenotypes were not observed consistently across all the strains, this data still shows that HIV-1 replication may be influenced by systemic *Mtb* infection.

TZM-bl cells are a modified cell line which provide insightful data on HIV-1 replication, but more applicable models, such as MDM, may provide more relevant data about individual host differences that impact replication and production of HIV-1. The MDM co-infection experiments showed that HIV-1 production is regulated differently between different donors and this regulation is mediated by cytokines. I have shown that donors that induced high CCL2 positively correlated with increased HIV-1 production, whereas donors with high IL-1β negatively correlates with HIV-1 production.

In addition to important phenotypic observations, the work I present here also represents an important technical accomplishment (that ultimately facilitated the phenotypic work). Using recombineering, I was able to introduce a single SNP into clinical *Mtb* strains to determine how the SNP might influence lipid biology and in turn, the immune environment. One of the approaches that allowed me to do this was a slight modification of the recombineering protocol to include a plasmid with a resistance marker, during electroporation, to make screening of transformants easier. After multiple attempts, I could not engineer the primary SNP of interest, and the SNP that was thought to be under HIV-1 selection, nevertheless I successfully changed a secondary SNP of interest in the different strains. This kind of genotype-phenotype investigation could be applied in other studies to understand the importance of key polymorphic variation in *Mtb* biology.

After successful recombineering, I used a trans-well assay to assess how introduction/replacement of the SNP may influence the phenotype of *Mtb* strains. Using the trans-well assay I was able to show that the question of co-infection and bystander cell effect can be answered simultaneously in a single experiment. Further, I was able to show that a single nucleotide change in *Mtb* strains has the potential to influence cytokine production in MDM and consequently HIV-1 productive infection in macrophages. This data can be taken as foundation to expand the influence of HIV-1 predicted positive selection on *Mtb* cytokine induction and HIV-1 replication.

In addition to these key findings, I was able to show that individual donor responses during co-infection determines the degree of HIV-1 production. This means that HIV-1 replication and progression of AIDS is different between donors, and that, donor variation should be considered when designing immune profiling experiments. Concordantly, I have shown that

the extent of inflammation of the donor is influenced by the genetic background of the infecting *Mtb* strain, which may be an indirect influence of *Mtb* to HIV-1 replication and production.

In summary, the genotype-phenotype investigation here provides interesting data that suggests that single SNP in *Mtb* can significantly change the immunological milieu during disease, that can in turn have important implications for the outcomes of HIV-1 co-infection. With study limitations in mind, I discuss areas for future research below.

7.9. Future research

There are several key experiments that could be completed, as a priority, to further the understandings that I have generated above. WGS of generated mutant strains is a crucial and urgent next step to determine if any additional mutations were introduced during the recombineering process. Furthermore, TLC data for strains that were generated via genetic engineering (and underwent two rounds of electroporation) will be important to determine what the impact of on the recombineering process was on cell wall lipid production. In addition to further characterisation via TLC, mass spectrometry of the cell wall lipids in the original strains and the mutant strains, could provide more granular insights into lipid production because mass spectrometry has the potential to generate data about the nature of lipids present and the quantity of the lipids.

To accomplish the desired mutation in *pks* position 1939 in future experiments, different mutagenic techniques, such as allelic exchange using a suicide vector, could be attempted.

The gene of interest, *pks2*, in these experiments is involved in the metabolism of SL-1. To elucidate the role of this lipid in the phenotypes involved, future experiments could use strains without *pks2* and consequently SL-1 on the cells wall. The strains without SL-1 can be used to infect MDM and analyse the effect of complete lipid absence on the phenotypes.

In terms of phenotype data, I focussed on understanding how infection of MDM with *Mtb* strains might create an immune milieu with the capacity to impact HIV-1 progression. Given that CD4+ T cells are the primary site of HIV-1 infection, future experiments that determine how T cells co-cultured with *Mtb*-induced SN should be conducted. TZM-bl cells showed an increased susceptibility HIV-1infection when *Mtb*-induced SN was added before infection. Measuring HIV-1 surface receptors during these kinds of experiments could provide insights

into the mechanism governing rapid uptake of HIV-1 into TZM-bl cells. Similarly, adding antagonising antibodies against the potential cytokines and chemokines which may mediate the regulation of viral uptake in the TZM-bl assay may help to elucidate which proteins in the cytokine mileu are having the greatest effect on HIV-1 infection.

A key area for future work would also be to measure the rate of cell death in co-infection experiments. Because HIV-1 depends completely on host cells for replication and production, variation in both these phenotypes should be interpreted in relation to the availability of cells. Furthermore, it would be important to add HIV-1 RNA detection to the suit of tools used to measure HIV-1 replication to avoid misinterpretation of the rates of HIV-1 replication due to lack of packaging of some defective RNA into a mature virion. Understanding levels of DNA integration could also be useful to understand (1) whether some donors resist HIV-1 DNA integration compared to others, and (2) does HIV-1 replication correlate with DNA integration between donors.

7.10. Conclusions

In the work presented above, I set out to answer whether phylogenetically close strains of *Mtb* with SNP predicted to be under HIV-1 positive directional selection in lipid metabolising genes have different cell wall lipid phenotypes. I also aimed to use the phylogenetically close strains to determine whether the SNP resulted in differential regulation of cytokines using macrophages *in vitro* in the presence and absence of HIV-1 co-infection and the consequence of the regulation on HIV-1 during co-infection. Finally, I wanted to validate the role of the SNP by genetic engineering, to assess whether the change would affect, cell wall lipid phenotypes, cytokine secretion *in vitro* in both *Mtb* mono-infected MDM and HIV-1 co-infected MDM, as well as determine the consequence of the SNP change in HIV-1 production in co-infected MDM and by-stander MDM. I was able to show that phylogenetically close strains of *Mtb* can have different cell wall phenotypes, which results in differential regulation of cytokine secretion by macrophages. *Mtb*-induced microenvironment increases susceptibility of cells to HIV-1 infection and leads to increased replication of HIV-1. A single nucleotide change has the potential to affect cell wall lipid phenotypes and cytokine secretion dynamics. This could consequently influence HIV-1 production and replication. I acknowledge that the primary SNP predicted to be under HIV-1 positive directional secretion was not successfully changed in these experiments and the full repertoire of lipids was not analysed following mutagenesis. These are as priority experiments for future works.

7.11. References

1. Comas, I., et al., *Out-of-Africa migration and Neolithic coexpansion of Mycobacterium tuberculosis with modern humans.* Nat Genet, 2013. **45**(10): p. 1176-82.
2. Sharp, P.M. and B.H. Hahn, *Origins of HIV and the AIDS pandemic.* Cold Spring Harb Perspect Med, 2011. **1**(1): p. a006841.
3. Bliven, K.A. and A.T. Maurelli, *Evolution of Bacterial Pathogens Within the Human Host.* Microbiol Spectr, 2016. **4**(1).
4. Warner, D.F., A. Koch, and V. Mizrahi, *Diversity and disease pathogenesis in Mycobacterium tuberculosis.* Trends Microbiol, 2015. **23**(1): p. 14-21.
5. Koch, A.S., et al., *The Influence of HIV on the Evolution of Mycobacterium tuberculosis.* Mol Biol Evol, 2017. **34**(7): p. 1654-1668.
6. Eldholm, V., et al., *Impact of HIV co-infection on the evolution and transmission of multidrug-resistant tuberculosis.* Elife, 2016. **5**.
7. Stucki, D. and S. Gagneux, *Single nucleotide polymorphisms in Mycobacterium tuberculosis and the need for a curated database.* Tuberculosis (Edinb), 2013. **93**(1): p. 30-9.
8. Reed, M.B., et al., *A glycolipid of hypervirulent tuberculosis strains that inhibits the innate immune response.* Nature, 2004. **431**(7004): p. 84-7.
9. Sandberg, J.K., et al., *HIV-1 Replication Is Differentially Regulated by Distinct Clinical Strains of Mycobacterium tuberculosis.* PLoS ONE, 2009. **4**(7).
10. Gago, G., L. Diacovich, and H. Gramajo, *Lipid metabolism and its implication in mycobacteria-host interaction.* Curr Opin Microbiol, 2018. **41**: p. 36-42.
11. Pieters, J., *Mycobacterium tuberculosis and the macrophage: maintaining a balance.* Cell Host Microbe, 2008. **3**(6): p. 399-407.
12. Glickman, M.S. and W.R. Jacobs, Jr., *Microbial pathogenesis of Mycobacterium tuberculosis: dawn of a discipline.* Cell, 2001. **104**(4): p. 477-85.
13. Goren, M.B., *Mycobacterial lipids: selected topics.* Bacteriol Rev, 1972. **36**(1): p. 33-64.
14. Chen, J.M., et al., *Roles of Lsr2 in colony morphology and biofilm formation of Mycobacterium smegmatis.* J Bacteriol, 2006. **188**(2): p. 633-41.
15. Korf, J., et al., *The Mycobacterium tuberculosis cell wall component mycolic acid elicits pathogen-associated host innate immune responses.* Eur J Immunol, 2005. **35**(3): p. 890-900.

16. Rousseau, C., et al., *Production of phthiocerol dimycocerosates protects Mycobacterium tuberculosis from the cidal activity of reactive nitrogen intermediates produced by macrophages and modulates the early immune response to infection.* Cell Microbiol, 2004. **6**(3): p. 277-87.
17. Jarlier, V. and H. Nikaido, *Mycobacterial cell wall: structure and role in natural resistance to antibiotics.* FEMS Microbiol Lett, 1994. **123**(1-2): p. 11-8.
18. Singh, P., et al., *Cell envelope lipids in the pathophysiology of Mycobacterium tuberculosis.* Future Microbiol, 2018. **13**: p. 689-710.
19. Gilmore, S.A., et al., *Sulfolipid-1 biosynthesis restricts Mycobacterium tuberculosis growth in human macrophages.* ACS Chem Biol, 2012. **7**(5): p. 863-70.
20. Ruhl, C.R., et al., *Mycobacterium tuberculosis Sulfolipid-1 Activates Nociceptive Neurons and Induces Cough.* Cell, 2020. **181**(2): p. 293-305 e11.
21. Daffe, M., et al., *Polyphthienoyl trehalose, glycolipids specific for virulent strains of the tubercle bacillus.* Eur J Biochem, 1988. **172**(3): p. 579-84.
22. Astarie-Dequeker, C., et al., *Phthiocerol dimycocerosates of M. tuberculosis participate in macrophage invasion by inducing changes in the organization of plasma membrane lipids.* PLoS Pathog, 2009. **5**(2): p. e1000289.
23. Cambier, C.J., et al., *Mycobacteria manipulate macrophage recruitment through coordinated use of membrane lipids.* Nature, 2014. **505**(7482): p. 218-22.
24. Lerner, T.R., et al., *Mycobacterium tuberculosis cords within lymphatic endothelial cells to evade host immunity.* JCI Insight, 2020. **5**(10).
25. Kalsum, S., et al., *The Cording Phenotype of Mycobacterium tuberculosis Induces the Formation of Extracellular Traps in Human Macrophages.* Front Cell Infect Microbiol, 2017. **7**: p. 278.
26. Indrigo, J., R.L. Hunter, and J.K. Actor, *Cord factor trehalose 6,6'-dimycolate (TDM) mediates trafficking events during mycobacterial infection of murine macrophages.* Microbiology (Reading), 2003. **149**(Pt 8): p. 2049-2059.
27. Middlebrook, G., R.J. Dubos, and C. Pierce, *Virulence and Morphological Characteristics of Mammalian Tubercle Bacilli.* J Exp Med, 1947. **86**(2): p. 175-84.
28. Dubey, V.S., T.D. Sirakova, and P.E. Kolattukudy, *Disruption of msl3 abolishes the synthesis of mycolipanoic and mycolipenic acids required for polyacyltrehalose synthesis in Mycobacterium tuberculosis H37Rv and causes cell aggregation.* Mol Microbiol, 2002. **45**(5): p. 1451-9.

29. Ghazaei, C., *Mycobacterium tuberculosis and lipids: Insights into molecular mechanisms from persistence to virulence.* J Res Med Sci, 2018. **23**: p. 63.
30. Trivedi, A., et al., *Thiol reductive stress induces cellulose-anchored biofilm formation in Mycobacterium tuberculosis.* Nat Commun, 2016. **7**: p. 11392.
31. Falvo, J.V., et al., *Arc of a vicious circle: pathways activated by Mycobacterium tuberculosis that target the HIV-1 long terminal repeat.* Am J Respir Cell Mol Biol, 2011. **45**(6): p. 1116-24.
32. Chun, T.W., et al., *Quantification of latent tissue reservoirs and total body viral load in HIV-1 infection.* Nature, 1997. **387**(6629): p. 183-8.
33. Vandergeeten, C., R. Fromentin, and N. Chomont, *The role of cytokines in the establishment, persistence and eradication of the HIV reservoir.* Cytokine Growth Factor Rev, 2012. **23**(4-5): p. 143-9.
34. Cocchi, F., et al., *Identification of RANTES, MIP-1 alpha, and MIP-1 beta as the major HIV-suppressive factors produced by CD8+ T cells.* Science, 1995. **270**(5243): p. 1811-5.
35. Herbein, G. and A. Varin, *The macrophage in HIV-1 infection: from activation to deactivation?* Retrovirology, 2010. **7**: p. 33.
36. Sirakova, T.D., et al., *The Mycobacterium tuberculosis pks2 gene encodes the synthase for the hepta- and octamethyl-branched fatty acids required for sulfolipid synthesis.* J Biol Chem, 2001. **276**(20): p. 16833-9.
37. Middlebrook, G., C.M. Coleman, and W.B. Schaefer, *Sulfolipid from Virulent Tubercle Bacilli.* Proc Natl Acad Sci U S A, 1959. **45**(12): p. 1801-4.
38. Gangadharam, P.R., M.L. Cohn, and G. Middlebrook, *Infectivity, Pathogenicity and Sulpholipid Fraction of Some Indian and British Strains of Tubercle Bacilli.* Tubercle, 1963. **44**: p. 452-5.
39. Goren, M.B., et al., *Prevention of phagosome-lysosome fusion in cultured macrophages by sulfatides of Mycobacterium tuberculosis.* Proc Natl Acad Sci U S A, 1976. **73**(7): p. 2510-4.
40. Pabst, M.J., et al., *Inhibition of macrophage priming by sulfatide from Mycobacterium tuberculosis.* J Immunol, 1988. **140**(2): p. 634-40.
41. Brozna, J.P., et al., *Monocyte responses to sulfatide from Mycobacterium tuberculosis: inhibition of priming for enhanced release of superoxide, associated with increased secretion of interleukin-1 and tumor necrosis factor alpha, and altered protein phosphorylation.* Infect Immun, 1991. **59**(8): p. 2542-8.

42. Augenstreich, J. and V. Briken, *Host Cell Targets of Released Lipid and Secreted Protein Effectors of Mycobacterium tuberculosis.* Front Cell Infect Microbiol, 2020. **10**: p. 595029.
43. Pasternak, A.O. and B. Berkhout, *What do we measure when we measure cell-associated HIV RNA.* Retrovirology, 2018. **15**(1): p. 13.
44. Prado, J.G., et al., *Lack of longitudinal intrapatient correlation between p24 antigenemia and levels of human immunodeficiency virus (HIV) type 1 RNA in patients with chronic hiv infection during structured treatment interruptions.* J Clin Microbiol, 2004. **42**(4): p. 1620-5.
45. Li, C.C., et al., *Detection and quantification of human immunodeficiency virus type 1 p24 antigen in dried whole blood and plasma on filter paper stored under various conditions.* J Clin Microbiol, 2005. **43**(8): p. 3901-5.
46. Platt, E.J., et al., *Effects of CCR5 and CD4 cell surface concentrations on infections by macrophagetropic isolates of human immunodeficiency virus type 1.* J Virol, 1998. **72**(4): p. 2855-64.
47. Wei, X., et al., *Emergence of resistant human immunodeficiency virus type 1 in patients receiving fusion inhibitor (T-20) monotherapy.* Antimicrob Agents Chemother, 2002. **46**(6): p. 1896-905.
48. Thayil, S.M., et al., *Mycobacterium tuberculosis complex enhances susceptibility of CD4 T cells to HIV through a TLR2-mediated pathway.* PLoS One, 2012. **7**(7): p. e41093.
49. Garrait, V., et al., *Tuberculosis generates a microenvironment enhancing the productive infection of local lymphocytes by HIV.* J Immunol, 1997. **159**(6): p. 2824-30.
50. Souriant, S., et al., *Tuberculosis Exacerbates HIV-1 Infection through IL-10/STAT3-Dependent Tunneling Nanotube Formation in Macrophages.* Cell Rep, 2019. **26**(13): p. 3586-3599 e7.
51. Mancino, G., et al., *Infection of human monocytes with Mycobacterium tuberculosis enhances human immunodeficiency virus type 1 replication and transmission to T cells.* J Infect Dis, 1997. **175**(6): p. 1531-5.
52. Goletti, D., et al., *Inhibition of HIV-1 replication in monocyte-derived macrophages by Mycobacterium tuberculosis.* J Infect Dis, 2004. **189**(4): p. 624-33.
53. Kedzierska, K. and S.M. Crowe, *Cytokines and HIV-1: interactions and clinical implications.* Antivir Chem Chemother, 2001. **12**(3): p. 133-50.

54. Webster, J.D. and D. Vucic, *The Balance of TNF Mediated Pathways Regulates Inflammatory Cell Death Signaling in Healthy and Diseased Tissues.* Front Cell Dev Biol, 2020. **8**: p. 365.
55. Dinarello, C.A., *Immunological and inflammatory functions of the interleukin-1 family.* Annu Rev Immunol, 2009. **27**: p. 519-50.
56. Fantuzzi, L., et al., *Endogenous CCL2 (monocyte chemotactic protein-1) modulates human immunodeficiency virus type-1 replication and affects cytoskeleton organization in human monocyte-derived macrophages.* Blood, 2003. **102**(7): p. 2334-7.
57. Poli, G., et al., *Interleukin 6 induces human immunodeficiency virus expression in infected monocytic cells alone and in synergy with tumor necrosis factor alpha by transcriptional and post-transcriptional mechanisms.* J Exp Med, 1990. **172**(1): p. 151-8.
58. Sabbatucci, M., et al., *Endogenous CCL2 neutralization restricts HIV-1 replication in primary human macrophages by inhibiting viral DNA accumulation.* Retrovirology, 2015. **12**: p. 4.
59. van Kessel, J.C. and G.F. Hatfull, *Efficient point mutagenesis in mycobacteria using single-stranded DNA recombineering: characterization of antimycobacterial drug targets.* Mol Microbiol, 2008. **67**(5): p. 1094-107.
60. Bol, S.M., et al., *Donor variation in in vitro HIV-1 susceptibility of monocyte-derived macrophages.* Virology, 2009. **390**(2): p. 205-11.
61. Klatt, N.R., et al., *Immune activation and HIV persistence: implications for curative approaches to HIV infection.* Immunol Rev, 2013. **254**(1): p. 326-42.
62. Massanella, M., R. Fromentin, and N. Chomont, *Residual inflammation and viral reservoirs: alliance against an HIV cure.* Curr Opin HIV AIDS, 2016. **11**(2): p. 234-41.
63. Waters, R., et al., *The Mtb-HIV syndemic interaction: why treating M. tuberculosis infection may be crucial for HIV-1 eradication.* Future Virol, 2020. **15**(2): p. 101-125.
64. Ajasin, D.O., et al., *CCL2 mobilizes ALIX to facilitate Gag-p6 mediated HIV-1 virion release.* Elife, 2019. **8**.
65. Lopez-Castejon, G. and D. Brough, *Understanding the mechanism of IL-1beta secretion.* Cytokine Growth Factor Rev, 2011. **22**(4): p. 189-95.
66. Summers, W.C., *Virus infection.* Viruses, 2009. **1**: p. 546 - 552.

67. Eisenreich, W., et al., *How Viral and Intracellular Bacterial Pathogens Reprogram the Metabolism of Host Cells to Allow Their Intracellular Replication.* Front Cell Infect Microbiol, 2019. **9**: p. 42.
68. Koch, A.E., et al., *Interleukin-8 as a macrophage-derived mediator of angiogenesis.* Science, 1992. **258**(5089): p. 1798-801.
69. Apostolopoulos, J., P. Davenport, and P.G. Tipping, *Interleukin-8 production by macrophages from atheromatous plaques.* Arterioscler Thromb Vasc Biol, 1996. **16**(8): p. 1007-12.
70. Lane, B.R., et al., *Interleukin-8 stimulates human immunodeficiency virus type 1 replication and is a potential new target for antiretroviral therapy.* J Virol, 2001. **75**(17): p. 8195-202.
71. Nookala, A.R. and A. Kumar, *Molecular mechanisms involved in HIV-1 Tat-mediated induction of IL-6 and IL-8 in astrocytes.* J Neuroinflammation, 2014. **11**: p. 214.
72. Pananghat, A.N., et al., *IL-8 Alterations in HIV-1 Infected Children With Disease Progression.* Medicine (Baltimore), 2016. **95**(21): p. e3734.
73. Richardson, R.M., et al., *Interleukin-8-mediated heterologous receptor internalization provides resistance to HIV-1 infectivity. Role of signal strength and receptor desensitization.* J Biol Chem, 2003. **278**(18): p. 15867-73.
74. Rollenhagen, C. and S.N. Asin, *IL-8 decreases HIV-1 transcription in peripheral blood lymphocytes and ectocervical tissue explants.* J Acquir Immune Defic Syndr, 2010. **54**(5): p. 463-9.
75. Csoma, E., et al., *Human herpesvirus 6A decreases the susceptibility of macrophages to R5 variants of human immunodeficiency virus 1: possible role of RANTES and IL-8.* Virus Res, 2006. **121**(2): p. 161-8.
76. Jacobs, E.S., et al., *Cytokines Elevated in HIV Elite Controllers Reduce HIV Replication In Vitro and Modulate HIV Restriction Factor Expression.* J Virol, 2017. **91**(6).
77. Gonzalez, E., et al., *Race-specific HIV-1 disease-modifying effects associated with CCR5 haplotypes.* Proc Natl Acad Sci U S A, 1999. **96**(21): p. 12004-9.
78. Gonzalez, E., et al., *The influence of CCL3L1 gene-containing segmental duplications on HIV-1/AIDS susceptibility.* Science, 2005. **307**(5714): p. 1434-40.
79. Arias, L., et al., *Cording Mycobacterium tuberculosis Bacilli Have a Key Role in the Progression towards Active Tuberculosis, Which is Stopped by Previous Immune Response.* Microorganisms, 2020. **8**(2).

80. Mittal, E., et al., *Single cell preparations of Mycobacterium tuberculosis damage the mycobacterial envelope and disrupt macrophage interactions.* bioRxiv, 2022.
81. Wong, J.K. and S.A. Yukl, *Tissue reservoirs of HIV.* Curr Opin HIV AIDS, 2016. **11**(4): p. 362-70.
82. Musyoki, A.M., et al., *Identification and genetic characterization of unique HIV-1 A1/C recombinant strain in South Africa.* AIDS Res Hum Retroviruses, 2015. **31**(3): p. 347-52.
83. Korb, V.C., A.A. Chuturgoon, and D. Moodley, *Mycobacterium tuberculosis: Manipulator of Protective Immunity.* Int J Mol Sci, 2016. **17**(3): p. 131.